UNIVERSITY OF SOUTHAMPTON

ABSTRACT

FACULTY OF LAW, ARTS AND SOCIAL SCIENCES
TEXTILE CONSERVATION CENTRE

Doctor of Philosophy

Investigating the Characterisation and Stability of Polyamide 6,6 in Heritage Artefacts

By Emma J C Richardson

Near-infrared reflectance spectroscopy (NIR) is investigated as a method of non-invasive, *in situ* analysis of contemporary textile material. Besides providing spectral signatures, the advantages of NIR include the non-contact nature of the reflectance technique and the use of a remote, flexible probe. A spectral database of well-defined reference material has been collected. This was recorded using a standardised protocol taking into account the need to interrogate objects within a collection. The differentiation of silk and synthetic polyamide can pose particular problems for curators of historic textiles due to the similarities in their visual appearance. NIR spectroscopy coupled with multivariate analysis is investigated for the differentiation of the polyamide sub-classes, found extensively within textile collections. Two multivariate methods of classification have been applied and it is shown that, with the appropriate spectral processing and calibration, both of these techniques are appropriate for sub-class discrimination.

Synthetic polyamides are frequently found in conjunction with natural organic materials, and are often exposed to the same pest treatments as natural polymers. In the event of an infestation there are a number of eradication measures possible, including the application of raised and lowered temperatures. However, these treatments take unaged aliphatic polyamides above, and well below, their glass transition temperature, respectively. For this reason the stability of new and aged polyamide textile material has been investigated.

Polyamide 6,6 test material was tested 'as received' and in an artificially aged condition. Samples were subsequently subject to -30°C, room temperature or 58°C. In addition, samples were treated with and without the application of a load, enabling an assessment of risk if treated whilst hanging and supporting their own weight. Structural alterations were monitored using polarized and non-polarized mid infrared spectroscopy, tensile testing and differential scanning calorimetry. In addition, dynamic mechanical thermal analysis creep experiments were carried out to supplement the information provided by the *in situ* creep tests. It is evident from the results that the thermal treatments have a significant effect on the behaviour and structure of the aged polyamide. The implication for *in situ* treatment of this material in collections is clear, and must therefore be approached with caution. Analysis of the experimental data suggest that the changes observed can be related to the degree of crystallinity produced by the changes in temperature and by the presence of stress during treatment.

Contents:

List of Figures:

Chapter 2

Chapter 3

Chapter 4

Chapter 5

Chapter 6

Chapter 7

Chapter 8

Chapter 9

Chapter 10

Chapter 11

Appendix 1

Appendix 2

List of Tables:

Chapter 10

Chapter 11

Appendix 1

Declaration of Authorship:

I, Emma Joanne Claire Richardson declare that this thesis entitled, *Investigating the Characterisation and Stability of Polyamide 6,6 in Heritage Artefacts*, and the work presented in the thesis are both my own, and have been generated by me as the result of my own original research. I confirm that:

• this work was done wholly or mainly while in candidature for a research degree at this University;

• where any part of this thesis has previously been submitted for a degree or any other qualification at this University or any other institution, this has been clearly stated;

• where I have consulted the published work of others, this is always clearly attributed;

• where I have quoted from the work of others, the source is always given. With the exception of such quotations, this thesis is entirely my own work;

• I have acknowledged all main sources of help;

• where the thesis is based on work done by myself jointly with others, I have made clear exactly what was done by others and what I have contributed myself;

• none of this work has been published before submission.

Signed:……

Date:……

Acknowledgments:

Many thanks are given to my supervisors, Dr Paul Wyeth and Prof. Graham Martin, for their encouragement, ideas and direction, and for ensuring I remained 'on track' even when I felt there was a mountain to climb. I would also like to thank Dr Paul Garside for his technical guidance during the early stages of this project.

I am most grateful for the funding provided by the Arts and Humanities Research Council, the Pasold Research Fund and the University of Southampton Postgraduate Conference Attendance Fund, which enabled this research to be brought to a successful conclusion.

Access to equipment was kindly provided by the Department of Physics, University of Surrey, the School of Engineering Sciences, University of Southampton and the Department of Biological and Chemical Sciences, Birkbeck College. Polymer reference samples were provided by Solutia, Goodfellows, Equipolymer, Hahl, Lati, Whaleys of Bradford Ltd and members of the Plastics Historical Society. Without this material the NIR spectral library would not have been possible.

Many thanks are given to my colleagues at the Textile Conservation Centre and the Victoria and Albert Museum. In particular I would like to thank Suzanne Smith, Keeper of Collections, and Sue Prichard, Curator of Flat and Hanging Textiles, Department of Furniture, Textile and Frames, Victoria and Albert Museum, for their willingness to provide access to the contemporary textile collections. Similar thanks are given to Sarah Howard, Textile Conservator, and Sue Washington, Keeper of Dress and Textiles, Hampshire County Council Museums and Archives Service. I would also like to acknowledge the support of Frances Hartog and Elizabeth-Anne Haldane, Textile Conservators, Department of Furniture, Textile and Frames, Victoria and Albert Museum, for their continuing enthusiasm.

Karen Roux and Paul Leary at Thermo Lignum® kindly facilitated access to the WARMAIR treatment chamber, without which this project would not have been possible.

On a personal note, warm thanks are given to my fellow PhD students, who have provided advice and support along the way. In particular, I am grateful to Naomi Luxford for the laughter and tears, and for making me realise that it was within my reach.

Last, but by no means least, I am most indebted to my family, even though they continuously asked “is it not done yet?”. To my mum and dad for supporting me emotionally, physically, intellectually and financially. For ensuring the fridge was always full and the kettle always boiled, and finally to my brother, “Technical” Tony, for his 24hour computer support.

Abbreviations:

a	slope
A	absorbance ($-\log_{10}R$)
θ	angle
b	intercept
BSI	British Standards Institute
c	velocity of light (299 792 458 m/s)
Cp	heat capacity
°C	degrees Celsius
Δ	difference
D	dichroic ratio
DA	Discriminant Analysis
D_e	dissociation energy
d_p	depth of penetration
Dp	degree of polymerisation
ATR	attenuated total reflectance
cm	centimetre
DMTA	Dynamic Mechanical Thermal Analyser
DSC	Differential Scanning Calorimetry
E	Young's modulus
Ep	photon energy
FTIR	Fourier Transform Infra-red Spectroscopy
FTR	Fourier Transform Raman
g	gram
GPa	gigapascals
h	Planck constant (6.63×10^{-34} J/s)
HCCMAS	Hampshire County Council Museums and Archives Service
Hm	heat of melting
HQI	Hit Quality Index
InGaAs	indium gallium arsenide
IPM	integrated pest managment
IRUG	Infrared and Raman Users Group
IS	integrating sphere

ISO	International Organization of Standardization
J	joule
kg	kilogram
l	litre
L^T	loadings matrix
m	metre
min	minute
MIR	mid-infrared
MoMA	Museum of Modern Art
µ	molecular mass
µm	micrometre (micron)
mm	millimetre
ml	millilitre
MPa	megapascals
MVA	Multivariate Analysis
N	Newtons
n_c	refractive index of the ATR crystal
n_s	refractive index of the sample
NIPALS	nonlinear iterative partial least squares
NIR	near-infrared
NIRA	near-infrared accessory
NMR	Nuclear Magnetic Resonance
%	percent
P	probe
PA 6	polyamide 6
PA 6,6	polyamide 6,6
PA 12	polyamide 12
PC	principal component
PCA	Principal Component Analysis
PLS	Partial Least Squares
Pol	polarized
R	reflectance (ratio of reflected over incident)
RH	relative humidity
RMSEP	Root Mean Squared Standard Error of Prediction

s	second
SIMCA	Soft Independent Modelling of Class Analogies
S/N	signal to noise parameter
T	scores matrix
Tb	Brill transition temperature
Tg	glass transition temperature
Tm	melting temperature
U	Y matrix
UV	ultra-violet
V	potential energy
v	quantum number
V & A	Victoria and Albert Museum
W	Watt
λ	wavelength (nm)
$\tilde{\nu}$	wavenumber (cm^{-1})
X	X matrix
XRF	X-ray Fluorescence
XRD	X-ray Diffraction

Introduction: New Materials, New Challenges

In recent years there has been growing interest in synthetic materials within the museum environment; both from an identification point of view and in order to determine their condition. Since their development in the late 19th Century, synthetic polymers have moved steadily into almost every area of life, and as a consequence, into a growing number of museum collections.

The increase in contemporary collecting has prompted a number of specialist conferences, focusing on the issues of characterisation and stabilisation of these relatively new heritage materials [1-3]. The most recent of these was entitled *Plastics: Looking at the Future and Learning from the Past*, held at the Victoria and Albert Museum, London, in May 2007. This was a multidisciplinary meeting, bringing together a broad spectrum of experts, from scientists and artists, to conservators and manufacturers. The conference encouraged discussions regarding the future practice of preservation and highlighted to a wider audience the issues faced by the conservation profession.

Many households these days are now required by their councils to recycle plastic waste, to avoid such material finding their way into landfill sites. The general perception of plastics is one of persistence, materials that do not readily biodegrade and pose significant environmental problems. Whist this may well be the case, the original form and condition of these plastics will likely alter over time even though their presence remains. It is these alterations in the physical nature of plastics that are of concern to the heritage profession. Organic polymeric materials will all degrade over time, whether natural, man-made or synthetic. However, man-made and synthetic types tend to pose significant stabilisation problems due to production methods, additives and treatments, which can introduce varying and complex routes of degradation.

The physical characteristics of polymers are based on their high molecular weights and the amorphous and crystalline nature of the chain aggregates. Therefore, processes of deterioration that alter the structure of these polymer chains are naturally going to affect their properties and stability. Such processes of degradation include, hydrolysis, photo-oxidation and mechanical stress [4].

Of the polymeric material held within museum and heritage collections, other than biopolymers, Keneghan [5] has identified five types of major concern regarding instability. These are cellulose nitrate, cellulose acetate, poly-vinyl chloride (PVC), polyurethane and

synthetic and natural rubbers. Their deterioration within collections is inevitable, but the rate at which the objects deteriorate can often be reduced by careful control of the environment. The degradation and stabilisation of these polymers vary through the classes, therefore illustrating the need for positive identification within collections, which is not always easy with limited sampling of artefacts.

One area of particular interest is that related to contemporary textile collections. Synthetic polymeric fibres have been used extensively within clothing, with industry exploiting physical and chemical possibilities through fibre synthesis. Synthetic polymers are found within textiles as fibres, interlinings of clothes, surface coatings, fastenings and adornments. As with other synthetic materials, these textiles are of growing concern to conservators and curators caring for textile collections.

Pritchard and Smith [6] describe the deterioration of a patent PVC coated jacket as "actively deteriorating and leaching plasticizer" where the "left lapel of the jacket had adhered to the left front". They note that when the jacket was acquired into the collection in the year 2000 (the jacket dating from the 1980's) it was in good condition, and thus highlighted the need for regular condition monitoring of potentially vulnerable material. However, even simple identification of materials within these collections is not straightforward. The very nature of textile artefacts constrains sampling and conventional microscopy, which, unlike natural fibres, does not readily distinguish the synthetic polymer classes. Fibre processing such as extrusion does not convey polymer-specific morphological features seen in natural fibres. In addition, by their very nature, materials such as interlinings are not readily accessible for sampling.

Through discussions with conservators and curators it has been highlighted that the *in situ* application of near-infrared spectroscopy for the non-invasive identification and condition monitoring of synthetic textile materials would greatly assist in the long-term preservation of contemporary collections. The ability to identify quickly modern textiles would provide museum professionals with the information required for a greater understanding of their collections, enabling informed long-term action plans and more immediate remedial conservation plans to be implemented.

I.1 A Question of Identification

Having spoken with the curators and keepers of the contemporary textiles collections at the Victoria and Albert Museum [I,II], it has become apparent that their knowledge of the materials held within the collections is limited. Object catalogues and accessioning are incomplete with regards to material types, thus making it difficult for them to identify and monitor the materials of possible future concern, as highlighted by Keneghan [5].

Two such areas were pinpointed during a visit to the V&A collections. These were the deterioration of a number of shoes and painted textiles within the collection.

The shoes were showing signs of a variety of different degradation paths. These ranged from sticky, buckling coated textiles to brittle and yellowing uppers. Similar problems were found in a collection of painted T-shirts. Many had become adhered to themselves due to 'tacky' paints, whilst others had logos with significant loss of flexibility.

Although this problem was prolific through their collections, the curators were not able to identify the material types without the aid of sampling and significant use of time from the curatorial and scientific departments. On application of portable NIR analysis, the majority of the problematic materials were readily and quickly identified as either polyurethane polyesters or polyvinyl chloride (Case Study II, Chapter 3).

Such problems are not unique to the V&A collections. Bechtold [7] describes: "discolouration, brittleness, cracking and detachment of the coating" to wet look polyurethane polyesters. Similarly, a pair of polyurethane coated trousers treated at the Textile Conservation Centre, Winchester, showed signs of significant delamination of the polyurethane coating. In this latter case corrosion of metal rivets was also seen due to out gassing of volatile organic acids during the polyurethane degradation [8]. This underlines the need for positive identification of materials that give volatile emissions within collections. Not only would this benefit the object of interest, but would allow such material to be segregated, reducing the risk to adjacent objects.

[I] Personal conversation with Sue Pritchard, Curator of Flat and Hanging Textiles, Furniture, Textile and Frames Section, Victoria and Albert Museum, 5 January 2006. Discussion regarding the types of artefacts that would benefit from on site characterisation and condition monitoring.

[II] Personal conversation with Susanne Smith, Keeper of Collections, Furniture, Textile and Frames Section, Victoria and Albert Museum, 31 July 2006. Discussion and site visit to assess the major areas of concern within the V&A's contemporary textiles collection.

I.2 A Question of Stability

Discussions with textile conservators and conservation scientists [III,IV,V,VI] have highlighted different priorities and concerns from those presented by curators. A lack of knowledge and understanding of these complex materials proves problematic when conservators are required to treat or advise on stability. A recurring area of concern is the possible detrimental effect that pest control measures have on synthetic materials. Many studies have been carried out into the effects of heat and freezing treatments on natural cellulosic and proteinacous materials [9-13], but their impact on synthetic materials has not been thoroughly studied in a museum collection context. Kite[v] has suggested that being able to identify the materials susceptible to chemical or physical damage during or after these treatments, would enable informed decisions when faced with pest infestations. Knowledge of their routes of degradation would enforce the ethical decisions made about the possible removal of vulnerable material from mixed media artefacts before treatment. An example of such a case is presented in Section 4.3, Chapter 4, where cellulose nitrate adornments were removed from a woollen garment before freezing, as it was feared that the treatment may cause irreversible damage[VII].

The following thesis will present the results of research carried out aimed at answering some of the questions facing conservators when caring for contemporary textile collections. The issues surrounding temperature treatments of synthetic textiles will be addressed, focusing on the differences of behaviour between new and aged material, and samples treated when flat or hanging under their own weight. The detection of polymers vulnerable to treatment enables such material to be separated or removed. Unfortunately, the visual nature of many of these materials precludes ready identification. It is for this reason that the development of near-infrared spectroscopy as a method of non-invasive characterisation has also been investigated. The aim of which was to provide museum professionals with collection management tools.

[III] Private conversation with Lynda Hillyer, Senior Textile Conservator, Furniture, Textile and Frames Section Victoria and Albert Museum, 28 October 2005.

[IV] Private conversation with Lesley Miller, Textile Curator, Furniture, Textile and Frames Section, Victoria and Albert Museum, 13 January 2006

[V] Private conversation with Marion Kite, Head of Furniture, Textile and Frames Section, Furniture, Textiles and Frames Section, Victoria and Albert Museum, 10 August 2006. Discussion regarding the treatment of synthetic textile artefacts.

[VI] Personal conversation with Anita Quye, Conservation Scientist, National Museums of Scotland, 06 December 2006.

[VII] Private communication with Elizabeth-Anne Haldane, Textile Conservator, Furniture, Textile and Frames Section Victoria and Albert Museum, 30 April 2009.

The first part of this thesis will address the issues surrounding the identification of synthetic material held within contemporary textile collections (a brief review of the chemistry of the various synthetic polymers is presented in Appendix 1). The development of a practical solution for collections management will be presented in the form of a near-infrared spectral library. The determination of experimental protocols to enable non-invasive, onsite characterisation of polymers will be presented. The acquisition of a reference database will be detailed, along with two case studies illustrating the application and limitations of the near-infrared technique onsite in collections. Attention will be given to the use of commercial library software and more sophisticated multivariate analyses for polymer discrimination.

In the latter half of the thesis, the issues arising from the application of raised and lowered temperature pest eradication treatments will be investigated. Focus will be given to the behaviour of unaged and aged synthetic polyamide textile material under these conditions. Here the importance of the glass transition temperature, and it's influence on physical properties, will be discussed. The occurrence of the glass transition in polyamides within the temperature range of interest will be highlighted, and the results of *in situ* testing and laboratory based experiments will be related back to this important property of polymers. The results from Fourier-transform mid-infrared spectroscopy, mechanical analysis and differential scanning calorimetry will be presented, enabling the condition of the control material to be assessed and the structural changes induced after pest control treatment to be monitored. Supplementary creep experiments were performed using a dynamic mechanical thermal analyser, and the creep/recovery curves will be presented. The intention of these tests was to mimic the behaviour of hanging textiles when subjected to the temperatures of interest, enabling the stability of treating hanging textiles to be determined.

I.3 References

1. Rogerson, C. and P. Garside. in *AHRC Research Centre for Textile Conservation and Textile Studies 2nd Annual Conference The Future of the 20th Century: Collecting, Interpreting and Conserving Modern Materials*. 2005. Winchester: Archetype Publications.
2. Corzo, M.A. in *Mortality Immortality? The Legacy of 20th Century Art*. 1998. Los Angeles: J. Paul Getty Trust.

3. Keneghan, B. and L. Egan. in *Plastics: Look at the Future and Learning from the Past*. 2007. London: Archetype Publications in association with the Victoria and Albert Museum.
4. Allen, N.S. and M. Edge, *Fundamentals of Polymer Degradation and Stabilisation*. 1992, Barking: Elsevier Science Publishers Ltd. 201.
5. Keneghan, B., *A Survey of Synthetic Plastic and Rubber Objects in the Collections of the Victoria and Albert Museum.* Museum Management and Curatorship, 2002. **19**(3): p. 321-331.
6. Prichard, S. and S. Smith. *Taking a Risk: Collecting for the Future*. in *Plastics: Looking at the Future and Learning from the Past*. 2007. London: Archetype Publications in association with the Victoria and Albert Museum.
7. Bechtold, T. *Wet Look 1960's Furniture Design: Degradation of Polyurethane-coated Textile Carrier Substrates*. in *AHRC Research Centre for Textile Conservation and Textile Studies Second Annual Conference: The Future of the 20th Century - Collecting, Interpreting and Conserving Modern Materials*. 2005. Winchester: Archetype Publications.
8. Garside, P. and D. Lovett. *Polyurethane Foam: Investigating the Physical and Chemical Consequences of Degradation*. in *AHRC Research Centre for Textile Conservation and Textile Studies Second Annual Conference: The Future of the 20th Century - Collecting, Interpreting and Conserving Modern Materials*. 2005. Winchester: Archetype Publications.
9. Beiner, G.G. and T.M. Ogilvie, *Thermal Methods of Pest Eradication: Their Effect on Museum Objects.* The Conservator, 2005/06. **29**: p. 5-18.
10. Berkouwer, M., *Freezing to Eradicate Insect Pests in Textiles at Brodsworth.* The Conservator, 1994. **18**: p. 15-22.
11. Ackery, P., R, et al., *Effects of High Temperature Pest Eradication on DNA in Entomological Collections.* Studies in Conservation, 2004. **49**: p. 35-40.
12. Xavier-Rowe, A., et al. *Using Heat to Kill Insect Pests - Is It Practical and Safe?* in *IIC Advances in Conservation: Contributions to the Melboune Congress*. 2000. Melbourne: IIC.
13. Carrlee, E., *Does Low-temperature Pest Management Cause Damage? Literature Review and Observational Study of Ethnographic Artefacts.* Journal of the American Society for Conservation, 2003. **42**: p. 141-166.

Chapter 1: The Possibilities for Non-invasive Analysis of Polymeric Material *in* Collections

This chapter will consider the difficult nature of historical artefacts within the context of conservation science and the need for representative samples to aid analysis. An overview will be given of the applications of non-invasive analyses within the heritage sector, with particular emphasis on organic material. Arguments will be provided for the application of near-infrared spectroscopy within contemporary collections, in an aim to provide keepers of collections with tools for successful collections management.

The principles of interventive and preventive conservation have their foundations in science. Whether, for example, it is the choice of adhesive for stabilisation of an artefact or the monitoring of environmental conditions to ensure that optimum preservation conditions prevail, conservation work relies on an intimate knowledge of materials and their behaviour. It is for this reason that conservation science is finding increasing importance within museums and the heritage sector. The ability to qualify and quantify deterioration and related degradation products, enables a move towards enhanced measures of preservation, with improved storage and stabilisation. However, the fragile and rare nature of heritage material requires minimum disturbance to the artefact, avoiding loss of key information and integrity, whilst gaining maximum information.

There are a number of analytical techniques available to the conservation scientist; these include destructive, non-destructive and non-invasive techniques. Non-invasive techniques are usually much preferred where available, this referring to methods of analysis requiring no sample removal and leaving the investigated area intact.

Such techniques have been researched and developed for application to inorganic materials in the main. Examples include, the application of a portable X-ray Fluorescence Spectrometer (XRF) for *in situ* analysis of wall paintings [1], Infrared

Reflectography to reveal underdrawings in oil paintings [2], Synchrotron X-ray Diffraction (SR-XRD) and X-ray Absorbance Spectroscopy (SR-XRA) for mineral characterisation in black gloss pottery [3].

Non-invasive methods have been less well developed for application to organic artefacts. Existing, commonplace techniques for organic materials analysis, readily accessible to museums and the heritage sector, usually rely on some degree of sampling, although the analysis may not cause any damage to the sample itself. These techniques include Fourier-transform mid-Infrared spectroscopy (FT-IR), ultra-violet/visible spectroscopy (UV-Vis), nuclear magnetic resonance spectroscopy (NMR) and Raman spectroscopy. The development of near-Infrared spectroscopy (NIR) as a truly non-invasive, portable method of analysis for organic artefacts is presently being investigated. It has already been successfully applied *in situ* within the food and textile industry and agriculture, and its potential for onsite application within museums is now being assessed.

It is particularly timely then to consider the use of non-invasive vibrational spectroscopy for characterising contemporary collections. The general application to heritage materials is reviewed below, with particular emphasis given to near infrared spectroscopy, especially in relation to synthetic textile material.

1.1 Vibrational Spectroscopy in Heritage

The two primary spectroscopic techniques for molecular determination within the museum environment are mid-infrared spectroscopy and Raman spectroscopy. However, as indicated above, a third vibrational spectroscopic technique, near-infrared spectroscopy, is also finding its way into the conservation science laboratory. An overview of the techniques will be given here alongside their applications within heritage, but the reader is directed to the general literature for expanded explanations[4-10].

1.1.1 Mid-Infrared Spectroscopy

Mid-infrared spectroscopy (MIR) is concerned with the vibrations of molecular bonds, brought about by the application of infrared radiation to matter. Bonds will vibrate at a frequency that is dependent on the masses of the two connected atoms and the strength of the interatomic bond. Radiation will be absorbed by a molecule if the incident radiation contains frequencies that exactly match that of a bond vibration, thus causing excitation from its ground state to an excited state. It is this specificity that allows the identification of molecular structures to be made. For organic molecules, fundamental vibrational modes are generally excited by mid-infrared radiation (2 500-50 000nm), although information on inorganic material is also available [11]. With spectral vibrations primarily originating from fundamental transitions, band assignments are readily made and changes in peak position easily monitored. This is a significant benefit for the monitoring of sometimes small changes seen during degradation of artefacts. There are a number of sampling techniques available for use in MIR spectroscopy, with their choice and application being dependent on the physical and chemical nature of the sample, cost and availability.

The presentation of the sample in a halide salt disk or nujol mull for transmittance spectroscopy is not generally favoured within the context of heritage and conservation. This is due to the destructive nature of the preparation technique and the relatively large sample sizes required for analyses [12]. Pielesz *et al* [13] have also raised concerns regarding the possible modifications imparted to the molecular structure of fibres during transmittance analyses. Other researchers have commented on the low reproducibility of the technique, which is an important factor when sampling is limited [4, 14].

Reflectance techniques, however, have been widely applied within heritage. Infrared microscopy is often employed for the study of paintings and coatings, as illustrated by the work of Spring *et al* for the study of pigment and medium interactions in oil paintings [15]. Here, samples in the region of 200µm across were mounted in a resin and reflectance spectra collected via a microscope attachment. The removal, mounting and polishing of material does mean that this technique is invasive. However, the sample preparation does not alter the

structural properties of the material and the sample is retained after data acquisition.

Attenuated Total Reflection spectroscopy (FTIR-ATR) has become one of the most applicable methods due to low level sampling and non-destructive capabilities [16-18]. The method is based on the penetration of radiation through a high-density crystal, producing an evanescent wave at the point of internal reflection. This interacts with the sample surface to depths approximating 2µm from the profile of the high density crystal, attenuating the beam. The short sampling capabilities of the technique requires good contact to be made between the sample and crystal window, thus requiring pressure from an anvil. Although ATR sample compartments generally allow ready access for un-mounted, flat material, the method is still regarded as an invasive technique due to the need for contact and compression [19, 20].

Recent studies have been carried out to investigate mid-infrared analyses outside of the sample compartment [21]. Thickett *et al* have reported on the identification of cellulose nitrate lacquers on silver objects via a chalcogenide optical probe setup [22]. This work made use of the reflective nature of the silver substrate to give a double pass through the surface coating, known as transflection. Although this technique provides non-destructive, non-invasive analysis, the optical fibres are brittle which can limit their application *in situ*. In addition, chalcogenide glass will absorb in the region of 2 200-2 050cm^{-1} due to the H-Se content, reducing signal strength within this region [23, 24]. However, this may not prove a difficulty for all samples due to the low infrared activity across this region.

Regardless of the sampling method employed, mid-infrared spectroscopy has become a routine method of analysis within museums and heritage. This is owed to the relative ease with which the technique can be applied and the molecular specific information acquired. Although mid-infrared spectroscopy will provide information on inorganic material, its primary applications within the sector have been organics. These are varied, and range from identification problems to more involved condition monitoring applications. Howard *et al* [25] used Fourier-

transform infrared with an ATR accessory (FTIR-ATR) for the rapid identification of a starch coating applied to a silk net substrate from the collections of Hampshire County Council Museums and Archives Service. This was achieved using a spectral subtraction method and comparison with the relevant reference spectra. Meincke and co-workers [26] applied FTIR-ATR for the identification of cross-sectional layers taken from a number of pieces of furniture dating from the early 20th Century. They identified the ground layers as shellac and the uppermost layers of the wood lacquers cellulose nitrate. One piece of furniture was showing increased deterioration compared to the others being studied. The corresponding mid-infrared analyses indicated an increased absorbance in the ester peak. This indicates the condition monitoring capabilities of the technique, but in this case, was not taken further by the authors. One application of mid-infrared spectroscopy for condition monitoring has been the use of Polarised FTIR-ATR experiments applied to textile artefacts. The directionality of the infrared beam has been successfully exploited to study orientation within protein and cellulose fibres. Orientation parameters are determined and used as a measure of crystallite order and polymer stability [27-29].

1.1.2 Raman Spectroscopy

Raman spectroscopy, like infrared spectroscopy, is concerned with molecular vibrations. However, in the case of Raman spectroscopy information is gained through the application and absorption of UV, visible or NIR laser radiation. When light is incident on matter, the atoms present cause a small proportion of the radiation to be scattered in all directions. This is in addition to the processes of reflection, absorption or transmission [30]. Raman Spectroscopy results from the detection of the scattering of this photon energy. Scattering occurs in three forms. If the scattered light energy exactly matches that of the incident radiation, then the scattering is said to be elastic, and is known as Rayleigh scattering. If the scattered light is found to be at lower or higher energy from that of the incident beam, then this is due to inelastic Raman scattering, and is known as Stokes and anti-Stokes scattering, respectively. The energy difference between Stokes or anti-Stokes scattering and that of the excitation radiation exactly matches the vibrational energy found in the mid-infrared spectra for the same bond.

Although both infrared and Raman spectroscopies rely on molecular vibrations, they provide complementary information to one another. This is owing to spectral activity arising from dipole fluctuations and polarization, respectively. This is illustrated by the study carried out by Pielesz and Weselucha-Birczynska into the destruction of keratin di-sulfide bonds during dye processing and penetration of wool fibres using Raman and infrared analysis [13]. The di-sulfide bond is infrared inactive because there is no fluctuation in the dipole moment, and MIR is therefore not suitable for monitoring structural changes during such treatments. Infrared measurements did enable the transformation of the α-helix structure to β-sheet conformations to be monitored through Amide I and II vibrations. In such cases a combination of both techniques may prove necessary to gain a wider picture.

The application of Raman spectroscopy has only recently found widespread use within conservation science. This is, in part, due to the high cost of instrumentation [30], but other drawbacks can include localised burning, thermal phase transitions and high fluorescence. Macdonald *et al* reported the false positive identification of litharge pigment applied to a historic textile, which they later found to be red lead [31]. Thermal degradation had converted dilead(II)lead(IV)oxide (Pb_3O_4) to tetragonal lead(II)oxide (PbO), highlighting the need for a low lasing power. The presence of impurities or enzymes have also been reported to be a problem by inducing fluorescence [19, 30, 32-34]. For every 10^6 molecules undergoing Rayleigh scattering there is only one, approximately, emitting Stokes or anti-Stokes photons. With Raman bands being so weak, any fluorescence is naturally going to saturate the spectrum and hinder characterisation. This said, with careful laboratory protocols Raman can be successfully applied to artefacts in a non-invasive, non-destructive manner.

Fourier-transform Raman Spectroscopy (FTR) has been successfully applied to the characterisation of degraded archaeological linen textiles by Edwards and co-workers [35]. Low laser powers of 50 mW were applied to prevent degradation of these fragile samples. Issues of high fluorescence were also circumvented by the application of a neodymium-doped yttrium-aluminium-garnet laser (Nd/YAG) with

a near-infrared lasing wavelength of 1 064nm. The advantage of longer wavelength lasers being that the energies involved are generally not sufficiently high to excite fluorescent transitions. Other examples of the application of near-infrared lasers include the monitoring of structural changes in wool fibres induced by enzyme treatments used to assist dye penetration [36], and the identification of semi-synthetic cellulose-based polymers, and additives such as camphor, from a collection of fans at the Musée Galliéra in Paris [37]. In this latter case the authors commented on the limitation of the technique with regards to the height of the spectrometer compartment for whole sample analyses. This problem can be resolved by use of a spectrometer with a microscope attachment [38].

Confocal Raman spectroscopy has been used successfully for identification and discrimination of thin polymeric adhesives applied to historic textiles [39]. Characterisation of previous conservation treatments or repairs is essential for informed collections care. However, thin surface coatings can prove difficult to analyse non-invasively. Confocal Raman spectroscopy allows for a sample layer to be isolated and data collected from a single plane of focus, thus removing any interference effects from highly scattering substrates.

1.1.3 Near-Infrared Spectroscopy

Near-infrared spectroscopy (NIR) is concerned with the application of near-infrared radiation (780-2 500nm, 12 800-4 000cm^{-1}). NIR spectra are produced by the absorption of radiation at shorter wavelengths than that found in the more widely applied mid-infrared spectroscopy discussed above (2 500-50 000nm, 4 000-400cm^{-1}). The higher energy NIR radiation excites overtone and combination bands of the fundamental vibrations found in MIR spectroscopy. These are multiples of the fundamental vibrations experienced in the mid-infrared region and simultaneous excitation of two or more fundamental vibrations, respectively. Overtones and combination bands are discussed further in Section 2.1.3, Chapter 2. Generally NIR spectra are dominated by molecular bonds to hydrogen, as, due to the low atomic weight of hydrogen and the relative strength of the bonds, the associated vibrations are at relatively high frequency.

The existence of overtone and combinations of fundamental vibrations, as seen in near-infrared spectra, is not consistent with the simple harmonic oscillator and demands a more involved theory, the anharmonic oscillator. There are two types of anharmonicity which occur, mechanical and electrical. The former arises because of Coulombic effects of repulsion and attraction, and the latter is related to the non-linear relationship between the dipole and the internuclear distance [40]. For a more in depth discussion of the anharmonic model the reader is guided to Chapter 2 and the literature [40-42].

In comparison with the spectral bands seen in MIR spectroscopy, the NIR spectrum is less well resolved, owing to the large number of combination and overtone transitions possible for each fundamental vibration. The complexity of the spectra can preclude simple band assignments. Therefore it is often necessary to apply a statistical approach to classification, to highlight minor differences between data sets [43].

In its reflectance mode, NIR spectroscopy is a diffuse reflectance technique which can be readily coupled with a flexible fibre optic probe. This removes the need for sampling, ensuring a truly non-invasive method of analysis. In addition, sampling depths in organic materials are generally 1 mm or more, allowing successful analysis whilst removing the need for contact and intervention. Such advantages have enabled the technique to be used successfully within the food industry, agriculture, polymer manufacturing and recycling since the 1970's.

Coates *et al* illustrated the strength of NIR spectroscopy through in-process analyses during co-polymer production [44]. Comparisons were made between vibrational spectroscopic techniques and ultrasonic measurements for monitoring blend composition during the manufacture of polyethylene/polypropylene copolymer. The low absorption coefficients seen in the near-infrared analyses enabled an online and inline setup within the bulk flow. This was not possible using mid-infrared spectroscopy, which required offline sampling, therefore not providing representative data. The Raman analysis provided concentration predictions within $\pm$0.95 wt% of the co-added polymer. This was higher than that shown for the near-infrared analysis which was resolved within $\pm$0.39 wt%. This

difference was attributed to the presence of fluorescence and increased noise in the Raman spectra. Ultrasound measurements were shown to be the most sensitive to change, but were not able to provide molecular information and therefore could not identify what change was occurring. NIR spectroscopy proved the best all round method for this type of analysis. These findings correlate well with those of other researchers in the field [45-47].

Similar studies have been carried out using NIR spectroscopy for the discrimination of polymer classes within the recycling industry. Kumagi *et al* have reported on the clear discrimination of polyethylene, polypropylene and polyvinyl chloride by the application of Principal Component Analysis (PCA) [48]. Multivariate analysis readily identified distinct clusters relating to the different polymer classes. A Partial Least Squares (PLS) method was applied by Cleve and co-workers to optimise the analysis of fibre blends [49]. A calibration set was produced covering 50:50 mixtures of cotton, polyester, viscose, silk, wool, polyacrylonitrile and cellulose acetate. In total, twenty one different blends enabled an unknown matrix parameter to be determined by the chemometric method, allowing successful identification of unknown textile combinations. Polymer components within polyvinyl chloride (PVC), such as plasticisers, were studied by Saeki *et al* [50]. The application of Neural-network Analysis enabled qualification and quantification of five plasticisers. This is of great importance during the recycling of PVC, due to the varying impact that plasticisers have on the physical properties of the polymer. Further industrial applications include real-time production monitoring and quality control during polymer manufacturing, providing chemical data on reactants, intermediates and products in less than one minute [51-55].

Near-infrared spectroscopy has found a range of applications within the textile industry, from quantification of textile blends for consumer information [56, 57] to quality control of processing methods such as fibre retting [58] and fibre sizing [59, 60]. The fibre diameter and the grease content are the two most important factors regarding the commercial value of wool. The former governs the potential applications within textiles, whilst the level of residual grease affects the spinning process. Both of these characteristics have previously been determined through

time consuming methods, by microscope analysis and wet chemical processes, respectively. Larsen and Kinnison compared NIR data with that of a microprojector measurement for the mean fibre diameter of greasy and washed wool samples [61]. Correlation coefficients of R = 0.93 were achieved for measured against predicted in both sets of samples. During the same study reflectance values were compared to known grease content of wool base by means of multiple linear regression. Correlation coefficients of 0.91 and higher were found, which are in good agreement with those from a similar study by Connell [62] and another applying PLS modelling by Innocenti and Zoccola [63]. Ghosh has successfully applied NIR spectroscopy to the determination of cotton maturity. Immature cotton shows surface defects and can be difficult to dye successfully [64, 65]. Least squares regression calibration produced a correlation of R = 0.97 for predicted maturity values by microscope analysis vs absorption at four pre-determined wavelengths. Differential packing and fibre fineness caused variations in scattering producing raising baselines. These were overcome by applying a second derivative function to the data set.

Within the context of heritage science, near-infrared spectroscopy is a relatively new analytical technique. The applications to date have been limited, but its ready application as a non-invasive technique means that interest is growing. This was illustrated by the recent European Union funded COST D42 workshop in Ljubljana, focussing on the application of near-infrared spectroscopy and chemometrics in cultural heritage[l].

The applicability of the technique for archival material has recently been illustrated by the SurveNIR project. This was a European Community funded project, under the Framework Six Energy, Environment and Sustainable Development Programme. Co-ordinated by the University of Ljubljana, but with many collaborative partners such as the British Library, Victoria and Albert Museum and the National Museum of Denmark, this project aimed to provide an *in situ* method for monitoring the condition of archival paper. It was shown that with the relevant spectral reference set and multivariate technique, the method could monitor chemical and physical properties such as lignin content, pH levels,

[l] Postprints from the meeting held on 14 November 2008 still awaiting publication.

degree of polymerisation and tear strength, all important markers for the stability of paper [66].

The dominance of the near-infrared spectrum by hydrogen containing species has been exploited by Zhang and Wyeth [67]. In their work, sorption experiments were carried out to investigate the moisture content of silk fibres, which they showed to be an indicator of condition. Further work investigating the condition of silk has involved non-invasively monitoring tensile stresses in hanging textiles. Richardson and Garside [68] illustrated the applicability of the technique for quantitative stress determinations, when coupled with multivariate analyses. Test samples were subjected to mechanical testing whilst NIR spectra were acquired. These were then used for multivariate calibration, providing a means of identifying regions of stress in unknown silk samples.

The depth sensitivity of the technique has been highlighted by a study into the deterioration of polyurethane foam. Garside and Lovett [69] used a spectral subtraction method to determine the composition of a number of internal supports sewn into textile garments, thus removing the need for invasive sampling

1.2 Conclusions

Vibrational spectroscopy has found extensive application in the heritage sector, as it offers a rapid means of materials characterisation with limited sample preparation. Mid-infrared spectroscopy is routinely used as a means of identification and condition monitoring. Various non-destructive sampling techniques have been applied, but they usually require sample removal or compression and are therefore invasive techniques. Raman spectroscopy offers the possibility of non-invasive analysis particularly when used in confocal mode. The disadvantages of the technique lie in the spectral interference from fluorescing species and the possibility of sample degradation caused by the use of lasers. The availability of non-destructive, non-invasive technique with analysis capabilities outside of the sample compartment would benefit both conservators and conservation scientists. Near-infrared spectroscopy has been successfully applied in other fields for a number of decades, but is only now receiving interest from museums and archives. The ability to use flexible fibre optic probes, coupled

with the depth sensitivity of the technique, means that NIR spectroscopy offers a truly non-invasive method of analysis that can be applied in collections. The primary limitation of the technique lies with the spectral bands originating from overtone and combination vibrations. This produces low resolution peaks, necessitating comprehensive reference spectra.

The following two chapters will present the steps taken to build a near-infrared spectral database for the non-invasive characterisation of synthetic material housed in textile collections. Discussion will be given to the experimental protocols required for onsite analyses and two case studies will be presented, illustrating the advantages and limitations of this technique.

1.3 References

1. Cesareo, R., et al., *Portable Equipment for Energy Dispersive X-ray Fluorescence Analysis of Giotto's Frescoes in the Chapel of Scrovegni.* Nuclear Instruments and Methods in Physics Research B, 2004. **213**: p. 703-706.
2. Bomford, D., *Art in the Making: Underdrawings of the Renaissance Paintings* 2002, London: National Gallery Company Limited.
3. Gliozio, E., et al., *Black Gloss Pottery: Production Sites and Technology in Ancient Tuscany. Part II: Gloss Technology.* Archaeometry, 2004. **46**: p. 227-246.
4. Derrick, M.R., D. Stulik, and J.M. Landry, *Infrared Spectroscopy in Conservation Science: Scientific Tools for Conservation*. 1999, Los Angeles: The Getty Conservation Institute.
5. Long, D.A., *Raman Spectroscopy*. 1977, London: McGraw-Hill.
6. Schrader, B., *Infrared and Raman Spectroscopy: Methods and Applications*. 1995: Wiley-VCH.
7. Skoog, D.A., F.J. Holler, and T.A. Nieman, *Principles of Instrumental Analysis*. 5th ed. 1998: Thompson Learning Inc. .
8. Schrader, B., *Chemical Applications of Raman Spectroscopy.* Agnew. Cham. International Edition, 1973. **12**(11): p. 884-905.
9. Gardiner, D.J., *Practical Raman Spectroscopy*. 1989, Berlin: Springer-Verlag.
10. Colthup, N.B., *Introduction to Infrared and Raman Spectroscopy*. 2nd ed. 1975, London: Academic Press.
11. Schrader, B., et al., *Non-Destructive NIR-FT-Raman Spectroscopy of Plant and Animal Tissues, of Food and Works of Art.* Talanta, 2000. **53**: p. 35-45.
12. Ferrero, F., et al., *Thermal Degradation of Linen Textiles: The Effects of Aging and Cleaning.* Journal of the Textile Institute, 1998. **89**(3): p. 562-569.
13. Pielesz, A. and A. Weselucha-Birczynska, *The Identification of Structural Changes in the Keratin of Wool Fibre Dyed with Azo Dye using Raman and Fourier Transform Infrared Spectroscopy Methods.* Journal of Molecular Structure, 2000. **555**: p. 325-334.

14. Garside, P., *Investigations of Analytical Techniques for the Characterisation of Natural Textiles Fibres Towards Informed Conservation*. 2002, Department of Chemistry, University of Southampton.
15. Spring, M., C. Higgitt, and D. Saunders, *Investigation of Pigment-Medium Interaction Processes in Oil Paint Containing Degraded Smalt.* National Gallery Technical Bulletin, 2005. **26**: p. 56-69.
16. Garside, P. and P. Wyeth, *Identification of Cellulosic Fibres by FTIR Spectroscopy: Thread and Single Fibre Analysis by Attenuated Total Reflectance.* Studies in Conservation, 2003. **48**(3): p. 269-275.
17. Buzio, R., et al., *Surface Analysis of Paper Documents Damaged by Foxing.* Applied Physics A, 2004(79): p. 838-387.
18. Shashoua, Y. and K.B. Johansen. *Investigation of ATR-FTIR Spectroscopy as an Alternative to the Water-Leach Free Acidity Test for Cellulose Acetate-based Film*. in *14th Triennial Meeting ICOM Committee for Conservation*. 2005. The Hague.
19. Richardson, E., *Infrared and Raman Analysis of Metal Soap Formation Through Pigment and Binder Interactions in Oil Paintings*. 2004, MSc Dissertation, Sheffield Hallam University.
20. Morris, N.M., *A Comparison of Sampling Techniques for the Characterization of Cotton Textiles by Infrared-Spectroscopy.* Textile Chemist and Colorist, 1991. **23**(4): p. 19-22.
21. Milosevic, M., et al. *The Flexible Opto-Mechanical Arm for FTIR Analysis of Samples Outside the Sample Compartment*. in *The Seventh Biannial Gathering of the Infrared and Raman Users Group*. 2006. MoMA, New York.
22. Thickett, D. and N. Luxford, *FTIR Analysis of Protective Coatings*, in *The Seventh Biannial Gathering of the Infrared and Raman Users Group*. 2006: MoMA, New York. p. 38.
23. Bacci, M., et al., *Non-invasive Fibre Optic Fourier-transform Infrared Reflectance Spectroscopy on Painted Layers Identification of Materials by Principle Componant Analysis and Mahalanobis Distance.* Analytica Chimica Acta, 2001. **446**: p. 15-21.
24. Miliani, C., et al. *Using Fibre Optic Infrared Spectroscopy from Mid to Near Infrared to Assess Non-invasively the Polychromy Composition of Easel Paintings*. in *The 7th Biannial Gathering of the Infrared and Raman User's Group*. 2006. MoMA, New York.
25. Howard, S. and P. Garside. *'Net' What it Seems! Conservation of Two Machine-made Net Dresses*. in *AHRC Research Centre for Textile Conservation and Textile Studies First Annual Conference Scientific Analysis of Ancient and Historic Textiles, Informing Preservation, Display and Interpretation*. 2004. Winchester: Archetype Publications.
26. Meincke, A., et al. *Early Cellulose Nitrate Coatings on Furniture of the Company of Modern Craftsmen*. in *Plastics: Looking at the Future and Learning from the Past*. 2007. London: Archetype Publications.
27. Garside, P. and P. Wyeth, *The Use of Polarised Spectroscopy as a Tool for Examining the Microstructure of Cellulosic Textile Fibres.* Applied Spectroscopy 2007. **61**(2): p. 218-222.
28. Garside, P., S. Lahlil, and P. Wyeth, *Characterisation of Historic Silk by Polarised ATR FT-IR Spectroscopy for Informed Conservation.* Applied Spectroscopy, 2005. **59**(10): p. 1242-1247.

29. Boulet-Audet, M., et al., *Golden Gate Attenuated Total Reflectance Infrared Spectroscopy: An Efficient Technique to Determine Quantitatively the Orientation and Conformation of Proteins in Single Silk Fibres.* Applied Spectroscopy, 2008. **62**: p. 46-52.
30. Smith, G.D. and R.J.H. Clark, *Raman Microscopy in Art History and Conservation Science.* Reviews in Conservation, 2001(2): p. 92-105.
31. Macdonnald, A.M., P. Wyeth, and C. Rogerson, *Raman Spectroscopy Interrogating Historic Painted Textiles.* Microscopy and Analysis, 2003. **97**: p. 5-7.
32. Andreev, G.N., et al., *Non-Destructive NIR-FT-Raman Analysis in Practice. Part 1. Analyses of Plant and Historic Textiles.* Fresenius Journal of Analytical Chemistry, 2001. **371**: p. 1009-1017.
33. De Faria, D.L.A. and H.G.M. Edwards. *Raman Spectroscopy in Art and Archaeology: Some Pitfalls*. in *The Seventh Biannial Gathering of the Infrared and Raman Users Group*. 2006. MoMA, New York.
34. Macdonnald, A.M., et al. *Raman Microscopy Interrogating 19th and 20th Century Painted Trade Union Banners*. in *AHRC Research Centre for Textile Conservation and Textile Studies 1st Annual Conference: Scientific Analysis of Ancient and Historic Textiles*. 2004. Winchester: Archetype Publications.
35. Edwards, H.G., et al., *Preliminary Study of the Application of Fourier Transform Raman Spectroscopy to the Analysis of Degraded Archaeological Linen Textiles.* Journal of Raman Spectroscopy, 1996. **27**: p. 663-669.
36. Wojciechowska, E., et al., *The use of Fourier Transform Infrared (FTIR) and Raman Spectroscopy (FTR) for the Investigation of Structural Changes in Wool Fibre Keratin after Enzymatic Treatment.* Journal of Molecular Structure, 2004. **704**: p. 315-321.
37. Paris, C. and C. Coupry, *Fourier Transform Raman Spectroscopic Study of the First Cellulose-based Artificial Materials in Heritage.* Journal of Raman Spectroscopy, 2005. **36**: p. 77-82.
38. Burgio, L., *Case Study: Raman Spectroscopy: A Powerful Tool for the Analysis of Museum Objects*, in *Raman Spectroscopy in Archaeology and Art History*, H.G.M. Edwards and J.M. Chalmers, Editors. 2005, The Royal Society of Chemistry: Cambridge. p. 179-191.
39. Macdonnald, A.M., A.S. Vaughan, and P. Wyeth, *Application of Confocal Raman Spectroscopy to Thin Polymer Layers on Highly Scattering Substances: A Case Study of Synthetic Adhesives on Historic Textiles.* Journal of Raman Spectroscopy, 2005. **26**: p. 185-191.
40. Pasquini, C., *Near Infrared Spectroscopy: Fundamentals, Practical Aspects and Analytical Applications.* Journal of the Brazilian Chemical Society, 2003. **14**(2): p. 198-219.
41. Burns, D.A. and E.A.e. Ciruczak, *Handbook of Near-Infrared Analysis*. 2001, New York: Marcel Dakker Inc. 814.
42. Siesler, H.W., *Near-Infrared Spectroscopy: Principles, Instrumentation, Applications*, ed. H.W. Siesler, et al. 2002, Weinheim: Wiley-VCH.
43. Visco, G., ed. in *1st International Meeting on Chemometrics and Multivaritate Analysis Applied to Cultural Heritage and Environment*. 2006. Rome: Aracne.
44. Coates, P.D., et al., *In-process Vibrational Spectroscopy and Ultrasound Measurements in Polymer Melt Extrusion.* Polymer 2003. **44**: p. 5937-5949.

45. Furukawa, T., et al., *Discrimination of Various Polypropylene Copolymers and Prediction of Their Ethylene Content by Near Infrared and Raman Spectroscopy in Combination with Chemometric Methods.* Journal of Applied Polymer Science, 2002. **87**: p. 616-625.
46. Lee, J., S and H. Chung, *Rapid and Nondestructive Analysis of the Ethylene Content of Polypropylene/Ethylene Copolymer by Near Infrared Spectroscopy.* Vibrational Spectroscopy, 1998. **17**: p. 193-201.
47. Camacho, W. and S. Karlsson, *NIR, DSC and FTIR as Quantitative Methods for Compositional Analysis of Blends of Polymers Obtained from Recycled Mixed Plastic Waste.* Polymer Engineering and Science, 2001. **41**(9): p. 1626-1635.
48. Kumagai, M., et al., *Discrimination of Plastics Using a Portable Near Infrared Spectrometer.* Journal of Near Infrared Spectroscopy, 2002. **10**: p. 247-255.
49. Cleve, E., E. Bach, and E. Schollmeyer, *Using Chemometric Methods and NIR Spectrophotometry in the Textile Industry.* Analytica Chimica Acta, 2000. **420**: p. 163-167.
50. Saeki, K., K. Funsatu, and K. Tanabe, *Discrimination of Polyvinyl Chloride Samples with Different Plasticizers and Prediction of Plasticizer Contents in Polyvinyl Chloride Using Near Infrared Spectroscopy and Neutral-network Analysis.* Analytical Sciences, 2003. **19**: p. 309-312.
51. DeThomas, F.A., *Real-time Monitoring of Polyurethane Production Using Near-infrared Spectroscopy.* Talanta, 1994. **41**(3): p. 425-431.
52. Nagata, T., M. Tanigaki, and M. Ohshima, *On-line NIR Sensing of Carbon Dioxide Concentration for Polymer Extrusion Foaming Process.* Polymer Engineering and Science, 2000. **40**(8): p. 1843-1849.
53. Blanco, M., et al., *Use of Near-infrared Spectroscopy in Control Analyses of Acrylic Fibre Manufacturing Processes.* Analytica Chimica Acta, 1999. **383**: p. 291-298.
54. Khettry, A. and M. Hansen, G, *Real-time Analysis of Ethylene Vinyl Acetate Random Co-polymers using Near Infrared Spectroscopy During Extrusion.* Polymer Engineering and Science, 1996. **36**(9): p. 1232-1234.
55. Sasic, S., et al., *Monitoring the Melt-extrusion Transesterification of Ethylene-vinylacetate Copolymer by Self-Modelling Curve Resolution Analysis of On-line Near Infrared Spectra.* Analyst, 2000. **125**: p. 2315-2321.
56. Church, J.S., J.A. O'Neill, and A.L. Woodhead, *A Comparison of Vibrational Spectroscopic Methods for Analyzing Wool/Polyester Textile Blends.* Textile Research Journal, 1999. **69**(9): p. 676-684.
57. Ruckebusch, C., et al., *Quantitative Analysis of Cotton-Polyester Textile Blends from Near Infrared Spectra.* Applied Spectroscopy, 2006. **60**(5): p. 539-544.
58. Sohn, M., et al., *A New Approach for Estimating Purity of Processed Flax Fibre by NIR Spectroscopy.* Journal of Near Infrared Spectroscopy, 2004. **12**: p. 259-262.
59. Ghosh, S. *On-line NIR Measurements for Textile Process Control*. in *Making Light Work: Advances in Near Infrared Spectroscopy, 4th International Conference on Near Infrared Spectroscopy*. 1991. Aberdeen, Scotland: VCH.

60. Kitagawa, K., S. Hayaskai, and Y. Ozaki, *In situ Analysis of Sizing Agents on Fibre Reinforcements by Near Infrared Light Fibre Optics Spectroscopy.* Vibrational Spectroscopy, 1997. **15**(1): p. 43-51.
61. Larsen, S.A. and J.L. Kinnison, *Estimating Quality Components of Natural Fibres by Near Infrared Reflectance.* Textile Research Journal, 1982(January): p. 25-31.
62. Connell, J.P., *Predicting Wool Base of Greasy Wool by Near Infrared Reflectance Spectroscopy.* Textile Research Journal, 1983(November): p. 651-655.
63. Innocenti, R. and M. Zoccola, *Near Infrared Reflectance Spectroscopy as a Tool for the Determination of Dichloromethane Extractable Matter and Moisture Content in Combed Wool Slivers.* Journal of Near Infrared Spectroscopy, 2003. **11**: p. 333-340.
64. Ghosh, S. *Use of an Automated NIR High Volume Tester to Determine Cotton Maturity*. in *Making Light Work: Advances in Near Infrared Spectroscopy, 4th International Conference on Near Infrared Spectroscopy*. 1991. Aberdeen, Scotland: VCH.
65. Ghosh, S., *At-line and On-line Characterization of Textile Products using the NIR Spectroscopy Method*, in *Leaping Ahead with Near Infrared Spectroscopy*, G.D. Batten, et al., Editors. 1994. p. 450-460.
66. Trafela, T., et al., *Nondestructive Analysis and Dating of Historical Paper Based on IR Spectroscopy and Chemometric Data Evaluation.* Analytical Chemistry, 2007. **79**: p. 6319-6323.
67. Zhang, X. and P. Wyeth, *Moisture Sorption as a Potential Condition Marker for Historic Silks: Noninvasive Determination by Near-Infrared Spectroscopy.* Applied Spectroscopy, 2007. **61**(2).
68. Richardson, E. and G. Garside. *The Use of Near Infrared Spectroscopy as a Diagnostic Tool for Historic Silk Artefacts*. in *IRUG 8*. 2009. Vienna: e-Preservation Science.
69. Garside, P. and D. Lovett. *Polyurethane Foam: Investigating the Physical and Chemical Consequences of Degradation*. in *AHRC Research Centre for Textile Conservation and Textile Studies Second Annual Conference: The Future of the 20th Century - Collecting, Interpreting and Conserving Modern Materials*. 2005. Winchester: Archetype Publications.

Chapter 2: Near-infrared Spectroscopy and the Determination of On-site Protocols

The application of near-infrared spectroscopy in fields such as polymer manufacturing and agriculture illustrates the possibility of rapid, *in situ* analysis for organic material. The technique is relatively new to the heritage sector, but widespread interest is growing, due to the possibilities for non-invasive sampling *in* collections. It is that potential that is investigated in this thesis, with the aim of providing museum professionals with collections management tools. Here, a broad overview of infrared spectroscopy will be given with the details of sampling techniques, focusing on near-infrared spectroscopy and the methods employed for this work. The later sections of this Chapter will describe the methodologies adopted and the results of experiments which were carried out in order to optimise the on-site protocols for successful *in situ* data acquisition.

2.1 Infrared Spectroscopy

Infrared Spectroscopy is concerned with molecular vibrations of molecular bonds, brought about by the absorption of infrared radiation. Molecular bonds vibrate at a frequency that is dependent on the masses of the two connected atoms and the strength of the interatomic bond. If the frequency of a molecular bond vibration is the same as the incident radiation then infrared radiation may be absorbed, causing excitation from its ground state to an excited state. For organic molecules, fundamental vibrational modes are generally excited by mid-infrared radiation (400 – 4 000 cm^{-1}).

As a result of infrared radiation absorption by a molecule, there must be a change in the dipole moment with the vibration. The permanent dipole moment exists when a molecule experiences an unequal sharing of electrons caused by chemically different atoms. As these molecules vibrate, under certain modes there can be fluctuations in this dipole. If the incoming radiation frequency exactly matches that of a natural vibrational frequency of the molecule, a net increase in the amplitude of the vibration is experienced through absorption of radiation [1]. The energy transferred from the photon of radiation (Ep) at a given wavelength is given by:

$$Ep = h\nu = hc/\lambda$$

Eq. 2.i

Where *h* is Planck constant and *c* is the velocity of light.

Wavelength (λ) is inversely proportional to energy, so in vibrational spectroscopy it is common to use the reciprocal of wavelength, wavenumber $\tilde{\nu}$ (cm^{-1}):

$$Ep = hc\tilde{\nu}$$

Eq. 2.ii

The absorption of infrared radiation is common to most polyatomic molecules. There are some exceptions; homodiatomics such as oxygen, do not experience a permanent dipole, and are therefore infrared inactive. In addition, not all molecular vibrations give rise to absorption, due to symmetry restrictions. For example, carbon dioxide (CO_2) will only show infrared absorption with certain vibrations (Figure 2.1).

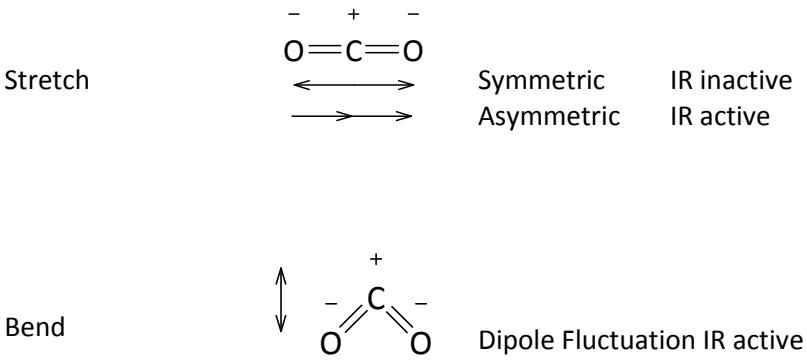

Figure 2.1 Infrared vibrations of carbon dioxide

When dealing with a molecule such as carbon dioxide a symmetrical stretch is IR inactive. This is not the case for all triatomic molecules, water being one example.

2.1.1 Near-infrared Spectroscopy

Near-infrared spectroscopy (NIR) is concerned with near-infrared radiation (λ=780-2 500nm, $\tilde{\nu}$ =12 800-4 000cm^{-1}). NIR spectra are produced by the absorption of radiation at higher wavenumbers than that found in more conventional mid-infrared spectroscopy (λ=2 500-50 000nm, $\tilde{\nu}$ =4 000-200cm^{-1}) (MIR). The higher energy NIR radiation excites overtone and combination bands of the fundamental vibrations found in the MIR. However, some of these bands can occur in the MIR too. For example, carboxyl dimers exhibit a combination band at 2 650cm^{-1}, caused by an interacting C-O stretch and O-H deformation [2]. Generally NIR spectra are dominated by hydrogen containing bonds, as, due to the low atomic weight of hydrogen and the relative strength of the bonds, the associated vibrations are at relatively high frequency.

2.1.2 Harmonic Oscillator

Reference to a simple molecular model allows a clearer understanding of the interaction of radiation with matter: two spherical masses (m_1 and m_2) are connected by a spring with a force constant *k*.

The potential energy of this system is given by:

$$V = \tfrac{1}{2}k\,(r - r_e)^2$$

Eq. 2.iii

Where r is the intersphere distance and r_e is the distance at equilibrium [3].

In this model the fundamental frequency of the stretching vibration is defined by:

$$\nu = \tfrac{1}{2\pi}\sqrt{k/\mu}$$

Eq. 2.iv

where μ is the reduced molecular mass ($\mu = m_1m_2/m_1+m_2$).

The harmonic oscillator is governed by quantum mechanics, which only allows for quantised vibrational states (corresponding to quantum numbers of integer values) [4]. These levels (Ev) are defined as:

$$Ev = h\nu(v + \tfrac{1}{2})$$

Eq. 2.v

h = Planck's constant

ν = vibrational frequency

v = quantum number (0, 1, 2 …)

Transitions are restricted to adjacent energy levels.

This model does not take into account Coulombic interactions and excludes the phenomena of overtones and combinations.

2.1.3 Anharmonic Oscillator

The existence of overtone and combinations of fundamental vibrations, as seen in near-infrared spectra, is not consistent with the simple harmonic oscillator and demands a more involved theory, the anharmonic oscillator. Overtone vibrations are multiples of the fundamental vibrations experienced in the mid-infrared region, whereas combinations are simultaneous excitation of two or more fundamental vibrations.

Two types of anharmonicity occur, the first is mechanical, and is caused by Coulombic effects of repulsion and attraction[I], and the second is electrical, related to the non-linear relationship between the dipole and the internuclear distance [3, 5].

Due to Coulombic forces, a bond is more easily stretched than compressed, so the potential energy represented by the harmonic oscillator model is not true. The energy levels are unevenly spaced, as represented by the anharmonic Morse function [3]:

$$V = D_e (1 - e^{-\beta x r})^2$$

Eq. 2.vi

[I] Coulombic effects refer to electrostatic forces of repulsion and attraction between two particles that have charge and are at a distance from each other (r) [5].

x = displacement ($r-r_e$)

β = a constant

D_e = dissociation energy

The dissociation energy, D_e, is given by:

$$D_e = \tilde{\nu}/4x_e$$

Eq. 2.vii

Relating back to Figure 2.6, anharmonic vibrational levels are described as:

$$Ev = h\nu(v + \tfrac{1}{2}) - x_e h\nu(v + \tfrac{1}{2})^2$$

Eq. 2.viii

x_e = anharmonic constant [3].

2.1.4 Degrees of Freedom

The number of fundamental vibrations is governed by the degrees of freedom of a molecule. Each atom contained within a molecule can move in three directions; these movements correspond to three independent degrees of freedom, along the x, y and z co-ordinates. A molecule then has 3N degrees of freedom (N = number of atoms) [6], but three of these are required to describe the position of the centre of gravity (or its translation), and a further three will identify the molecular orientation about the centre of gravity (or its rotation). The number of vibrational degrees of freedom for a non-linear molecule is therefore 3N-6. (This reduces to 3N-5 for a linear molecule, because only 2 degrees of freedom are required to describe rotational orientation).

A triatomic molecule may then show three fundamental absorptions, but the infrared spectrum will be more complex due to overtones and combinations of the fundamental modes. In addition 'hot band' transitions are also experienced. Fundamental vibrations, from v=0 → v=1, have the highest absorption coefficients due to most molecules being in their ground state at room temperature (Boltzmann distribution). 'Hot band' transitions originate from excited vibrational states, which are weak at room temperature, but increase with temperature.

2.1.5 Degenerate Vibrations

Degeneracy occurs when two or more of a molecule's normal modes of vibration have the same vibrational frequency. When two modes occur at a single frequency they are said to be doubly degenerate, three modes are triply degenerate. See Figure 2.2 for a simplistic case of a side group vibration along a polymer backbone. Both the in-plane and out-of-plane deformations occur at the same frequency but are different vibrational modes.

2.1.6 Fermi Resonance

Resonance occurs when an overtone or combination vibrational frequency of one mode has the same, or closely matched, frequency of a fundamental vibration. Resonance occurs between both modes, with each contributing to the other, thus causing one frequency of vibration to be lowered whilst the second is raised, and affecting the intensities of the two bands.

2.1.7 Forms of Vibration

In-plane Deformation Out-of-plane Deformation

Figure 2.2 In-plane and out-of-plane vibrational deformation (+/- out of plane with the page)

2.1.8 Group Frequencies

Due to the energies involved in near-infrared spectroscopy, the vibrations excited are anharmonic high frequency overtone and combinations of the fundamental modes seen in mid infrared spectroscopy. For organic molecules, these relate primarily to bonds containing hydrogen (the lightest atom) in particular C-H, O-H and N-H bonds. The intensity of the spectral bands are dependent on the magnitude of the dipole fluctuation and degree of anharmonicity. Figure 2.3 shows the position of some of the major bands seen in the near-infrared, with their approximate wavenumber.

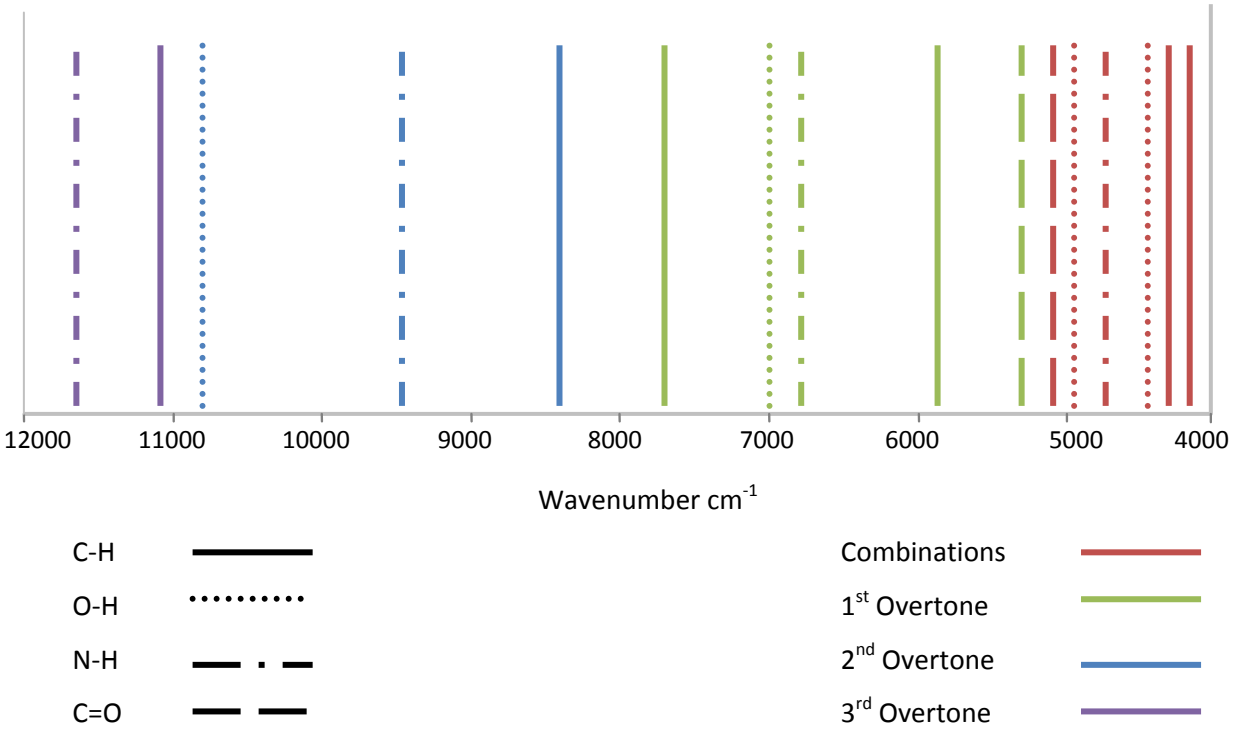

Figure 2.3 Approximate near-infrared band assignments [4]

It is apparent that near-infrared spectra will contain many bands and therefore be quite complex. In comparison with the spectral bands seen in mid infrared spectroscopy, the NIR spectrum contains many overlapping bands, owing to the large number of combination and overtone transitions possible for each fundamental vibration.

The complexity of the spectra can preclude simple band assignments. However, the spectra are still characteristic, and comparison with a suitable spectral reference set usually allows for ready identification of unknowns.

2.2 Instrumentation

All analytical work has been carried out using a Perkin Elmer Spectrum One Fourier Transform Near-infrared spectrometer (FT-NIR), using an integrating sphere accessory (NIRA) and/or Axiom probe attachment. Spectral processing was carried out using Thermo Galactic Grams AI software. The background reference was Spectralon®. All data were collected in Absorbance, calculated as $A = -\log_{10}R$ (R = ratio of reflected over incident radiation).

The near-infrared source is a quartz halogen lamp, emitting thermal radiation [4]. The spectrometer is fitted with a Michelson Interferometer, with subsequent application of a

Fourier transform converting the resultant interferogram from time domain (intensity vs. time) to a frequency domain spectrum (intensity vs. frequency). A near-infrared laser is housed within the spectrometer, which acts as a distance reference for the moving mirrors in the Interferometer. The reflected radiation is detected by an indium gallium arsenide (InGaAs) semi-conductor.

2.2.1 Integrating Sphere

For all the work reported here, samples were interrogated using diffusely reflected radiation. During diffuse reflectance the radiation incident on finely divided particles and powders penetrates the sample and undergoes scattering, becoming reflected in all directions due to the orientation of the particles.

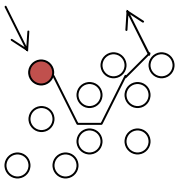

Figure 2.4 Schematic of diffuse reflectance

When analysing thin and transparent sample the use of a ceramic or aluminium reflector behind the sample will allow radiation to be scattered back through the sample and into the detector [7]. This type of sampling is known as transflection.

The integrating sphere is a hollow sphere with a diffusely reflecting coating. The radiation enters from one side and is reflected towards the sample window. The returning light from the sample is diffusely scattered off the interior of the sphere and focussed on to the detector window. A baffle is placed between the detector and the sample to prevent saturation from specular reflectance. From here on the integrating sphere will be referred to as the Near-infrared Accessory (NIRA)

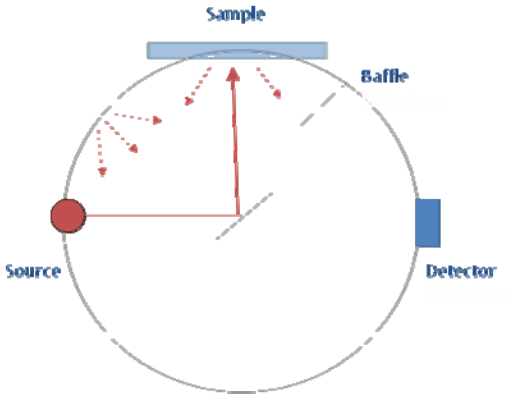

Figure 2.5 Schematic of an integrating sphere

2.2.2 Probe

The use of an Axiom probe attachment allows for remote diffuse reflectance sampling. Light is transmitted and collected along bifurcated optical fibres, which are arranged in a random manner. The fibre optic bundle has an acceptance angle of plus or minus 12.7 degrees. Therefore, the probe will also detect specular reflected light, in addition to diffuse reflected light, as long as the normal to the surface falls within this range of angles. However, the centre of the optical field of view is inclined at approximately 18 degrees from the probe axis reducing the amount of specular reflectance reaching the optical fibres.

The fused silica optical fibres are housed in a stainless steel casing with a sapphire window at the sampling end. The optical fibre length measures 1.90 metres, enabling spectral acquisition on site within textile collections.

Figure 2.6 Image of fibre optic probe (V&A T97-1988) (Copyright V&A)

2.3 Data Processing

Data processing is applied to spectra to standardise and optimise the signal. Its aim is to reduce effects outside the control of the analytical methodology, such as variations in light scattering, instrument noise and rising baselines.

2.3.1 Smoothing

Smoothing methods can be applied after data acquisition to reduce the effects of noise. Noise is caused by random, inhomogeneous electrical charges experienced by conducting instrumental components [1]. The random nature of noise allows it to be averaged, with the aim of reducing noise without distortions or reduction to the signal of interest.

A moving average is often applied as a smoothing method, calculated as the sum of the Y values within a chosen filter window divided by the number of data points within that window [8]. The drawback of a moving average is that all data points are given equal weighting, so definition of spectral peaks can be lost. Data points on the outer edge of the moving average are given the same weighting as those close to the point of interest. This can cause a broadening of spectral peaks and loss of visual resolution. This effect increases with increasing filter width.

The method applied during this work was a five point Savitzky-Golay filter [9]. This works in a similar way to the moving average filter, but the raw data points are weighted by the application of a polynomial to the data within the filter window. For a five point window, Y_k is weighted by 17 (central data point), Y_{k+1} and Y_{k-1} are weighted by 12, and Y_{k+2} and Y_{k-2} by –3. The sum of these is then divided by the *total* number of coefficients, not the filter width [8]. The Savitzky-Golay filter does not give equal weighting to data points at a distance from the central point of interest. This prevents the height and width of a peak becoming ill-defined.

2.3.2 Derivatives

The first and second derivative spectra are commonly used to reduce baseline affects and to increase resolution. Derivatives reduce low frequency components whilst increasing signal, but also noise.

The Savitzky-Golay method may also be applied here, by differentiation of the polynomial fitted to the curve. The first, through to the ninth, derivatives can be established [8].

However, the method used throughout this work is the Norris differentiation, or Gap method. This calculates the absorption differences between two X values. The points of subtraction are determined by the gap value, which moves a set number of points along the X axis. The larger the gap value the lower the visual resolution.

By using the second derivative the peak maximum is inverted to a minimum. In calculating the second derivative the full width at half height is narrower than for the original spectrum, allowing greater visual resolution.

Although the Gap method is not a true derivative function, the resultant derivative spectra tend to contain less noise than those generated by the Savitzky-Golay method, without notable loss of signal.

2.3.3 Spectral Subtraction

The spectral subtraction application allows one data set to be subjectively removed from another. This function has been applied during noise calculations in the determination of the signal to noise parameter (S/N). First the raw data were smoothed using a five point moving average filter (Section 2.3.1). The smoothed data were then subtracted from the raw, with the residual spectrum used to represent the random noise.

The subtraction application method has also been applied to reveal low level components within samples. This is presented in later chapters.

2.4 Determination of Experimental Parameters for NIR Spectral Acquisition

All analytical work was carried out using a Perkin Elmer Spectrum One Fourier Transform Near-infrared spectrometer (FT-NIR), using an integrating sphere accessory (NIRA) and/or Axiom probe attachment. The background reference was Spectralon® and all data were collected in Absorbance. Single scans were acquired using a wavenumber resolution was set to 8 cm^{-1}, with a scan speed of 1 cm/s over a spectral scan range of 12 000-4 000 cm^{-1}.
In the majority of cases the standard material used during the experimental work was a polyester test fabric supplied by SDC Enterprises. For the determination of polarization effects a polyamide material was employed, and for determining the effects of RH a number of different materials were used. The NIR absorbance spectrum of the polyester fabric is shown

below (Figure 2.7). Unless otherwise stated, the ambient conditions in the laboratory were 20°C ±3 and RH 50% ±4.

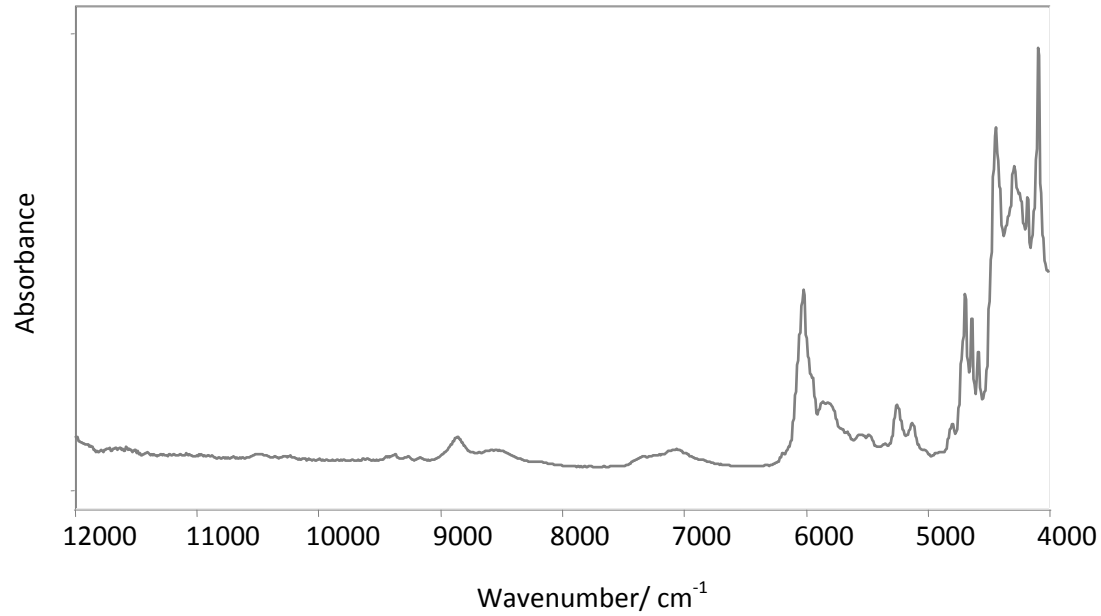

Figure 2.7 NIRA absorbance spectrum of a standard polyester fabric

Parameters under consideration were:

Parameters	Sampling Accessory
Optimum number of scans	NIRA
Optimum depth of sample	NIRA & Probe
Point of infinite thickness	NIRA & Probe
Geometry of fabric and probe window	Probe
Distance of fabric from probe window	Probe
Polarising affects	Probe
Geometry of optical fibres	Probe
Effect of colour	NIRA
Effects of RH	Probe
Effects of Stray Light	Probe

Table 2.1 Parameters under consideration for spectral optimisation

2.4.1 Methodology

2.4.1.1 Optimum Number of Scans

1 ply polyester fabric, measuring approximately 0.26mm depth, was analysed using the NIR accessory with increasing scan numbers: 1, 2, 4, 8, 16, 32, 64, 128 and 256. A signal to noise parameter (S/N) for each spectrum was then manually calculated, after pre-treatment methods were used to determine the spectral noise, as follows:

Savitzky-Golay smoothing was applied to all spectra, with points set at 101 (Figure 2.8). The smoothed spectra were then subtracted from the original (Figure 2.9). The noise was then calculated by the spectral software, using the integrating function, for a region of the spectrum devoid of major peaks with x = 11 900-9 500 cm^{-1}. The absolute area output calculated by the integration function was used to represent the spectral noise, with the signal taken as the intensity of the strong absorbance at 6 020cm^{-1} after smoothing. This method was applied throughout the preliminary studies.

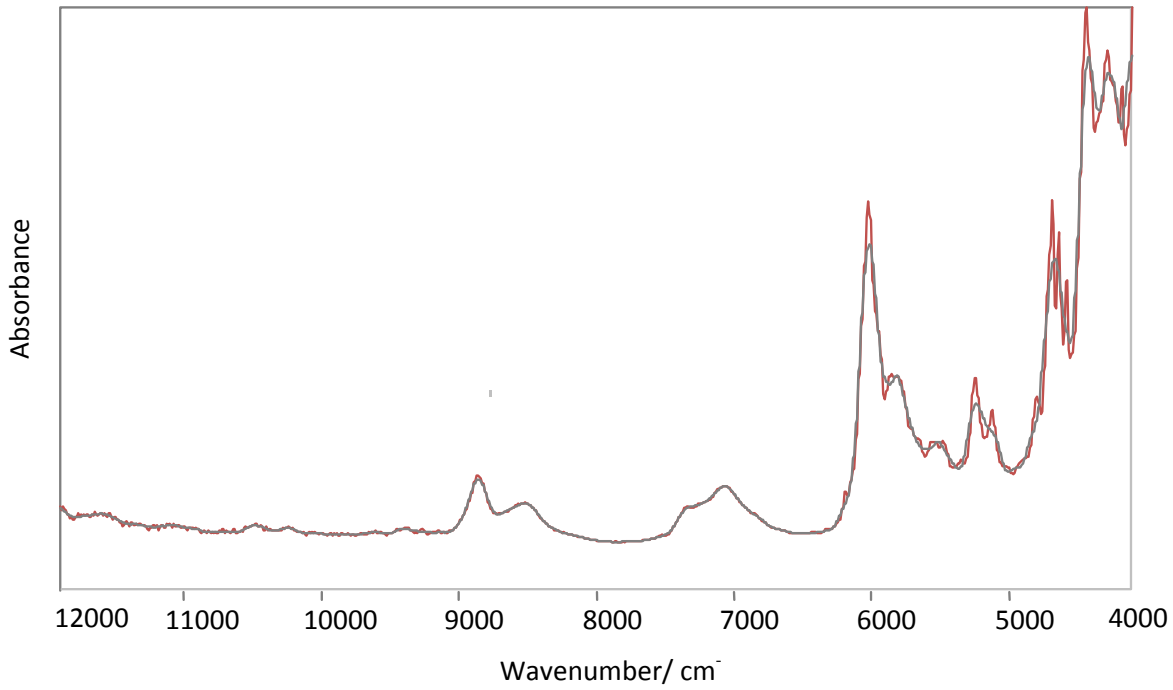

Figure 2.8 Overlaid NIR absorbance spectra of polyester before and after Savitzky-Golay smoothing

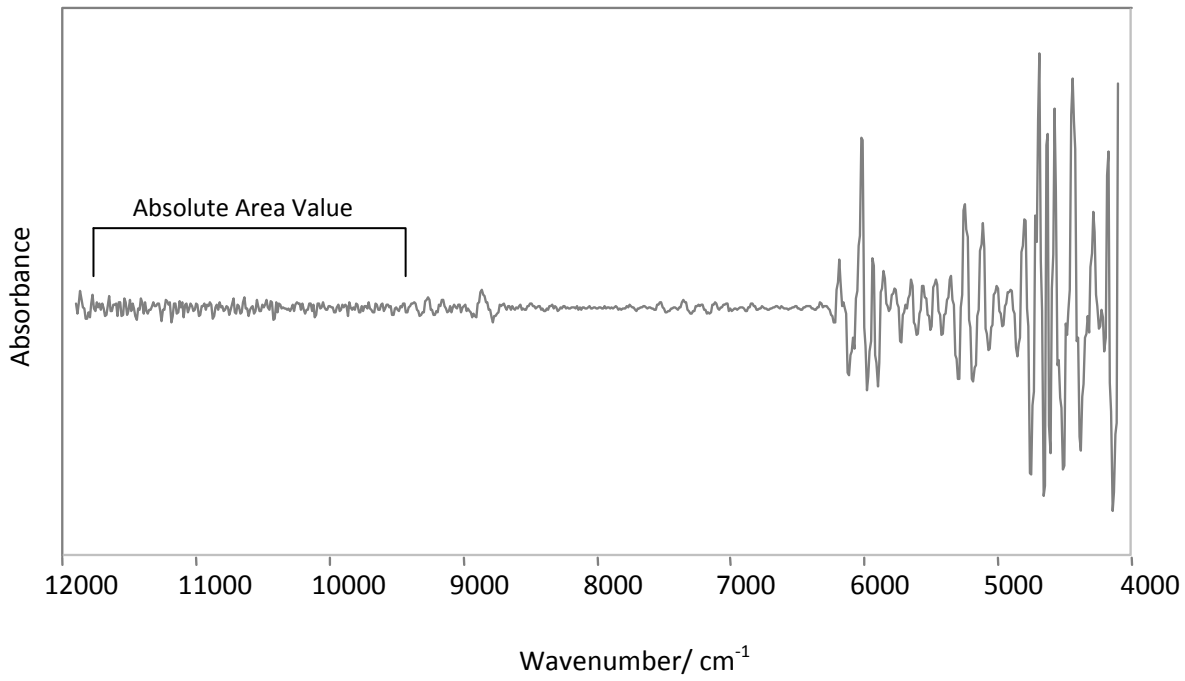

Figure 2.9 Polyester spectrum after the subtraction of the smoothed spectrum indicating the region over which the absolute area was calculated

2.4.1.2 Optimum Depth of Sample

To identify the optimum sample depth for data acquisition, polyester fabric, of increasing ply, was analysed using both the NIR accessory and probe attachment (thickness was measured using a micrometer gauge):

Number of Layers /ply	Thickness/ mm
1	0.26
2	0.50
4	1.46
8	2.41
16	4.41

Table 2.2 Thickness of samples for determining optimum sample depth

The signal to noise parameter was calculated using the method described in Section 2.4.1.1. A baseline correction was applied to the signal, after smoothing, to account for the increase in background with increasing ply. It was calculated using a correction function of 2 points and a levelling mode set to zero. These were forced to the data points at two troughs either side of the peak of interest, 6 400 and 5 000cm^{-1} (Figure 2.10).

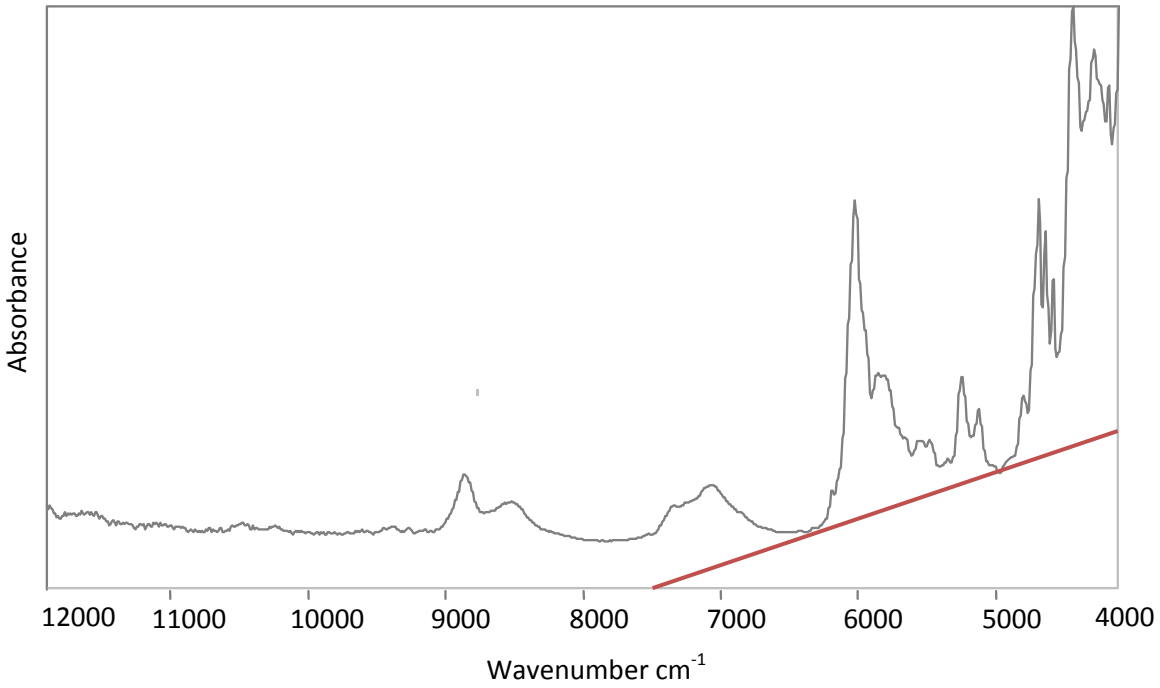

Figure 2.10 Example of the forced baseline correction function at 6 400cm^{-1} and 5 000cm^{-1}

2.4.1.3 Point of Infinite Thickness

To identify the point of infinite thickness, a polystyrene sample was placed behind increasing ply of polyester fabric (depths as above) and the combination analysed using the accessory and probe attachment (Figure 2.11). A subtraction function was applied to the spectra, removing the pure polyester spectrum from that of the combination. The resulting spectra were compared to that of polystyrene, identifying the point at which the upper material is no longer visible in the spectra.

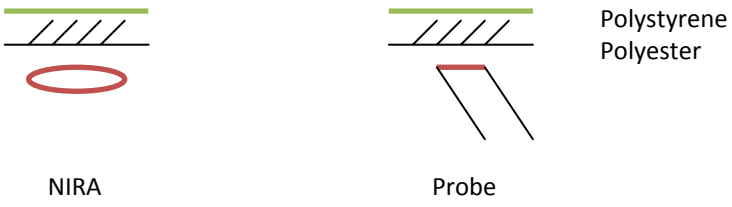

Figure 2.11 Schematic of the sampling of second material

2.4.1.4 Geometry of Fabric with Respect to Probe Window

To identify the optimum geometry of the probe window in relation to the sample, 4 ply polyester was analysed by placing the probe with the window parallel to the fabric, or such that the probe optical path was perpendicular to the fabric (Figure 2.12). Signal to noise parameters were calculated as described above.

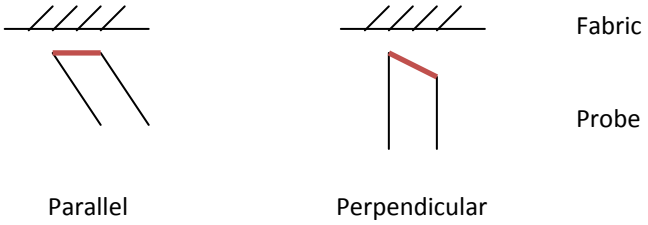

Figure 2.12 Schematic of sampling geometry

2.4.1.5 Distance of Fabric from Probe Window

Four ply polyester fabric was placed flush to, and at increasing distances from, the probe window to determine the maximum distance of sampling from the fabric (Figure 2.13). Using a retort stand the fabric was held at distances of 0, 1, 2, 4, 8, 16, and 32 mm from the probe window and parallel to it. The analyses were repeated nine times. The baseline correction was applied for calculating the signal to noise parameter, following the method described in Section 2.4.1.2.

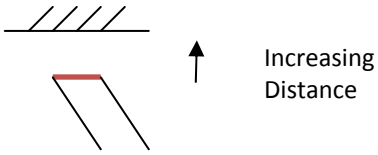

Figure 2.13 Schematic of Sampling Distance

2.4.1.6 Polarizing Effects

Polarization effects were monitored using the probe and three standard polyamide 6,6 yarns. Polyamide fibres were studied rather than polyester as they are semi-crystalline materials with isotropic properties, whereas polyesters have relatively low crystallinity due the aromatic groups along the polymer chain (Appendix 1). The NIR accessory was not considered here, as the integrating sphere provides non-linear, diffusely reflected light and therefore will not experience polarizing effects.

Warp yarns taken from the polyamide 6,6 fabric was arbitrarily orientated across the accessory window from the front to back of the accessory (0°), and rotated through 45 and 90 degree angles (Figure 2.14). The spectra were processed using a second derivative Norris function, with a gap value of 19 (Section 2.3.2). This gap value was chosen to reduce noise levels without significant loss of visual resolution. The second derivatives were then overlaid at a peak at 4364cm^{-1} to highlight subtle absorbance variations not immediately apparent in the raw data, and comparisons made.

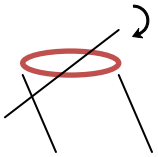

Probe window

Figure 2.14 Schematic of yarn orientation

2.4.1.7 Geometry of Optical Fibres

Four ply polyester was analysed using the probe attachment, with the optical fibre lengths orientated in a coiled and linear geometry (with the geometry fixed for both background and sample spectrum acquisition). The signal to noise parameter was then calculated to determine whether the geometry of the optical fibres impact on the signal throughput.

2.4.1.8 Effect of Colour

Commercially purchased polymer blend fabrics of 65% cotton and 35% polyester, in seven different colours, were analysed using the NIR accessory. Signal to noise parameter were calculated to identify whether there was any significant loss of information caused by highly absorbing species at the higher wavenumber region of the NIR spectrum. Fabric colours studied: Yellow, Pink, Red, Beige, Pale Blue, Navy and Black.

2.4.1.9 Effect of Relative Humidity

In order to determine whether fluctuations in relative humidity (RH) alter the NIR spectrum, and therefore adversely affect the identification of textiles, fabric material of five polymer classes were subjected to three levels of humidity and analysed using the NIR probe. Saturated salt solutions were made up to maintain RH levels of 22.5% ±0.3%, 43.2% ±0.4%and 68.9% ±0.2% by aqueous dissolution of potassium acetate, potassium carbonate and potassium iodide, respectively [10]. These were sealed in individual containers with samples of

polyamide, polypropylene, viscose, cotton and wool to reach equilibrium (Figure 2.15). The salts show different levels of water sorption due to their hygroscopic or hydrophobic nature, therefore maintaining an equilibrium at each respective RH within the containers.
After allowing the fabrics to equilibrate they were transferred to a controlled humidity chamber which had been allowed to reach the respective RH levels. The samples were removed from the containers and analysed using the probe attachment inside the chamber.

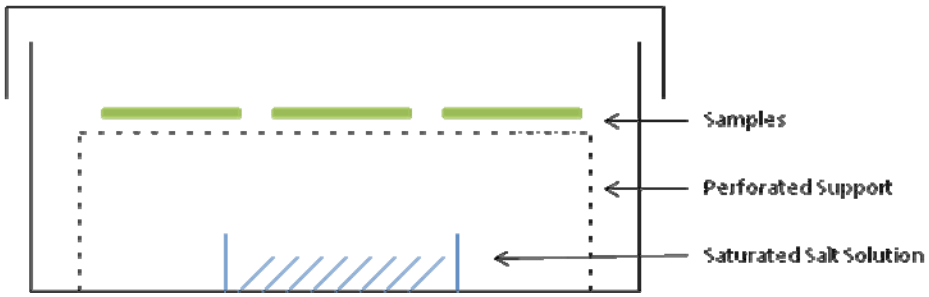

Figure 2.15 Schematic of fabric conditioning in relative humidity experiment

2.4.1.10 Effect of Stray Light

Stray light can have the effect of saturating the detector, so may be problematic when analysing thin samples or when sampling at a distance from the textile. In such cases it may be necessary to cover the end of the acceptance end of the probe or acquire data with the room lights turned off [11].

A foam cover was formed to slip over the end of the probe without itself being sampled (Figure 2.16). The spectrometer was moved into a work room with East facing windows with bright natural daylight. Analyses were carried out with and without the probe cover at a distance of 1mm from the sample surface to determine whether natural lighting would adversely affect the spectrum.

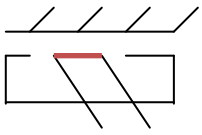

Figure 2.16 Schematic of stray light probe cover

Two further analyses were carried out in an inner room without natural light. The sample was again analysed at a distance of 1mm from the probe window, with and without the probe

cover, to observe the effect of the artificial fluorescent strip lighting, which was approximately 2 m above the sample.

2.4.2 Results and Discussion

2.4.2.1 Optimum Number of Scans

Figure 2.17 shows the signal to noise parameter calculated for increasing scan numbers. It can be seen that there is a proportional increase in the parameter with increasing number of scans. Figure 2.18 shows the S/N parameter plotted on a logarithmic scale illustrating a linear relationship between increasing scan numbers and increasing signal to noise for the first four data points. The signal to noise is expected to have a linear relationship with the number of scans; this is only true up to 8 scan numbers. It is likely that this behaviour at greater scans is related to the amount of signal removed during the smoothing process, as seen at the lower wavenumber region in Figure 2.9.

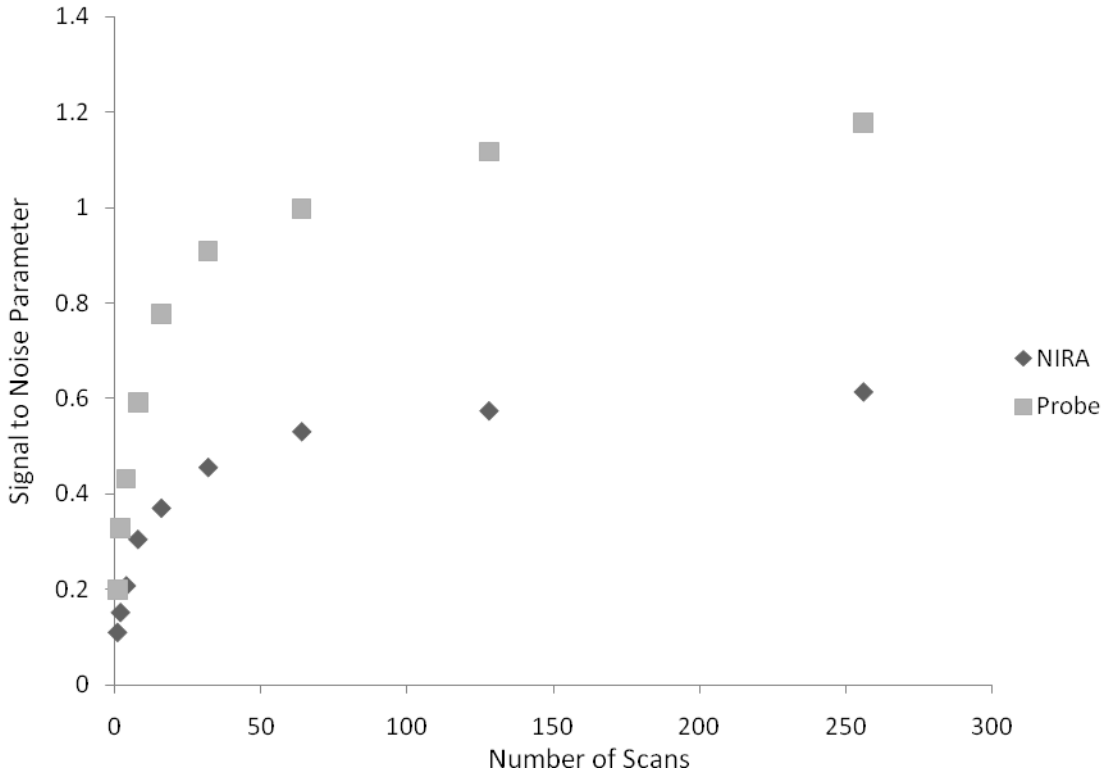

Figure 2.17 A Plot of the increasing signal to noise parameter against increasing number of scans

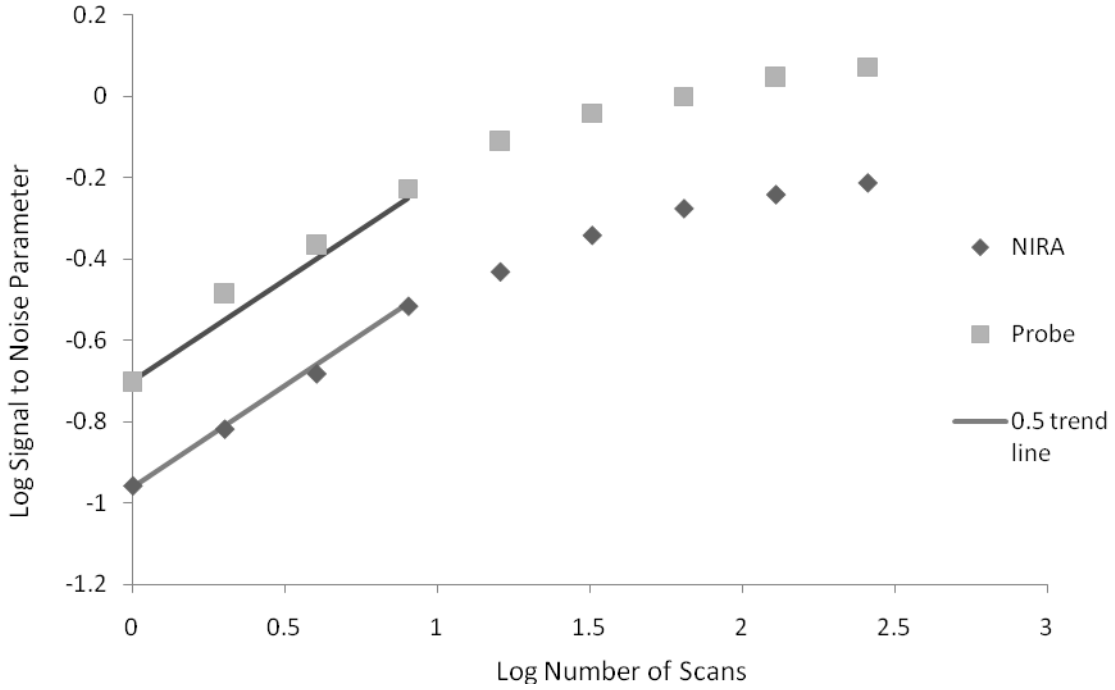

Figure 2.18 A plot of the log of the signal to noise parameter against the log of increasing number of scans. The trend lines have slopes of 0.5

Although not matching the theoretical increase, nonetheless, the signal to noise continues to improve with additional scans, though ever more gradually. When determining experimental parameters a balance needs to be struck between optimum S/N and acquisition times. A scan number of 64 appeared to offer the best compromise, with a good signal to noise and an acquisition time of only around one minute.

2.4.2.2 Optimum Depth of Sample

A plot of the signal to noise parameter against increasing sample thickness illustrates that with increasing ply the noise increased (Figure 2.19). While a proportionate increase in the S/N might be expected, the converse seems to be true. This may be attributed to an increase in scattering, and therefore noise, with increasing textile ply. Since the quality of the spectrum was not improved by increasing sample thickness, it was decided that reference data would be collected using only a single ply of fabric.

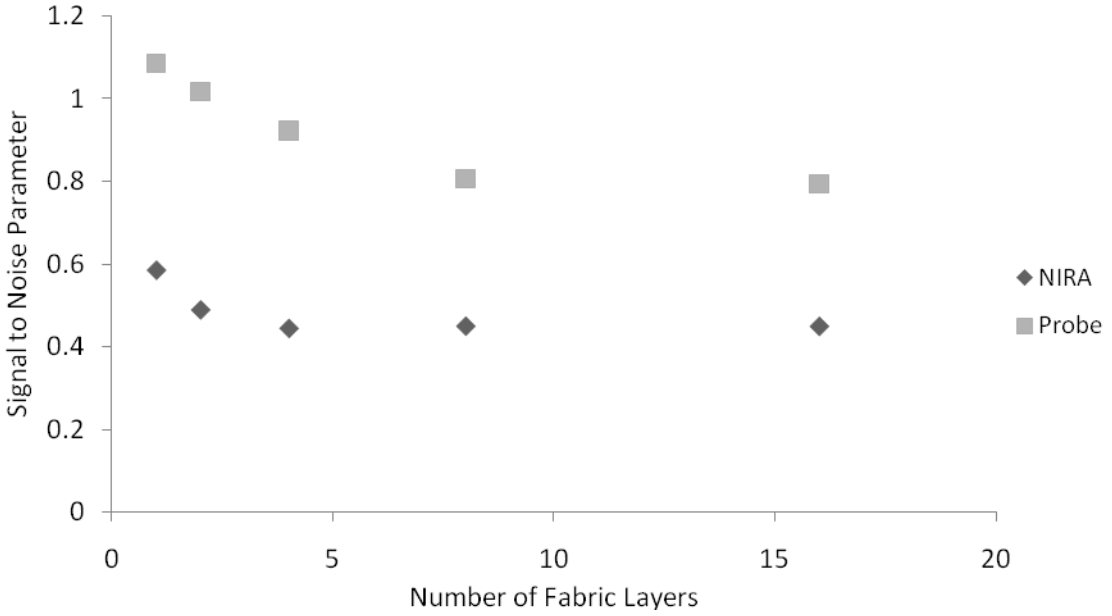

Figure 2.19 Plot of decreasing signal to noise parameter against increasing number of fabric layers

2.4.2.3 Point of Infinite Thickness

The subtraction spectra in Figures 2.20 and 2.21 confirm that the sampling depth is around 1.5 mm (4 ply), though for the probe this may be somewhat shallower as the polystyrene can still be seen in the 2ply spectrum, but is not visible in that of the 4ply. The residual negative spectrum in Figure 2.20 is due to moisture.

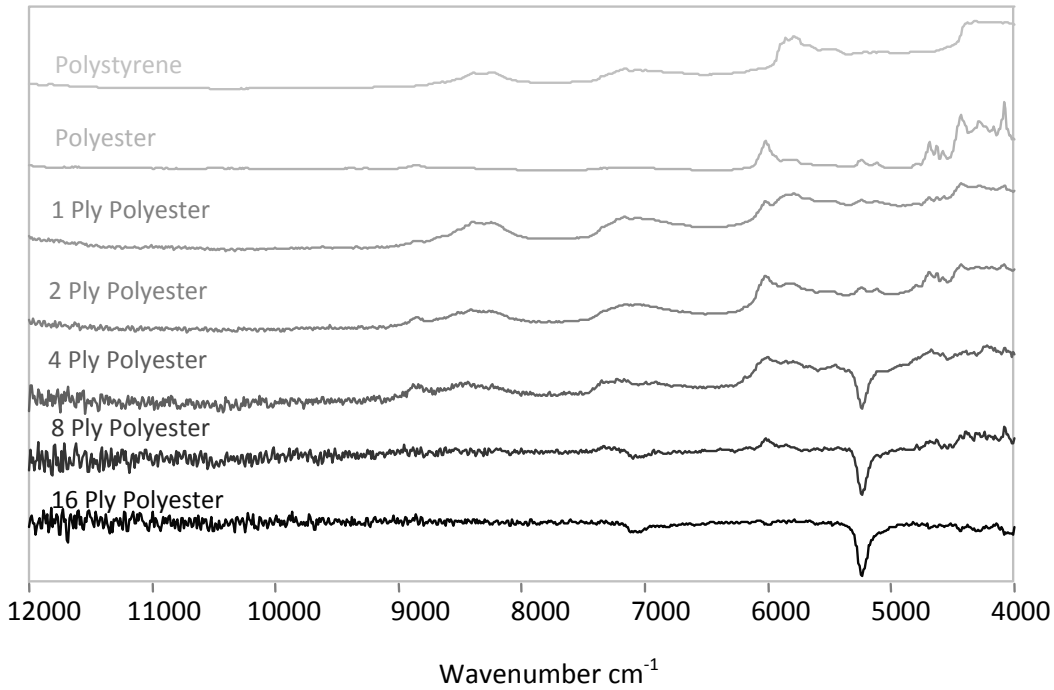

Figure 2.20 Subtracted spectra for the determination of sampling depth with the NIRA

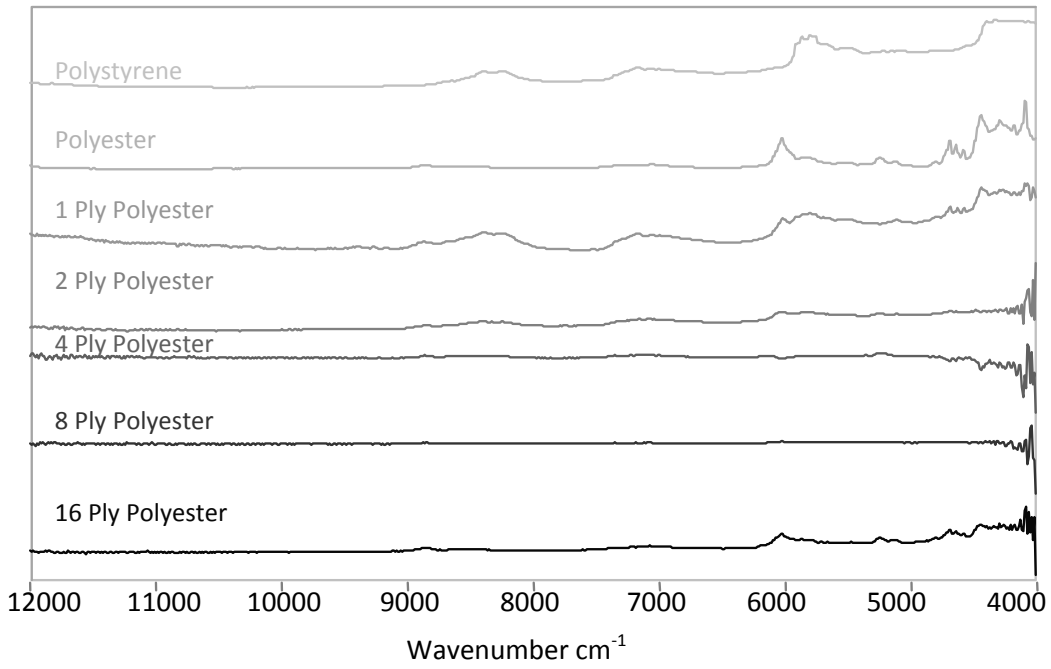

Figure 2.21 Subtracted spectra for the determination of sampling depth with the probe

2.4.2.4 Geometry of Fabric with Respect to Probe Window

The signal to noise is greater when the sample is parallel and flush to the probe window, as opposed to positioning the sample perpendicular to the probe optical path: 0.53 and 0.46 respectively. The reason for this is thought to lie in the fact that when sampling perpendicular to the probe's optical path, there is an increase in the detection of specular reflectance from the sample, due to the angle of incidence and collection. Sampling flush against the textile increases the detection of diffusely reflected light relative to specular reflectance. In addition this conformation increases the efficiency of collection of the scattered radiation, and reduces the effects from atmospheric interferences, such as stray light, which may increase background noise.

2.4.2.5 Distance of Fabric from Probe Window

Depending on the fragility of an artefact, or its accessibility, it may not always be possible to hold the probe window against the textile. Through visual examination of the spectra it was determined that the absorbance of key polyester peaks showed sufficient intensity up to approximately 4mm from the surface of the fabric; ensuring non-invasive analysis. However the signal to noise parameter decreases (Figure 2.22) due to an increasing background as the probe is moved away from the sample surface.

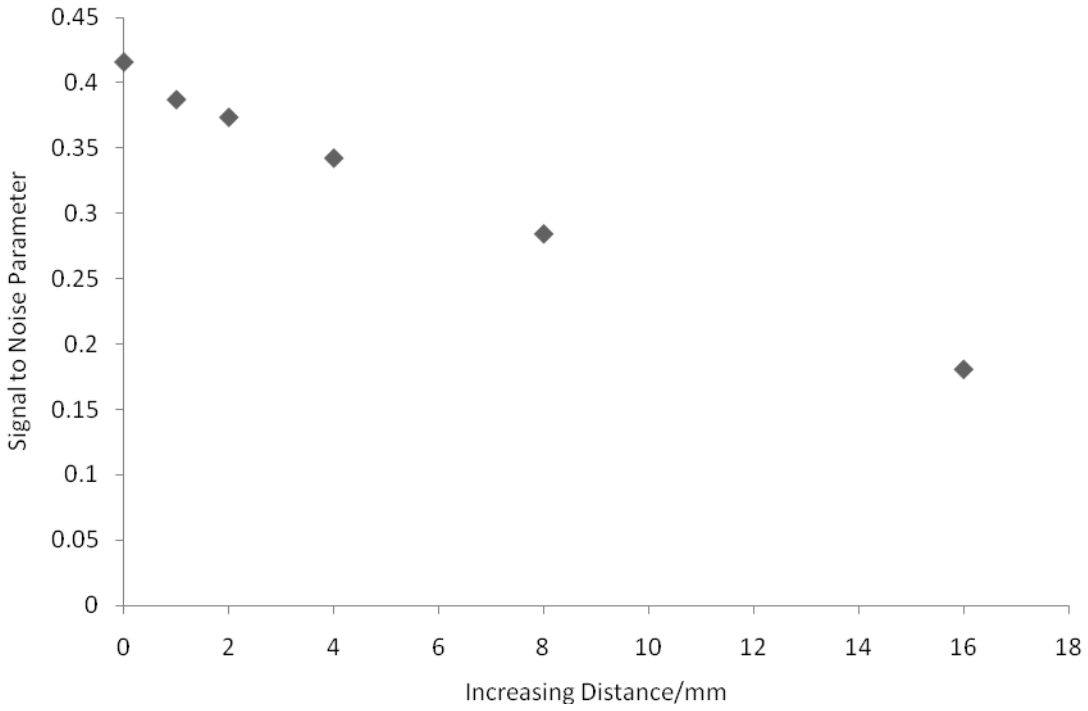

Figure 2.22 Plot of the decreasing signal to noise parameter against increasing distance of fabric from the probe window

2.4.2.6 Polarizing Effects

Polarizing effects occur when polymer chains are orientated in alignment, such as crystalline regions along a fibre's length. If the radiation incident on the fibre is polarized, then there will only be absorptions when the electric vector is aligned with the bond of interest; therefore making spectra reliant on the fabric's geometry. Figures 2.23 – 2.25 show the overlaid second derivative spectra of three polyamide 6,6 samples. Focus has been given to the region between 4 200-5 000cm^{-1} as this has been shown to contain Amide I combination vibrations [4]. These vibrations originate from carbonyl bonds and are highly orientated in the crystalline domains. They are known to exhibit polarization effects in mid infrared spectroscopy [12]. This will be discussed to a greater extent in Chapters 9, 10 and 11 of this thesis, but here focus is given to how this might adversely affect the near-infrared spectrum.

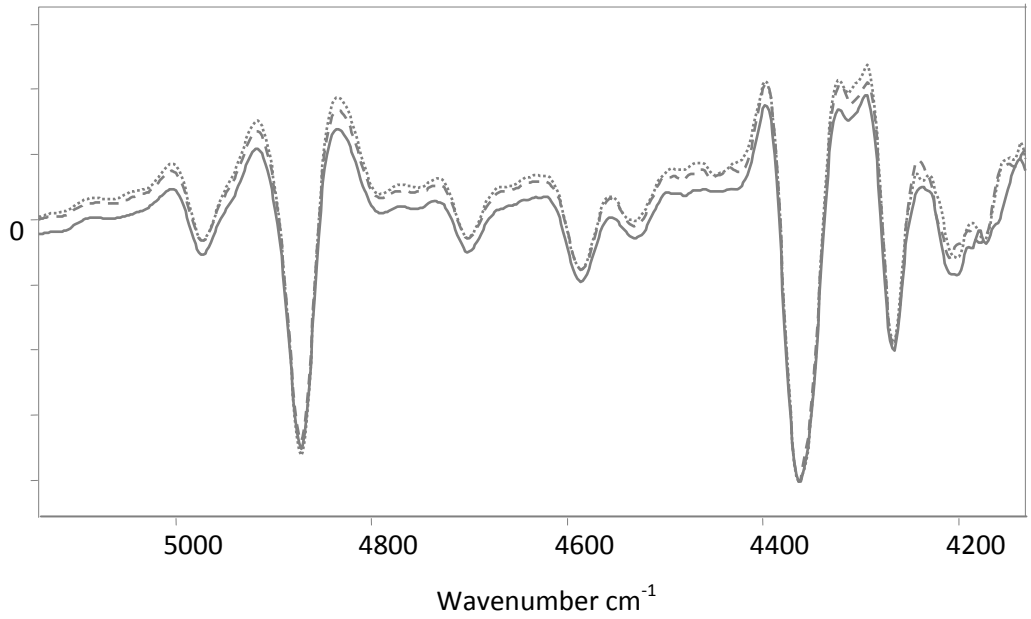

Figure 2.23 Expanded NIR second derivative spectra of a polyamide 6,6 reference sample supplied by Test Fabrics Inc. 0 degrees (solid), 45 degrees (dotted) and 90 degrees (dashed)

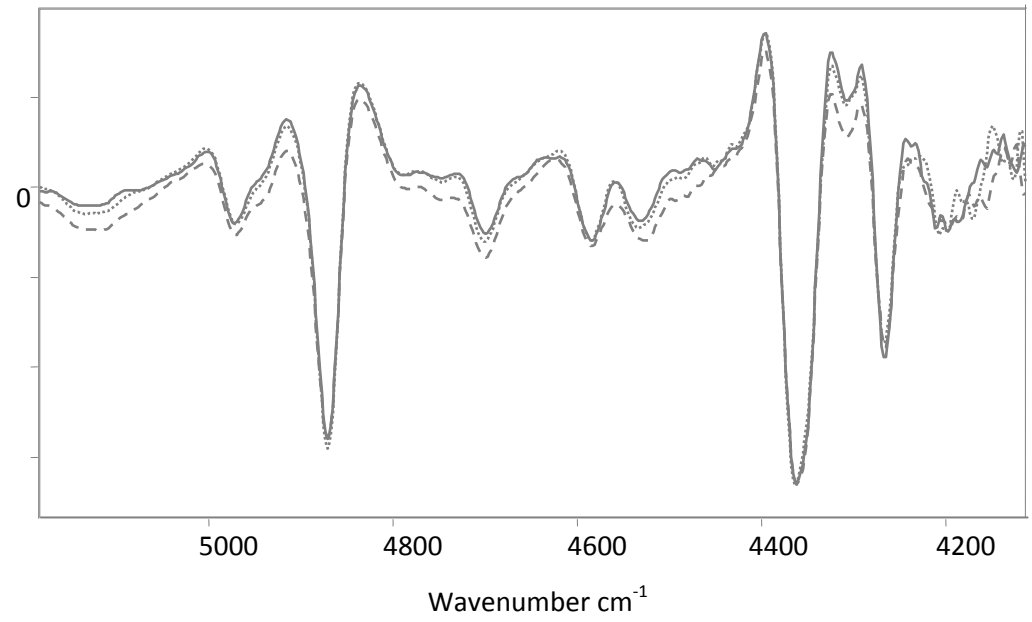

Figure 2.24 Expanded NIR second derivative spectra of a polyamide 6,6 reference sample supplied by Test Fabrics Inc., manufactured by Du Pont. 0 degrees (solid), 45 degrees (dotted) and 90 degrees (dashed)

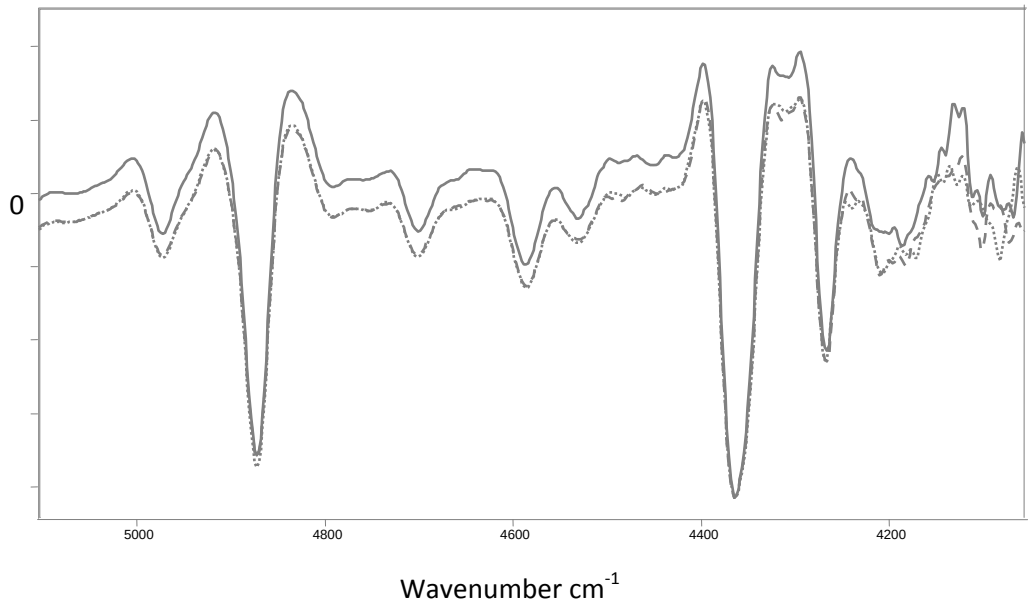

Figure 2.25 Expanded NIR second derivative spectra of a polyamide 6,6 reference sample supplied by the Society of Dyers and Colourists. 0 degrees (solid), 45 degrees (dotted) and 90 degrees (dashed)

It is apparent from the derivative spectra that there are alterations in the absorbance intensities as the yarns are rotated through 90 degrees. This therefore suggests that a degree of polarization is present when analysing highly oriented polymers with the fibre optic probe. This leads to the conclusion that such material should, where appropriate, be analysed using the integrating sphere attachment.

2.4.5.7 Geometry of Optical Fibres

There is a small improvement in the signal to noise parameter when the optical fibres are in a linear geometry, than when coiled: 3.00 and 2.73 respectively. This is probably due to a higher throughput of radiation. Where possible on site experimental parameters will be optimised using a linear setup. However, the signal to noise ratio when the fibres are coiled is still high enough for quality data acquisition.

2.4.2.8 Effect of Colour

Dyes do not appear to prevent detection of characteristic absorbance bands at lower wavenumbers, towards the mid-IR, although the tail of the electronic absorption of some dyes (blue and black) masks weaker bands at higher wavenumbers (Figure 2.26). Collection of reference spectra will be carried out, where possible, using undyed samples over the entire

NIR spectral range. For highly coloured material it may be necessary to acquire spectra over a smaller spectral range to prevent interferences.

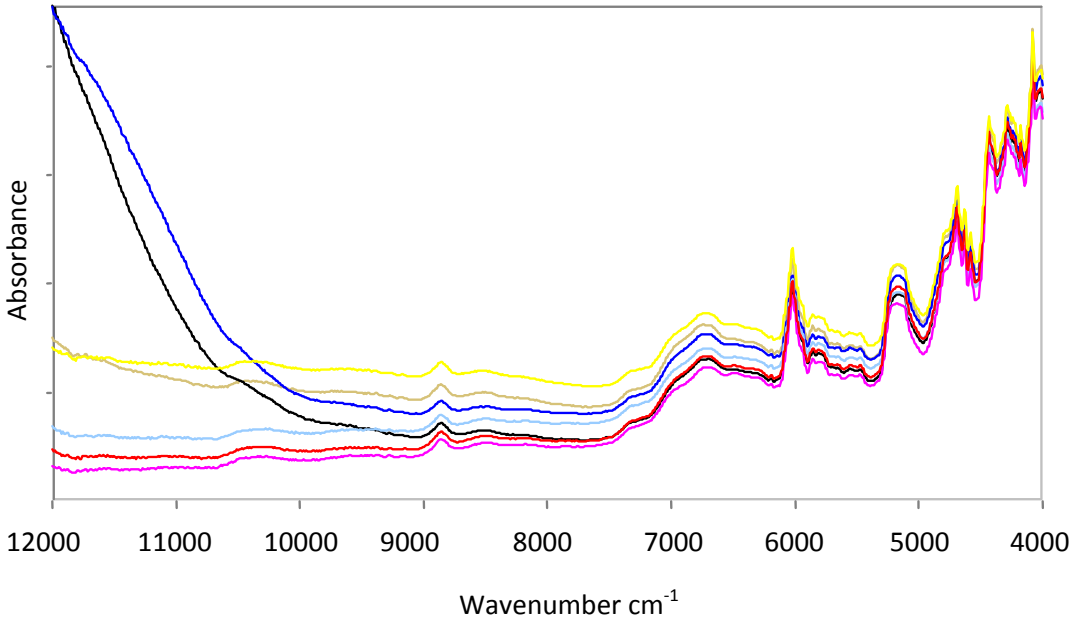

Figure 2.26 Overlaid NIRA spectra for varying colours of a polyester/cotton blended fabric

2.4.2.9 Effect of RH

The offset second derivative spectra for each polymer at increasing RH are presented in Figures 2.27-2.31. The combination bands relating to water are found at approximately 5 150-5 200cm^{-1} and the first overtone in the region of 6 800-7 000cm^{-1} [4]. It can be seen in spectra of viscose, cotton and wool that there are significant increases in the sorbed H_2O peaks, in particular those relating to the OH stretching and bending combination band. The relative peak increases are less obvious in that of the polyamide sample, with virtually no moisture sorption by the polypropylene. These results are consistent with the polymer structures of each of the samples (Appendix 1), which will affect the degree of moisture penetration.

Viscose and cotton are both cellulosic materials, but with the former having a much higher amorphous content; the presence of alcohol groups readily permitting a high degree of hydrogen bonding. Wool also shows high moisture sorption due to relatively low ordering of the keratin polyamide, and ready penetration by water of the hydrophilic amorphous zones. Polyamide 6,6 is a more crystalline structures with fewer sites for intramolecular bonding and hence exhibits lower moisture sorption. Polypropylene is a highly hydrophobic polymer, showing high crystallinity and no polar groups available for attraction of water molecules.

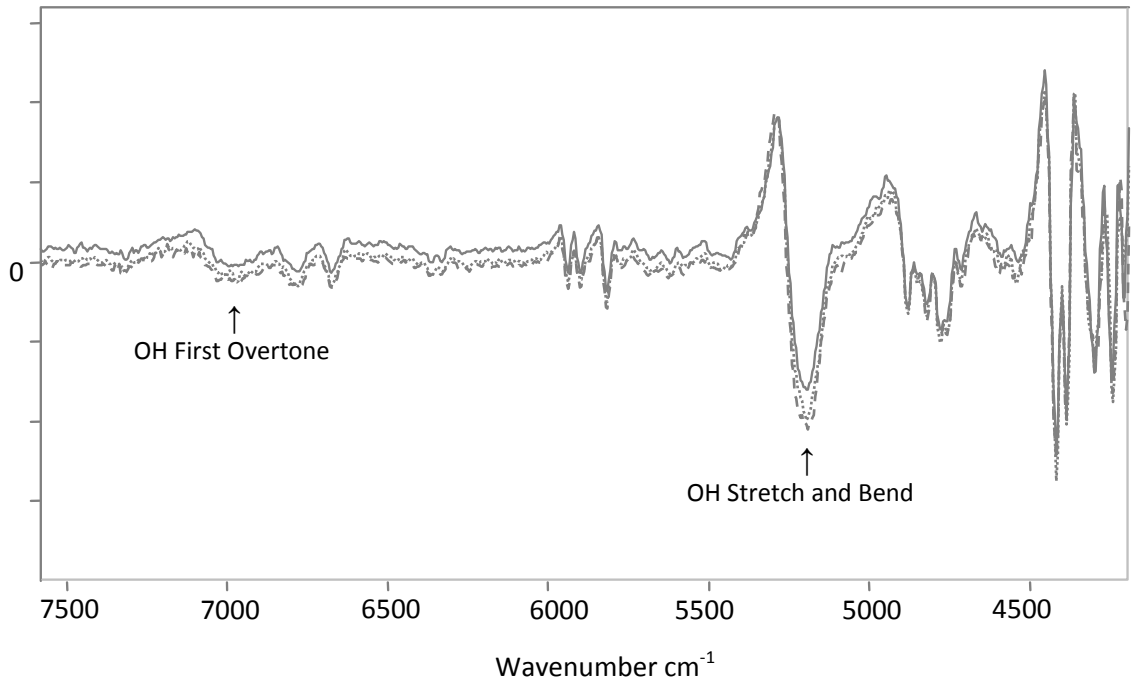

Figure 2.27 Offset second derivative NIR probe spectra of viscose at increasing RH levels. 20% (solid), 45% (dashed) and 70% (dotted)

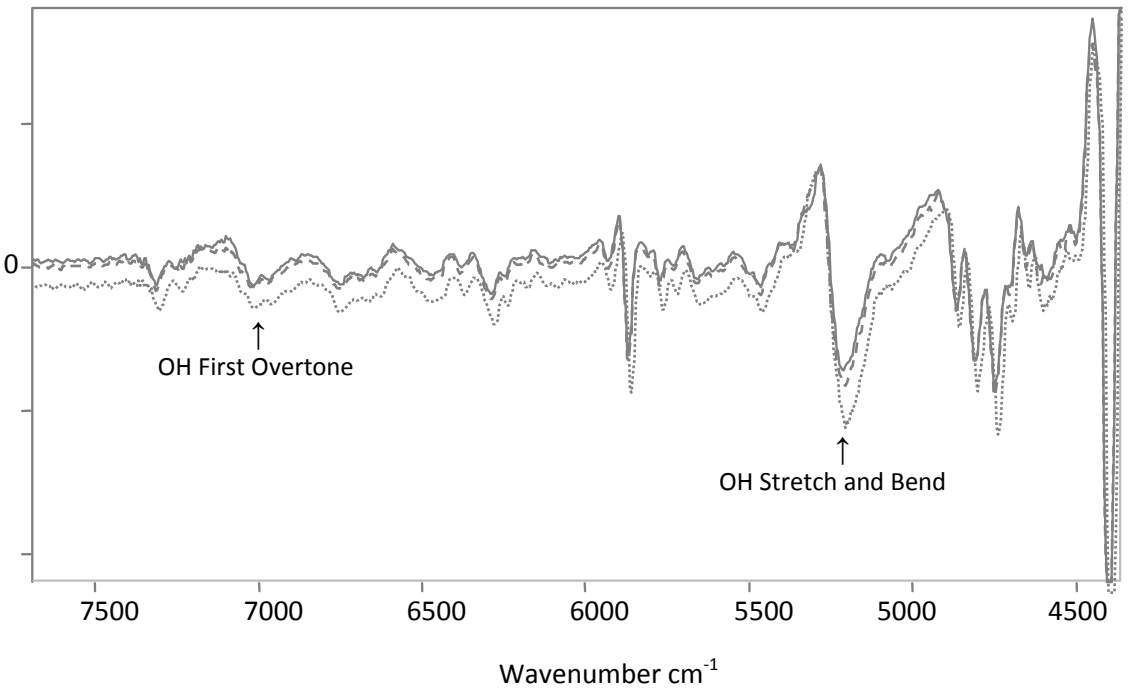

Figure 2.28 Offset Second Derivative NIR Probe Spectra of Cotton at Increasing RH Levels. 20% (solid), 45% (dashed) and 70% (dotted)

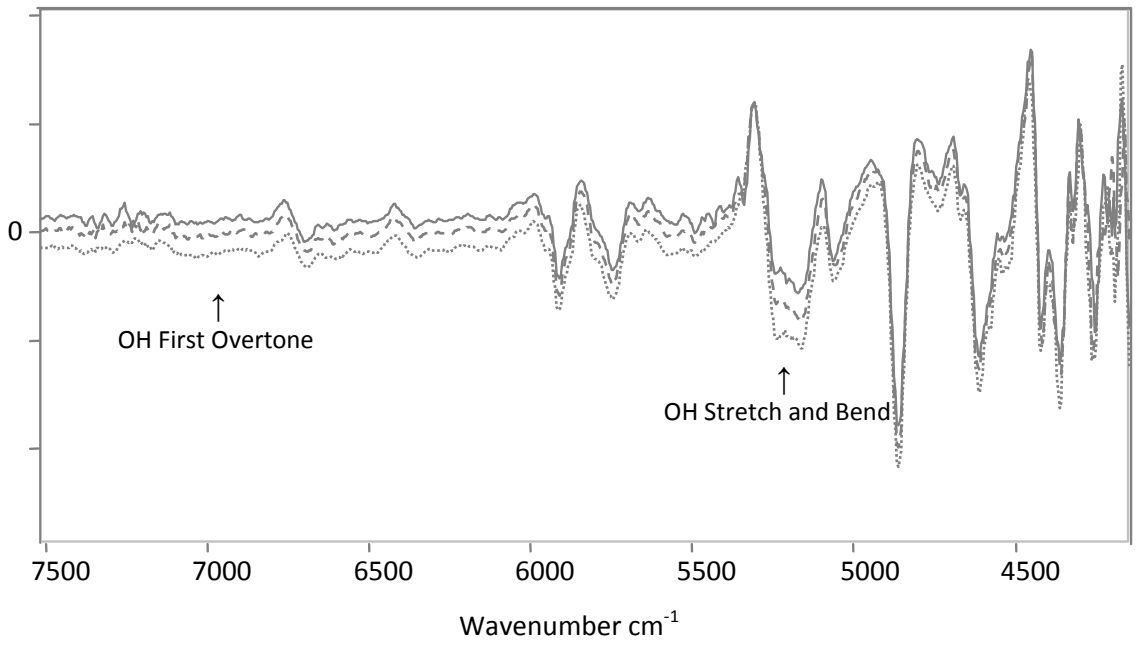

Figure 2.29 Offset Second Derivative NIR Probe Spectra of Wool at Increasing RH Levels. 20% (solid), 45% (dashed) and 70% (dotted)

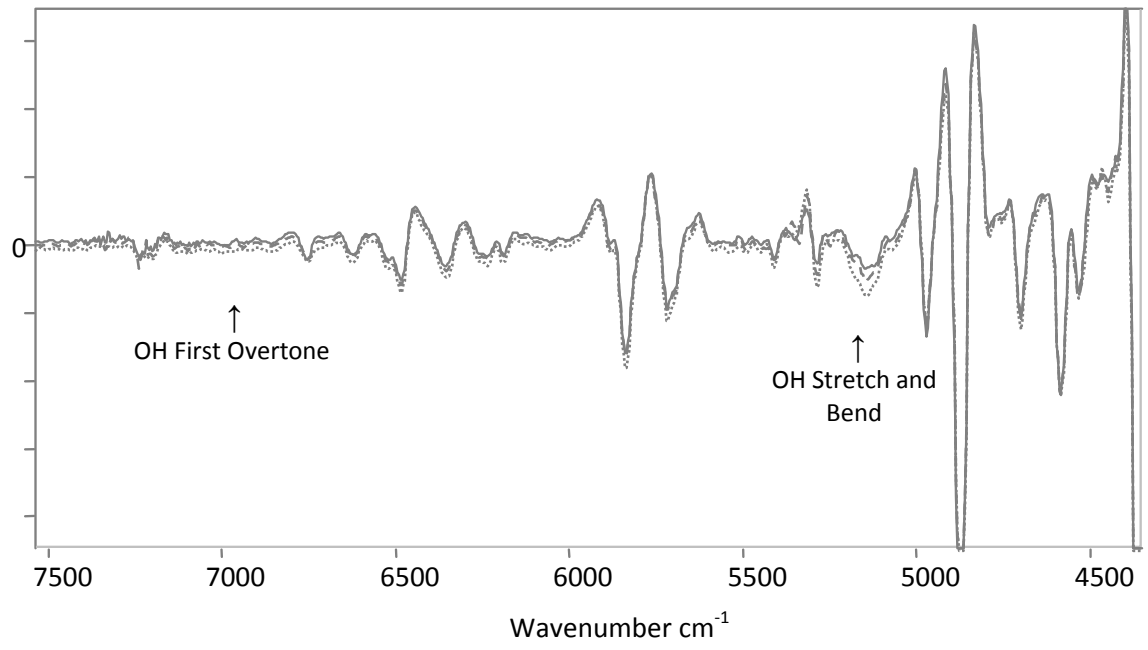

Figure 2.30 Offset Second Derivative NIR Probe Spectra of Polyamide 66 at Increasing RH Levels. 20% (solid), 45% (dashed) and 70% (dotted)

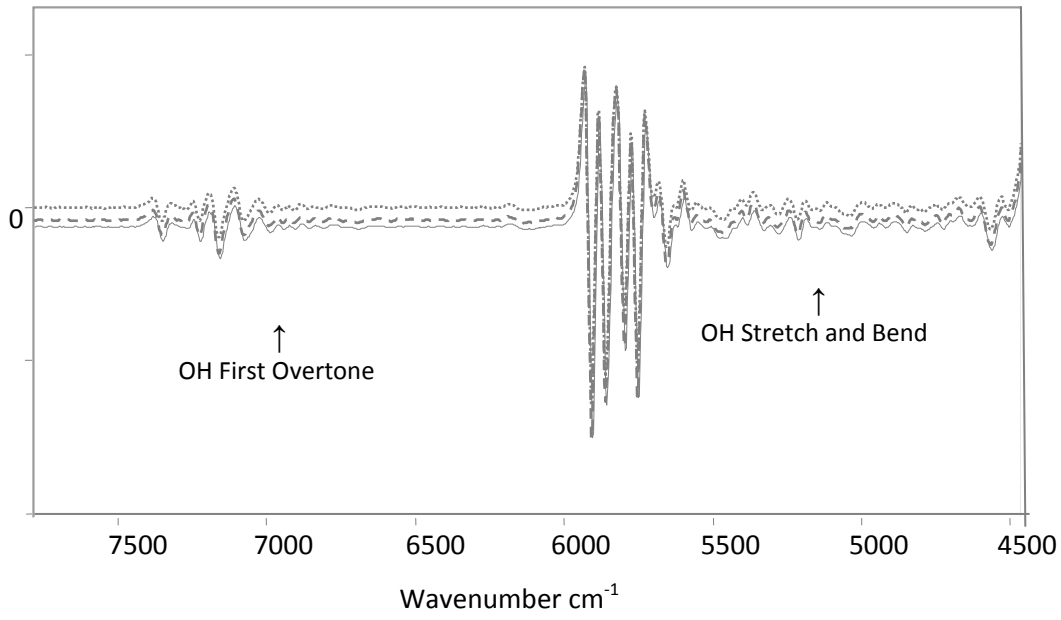

Figure 2.31 Offset Second Derivative NIR Probe Spectra of Polypropylene at Increasing RH Levels, 20% (solid), 45% (dashed) and 70% (dotted)

In order to determine whether the increased moisture content would have an effect on the identification of these textiles, the raw spectra were submitted to the Spectral ID library (to be discussed in Section 3.1.1, Chapter 3) using the first derivative least squares algorithm for matching. All samples could be readily identified, even at raised RH.

2.4.2.10 Effect of Stray Light

Figure 2.32 shows two second derivative NIR spectra of a polyethylene foam analysed with and without the stray light cover. It can be seen from the spectra that there is a negligible effect on the spectrum when analysed in natural daylight.

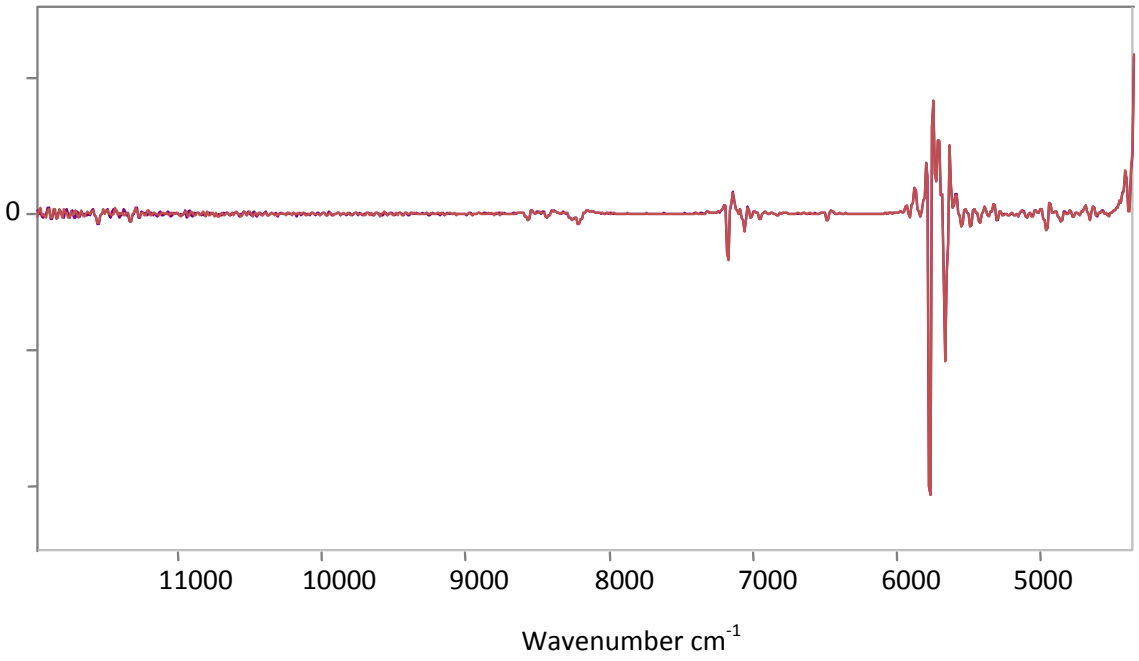

Figure 2.32 Overlaid Second Derivative Probe Spectra With (Grey) and Without (Red) Stray Light Cover

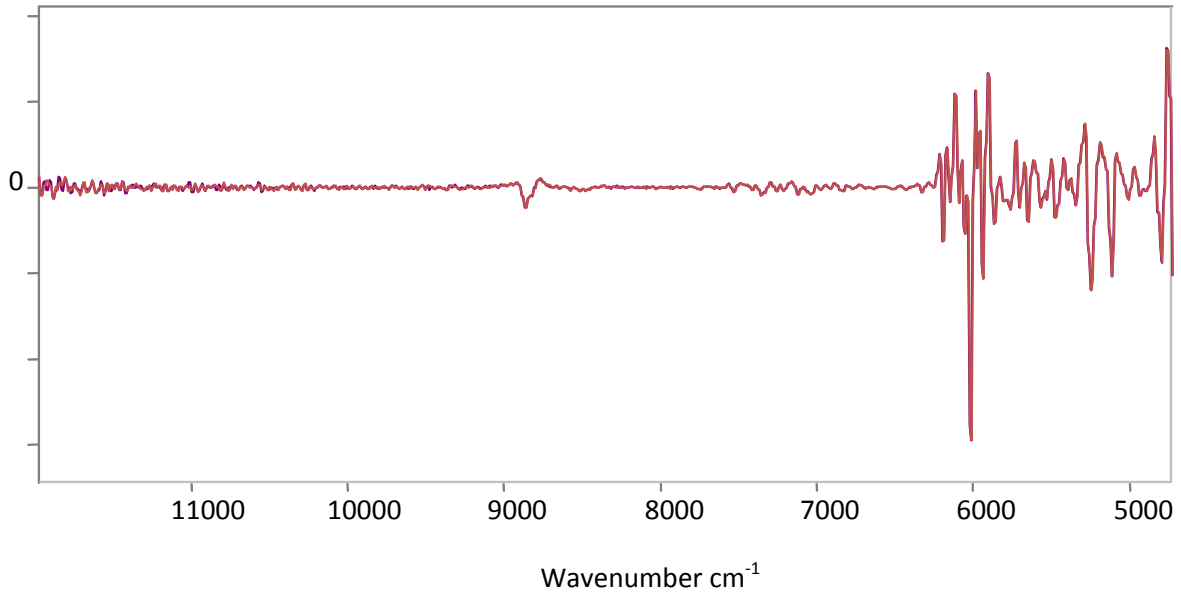

Figure 2.33 Overlaid Second Derivative Probe Spectra With (Red) and Without (Grey) Artificial Lighting

Figure 2.33 shows the second derivative spectra of two further analyses with and without artificial lighting. Again the effects of stray light appear to be low, indicating that on site analysis is unlikely to be compromised by lighting conditions.

Due to the often fragile nature and accessibility of the materials under investigation, it may not be possible to position the probe in close contact with the sample surface. In such cases it is recommended that the light cover be employed to ensure minimal interference and optimum conditions.

2.5 Conclusions

The spectra are characteristically complicated, as a consequence of near-infrared vibrations originating from overtones and combinations of the fundamental vibrations found in mid-infrared spectroscopy. This results in absorption bands of low resolution, restricting band assignments and necessitating spectral comparisons for robust classification. The following chapter will discuss this further, and present the acquisition and application of a NIR spectral reference library.

The preliminary experimental work allowed the analytical protocols to be determined and optimised for on-site interrogation of objects. The signal to noise parameter was shown to improve with an increase in scan number.

As a compromise between increased signal and sampling time a decision was taken to acquire all future NIR spectra using 64 scans, equating to approximately one minute.

On increasing the depth of the textile sample it was apparent that the signal decreased relative to the spectral noise. This was attributed to increased scattering from multiple woven layers. To reduce such affects all subsequent sampling, whether for the reference library or from a heritage artefact, were carried out using a single ply of fabric (where appropriate).

The shorter wavelengths associated with the near-infrared provide a method of analysis capable of sampling to some depth. It was shown that depth sampling in the region of 1-2mm was possible, analysing all material to this depth unless there is significant scattering from the upper layers. The ability to analyses material not easily accessible, through an upper layer removes the need for invasive sampling and will aid conservators and curators.

Although the signal to noise parameter was shown to decrease as the distance between the sample and analysis window was increased, it was still possible to detect the signal from up to 4mm from the sample surface. This means that for fragile samples, where contact may not be possible, a near-infrared spectrum may still be obtained.

The polarization experiments indicted that there was a degree of polarization when studying highly oriented fibres with the fibre optic probe. Therefore, the reference library spectra were obtained using the integrating sphere, where the light is non-linear and diffusely scattered.

Coloured fabrics experienced high absorption towards the visible region of the spectrum

(9 000-12 000cm^{-1}).The effect of this on materials identification will be considered in Chapter 6.

External, environmental factors were assessed through RH and stray light experiments. Although variations in RH caused changes in the OH absorption bands for some polymers, subsequent identification using the spectral library indicated that this did not hinder correct classification. The effects of stray light were not shown to adversely affect the NIR spectrum.

Following a discussion on building a NIR reference database and searching library, the next chapter will present two heritage case studies. This will serve to illustrate the application of NIR spectroscopy for the onsite identification of modern materials, whilst highlighting some of the limitations of the technique.

2.6 References

1. Skoog, D.A., F.J. Holler, and T.A. Nieman, *Principles of Instrumental Analysis*. 5th ed. 1998: Thompson Learning Inc. .
2. Colthup, N.B., *Introduction to Infrared and Raman Spectroscopy*. 2nd ed. 1975, London: Academic Press.
3. Pasquini, C., *Near Infrared Spectroscopy: Fundamentals, Practical Aspects and Analytical Applications.* Journal of the Brazilian Chemical Society, 2003. **14**(2): p. 198-219.
4. Siesler, H.W., *Near-Infrared Spectroscopy: Principles, Instrumentation, Applications*, ed. H.W. Siesler, et al. 2002, Weinheim: Wiley-VCH.
5. Halliday, D., R. Resnick, and J. Walker, *Fundamentals of Physics*. 4th ed. 1993, Chichester: John wiley & Sons, Inc.
6. Schwedt, G., *The Essential Guide to Analytical Chemistry*. 1997, Chichester: John Wiley & Sons Ltd.
7. Thickett, D. and N. Luxford, *FTIR Analysis of Protective Coatings*, in *The Seventh Biannial Gathering of the Infrared and Raman Users Group*. 2006: MoMA, New York. p. 38.
8. Otto, M., *Chemometrics: Statistics and Computer Application in Analytical Chemistry*. 1999, Frieberg: Wiley-VCH.
9. Savitzky, A. and M.J.E. Golay, *Smoothing and Differentiation of Data by Simplified Least Squares Procedure.* Analytical Chemistry, 1964. **36**(8): p. 1629-1630.
10. Greenspan, L., *Humidity Fixed Points of Binary Saturated Aqueous Solutions.* Journal of Research of the National Bureau of Standards - A. Physics and Chemistry, 1977. **81A**(1): p. 89-96.
11. Vintzileos, A.M. *Transabdominal Fetal Pulse Oximetry Using Near-infrared Spectroscopy*. 2005 [cited 2006]; Available from: http://www.umdnj.edu/research/publications/spring05/05_fetal_pulse.htm.
12. Brooks, M. and P. Garside. *Probing the Microstructure of Protein and Polyamide Fibres*. in *AHRC Research Centre for Textile Conservation and Textile Studies Second Annual Conference The Future of the 20th Century - Collecting, Interpreting and Conserving Modern Materials*. 2005. Winchester: Archetype Publications.

Chapter 3: A Question of Identification: The Acquisition of a Spectral Library and the Application to Two Heritage Case Studies Illustrating Non-invasive, *in situ* Analysis

Decisions regarding the long term storage and display of artefacts within heritage collections rely on an intimate knowledge of materials and their behaviour. Over time deterioration is inevitable, but the rate at which objects deteriorate may be greatly reduced by careful control of the environment. Degradation routes and stabilisation vary through the material classes, illustrating the need for an intimate knowledge of their behaviour and for positive identification within collections, this is not always easy with limited sampling of artefacts.

The *in situ* application of NIR spectroscopy for the non-invasive identification and condition monitoring of synthetic material held in textile collections should greatly assist in the long-term preservation of contemporary artefacts. The ability to identify quickly modern textiles, accessories and adornments, found in conjunction with natural organic material, would provide museum professionals with the information required for a greater understanding of their collections. This should enable informed long-term action plans and more immediate remedial conservation plans to be implemented.

The first half of this Chapter will focus on the collection of a spectral database of reference polymers and the development of a searching library. Later in the Chapter two Case Studies will be highlighted that illustrate the on-site applicability of the near-infrared technique within heritage settings. The artefacts studied cover a range of materials, which is not limited to fabric. This illustrates the mixed nature of collections and demonstrating that, whilst the physical form may vary, the chemical composition of modern materials remain the same across different manufacturing applications.

3.1 Spectral Database and Searching Library

It has been previously highlighted that the ability to identify the major classes of polymeric material found in heritage collections would greatly benefit the curators and conservators. Chapter 2 presented the experimental protocols for the use of NIR spectroscopy and illustrated the non-invasive capabilities of the technique. One of the most important features of the NIR technique relates to the high number of absorption bands seen to occur across this spectral region. These originate from overtone and combination vibrations and mean that the NIR spectrum appears characteristically unresolved. Where absorption bands are often readily assigned to vibrational modes in the mid-infrared, this is not possible when dealing with near-infrared spectroscopy. To this end, the successful application of near-infrared spectroscopy requires a comprehensive set of references to accompany any analyses.

In order to enable unequivocal identification, a reference set of the major classes of polymers found in contemporary collections was acquired from a number of manufacturers and suppliers. Near-infrared spectral scans were then taken and each spectrum individually uploaded to commercial library software. This library was then used to enable unknown samples to be identified following the NIR analysis. All reference spectra are included on the accompanying CD-ROM, alongside a spreadsheet containing details of the respective suppliers.

3.1.1 Spectral Library Matching

3.1.1.1 Reference Library

Due to the origin and complexity of the spectral bands exact functional assignments can be problematic. However, the spectra are still characteristic, and comparison with a suitable spectral reference set usually allows ready identification of unknowns. For this reason a comprehensive spectral library of well-defined modern materials was acquired. At this point approximately 300 samples have been obtained, covering the major classes of synthetic textile material found within contemporary collections. Table 3.1 lists the major classes of polymers that were included in the reference library and the number of samples acquired for each class.

Polymer Class	Abbreviation	Number of Samples
Acrylonitrile Butadiene Styrene	ABS	2
Casein Formaldehyde	CF	1
Cellulose Acetate	CA	10
Cellulose Nitrate	CN	12
Cotton/linen	C/LN	25
Epoxy Resin	EXR	2
Gelatine	G	2
Glass Reinforced Polyester	GRP	2
Kevlar/Nomex	K	7
Natural Rubber	NR	1
Melamine Formaldehyde	MF	3
Nitrile Rubber	NR	3
Polyacrylonitrile	AN	8
Polyamides	PA	83
Polycarbonate	PC	4
Polyethylene Terephthalate	PET	58
Polybutylene Terephthalate	PBT	1
Polyethylene	PE	4
Polymethylmethacrylate	PMMA	1
Polypropylene	PP	3
Phenol Formaldehyde	PF	4
Polyimide	PI	2
Polystyrene	PS	3
Polyurethane Polyester	PU-PES	3
Polyurethane Polyether	PU-PETH	2
Polyvinyl Acetate	PVA	2
Polyvinyl Chloride	PVC	5
Silk	SK	29
Soya	S	2
Urea Formaldehyde	UF	2
Viscose/Rayon	V/R	4
Wool	W	38

Table 3.1 Major polymer classes and abbreviations contained in the reference library and their corresponding number of samples for each

3.1.1.2 Spectral Parameters and Data Acquisition

The spectral parameters and the protocols for collecting the reference spectra were determined by the preliminary studies presented in Chapter 2.

Spectral Parameter and Data Acquisition	
Spectral Range	4 000-12 000cm^{-1}
Wavenumber Resolution	8 cm^{-1}
Scan Accumulation	64
Sample Depth for Textile Samples	Single ply
Accessory	Integrating Sphere
Relative Humidity	Ambient RH (50% ±4)
Spectral Averaging	3

Table 3.2 Spectral parameters and data acquisition protocols for collection of the near-infrared reference spectra used to build the searching library

3.1.1.3 Choice of Library

Two spectral library searching facilities were available within the laboratory, Perkin Elmer Spectrum Library and Thermo Galactic Spectral ID. On application of test libraries, the Thermo Galactic informatics package was found to be the most "user friendly", with the ability for data manipulation and algorithm searching facilities. During the 7th Biannual IRUG meeting at the MoMA, New York, Hall *et al* [1] indicated that the Thermo Galactic Spectral ID was a good all round spectral searching package and was preferred to two rival programmes, KnowItAll (Bio-Rad) and Curve Manager (Advanced Chemical Development).

The library matching software allows for the creation of new search libraries with specified parameters. These are manually input and allow the spectra to be accompanied by the compound name, molecular formula, source, comments and the attachment of chemical structures.

3.1.1.4 Matching Algorithms in Spectral ID

Unknown spectra are assigned through the searching and retrieval capabilities of the software's matching algorithms, which are based on cluster analysis, finding the closest match held within the reference set. The data files are opened in the library software, and with the application of matching algorithms to the reference set, the closest matches to that of the unknown are generated (Figure 3.1). A Hit Quality Index (HQI) is generated by the software, which is used as a measure of confidence. These range from 0 as a perfect

match to 1 as an indication of a poor correlation. This is opposite to normal statistics where 1 refers to a perfect correlation.

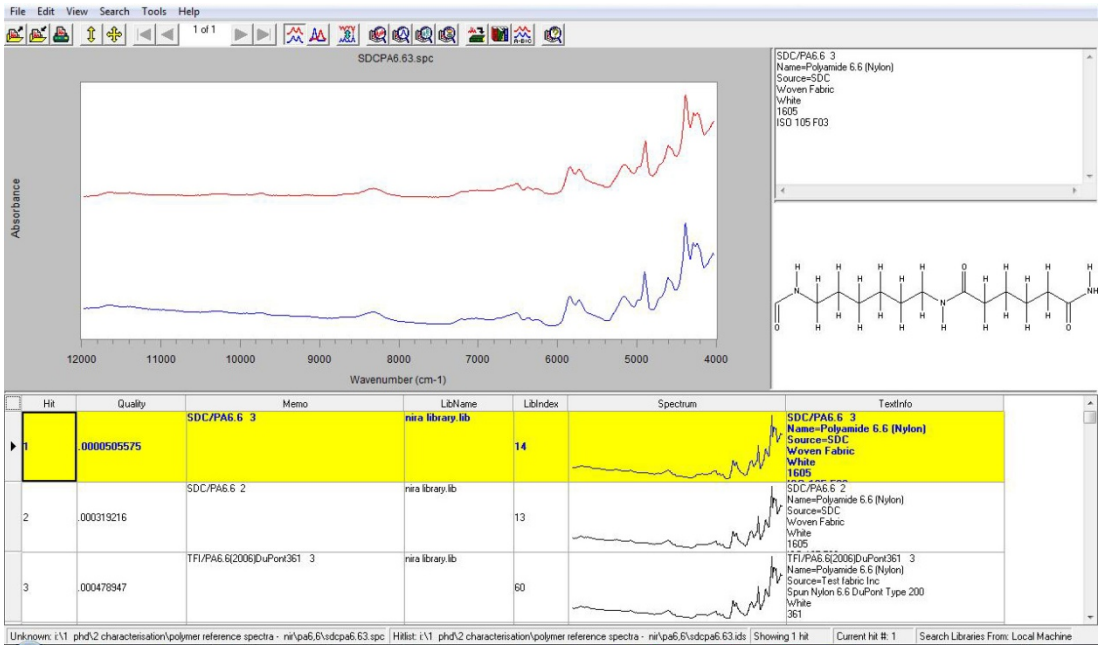

Figure 3.1 Image of the Spectral ID software finding the closest match (blue curve) to the unknown sample (red curve). The sample was identified as polyamide using the correlation algorithm and returning a Hit Quality Index of 0.0

Due to the complicated nature of the spectra and spectral interferences caused by bulk scattering, the matching algorithms can give disproportionate weighting to raising baselines and noise. It is not possible to apply the library matching as a “black box” method. Therefore, all classifications were accompanied by visual inspection of the spectra and, if deemed appropriate, data processing methods employed. This ensured false positive classification was avoided. This means that the matching of an unknown sample is still to some degree subjective. However, the ability to search through a library of NIR spectra enabled the samples with similar spectral patterns to be highlighted, providing an indication of the material present[I].

Within the literature [2-4] it is common practice to normalise NIR spectra throughout a data set by the application of scatter correction methods, reducing the effects of sloping baselines and offsets whilst maintaining the signal. The spectra input into the library

[I] Private conversation with Professor J. Frey, Department of Chemistry, University of Southampton, 4 October 2006. Discussion regarding the application of spectral library matching algorithms.

discussed here have not been normalised as the collection of reference spectra is ongoing, thus preventing the calculation of a mean 'ideal' spectrum for normalisation. Problems may also be encountered if applying the library to an unknown sample that contains spectral features that have been removed by the normalisation process. The particular software is not able to apply the same pre-treatment to the unknown[II].

The computer software allows the first derivative to be applied to the raw spectral data. The method applied by the software is the Gap method, with a gap value of 1 (Section 2.3.2). The derivative function is used to remove baseline error, which is useful for non-linear baselines often experienced in the NIR spectral region [5].

The software is capable of applying a number of test matching algorithms. In order to determine the most appropriate algorithms for application, a number of samples of known classification were tested against the spectral library. This validation step indicated that least squares algorithm and the correlation algorithm performed better at correct classification than the other algorithms available.

The former is based on the least squares regression method to find the best-fit curve to a given set of data points, by reducing the sum of the squares of the residuals. The algorithm treats the library Y values as residuals to the line of best fit, in this case the unknown Y values. Therefore, the best fitting library spectrum is that which minimises the sum of the squares of the deviations, calculated by:

$$HQI = \frac{\sum_{i=1}^{n} \left(Lib_i - Unkn_i \right)^2}{n}$$

Eq. 3.i

In calculating the square cancelling out is avoided, but as found with conventional linear least squares regression, this can cause outliers to have a disproportionate leverage in determining the line of best fit. The resultant estimate of correlation is known as the Hit

[II] This approach was deemed appropriate within the capabilities of the software. More advanced multivariate software packages are capable of applying the normalisation function to the unknown spectrum in addition to the training samples. However, these still preclude the insertion of new samples in to the calibration, therefore requiring the classification models to be re-built if new reference samples are acquired. Private conversation with Professor T. Fearn, Department of Statistical Science, University College London, 14 April 2008.

Quality Index, returning 0 as an indication of best fit and 1 where no correlation is found. The influence of outliers resulting from baseline variations can be reduced by applying the algorithm to the spectral derivative.

The second algorithm used was the correlation algorithm. In two dimensional space, a vector relates the distance of a data point to the origin. This algorithm calculates the cosine of the angle between the corresponding vectors for the spectra of the known and unknown, after the spectra have both been mean centred. When the vectors are parallel the cosine is equal to 1, and they are said to be the same. A more in depth discussion can be found on distance measures, and cluster analysis in general, in Anderberg [6]. The equation for the correlation matching algorithm is given below:

$$HQI = 1 - \frac{\left(Lib_m \bullet Unkn_m\right)^2}{\left(Lib_m \bullet Lib_m\right)\left(Unkn_m \bullet Unkn_m\right)}$$

Eq. 3.ii

The spectra are mean centred to scale the variables. This is done by calculating the mean of the data sets and then subtracting this from each data point, as follows:

$$Lib_m = Lib - \frac{\sum_{i=1}^{n} Lib_i}{n} \qquad Unkn_m = Unkn - \frac{\sum_{i=1}^{n} Unkn_i}{n}$$

Eq. 3.iii

3.2 Case Studies

As discussed in the Introduction, the ability to identify a material on site without the need for sampling would provide museum professionals with a useful tool for successful collections management. This is especially true when interventive methods of conservation are to be applied, such as in the case of pest control, when the rapid identification of vulnerable material is of paramount importance. The optimisation of analytical conditions enabled the initial compilation of the spectral database and searching library. Following this, two site visits were made to heritage collections to test the near-infrared protocols and aid in the identification of a number of modern materials housed within the

collections. The value of the technique will be illustrated in the follow sections, whilst also highlighting areas of application that proved problematical. An overview of some of the artefacts studied during the visits will be discussed, but will not be exhaustive.

3.2.1 Methodology

The protocol adopted was influenced by the outcomes of the preliminary studies reported in Chapter 2. All analytical work was carried out using a Perkin Elmer Spectrum One Fourier-transform Near-infrared spectrometer (FT-NIR), using the Axiom probe attachment (Section 2.2.2) employing a scan range of 4 000-12 000 cm^{-1}, resolution of 8cm^{-1} and scan accumulation of 64. Spectral processing was carried out using Thermo Galactic Grams AI version 7. The background reference was Spectralon® [III]. All data were collected in Absorbance.

Textile material was analysed as a single ply, shown during the preliminary studies to reduce the effects of spectral scattering (Section 2.4.2.2, Chapter 2). The probe window was oriented parallel with the surface of interest, and where possible, in close proximity to the surface. In cases where the probe could not be in close contact with the artefact, such as where the surface of an object had become sticky due to plasticiser migration, the probe cover was used to reduce interference (Section 2.4.2.10, Chapter 2).

Spectral matching was carried out using Thermo Galactic Spectral ID library, with the application of matching algorithms to search the reference set. As explained in Section 3.1.1.4, library matching requires a degree of caution. Therefore visual comparisons and data processing, such as spectral subtractions, were applied alongside the Hit Quality Index output generated by the library. In the majority of cases the raw spectra were sufficiently characteristic to make class assignments, but on occasion the derivative spectra were calculated to maximise the signal whilst suppressing interferences.

3.2.2 Case Study I: Hampshire County Council Museums and Archives Service

The aim of the site visit to Hampshire County Council Museums and Archives Service (HCCMAS) was to study a range of garments dating from the early 20th Century, which had uncertain composition and were of interest to the conservation and curatorial departments. A list of the garments studied during the visit are presented in Table 3.3, along with the results from the library and visual spectral matching. Abbreviations for the polymer identifications are provided in Table 3.1.

[III] Spectralon® is a high reflectance, low particulate disk of polytetrafluoroethylene (PTFE).

Artefact	Acquisition Number	Area of Interest	Polymer	Processing	Matching Algorithm	HQI
Black Sequin Dress	C2000.60/38	Black Fabric	SK		Δ/*	0.2
		Sheer Black Lining	SK		Δ/*	0.0
		Black Backing Fabric	SK		Δ/*	0.0
		Shiny Black Sequins	G		Δ/*	0.0
		Dull Black Sequins	G		Δ/*	0.0
		Dull Circular Beads	G		Δ/*	0.0
		Small Black Beads	Glass		No Spectrum	
		Bugle Beads	Glass		No Spectrum	
Blue Jacket	1963.43	Blue Fabric	LN		Δ/*	0.0
		Lining	LN/SK	Subtraction	Δ/*	0.0
		Button	CN		Δ/*	0.0
Sequin Dress	C1997.65	Purple Sequins	G		Δ/*	0.0
		Gold sequins			Δ/*	0.0
		Bronze Sequins			Δ/*	0.0
		Beige Sequins			Δ/*	0.0
Jacket & Skirt	C2000.158/26	B&W Fabric	CA/VR		Δ/*	0.0
		White Lining	CA/VR		Δ/*	0.0
		Shoulder Pads	C	Subtraction	Δ/#	0.3
Stockings	C1989.41.53	Beige Leg	V/R		Δ/*	0.0
Parachute 'Silk' Slip	No accession number	White Fabric	PA		Δ/*	0.0
Parachute 'Silk' Dressing Gown	No accession number	White Fabric	PA		Δ/*	0.0

Evening Dress	C2000.67.9	Purple Taffeta	CA		Δ/*	0.0
		Blue Gauze	SK		Δ/*	0.0
Tea Gown	C2006.370	Brown Fabric	SK		Δ/*	0.0
		Cream Netting	SK		Δ/*	0.0
		Collar Lining	C		Δ/*	0.0
Tea Gown	No accession number	Pale Blue Fabric	SK		Δ/*	0.0
		Cream Netting	LN		Δ/*	0.0
Black Mantle	1966.1297	Black Fabric	SK		Δ/*	0.0
		Black Sequins	G		Δ/*	0.1
		Lining	LN		Δ/*	0.0
		Interlining at Necking	Unidentified	Subtraction	Δ/#	
Set of Pyjamas	1965.736/1	Lime Fabric	V/R		Δ/*	0.0
		Cream Lace	LN		Δ/*	0.0

Table 3.3 Library and visual matching results from the onsite analysis of the textile and dress collection at HCCMAS. Least squares algorithm (*), correlation algorithm (#) and visual comparison (Δ)

The following section will highlight the methods used to identify the various components of a sequin dress studied at HCCMAS. The application of the two different matching algorithms is illustrated and their application discussed. In addition, an example of spectral processing is given, along with an example of one of the limitations of the NIR technique. This example is provided as a means of interpreting the remaining classifications presented in this, and the following two, onsite Case Studies.

3.2.2.1 Results and Discussion

3.2.2.1.1 Sequin Dress

Two sequin dresses were of particular interest, due to the deterioration of the sequin adornments. In both cases some of the sequins had started to curl, accompanied by a dull surface and loss of lustre (Figure 3.34). In the image below it is possible to see the Spectralon® reference tile. This was used when acquiring spectra from thin layers of textile, preventing the material behind the layer of interest being sampled.

Figure 3.2 Image of one of two dresses found to have gelatine based sequins within the HCMAS textile collection (HCCMAS C200.60/38)

It can be seen from Table 3.3 that different searching algorithms were required for the identification of the garments. As mentioned in Section 3.1.1.3, visual inspection accompanied the application of the matching algorithms, as the library software always provides a result, even if the sample of interest is not held within the dataset. The software interface enables the matched spectra to be viewed with that of the unknown for ready visual inspection. Figure 3.3 shows the searching result for the sequins from the black sequin dress. A classification of melamine formaldehyde was given as the closest spectral match when using the correlation algorithm. On inspection of the two curves it is clear that the two spectra are distinctly different from each other.

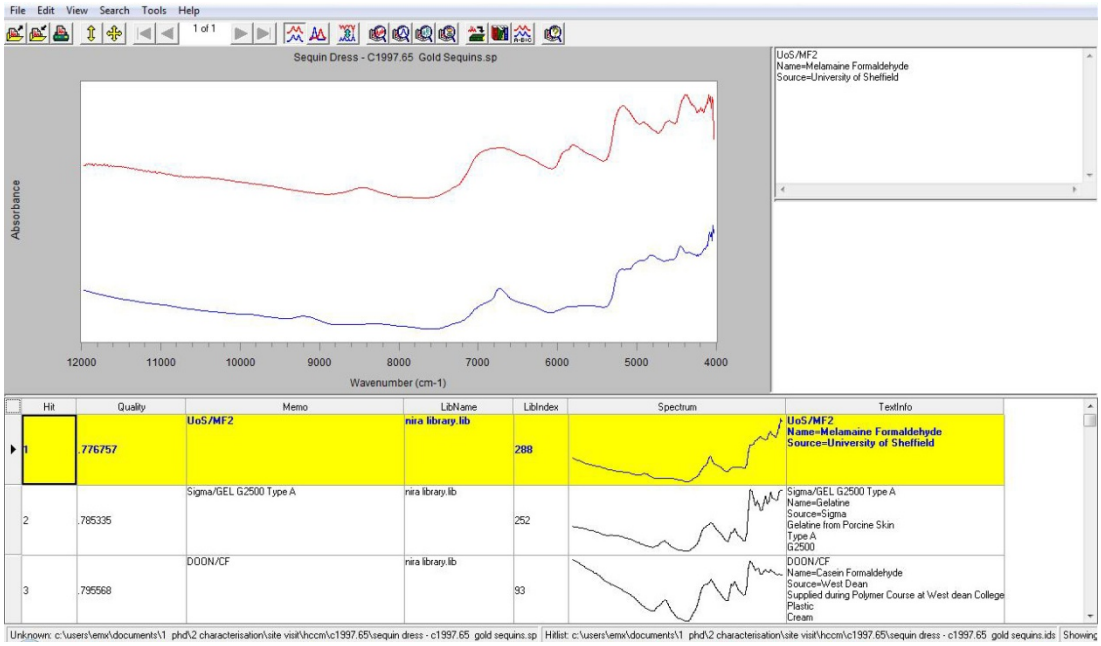

Figure 3.3 Misclassification of black sequins using the correlation algorithm in SpectralID. The closest match being melamine formaldehyde (blue curve) to the unknown sample (red curve).

The clear differences in the two curves indicated that the match provided by the algorithm was not correct. Therefore, the least squared algorithm was applied to the same unknown sample. Figure 3.4 shows the results from this spectral match, returning gelatine as the closest spectrum within the library. On visual inspection it is apparent that the two samples have similar spectral features. Coupled with the fact that gelatine has been used widely as a base for sequins, they were classified as gelatine [7].

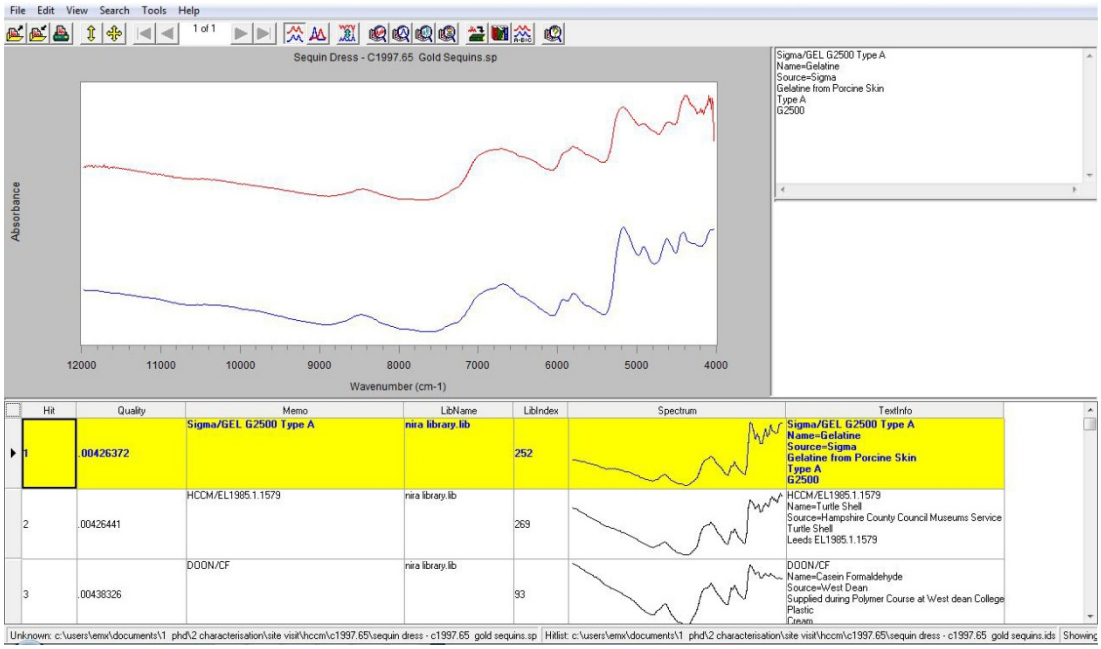

Figure 3.4 Classification of black sequins using the least squares algorithm in SpectralID. The closest match being gelatine (blue curve) to the unknown sample (red curve).

Sequins dating from the time of this dress (early 20th Century) were often found to contain cellulose nitrate. The raw spectrum was processed using the spectral subtraction method mentioned in Section 2.3.3, Chapter 2, with a subtraction factor of 0.3, where a reference gelatine spectrum was subtracted from that of the sample. The presence of cellulose nitrate was not apparent in the remaining spectrum (Figure 3.5). The ability to establish whether such unstable material is present or not aids informed storage and highlights one of the beneficial applications of the NIR technique.

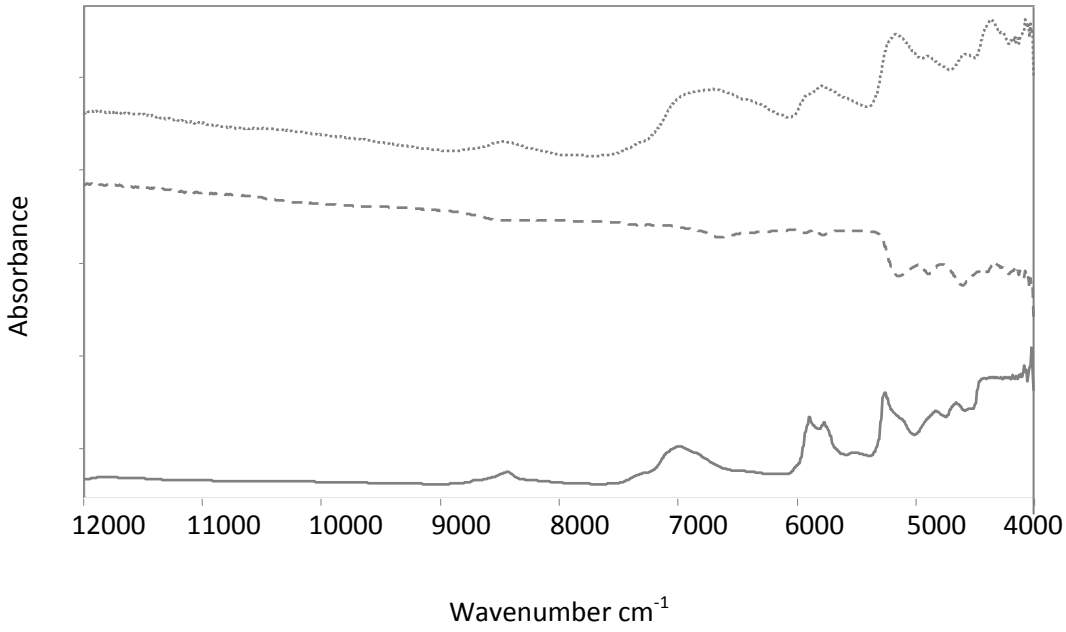

Figure 3.5 Offset, subtracted NIR spectra to assess the presence of cellulose nitrate within the gelatine sequins. Raw spectrum of sequin (dotted), spectra after spectral subtraction (dashed) and cellulose nitrate reference (solid)

There were a large number of small beads attached to the black sequin dress. Figure 3.6 shows the raw NIR spectra of a sample of beads. The lack of spectral information is apparent, and leads to the conclusion that the beads were made of glass rather than a synthetic polymer. Silica glass is transparent in the NIR region of the spectrum, and it is this property that is exploited when using fibre optic probes for remote analyses. Therefore it is not possible to gain NIR spectral information from such samples.

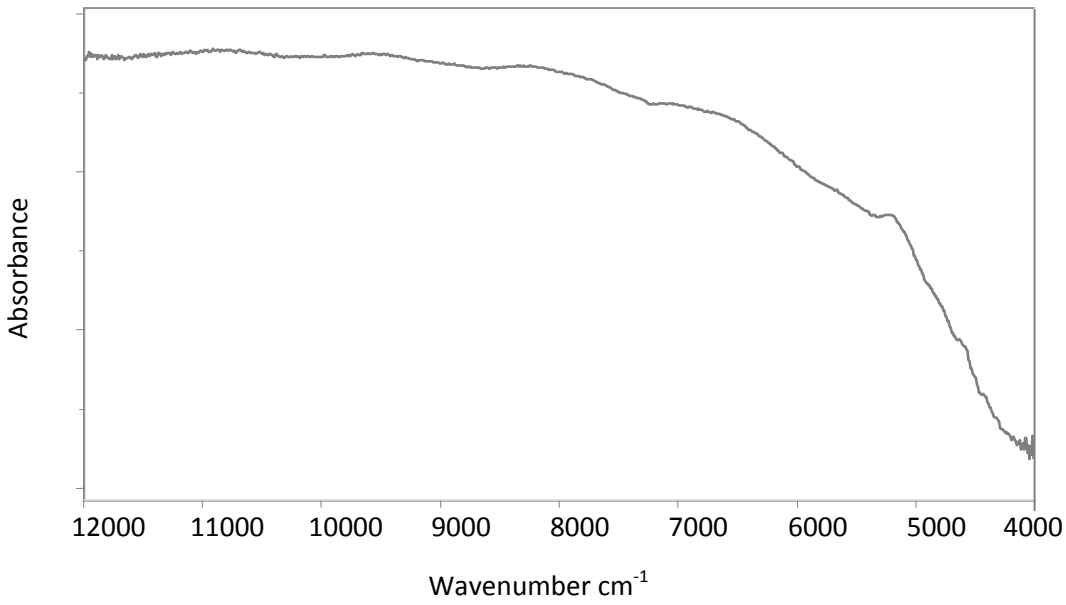

Figure 3.6 NIR absorbance spectrum of a glass bead

3.2.2.1.1 Parachute 'Silk' Slip

During the Second World War rationing had a major effect on the availability of luxury items, with textiles being no exception. Fabrics such as lace and satin were not available, and it was not uncommon to adapt material from other applications. The silk from discarded or surplus parachutes was often used for wedding gowns and undergarments, and the slip studied here was catalogued as such. The results from the NIR analysis showed the garment to be in fact polyamide and not silk. Figure 3.7 shows similar spectral features between polyamide and silk, this is owing to the amide vibrations experienced in both polymers. Conversely the second derivative spectra exhibit clear distinction between the silk reference sample and that of the unknown and polyamide reference (Figure 3.8).
This case illustrates the benefit of spectral processing to highlight subtle differences in the NIR spectrum. It also serves to illustrate the types of problem curators and conservators face when cataloguing a collection. The visual characteristics of silk and polyamides can be very similar, and without the necessary means of identification, misclassification can occur.

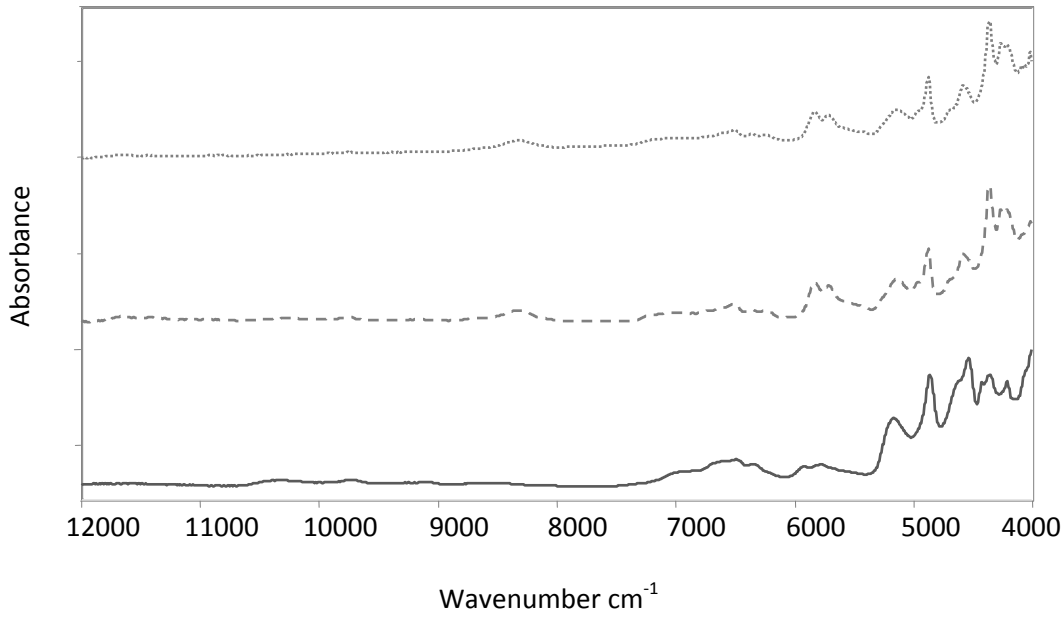

Figure 3.7 Offset NIR absorbance spectra of the Parachute 'Silk' Slip (dotted), polyamide reference (dashed) and silk (solid)

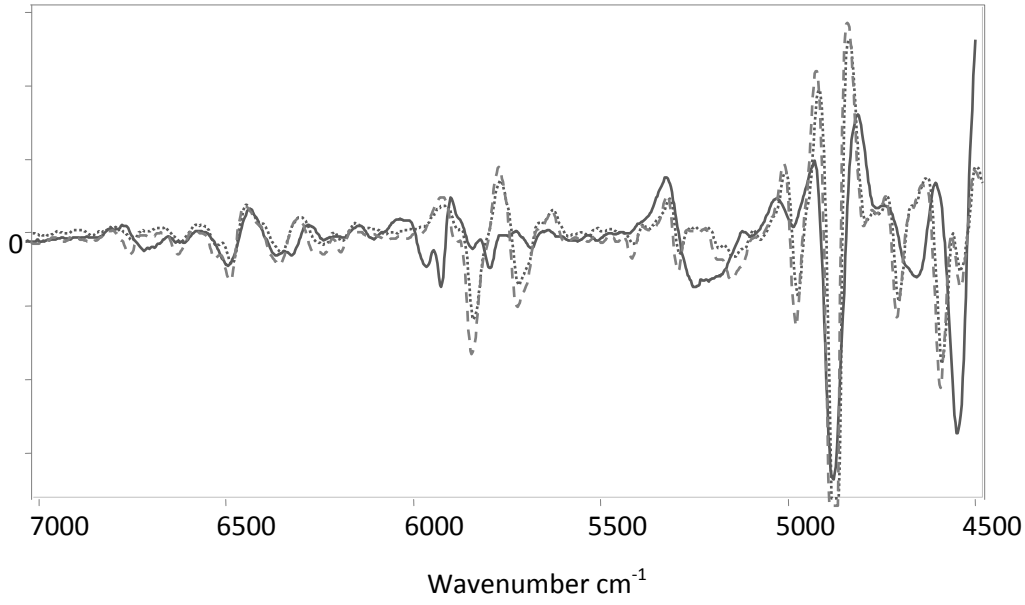

Figure 3.8 Overlaid second derivative NIR spectra of the Parachute 'Silk' Slip (dotted), polyamide reference (dashed) and silk (solid)

3.2.3 Case Study II: Contemporary Textiles Collection, Victoria and Albert Museum

Having spoken at length with the textile curatorial department at the V&A [IV,V], it became apparent that there were two distinct categories within the contemporary textile collection that were cause for concern. These were the shoe collection and the painted T-shirt collection. Both showed similar signs of degradation such as sticky surfaces, yellowing and brittleness. Although these artefacts had been flagged as requiring attention the materials of construction had not been ascertained.

The physical structure of these artefacts made removal of sample material difficult. This presented an ideal opportunity to demonstrate the application of NIR spectroscopy via a remote optical probe, which enabled rapid identification without the need for sampling.

A two week site visit was made to the Contemporary Textile Collection at the Victoria and Albert Museum, to study a cross section of artefacts. Table 3.4 contains the details of a selection of the objects studied during the visit.

[IV] Personal conversation with Sue Pritchard, Curator of Flat and Hanging Textiles, Furniture, Textile and Frames Section, Victoria and Albert Museum, 5 January 2006.

[V] Personal conversation with Susanne Smith, Keeper of Collections, Furniture, Textile and Frames Section, Victoria and Albert Museum, 31 July 2006. Discussion and site visit to assess the major areas of concern within the V&A's contemporary textiles collection.

Artefact	Acquisition Number	Area of Interest	Polymer	Processing	Matching Algorithm	HQI
Black Patent Shoes	T458 1974	Black Upper	PU-PE		Δ	
		Brown Lining	Leather		Δ/*	
		Black Sole	Leather		Δ/*	
Clear Shoe with Black Bow detail	T331 1978	Clear Upper	PVC		Δ/*	0.0
		Cream Lining	Leather		Δ/*	0.0
		Black Fabric	Silk/Polyamide		Δ/*	0.0
		Black Sole	Poor Spectrum		Δ/*	
Clear upper with pink patent edging	T380 1974	Clear Upper	PVC		Δ/*	0.0
		Pink Patent	PU-PET		Δ/*	0.0
		Cream Lining	Leather		Δ/*	0.0
		Sole	Leather		Δ/*	0.0
Yellow Patent	T3561 1974	Yellow Upper	PU-PE			0.0
		Beige Lining	Leather		Δ/*	0.0
		Sole	Leather		Δ/*	0.0
Silver upper with clear ankle strap	T97 1988	Silver Upper	Leather		Δ/*	0.0
		Clear strap	PVC		Δ/*	0.0
White Patent Loafers	T226 1990	White Upper	PU-PE		Δ/*	0.0
		Black Lining	Leather		Δ/*	0.0
		Black Sole	Poor Spectrum			

Blue ‘jelly’ shoes	T644:1-1996	Blue Upper	PVC		Δ#	0.1
		Blue Inner	PVC		Δ/#	0.2
		Clear Heel	PMMA		Δ/#	0.1
Timberland Boots		Beige upper	Leather		Δ/*	0.0
		Cream sole	PU-PET		Δ/#	0.0
Guns and Roses t-shirt	T608 1997	Black Fabric	C		Δ/*	0.0
		White Paint	PVC		Δ/*	0.0
		Orange Paint	PVC		Δ/*	0.0
Grateful Dead t-shirt	T607 1997	White Fabric	C		Δ/*	0.0
		White Paint	PVC		Δ/*	0.0
		Red Paint	PVC		Δ/*	0.0
		Blue Paint	PVC		Δ/*	0.0
Tiedye t-shirt	T629 1997	Green Fabric	C		Δ/*	0.0
		Yellow Paint	PVC		Δ/*	0.0
Pink Swirl t-shirt		Pink Fabric	C		Δ/*	0.0
		Pink paint	PVC	Subtraction	Δ/#	0.0
		Orange paint	PVC	Subtraction	Δ/#	0.0
		Black paint	PVC	Subtraction	Δ/#	0.1
		White paint				
Green ‘Paper’ Jacket	T6791-1991		PE ‘Tyvek’		Δ/*	0.0
White ‘Bauble’ Scarf		White Fabric	PA		Δ/*	0.0
		Baubles	PS	Subtraction	Δ/#	0.2
Wedding Dress	T81:2-2003	Coated Fabric Head Dress	PA		Δ/#	0.0

		Head Dress, Coating	CA		Δ/#	0.0
		Mesh Fabric	PA		Δ/#	0.0
		White Netting	PA		Δ/#	0.0
		Cream Thread	PET/C		Δ/#	0.0
		Quilting	C		Δ/#	0.0
		White Lace	PA		Δ/#	0.0
Textile Wall Hanging 'Diaspara'	New Acquisition	Brown Square Patch	PU-PE		Δ/#	0.0
		Grey Netting Ground	SK		Δ/#	0.0
		Cream Patch	PU-PE		Δ/#	0.0
		Raised Circular Decoration	LR		Δ/#	0.0
		Brown Printed Fabric	SK		Δ/#	0.0
Treaded Wall Hanging	T486-2003	Pink Weft	PA		Δ/#	0.0
		Red Weft	SK		Δ/#	0.0
		White Weft	PA		Δ/#	0.0
		Orange Weft	SK		Δ/#	0.0
		Fusia Weft	SK		Δ/#	0.0
		Transparent Warp	PA		Δ/#	0.0
Fake Fur Coat	T81-1991	Black Fur	V/R		Δ/#	0.0
		Lining	V/R		Δ/#	0.0

Table 3.4 Library and visual matching results from the onsite analysis of the Contemporary Textile Collection, V&A. Least squares algorithm (*), correlation algorithm (#) and visual comparison (Δ)

3.2.3.1 Results and Discussion

Textile material from a number of shoes within the V&A's collection were examined, dating from the 1960's to the present day. Those under investigation were showing visible signs of degradation and required materials identification before discussions with the conservation department to assess future treatment, stabilisation and storage.

3.2.3.1.1 Silver Shoes with Transparent Ankle Straps

One such example was the yellowing of once clear, transparent material, accompanied by the formation of a stiff and rigid structure of the straps of a pair of Charles Jourdan shoes (Figure 3.9). This type of deterioration was seen throughout the shoe collection, with the near-infrared analysis revealing the material as polyvinyl chloride (PVC) (Figure 3.10). Such yellowing is likely to be caused by an increase in unsaturation during polymer degradation, with the stiffening of the material caused by loss of plasticizer [8, 9].

Subsequent analyses have shown that the twin peaks visible at 4 669 and 4 625cm^{-1} and the single peak at 6 018cm^{-1} are only seen in the NIR spectrum of plasticized PVC. On subsequent comparison with a phthalic acid reference supplied by Sigma Aldrich, two peaks can be seen in this region of the spectrum (Figure 3.11), which relate to the second overtones of two carbonyl stretches [10]. This suggests a contribution from phthalate ester plasticizer in the ankle strap, and illustrates the possibility of using NIR spectroscopy for the determination of polymer additives.

Figure 3.9 Image showing the deterioration of a degraded polyvinyl chloride ankle strap on a pair of shoes within the V&A's Contemporary Textile Collection (V&A T97 1988)

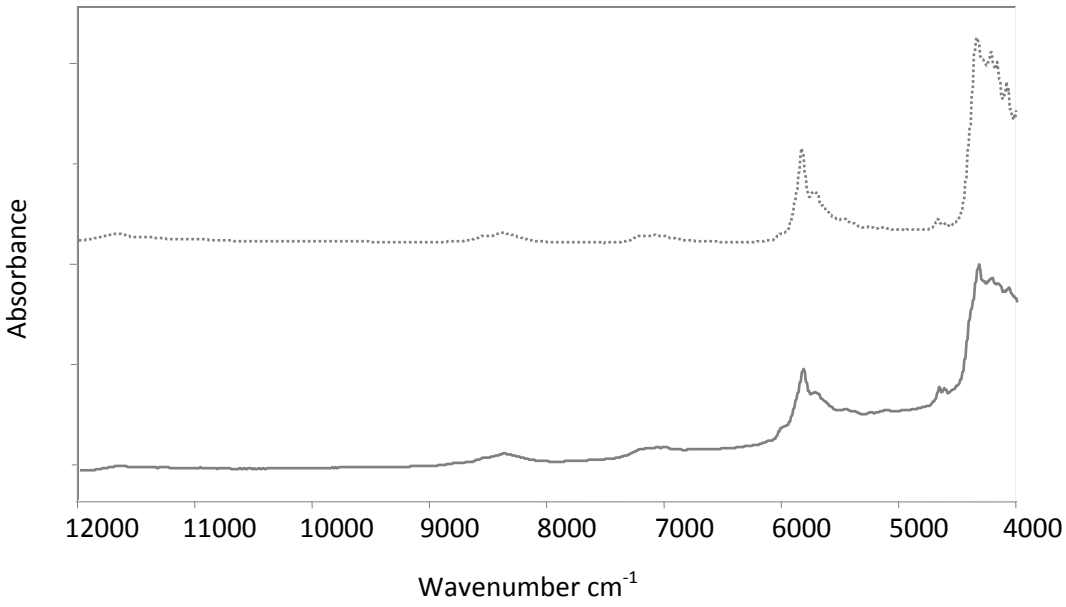

Figure 3.10 Offset NIR absorbance spectra of the unknown clear ankle strap (dotted) and a plasticised polyvinyl chloride reference (solid)

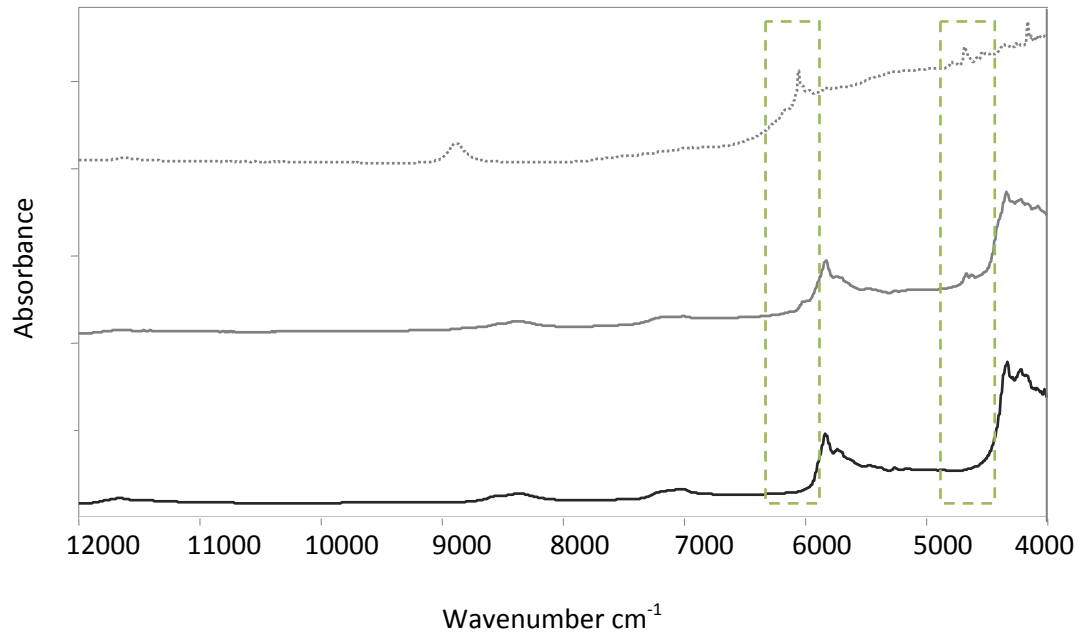

Figure 3.11 Offset NIR absorbance spectra of phthalic acid reference (dotted), plasticised PVC reference (solid grey) and unplasticised PVC (solid black). Boxed regions highlighting the peaks related to phthalate ester plasticiser content

3.2.3.1.2 Black Patent Shoes

Two pairs of patent leather shoes by the designer Roger Vivier, dating from 1963 and 1966, were of particular interest. Both pairs were of identical design and construction, but the later pair was showing significant signs of deterioration in the patent coating. The coating had become very sticky, possibly caused by the migration of plasticizer, which had resulted in both shoes becoming adhered together (Figure 3.12). Recent storage of the shoes had involved the insertion of padding into the shoes and wrapping with acid free tissue paper (Figure 3.13). Unfortunately, the tissue paper had become attached to the sticky surface, preventing future display and enforcing difficult decisions regarding conservation treatment.

The application of near-infrared spectroscopic analysis proved difficult due to the high specular reflectance from the patent surface. The resultant spectrum of the coating is weak, containing limited information. The low signal and high noise prevented the library algorithms from finding a suitable match (Table 3.4). On visual inspection the spectral signal is sufficient to identify the coating as polyurethane polyether. This highlights one of the limitations of the technique, which is dominated by diffuse reflectance (Figure 3.14). In such cases, alternative methods, such as attenuated total reflectance Fourier transform infrared spectroscopy, may prove more productive. However, this would require a sample to be removed, or if applied directly the ATR crystal may leave an impression on the surface of the shoe. The importance of identification would then need to be weighed up against potential loss of material.

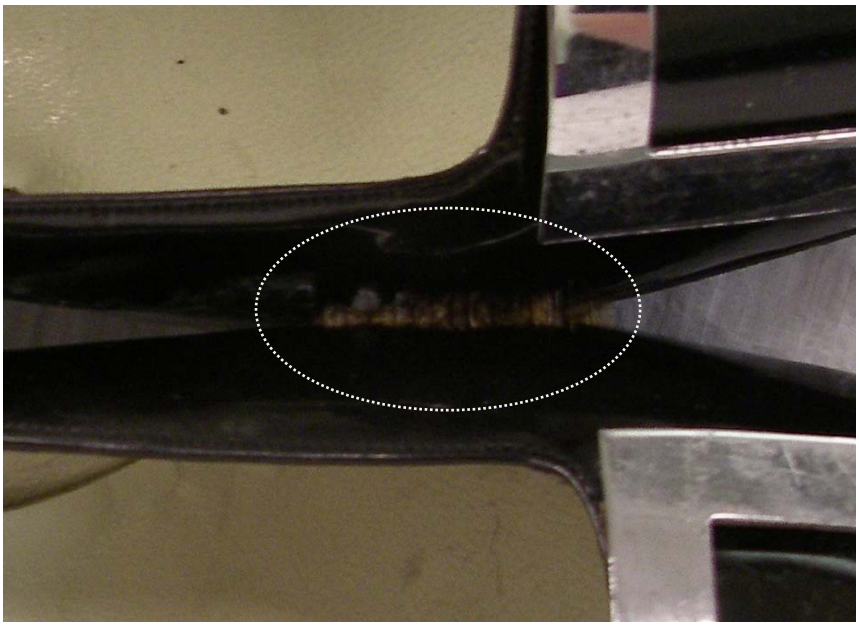

Figure 3.12 Image showing the migration of plasticizer and adhesion of two patent shoes dating from 1966 by Roger Vivier held within the V&A's Contemporary Textile Collection (V&A T458 1974)

Figure 3.13 Image of the deterioration and adhesion of paper to the patent coating

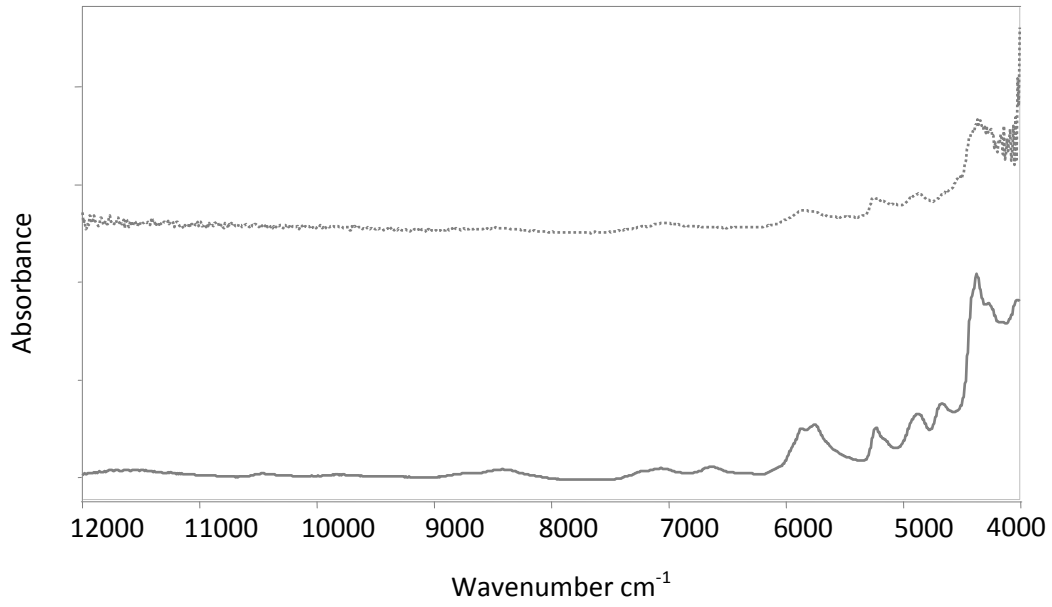

Figure 3.14 Offset NIR absorbance spectra of the black patent coating (dotted), showing weak spectral bands due to high reflectance and a polyurethane polyether reference (solid)

3.2.3.1.2 'Bauble' Scarf

Near-infrared spectroscopy can achieve sampling depths in the region of a few millimetres, making this a non-contact method of analysis with the possibility of depth sensitivity (Section 2.5.2.3, Chapter 2). This depth sensitivity can be exploited to analyse material that is not readily accessible, removing the need for invasive sampling. The image in Figure 3.15 is of a white 'bauble' scarf, comprising of a woven tube of fabric within which a number of spherical structures were inserted and stitched into place.

Figure 3.15 Image of the white 'bauble' scarf (no accession number)

By applying the spectral subtraction method it was possible to identify the internal architecture of the scarf. This was achieved by analysing a region comprising both the upper fabric and the substrate layers in addition to sampling the fabric alone. The upper fabric was identified as polyamide (using the least squares algorithm) and was subtracted from the combined spectra. The substrate was identified as polystyrene using the correlation algorithm, without the need for invasive sampling (Figure 3.16). It is worth noting that the correlation algorithm has proved particularly useful for subtracted data (Table 3.4), where peaks reminiscent of derivatives are often found in the residual spectrum. By centring the spectral data points about their respective means rather than forcing a baseline of zero, effective matches between the library and unknown spectrum have been found more readily found.

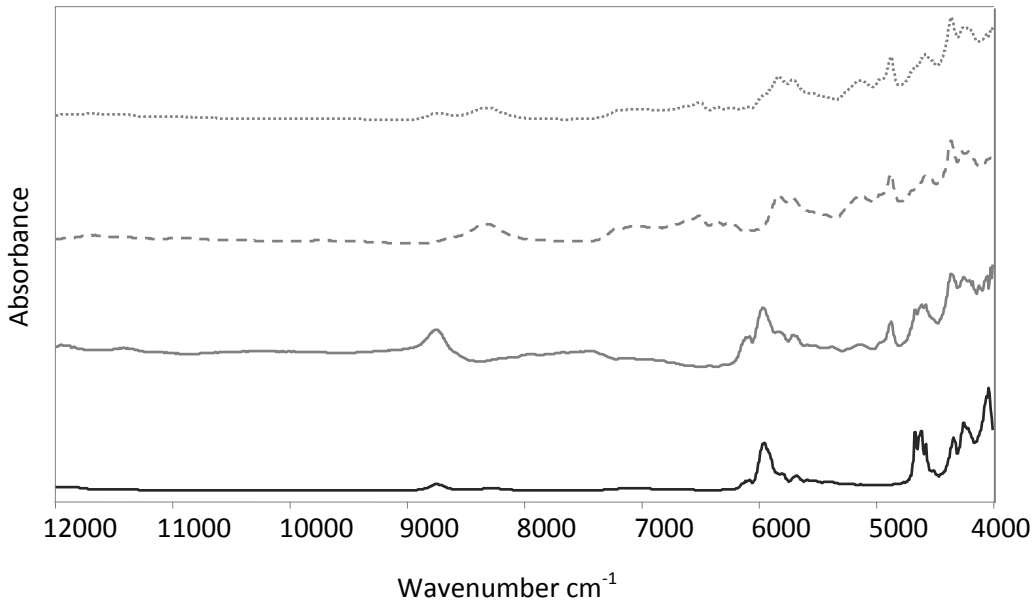

Figure 3.16 Offset NIR absorbance spectra revealing the underlayers of the 'bauble' scarf as polystyrene. Substrate and fabric (dotted), fabric without substrate (dashed), substrate after subtraction method (solid grey) and polystyrene reference (solid black)

3.3 Conclusions

Due to the number of different synthetic polymer classes composing contemporary textiles and their range of behaviour, the issues facing conservators and curators of 20th Century collections are varied. Unlike natural fibres, the polymer processing methods for synthetic fibres generally preclude classical methods of identification, such as microscopy, due to limited surface features. In addition, the physical form of an artefact can often restrict the removal of a representative sample. This illustrates the need for a non-invasive method of characterisation, readily enabling collections surveys and providing conservators with a means of materials identification to inform decisions regarding preventive and interventive treatment. The collation of a reference database was the first step in achieving the goal of onsite characterisation. Coupled with commercial library software, the searching of unknown samples was made possible.

Two site visits showed that it was possible to distinguish between the major classes of synthetic material held within contemporary collections. However, factors such as patent reflective surfaces did have a detrimental effect on the NIR spectrum, reducing signal and

increasing spectral interferences. These factors do not in all cases prevent positive characterisation, but may limit the application of the technique to identification purposes. There was no evidence that spectral matching was hindered by the condition of the sample material, but this is one area of research that would benefit from further work. The samples used for the spectral database were all new, subsequently being used for the discrimination of aged textile artefacts. For the objects studied here the spectra remained characteristically distinct, enabling positive identification. However, for lesser additive components, or for heavily degraded material, spectral alterations may prevent ready identification.

Due to the complicated nature of the spectra and spectral interferences caused by scattering, the matching algorithms can give disproportionate weighting to variations in light scattering, instrument noise and rising baselines. The application of cluster analysis algorithms must be undertaken with caution, with spectral variations and features not held in the data set producing poor correlations and false positive results (Section 3.2.2.1.1). It is not possible to apply the analysis as a "black box" method, as it still requires a significant amount of data interpretation [11]. Therefore visual comparisons and spectral processing, such as first and second order derivatives, accompany data analysis. It was with this in mind that multivariate analysis methods were subsequently investigated as an alternative means of providing a more robust method of classification. The results of these are presented and discussed in Chapters 6 and 7.

3.4 References

1. Hall, G.S. *Use of Commercial Software to Create FTIR, EDXRF and Raman Spectral Databases to Assist in Pigment Identification*. in *7th Biannual IRUG Conference*. 2006. Museum of Modern Art, New York.
2. Fischer, D., T. Bayer, and M. Otto, *In-line Process Monitoring on Polymer Melts by NIR-spectroscopy.* Fresenius Journal of Analytical Chemistry, 1997. **359**: p. 74-77.
3. Hall, J., W, D. Grzybowski, E, and S. Monfre, L, *Analysis of Polymer Pellets Obtained Form Two Extruders Using Near Infrared Spectroscopy.* Journal of Near Infrared Spectroscopy, 1993. **1**: p. 55-62.
4. Blanco, M., et al., *Use of Near-infrared Spectroscopy in Control Analyses of Acrylic Fibre Manufacturing Processes.* Analytica Chimica Acta, 1999. **383**: p. 291-298.
5. Dhanoa, M.S., et al., *The Link Between Multiplicative Scatter Correction (MSC) and Standard Normal Variate (SNV) Transformations of NIR spectra.* Journal of Near Infrared Spectroscopy, 1994. **2**: p. 43-47.
6. Anderberg, M.R., *Cluster Analysis for Application*. 1973, London: Academic Press.

7. Chung, A. *A Study of Sequins on a Cantonese Opera Stage Dress* in *AHRC Research Centre for Textile Conservation and Textile Studies Second Annual Conference: The Future of the 20th Century - Collecting, Interpreting and Conserving Modern Materials*. 2005. Winchester: Archetype Publishers.
8. Garcia, D. and M. Cibulsky, *Near Infrared Studies of PVC Film Photodegradation.* Journal of Vinyl and Additive Technology, 2005: p. 39-46.
9. Owen, E.D.e., *Degradation and Stabilisation of PVC*. 1984, Barking: Elsevier Applied Science Publishers Ltd.
10. Siesler, H.W., *Near-Infrared Spectroscopy: Principles, Instrumentation, Applications*, ed. H.W. Siesler, et al. 2002, Weinheim: Wiley-VCH.
11. Esbensen, K.H., *Multivariate Data Analysis: In Practice*. 5th ed. 2002, Esbjerg: Camo.

Chapter 4: A Question of Stability: The Effect of Pest Eradication Treatments on Synthetic Polymers

The following Chapter will provide a review of the current literature relating to the stability of polymers subjected to pest eradication methods. The application of raised and lowered temperatures to combat the problem of pest infestations are common within the museum and heritage sector. Since natural organic polymers are a source of food for insect pests, their behaviour during treatment has been studied widely. However, the effect of treating synthetic material with pest control methods has been largely overlooked. This is due to the fact that synthetic polymers are not eaten by insects. However, they are widely found in conjunction with natural polymers, in composite materials or applied as conservation treatments. As such, it may be necessary to concurrently treat such material during an infestation.

Many conservation professionals have raised concerns about applying these methods to synthetic material, with some opting to remove such material before treatment. These concerns stem from the changes in thermal properties known to occur over the range of temperatures in question. In the later sections of this chapter, an overview of the issues will be provided, setting the scene for a more in depth discussion of the physical properties in the next Chapter.

4.1 Pest Eradication Treatments in Heritage Collections

The issue of pest control and pest management within museums and the heritage sector has received increasing interest in recent years, resulting in a number of conferences devoted to the subject, the most recent being the multidisciplinary conference, 2001: A Pest Odyssey [1], organised jointly by the Science Museum, English Heritage and the National Preservation Office. The aim of the meeting was to highlight the developments within the sector to combat the problem of pest infestations, and raise awareness of these widespread issues in collections.

Pinniger [2] states that pests need just four key things for sustainable life: food, harbourage, warmth and water (or humidity). This therefore makes all organic based museum collections vulnerable to attack by insect pests, as they supply a ready source of food. The materials most at risk from attack and infestations are protein based artefacts, which will provide nourishment. These include materials such as silk, wool, feathers, fur and leather. Cellulosic materials are not so commonly eaten in isolation, unless in the presence of silverfish or carpet beetle [3]. However, they will often be subject to attack if this will allow access to proteinacous material.

Museums and keepers of heritage collections have, of late, focused on preventative rather than reactionary measures of pest control, dealing with the problem in a holistic manner, through the implementation of Integrated Pest Management programmes (IPM). The principles of IPM include the monitoring of pest traps, monitoring of the types of pests found, temperature and humidity regulation and thorough housekeeping. Reactionary measures of eradication are only used when absolutely necessary, thus reducing the risks both to objects and personnel [4-7]. The role of IPM is to prevent infestations from occurring, and although the monitoring of traps and ventilation systems are methodical and rigorous, it is still common for infestations to occur, posing a major threat to artefacts and collections as a whole [8]. In such an event, the priority for the keeper of the collection is to quickly and efficiently apply the most appropriate method of eradication to ensure 100% mortality, without endangering the object in question, or the personnel implementing these treatments.

When such cases arise there are a number of options available to the conservator or curator designed to resolve the problem. These include fumigation with toxic gases, anoxia, or raised and lowered temperature treatments.

The first of these methods introduces toxic gases, such as methylene bromide, ethylene oxide or phosphine, into the space surrounding the object or collection in question [2]. These gases, known to be lethal to all stages of insect life, are allowed sufficient exposure time to permeate the material and poison the insects [9]. However, the use of fumigation has been placed under tight restrictions in many countries due to concerns regarding human health and the environment. Therefore, other methods of eradication have been investigated to identify safer, alternative methods of treatment.

4.1.1 Anoxic Environments

Low oxygen techniques, known as anoxia, cause mortality in insects through a double process of asphyxiation and desiccation [10]. This is achieved either by purging the surrounding environment with nitrogen or argon [11] or by removal of oxygen using oxygen scavengers, such as Ageless®, a sacrificial iron based absorber. During both methods, oxygen will decrease in supply causing the insect to open their spiracles. These are a number of orifices leading to their trachea, and this action in turn leads to the dehydration of the insect. Although the mortality success rates are high, there are a number of drawbacks to both these approaches. In order to lower oxygen successfully to a level that is capable of killing insects (0.2% ± 0.1), large objects need to be placed within sealed enclosures, which can be costly to achieve [12, 13]. For smaller objects, oxygen scavengers placed with the object in oxygen barrier bags prove more viable, but again the cost of the scavengers can be high [2]. Another limitation can be the length of time required for these methods to ensure complete mortality. This can be in the region of 2-3 weeks, therefore preventing the method from being applied rapidly and routinely, as is often required, for example during the treatment of travelling exhibitions.

The anoxic environment is known to be of benefit to many objects, organics in particular, through inhibiting oxidative reactions [14]. However, where composite material is being treated care must be taken to ensure that materials which are readily reduced are not exposed to these environments. Rowe [15] has recently reported on the effects of anoxic insect fumigation on textiles dyed with Prussian blue. The experiments were carried out on modern textiles dyed with traditional methods. The colour measurements and FTIR analyses supported the concerns that anoxia may cause partly irreversible changes to the dye, thus prompting the recommendation that these treatments should be avoided in the presence of such colourants. However, Maekawa and Elert [16] have reported that the timescales used to eradicate insects under these conditions are not sufficient to induce fading of pigments and dyes. They did however, raise the issue of damage to artefacts caused by rapid moisture loss, owing to the low humidity levels of nitrogen atmospheres. This difficulty can be circumvented by the use of humidification pump.

4.1.2 Raised Temperature Treatments

The use of raised temperature disinfestation as an alternative has become popular within museums and heritage due to the relatively low cost of implementation and the short time periods required to achieve mortality. None the less there are still serious concerns held by

the heritage profession regarding the possible detrimental effects they might have on the objects under their care[I].

Ackery *et al* [17] reported on work during the 1980's into the application of raised temperatures to overcome an infestation of furniture beetle in the Entomology department at the National History Museum, London. Temperatures of 55°C were applied to part of the collection housed in wooden storage containers, which resulted in warping and deformation of the storage. This raised concerns and prevented the practice from developing further, even though the infestation was successfully curtailed. More recent work by the same co-workers reported that this deterioration was due to fluctuations in RH, rather than changes in temperature [18].

The majority of the stages in insect pest life cycles, from eggs through to adult, are killed when exposed to temperatures of 52°C, with the exception of the House Longhorn beetle, which requires temperatures of 55°C [2, 19]. As highlighted in the above example, these temperatures can cause problems of stability unless the relative humidity[II] surrounding the object remains stable. The RH surrounding the object is key to it maintaining physical stability, due to the moisture equilibrium of an object within its surrounding atmosphere [19]. If the surrounding RH is too low then the object will lose moisture, too high and it will take moisture up, causing contraction or expansion, respectively. This can be avoided either by enclosing small objects in sealed bags [20], or on a larger scale, via the Thermo Lignum WARMAIR® process. This latter case is a commercial process that employs a large temperature controlled, insulated chamber. The issues of moisture loss and dehumidification of the object are then overcome by careful control of the RH as the temperature rises and falls. The RH within the chamber is monitored throughout the cycle, which is usually in the region of 16-24 hours. A solid piece of wood, into which a Protimeter[III] has been placed, is used as a guide to monitor the thermal penetration of the treatment and the environment adjusted accordingly [21].

[I] Personal conversations and communications with textile conservators at the Textile Conservation Centre, Victoria and Albert Museum, National Museums of Scotland, Glasgow Museums and Hampshire County Council Museums and Archives Service, to be discussed in Section 4.3.

[II] Relative humidity (RH) is the percentage of water vapour present at a given temperature relative to the amount needed for saturation.

[III] A Protimeter is used to measure the percentage moisture content of wood, determined by measuring the electrical resistance between two probes.

Due to the concerns expressed across the conservation profession regarding high temperature treatments, there have been a small number of recent studies looking into their effects on organic and inorganic material. Unfortunately, these have primarily concentrated on new material, rather than on aged samples, and so may not necessarily be representative of the condition of objects found within collections. Beiner and Ogilvie [22] were one of the few to report on the effects of these treatments applied to historical material, thus giving a clearer idea of how artefacts may behave. Their findings indicated that there were no chemical or physical changes to decorative wooden surfaces or to bone and teeth, as determined by FTIR and SEM analysis. There were on the other hand some changes in the surface character of papyrus samples highlighted by microscopy, and the results from tensile analysis of leather appeared to indicate a small degree of permanent deformation. However, the tensile changes were small and may have been due to variations in the hide samples. Ackery and co-workers [17] studied the short term effects of high temperature disinfestations on the structure of DNA and its impact on future molecular characterisation. DNA extraction was used to compare control samples of butterfly and moth specimens from the collection at the Natural History Museum, with extractions from the same species after Thermo Lignum® treatment at 52°C. They found that both new and naturally aged samples (20 years) could be successfully sequenced after treatment. In fact, for one set of samples there appeared to be an enhancement in the extractable matter gained after treatment, attributed to the increase in relative humidity used during treatment relative to the collection storage. Although this work proved promising for the successful application of heat disinfestations to entomological collections, the authors stated that further work was needed to clarify the long term effects of such treatments, and they proposed re-visiting the samples in future work.

4.1.3 Low Temperature Treatments

A survey carried out by Beiner and Ogilvie [22] showed that the most widely used method of pest control within UK museums is low temperature treatments. This is partly due to financial reasons restricting the use of external contractors, but also because of the relative ease with which the technique can be implemented, enabling in-house treatment and rapid execution when faced with an infestation. There is, however, a degree of concern within the heritage sector relating to the short and long term effects that low temperatures will have on museum collections.

Low temperature treatments rely on the fact that most insect pests will die when exposed to a rapid drop in temperature to below -18°C. Although there are some species which will

survive temperatures down to around -40°C, these are not problematic in the context of collections infestation [2]. The accepted protocol for low temperature eradication is to subject specimens to -18°C for 14 days or to -30°C for a duration of 72 hours [23]. The literature states that the drop in temperature needs to be rapid, although there are no timescales quoted [2, 24, 25]. This is to avoid acclimatisation by the insects, which will readily adapt to low temperature environments so that the treatment will not be successful. This can prove problematic if the ambient conditions of the samples are relatively low temperature before treatment and insects have already acclimatised.

For samples of varying thickness the temperature within the object should be monitored, in addition to the external atmosphere, to ensure that the desired temperature is reached. This can be carried out using data loggers [3]. Any object being placed in to freezing temperatures is bagged prior to treatment and as much air removed from the surrounding space as possible. This reduces the risk of condensation forming as the object is acclimatised after treatment. Condensation is formed if the temperature of the air is lowered below its saturation point, known as the Dew point, reaching a point where it is no longer capable of holding the same level of moisture, resulting in the precipitation of liquid [26]. As an object is brought back up to room temperature after treatment a microclimate exists at the surface, where the surrounding air temperature is lowered and converts water vapour into liquid. The benefits of using sealed bags to enclose an object is a reduction of the volume or pressure of air surrounding the object, decreasing the level of moisture available for condensation to form. These bags also act as a barrier between the external air and the object surface, reducing the risk of condensation on the object. If condensation does form on the surface of a porous material then moisture may be adsorbed. This poses problems for artefacts, such as dimensional changes at the surface of an object, alterations in elastic properties of material under tension, migration of colourants, and water staining.

Although the temperatures employed are below the freezing temperatures of water, the formation of ice crystals is not found to be a problem in dry samples. Williams *et al* [27] studied the effect of hydrothermal stability on collagen in rodent skin. Samples were treated via six different methods and subjected to a temperature of -8°C. Their findings showed that samples dried before treatment were more dimensionally stable. Conditions mimicking museum pest control showed no significant effect. There were however

significant alterations to those samples which were taken to freezing temperatures without initial drying. This was attributed to the disruption of hydrogen bonds during freezing.

Regardless of how rigorous a museum's IPM and housekeeping is, there are still high levels of recurring infestations, which will often result in collections being subjected to multiple treatments. Again, this process of cycling has only received limited attention. In a study by Holt *et al*, new and aged wool was subjected to 50 cycles of 120 minutes at -25°C [28]. Although there were no reported alterations in the tensile strength or abrasion resistance for the new wool fabric, there was a drop in strength and weight loss through abrasion in the aged samples after cycling. The alterations were found in most cases to be less than 10% and may not constitute a significant change when taking into account the standard deviation for each sample set. The authors concluded that further work was required to clarify whether or not these changes were caused by the cycling treatment. In a more recent study, multiple freeze-thaw treatments were applied to a range of natural fibres to elucidate further the effects of low temperatures on natural textile material [29]. Wet and dry samples were cycled over a number of different timescales at temperatures of either -20°C or -80°C. All cotton and silk samples remained unchanged after cycling up to 64 times. However, Peacock [29] reported alterations in the tensile strength and elongation at break for wet wool and linen yarns, at both temperatures. Dry wool yarn was not seen to experience any alteration after cycling and may therefore dispel the concerns raised by the Holt *et al* study [28]. There was a significant increase in the percentage elongation of wet yarns after 32 cycles at -20°C. Since moisture is known to act as a plasticiser in organic material, this would account for an increase in elongation at break. However, the reasons for a delayed increase after a given number of treatments in not clear. The author postulates that these changes may be due to greater physical compacting of the fibres within the yarns. The results of the study also showed that there was a significant increase in the tensile properties for all linen samples, wet and dry. Again, the author concludes that further work is needed to fully understand the origin of these changes and their possible implications for treated linens.

4.2 The Effects of Temperature on Polymeric Material

The above review covers the recent work carried out in the conservation sector regarding the effects of temperature treatments on organic artefacts in collections. Although the studies have been relatively limited, they have tended to indicate short term stability of the artefact material. However, their focus has been primarily related to structural changes induced by the phase change of moisture between object and the surrounding atmosphere. There has been limited attention given to the physical characteristics and chemical stability of the materials themselves, especially in relation to the aged and degraded states in which many museum objects are found. Shashoua [30] cites a case where the degradation of rubber had an adverse effect on its behaviour at low temperatures. Trial low temperature storage for the reduction in the rate of deterioration of synthetic polymers, at the National Air and Space Museum in Washington DC, resulted in a permanent loss of flexibility in sections of a space suit. The reduction in temperature was well above that stated for loss of elasticity in new vulcanised rubber, therefore this change in property was regarded as an artefact of deterioration. If this is the case, then it indicates that the types of material held within heritage collections do not necessarily behave in a manner to be expected in new material and highlights the need for a thorough understanding of the behaviour of aged material at temperature extremes.

In high molecular weight linear polymers, changes of state are not clearly defined and can occur over a finite temperature range [31]. The primary transition for such material is from a glassy state to a rubbery one and can be separated into two parts: a solid-rubbery transition, known as the glass transition temperature (Tg) and a rubber-liquid transition at higher temperatures that produces a material that is capable of viscous flow. The glass transition temperature is a second order visco-elastic transition, governed by the amorphous regions of a material, above which free volume begins to increase (Figure 4.1).

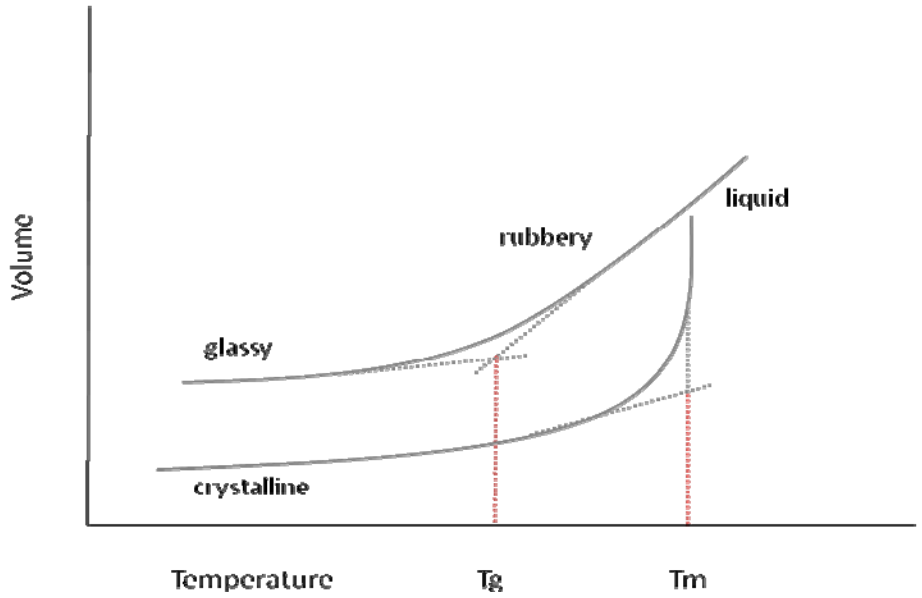

Figure 4.1 Relationship between volume and temperature in polymeric materials [32]

Raising the temperature above the Tg results in greater molecular motion of the long chain segments and eventual rupturing of the intermolecular bonds [33]. Below this temperature the molecules have reduced energy, becoming increasingly restricted preventing deformation. It is at this point that the material becomes brittle and will readily facture under the application of external forces or impact. Therefore, the mechanical properties of polymeric material are highly dependent on temperature, in addition to their structure and conformation.

Elasticity of polymeric material is the ability of a material to return to its original dimensions once an exerted load has been removed [34]. If the stress continues to be applied, then eventually the material will reach a point where it can no longer return to its original conformation, and is said to have reached its plastic limit and any further strain will cause inelastic deformation. As the temperature of a material is lowered or raised, the amount of elastic deformation that can be applied is changed. At temperatures above the glass transition the molecules increasingly move freely, and deform readily to external forces giving permanent deformation by a combination of elastic and viscous flow. Lowering a material to well below its Tg will produce a substance resistant to loading, which is stiff and rigid in nature.

It is these changes in physical properties that are of concern to conservators when applying thermal eradication techniques and thus requires them to be mindful when handling

objects [3]. At low temperatures there is a risk of a material becoming brittle and cracking under impact. At high temperatures, materials under particular threat are those bearing loads, such as costume mounted on a manikin or rolled carpets. These may deform by a visco-elastic process and remain in their new conformation on cooling.

These factors do not necessarily pose a problem for unaged material when careful protocols are adhered to, however, the situation for degraded materials may differ. There have been a couple of studies investigating their effects when applied to the aged materials, which make up a large proportion of museum collections. One of these studies, by Van Oosten and co workers [35] indicated that lowering the temperature of oxidised, isotactic polypropylene fibres exacerbated deterioration.

FTIR analysis of fibres from a tapestry indicated that the yellowing of the polypropylene fibres was caused by oxidation, accompanied by the absorption of moisture. This was determined by the presence of C=O and C-OH bands, respectively, in the infrared spectrum. The tapestry was subsequently treated for pest infestation at -20°C for three weeks. SEM imaging revealed cracks and defibrillation along the axis of the fibres, indicating that the polymer had become brittle as a result of the freezing treatment. The authors note that the isotactic form of polypropylene becomes brittle under stress at -20°C, which is below the Tg. The findings do suggest that caution is required when subjecting degraded polymers to sub-ambient temperatures. Further work needs to be carried out to clarify these effects.

The effects of external loads at different temperatures have been considered. However, in addition to these, stresses and strains can occur internally, through expansion and contraction of a substance at raised or lowered temperatures, respectively. An increase in temperature causes expansion due to molecular motion and a net increase in molecular separation. The converse is true for contraction. The degree to which a material will expand or contract can be determined by the thermal coefficient of linear expansion. It is calculated as the fractional change in length per degree of temperature change [36]. For theromoplastics the coefficients of linear expansion range from 5.0-30.0 x 10^{-5}/°C [32]. The impact of this becomes apparent when regarding an artefact of composite material or one where a material is already under tension, such as the canvas of a painting.
The effect of cold storage on the shrinkage of a variety of aged synthetic polymers has been studied by Shashoua [30, 37]. The focus was to look at the potential application of lowered

temperatures for the retardation of degrading polymers, as is already in use for cellulose nitrate photographic material. The samples included cellulose nitrate (CN), polyvinly chloride (PVC), polyacrylonitrile butadiene styrene (ABS), polystyrene (PS) and polyester (PET). They were chosen to represent the types of material commonly found in contemporary collections and covered a range of glass transition temperatures, from -40°C for plasticised PVC to 120°C for ABS [31]. They were chilled in the same manner as during low temperature eradication treatments, and taken down to temperatures reaching -30°C and then brought back up to ambient. During this time the temperature inside and out of the objects was monitored and the dimensional changes recorded and calculated as the percent linear shrinkage on cooling. For thin walled samples (less than 1cm thick) there were no irreversible dimensional changes on return to room temperature, with less than 1% change on lowering the temperature. Unexpectedly, the thick walled samples all increased in their dimensions. A PVC photograph album, which had lost plasticizer before the test resulting in shrinking and stiffening, was then found to buckle on freezing giving a net increase in size. This was a reversible effect, but the author notes that were any photographs to have been retained in the cover, then they would have been damaged in the process. Thicker samples were also shown to form condensation on their surfaces due to the increased temperature gradient experienced on cooling, therefore leading to the conclusion that although thin samples remain unaffected by low temperatures, thick materials or composite objects pose a potential problem when subjected to such conditions.

4.3 The Concern Regarding the Treatment of Synthetic Polymers

The above review highlights some of the main concerns surrounding the application of thermal pest control measures on art and artefacts.

Although much of the research already carried out suggests there is a relatively low risk of short term damage to objects, this has not served to dispel the concerns held by the heritage profession regarding the stability of aged polymers treated in this manner.

There appears to be widespread anxiety regarding their routine use, and a number of cases have been mentioned that have indicated further work is required to dispel or confirm such concerns.

Having spoken with a number of conservators and curators on this matter, it has become apparent that one area of particular apprehension is their application to synthetic

polymers[IV,V,VI,VII]. Although synthetic materials do not provide a source of food for pests, they are frequently found in conjunction with natural organic material and within composite artefacts or applied during conservation treatments. In these cases they are likely to be exposed to such treatments when other natural polymers are under attack.

One primary example is it that of polyamide, which is found extensively within contemporary textile collections in various forms. In addition to its occurrence as fibres, fabrics and fastenings, polyamide netting is applied routinely during conservation treatments to provide support to historic textiles and costumes [38]. In such situations it is repeatedly used on artefacts containing protein based material, which may subsequently undergo thermal treatment. The stability of polyamide netting has been raised as one of the primary concern to the textile conservators working at the National Museums of Scotland and at Glasgow Museums. Helen Hughes of The Burrell Collection, Glasgow, stated the material they were most concerned about under these conditions was polyamide, as found in garments, and as support for other textile objects, such as flags and banners[VIII]. The second material of concern was cellulose nitrate in the form of costume adornments.

Similar concerns were also raised by Elizabeth-Anne Haldane[v], textile conservator at the Victoria and Albert Museum, who took the decision to remove a set of cellulose nitrate eyes from a woollen costume before freezing. The Fate costume (Figure 4.2), on recent display during the V&A's Surrealists exhibition (2007), consisted of a knitted wool and cotton ballet costume onto which two cellulose nitrate eyes were sewn (Figure 4.3).

After de-installation of the exhibition, the costume was due to go into storage in crates over the summer, whilst the exhibition went on tour and awaited re-instillation at the next museum. Although there was no evidence of insect activity there were concerns about the warm climate, when insect eggs are laid[v]. Coupled with the fact the costume had previously suffered from insect damage, the decision was taken to freeze the costume

[IV] Personal conversation with Anita Quye, Conservation Scientist, National Museums of Scotland, 06 December 2006.
[V] Personal conversation with Elizabeth-Anne Haldane, Textile Conservator, Furniture, Textile and Frames Section, Victoria and Albert Museum, 17 January 2008.
[VI] Personal conversation with Sarah Howard, Textile Conservator, Hampshire County Council Museum and Archives Service, 19 March 2007.
[VII] Personal communication with Sarah Foskett, Textile Conservator, National Museums of Scotland, 15 February 2007.
[VIII] Personal conversation with Helen Hughes, Textile Conservator, The Burrell Collection, Glasgow Museums, 01 March 2007.

before storage. The cellulose nitrate eyes were showing signs of yellowing and had become brittle and cracked. After consulting a number of conservation scientists[IX], it was decided that the eyes would be removed prior to pest control treatment to avoid any possible damage. The eyes were stitched back in place subsequent to treatment.

This example illustrates the concerns that museum professionals have with regards to synthetic material. The lack of literature on the behaviour of aged polymers at these temperatures and the conflicting opinion between conservation scientists[V], leaves conservators with difficult ethical decisions with regards to treatment or removal.

Figure 4.2 Image of the Fate costume on recent display during the V&A's Surrealists exhibition. Mixed media costume comprising of wool, cotton and cellulose nitrate (V&A S.361&A-1985) (Copyright V&A)

[IX] Elizabeth-Anne Haldane, the textile conservator working on the Fate costume, consulted a number of conservation scientists and polymer specialists to determine whether the aged cellulose nitrate would be stable under freezing conditions[v]. This resulted in a number of conflicting opinions. Without a definitive answer, the decision was taken to remove the eyes as a precautionary measure.

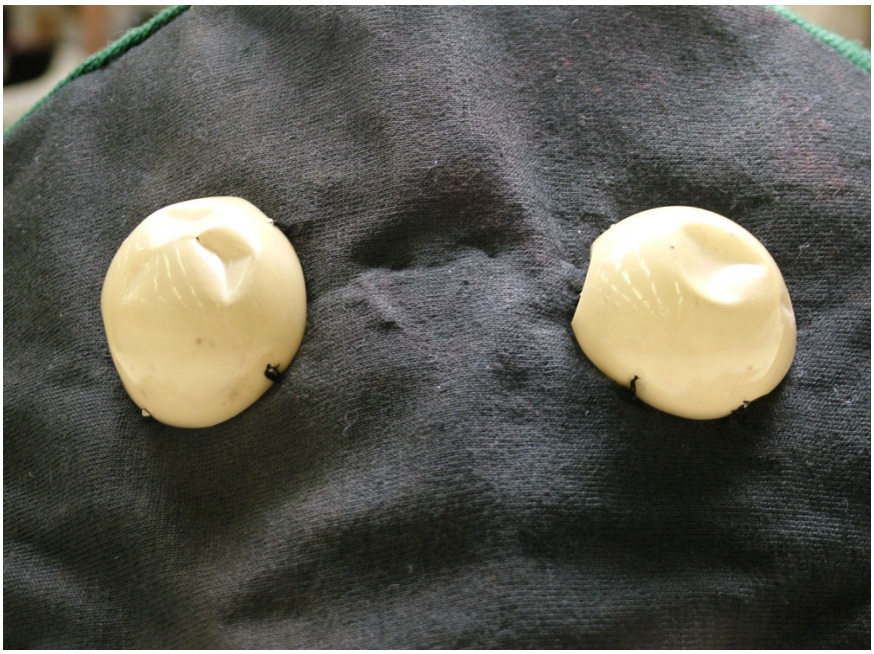

Figure 4.3 Image of the two cellulose nitrate eyes stitched to the hood of the Fate costume (V&A S.361&A-1985) (Image courtesy of Elizabeth-Anne Haldane)

4.4 The Application of Pest Eradication Treatments to Polyamides

Polyamides are long chain synthetic molecules formed through step polymerisation mechanisms and are characterised by the presence of the amide functional group linking one or more type of monomer unit. They can be divided into subclasses which, depending on the nature of the monomers employed during synthesis, result in the formation of aliphatic or aromatic polyamides, known as nylons and aramids respectively [31, 39, 40]. Aliphatic polyamides do not exceed more than 15% aromatic on either side of one amide group. Aromatic polyamide contain more than 85% aromatic species adjacent to an amide group [41].

The first commercially successful polyamide to be synthesised for manufacture was polyamide 6,6 in 1935 by W.H.Carothers and co-workers who were working for Du Pont Chemical Company (Hirsh). Previous experimentation to produce high molecular weight amides had not proven to be cost effective due to the time consuming preparation of the intermediate materials [42]. It was, however, the use of adipic acid ($HOOC(CH_2)_4COOH$), in conjunction with hexamethylendiamine ($H_2N(CH_2)_6NH_2$), that provided the first commercially viable process owing to their ready preparation from benzene, which in turn is derived from petroleum sources and coal industry by-products[42].

Although other mechanisms are used, commercially important polyamides are generally formed via three reaction routes: polycondensation (i), self polycondensation (ii) and the ring opening of a lactam (iii):

i. Polycondensation between a dicarboxylic acid and diamine. The product is an amide and the general equation for the reaction is:

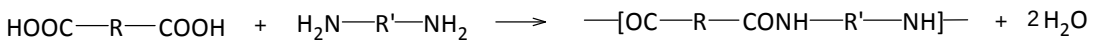

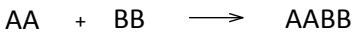

ii. Self polycondensation of an amino acid:

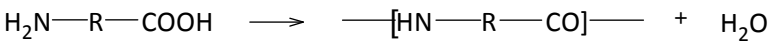

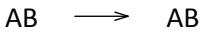

iii. Polyaddition via the ring opening of a lactam:

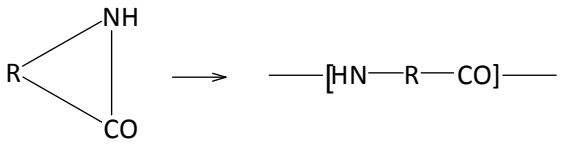

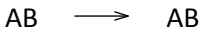

Those formed via polycondensation are referred to as AABB due to the end group functionalities, whilst those formed through self-condensation and ring opening of lactam structures are described as AB types.

There are a number of aliphatic and aromatic polyamide subclasses available, but those most frequently employed within the textile industry are polyamide 6,6 and polyamide 6, the former being used for conservation net. Aromatic polyamides, known as aramids, are produced in the form of fibres, and find specialist applications due to their high tensile strength and high temperature stability [31]. These include use as aviation materials, tire cords and protective clothing. As such they will not be covered in this thesis as they are unlikely to occur in significant quantities within a heritage setting.

The naming system of the polyamide subclasses is governed by the structure of the monomer units and are thus represented as polyamide X,Y or polyamide Z. The former relates to those formed though the polycondensation reactions of stoichiometric mixtures of dicarboxylic acids and diamides (AABB), and the latter referring to those formed by either amino acids or lactams (AB) [39].
The letters X and Y denote the carbon chain lengths of the diamine and the dicarboxylic acid backbones, respectively. Those referred to as polyamide Z, contain that number of carbons within the original amino acid or ring structure monomer. Hence, polyamide 6,9 refers to the six carbon chain of hexamethylene diamine and the nine carbons in azelaic acid, whereas polyamide 12 is formed thought the ring opening of the twelve membered ring structure of dodecanelactam. Where the polyamide is co-polymerised with one or more polyamide then the corresponding numbers are placed in decreasing order with regards to the percent content, and the ratio of the components stated [39].

Quoted values for the glass transition temperature of aliphatic polyamides tend to place it in the region of 45-55°C, depending on the subclass [43]. Therefore, when raising temperature levels during pest control treatments, unaged aliphatic polyamides will pass through their glass transition temperature. As previously touched upon this transition has implications for the physical strength of a material. It is therefore possible that museum objects containing these classes of polymers may become vulnerable to physical changes during such treatments, proving detrimental to their short and long term stability.
Although it has been shown by Egerton and Shah [44] that the degradative effects of raising the temperature of polyamide 6,6 to 100°C are negligible without UV radiation, when coupled with photooxidative reactions, an increase in temperature from ambient to just 40°C will result in a 10% loss in tensile strength. In the presence of delustrants and moisture, raising the temperature above 40°C causes a considerable effect on strength, and at 75°C tensile strength loss is as much an 87% over 95hrs.

It is well documented that polyamide fibres and nets suffer significant degradation in the presence of UV, causing the material to yellow and become brittle [45-47]. Photooxidative reactions are free radical reactions. These have been reported to continue after the incident radiation has been removed, caused by residuals remaining in the polymer structure [48]. This last point raises the question about the stability of aged polyamide within raised temperature treatments. Working above the Tg removes restrictions on

motion, potentially allowing radicals to move freely throughout the polymer structure, thus accelerating ageing.

The hygroscopic nature of polyamides is well known, and water has been shown to have a strong effect on their secondary, visco-elastic transitions [49-51]. The absorption of water into the structure of polyamides will significantly weaken intermolecular hydrogen bonding, as it interacts with the amide groups, thus lowering the glass transition temperature. During the degradation of the polymer chains two processes may be experienced: cross-linking or chain scission. The former route will produce a brittle material with a high glass transition temperature, whilst the latter will cause a break down in the amorphous regions, accompanied by a reduction in intermolecular bonding. As the polymer loses length along the chain aggregate there will be an increase in amorphous spaces for moisture uptake, and hence plasticization. As the moisture content in polyamides increases its glass transition can be suppressed considerably.

Vlasaveld *et al* [52] reported a drop in the glass transition temperature of 40°C with an increase of 3 wt% water. The equilibrium moisture content of the polyamide 6 nano-composite, at 23°C and 50% RH, was 2.5 wt% with a Tg of 65°C , which was reduced to 25°C with an increase in moisture. A further 3 wt% water lowered the transition to 0°C. As a consequence low temperature pest control measures at -30˚C are likely to pass such a polyamide from above its glass transition to below, regardless of its type or condition. This may have implications similar to those described in Section 4.2 for aged polypropylene.

The preliminary work carried out by Shashoua [30, 37] and Van Oosten [35] has illustrated the possible detrimental effects temperature can have on synthetic based museum artefacts, setting the scene for a more widespread investigation of modern materials under extreme conditions. In conjunction with a review of the wider literature, this highlights the need for a thorough investigation of the behaviour of polyamide textile material subjected to thermal pest control measures.

4.5 Conclusions

The application of raised and lowered pest control treatments are a common and widespread method of combating pest infestations in heritage collections. Their use ensures a rapid, cost effective means of action, without posing a risk to personnel. There has been a significant amount of research looking into the possible detrimental effects that such treatments may induce in artefacts, but these have primarily focused on natural polymeric material. Due to the fact that synthetic polymers do not provide a source of food for pests, these have been largely overlooked. However, the thermal properties of some classes of synthetics mean that they are vulnerable to physical alterations at the temperatures under question.

Polyamides are one such example of polymers that undergo changes in the physical properties over the temperature ranges applied to treat infestations. As raised temperature treatments are applied, aliphatic polyamides are taken through their glass transition, which has implications for increased molecular mobility and therefore deformation. As the temperature is lowered, polyamides become brittle, glass like materials, making them vulnerable to fracture.

A more in depth discussion into the physical properties of polyamides, pertinent to the issues surrounding temperature dependent pest control treatments, will be presented in the following Chapter.

4.6 References

1. *Integrated Pest Management for Collections. Proceedings of 2001: A Pest Odyssey*. 2001. National Preservation Office: James and James.
2. Pinniger, D., *Pest Management in Museums, Archives and Historic Houses*. 2001, London: Archetype Publications.
3. Berkouwer, M., *Freezing to Eradicate Insect Pests in Textiles at Brodsworth.* The Conservator, 1994. **18**: p. 15-22.
4. Strang, T.J.K. and J.E. Dawson, *Controlling Museum Fungal Problems*. Technical Bulletin No 12. 1991, Ottawa: Canadian Conservation Institute.
5. Blyth, V. *Training for Museum Staff is a Prerequisite for Successful Insect Pest Management*. in *Integrated Pest Management for Collections, Proceedings of 2001: A Pest Odyssey*. 2001. National Preservation Office.
6. Kingsley, H. and D. Pinniger. *Trapping Used in a Large Store to Target Cleaning and Treatment*. in *Integrated Pest Management for Collections, Proceedings of 2001: A Pest Odyssey*. 2001. National Preservation Office.

7. Xavier-Rowe, A. and D. Pinniger. *No Uninvited Guests: Successful Pest Management in Historic Houses*. in *Integrated Pest Management for Collections, Proceedings of 2001: A Pest Odyssey*. 2001. National Preservation Office.
8. Berry, J. *Battle of the Beasts: Treatment of a Pest Infestation of the Mounted Mammal Collection at Liverpool Museum*. in *Integrated Pest Management for Collections. Proceedings of 2001: A Pest Odyssey*. 2001. London: James & James.
9. Rossol, M., *Health and Safety: Textile Fumigation with Phosphine.* Textile Conservation Newsletter, 1990. **19**(Autumn): p. 15-20.
10. Selwitz, C. and S. Maekawa, *Inert Gases in the Control of Museum Insect Pests*. Research in Conservation. 1998, Los Angeles, USA: The Getty Conservation Institute.
11. Charles, S. and S. Maekawa, *Inert Gasses in the Control of Museum Insect Pests*. 1998, Los Angeles: The Getty Conservation Institute.
12. Rust, M.K., et al., *The Feasibility of Using Modified Atmospheres in Control of Insect Pest in Museums.* Restaurator, 1996. **17**(1): p. 43-60.
13. Bergh, J.E. *Current Research on Anioxic Insect Methods in Scandinavia*. in *Proceedings 3rd Nordic Symposium on Insect Pest Control in Museums*. 1998. Stockholm.
14. Maekawa, S., *Oxygen-free Museum Cases*. 1998, Los Angeles: Getty Conservation Institute.
15. Rowe, S., *The Effect of Insect Fumigation by Anoixa on Textiles Dyed with Prussian Blue.* Studies in Conservation, 2004. **49**: p. 259-270.
16. Maekawa, S. and K. Elert, *The Use of Oxygen-free Environments in the Control of Museum Insect Pests*. Tools for Conservation. 2003, Los Angeles, USA: The Getty Conservation Institute.
17. Ackery, P., R, et al., *Effects of High Temperature Pest Eradication on DNA in Entomological Collections.* Studies in Conservation, 2004. **49**: p. 35-40.
18. Ackery, P., R, A. Doyle, M, and D. Pinniger, *Safe High Temperature Pest Eradication - is the Answer in the Bag?* Biology Curator, 2002. **22**: p. 13-14.
19. Strang, T.J.K. *Principles of Heat Disinfestation*. in *Integrated Pest Management for Collections, Proceedings of 2001: A Pest Odyssey*. 2001. National Preservation Offices, London: James and James.
20. Xavier-Rowe, A., et al. *Using Heat to Kill Insect Pests - Is It Practical and Safe?* in *IIC Advances in Conservation: Contributions to the Melboune Congress*. 2000. Melbourne: IIC.
21. Child, B., *The Thermo Lignum Process for Insect Pest Control.* Paper Conservation News, 1994. **72**: p. 9.
22. Beiner, G.G. and T.M.A. Ogilvie, *Thermal Methods of Pest Eradication: Their Effect on Museum Objects.* The Conservator, 2005/6. **29**: p. 5-18.
23. Wellheiser, J.G., *Nonchemical Treatment Process for Disinfestation of Insect and Fungi in LIbrary Collections*, ed. K.G. Saur. 1991, Munich.
24. Carrlee, E., *Does Low-temperature Pest Management Cause Damage? Literature Review and Observational Study of Ethnographic Artefacts.* Journal of the American Society for Conservation, 2003. **42**: p. 141-166.
25. Florian, M.L., *The Freezing Process: Effects on Insects and Artefact Material.* Leather Conservation News, 1986. **3**(1): p. 1-14.
26. Incropera, F.P. and D.P. DeWitt, *Introduction to Heat Transfer*. 1985, Chichester: John Wiley & Sons.
27. Williams, S.L., S.H. Beyer, and S. Khan, *Effect of "Freezing" Treatments on the Hydrothermal Stability of Collagen.* Journal of the American Society for Conservation, 1995. **34**: p. 107-112.

28. Holt, L., C. Y, and W. Dodd, *The Effect of Wool Fabrics of Multiple Freeze Thaw Treatments for Insect Control.* Textile Conservation Newsletter, 1995. **29**(Autumn): p. 28-35.
29. Peacock, E.E., *A Note on the Effect of Multiple Freeze-thaw Treatment on Natural Fibre Fabrics.* Studies in Conservation, 1999. **44**: p. 12-18.
30. Shashoua, Y.R. *Freezing the Present to Preserve the Future*. in *AHRC Research Centre for Textile Conservation and Textile Studies Second Annual Conference: The Future of the 20th Century - Collecting, Interpreting and Conserving Modern Materials*. 2005. Winchester: Archetype Publishers.
31. Brydson, J., *Plastics Materials*. 7th ed. 1999, Oxford: Butterworth-Heinemann.
32. Shashoua, Y.R., *Conservation of Plastics: Materials Science, Degradation and Preservation*. 2008, London: Butterworth-Heinemann.
33. Murthy, N.S., *Hydrogen Bonding, Mobility, and Structural Transitions in Aliphatic Polyamides.* Journal of Polymer Science Part B: Polymer Physics, 2006. **44**(1763-1782).
34. Gillam, E., *Materials Under Stress*. 1969, London: Butterworth & Co.
35. Van Oosten, T., I. Joosten, and L. Megens. *Man-made Fibres from Polypropylene to Works of Art*. in *AHRC Research Centre for Textile Conservation and Textile Studies Second Annual Conference: The Future of the 20th Century - Collecting, Interpreting and Conserving Modern Materials*. 2005. Winchester: Archetype Publications.
36. Gere, J.M., *Mechanics of Materials*. 6th ed. 2006, Toronto, Canada: Thomson.
37. Shashoua, Y.R. *Storing Plastics in the Cold: More Harm than Good?* in *Modern Materials and Contemporary Art*. 2005. The Hague: ICOM Committee for Conservation.
38. Sinha, M.K., *An Investigation of Photodegradation of a Support Netting Used in the Conservation of Historic Textiles*. 2006, Heriott-Watt: Edinburgh.
39. Lewin, M. and E.M. Pearce, *Handbook of Fibre Chemistry*. 2nd ed. International Fibre Science and Technology Series, ed. M. Lewin. 1998, New York: Marcel Dekker Inc.
40. Brooks, M. and P. Garside. *Probing the Microstructure of Protein and Polyamide Fibres*. in *AHRC Research Centre for Textile Conservation and Textile Studies Second Annual Conference The Future of the 20th Century - Collecting, Interpreting and Conserving Modern Materials*. 2005. Winchester: Archetype Publications.
41. Hatch, K.L., *Textile Science*. 1993, Saint Paul: West Publishing Company.
42. Trossarelli, L. *The History of Nylon*. in *Nylon and Ropes*. 2002. Turin.
43. Gordon, G.A., *Glass Transitions in Nylons.* Journal of Polymer Science Part A-2, 1971. **9**: p. 1693-1702.
44. Egerton, G.S. and K.M. Shah, *The Effects of Temperature on the Photochemical Degradation of Textile Materials Part I: Degradation Sensitized by Titanium Dioxide.* Textile Research Journal 1968: p. 130-134.
45. Sinha, M.K., *An Investigation of Photodegradation of a Support Netting Used in the Conservation of Historic Textiles* 2006, Heriott-Watt: Edinburgh.
46. Do, C.H., et al., *FT-IR Spectroscopic Study on the Photo- and Photooxidative Degradation of Nylon.* Journal of Polymer Science Part A: Polymer Chemistry, 1987. **25**: p. 2301-2321.
47. Egerton, G.S., *Some Aspects of the Photochemical Degradation of Nylon, Silk and Viscose Rayon.* Textile Research Journal, 1948. **November**: p. 659-669.
48. Allen, N.S., M. Edge, and C.V. Horie, *Polymers in Conservation*. 1992, Cambridge: Royal Society of Chemistry.

49. Uddin, A.J., et al., *Influence of Moisture on the Viscoelectric Relaxations in Long Aliphatic Chain Contained Semiaromatic Polyamide, (PA9-T) Fibre.* Journal of Polymer Science Part B: Polymer Physics, 2003. **41**: p. 2878-2891.
50. Park, Y., et al., *Moisture Effects on the Glass Transition and the Low Temperature Relaxations in Semiaromatic Polyamides.* Journal of Polymer Science Part B: Polymer Physics, 1997. **35**(5): p. 807-815.
51. Choe, S., et al., *On the Visco-electric and Plastic Behaviour of Semiaromatic Polyamides.* Journal of Polymer Science Part B: Polymer Physics, 1999. **37**: p. 1131-1139.
52. Vlasveld, D.P.N., et al., *Moisture Absorption in Polyamide-6 Silicate Nanocomposites and its Influence on the Mechanical Properties.* Polymer, 2005. **46**: p. 12567-12576.

Chapter 5: The Structure, Thermal Behaviour and Deterioration of Polyamides

The physical properties of polymeric material are dependent on the underlying chemical and physical structure. For aliphatic polyamides, their properties are essentially governed by the length of the long chain methylene backbone, interspersed by polar amide linkages, the polymer processing methods and the overall chain length and inhomogenity. These factors govern their response to external stresses and as a consequence their application.

The methylene groups possess only weak interchain interactions and retain a degree of flexibility and disorder. Whereas the amide groups will readily form rigid, ordered regions through intermolecular hydrogen bonding. Depending on the proximity of the neighbouring chains, the polymer will attain different conformations of high and low order referred to as the crystalline and amorphous regions, respectively. The crystalline regions will exhibit long range order, whilst the amorphous regions will show some short range ordering but will be disordered over greater lengths.

The following Chapter will give an overview to the internal structure of aliphatic polyamides. Discussion will be given to the thermal characteristics related to the different regions, and highlighting the physical properties dependent on these. Particular focus will be given to the thermal properties of the amorphous region as these relate directly to the temperature range used for the eradication of pests in heritage collections.

Focus will be given to aliphatic polyamides, rather than aromatic types. Although aromatic polyamides are often used in fibre form, their specialist applications mean that collections are unlikely to house a significant quantity of these materials.

5.1. Crystalline Structure

The crystal structures of polyamides are dependent on the ability of opposing amide groups along the polymer chains to form strong intermolecular hydrogen bonds. Polyamide chains

take on an extended chain conformation enabling close lateral packing [1]. The –CONH- groups will take on different orientations depending on the particular type of polyamide, to optimise hydrogen bonding. This is as a consequence of the number of carbons in each chain and the orientation of the functional groups [2].

5.1.1 Orientation of the Polymer Chains

For even AB polyamides, formed either by amino acid polycondensation or the ring opening of a lactam, each neighbouring chain will be directionally antiparallel.

An example of this is shown in Figure 5.1, where the polyamide 6 (PA6) chain lengths run in opposing directions. If the PA6 chains were parallel in nature then only half of the carbonyl/amino groups could form interchain bonds without causing strain along the polymer, illustrated in red in Figure 5.2 [1, 2]. For odd AB polyamides, such as PA7, the chains are also found to adopt the antiparallel arrangement [2].

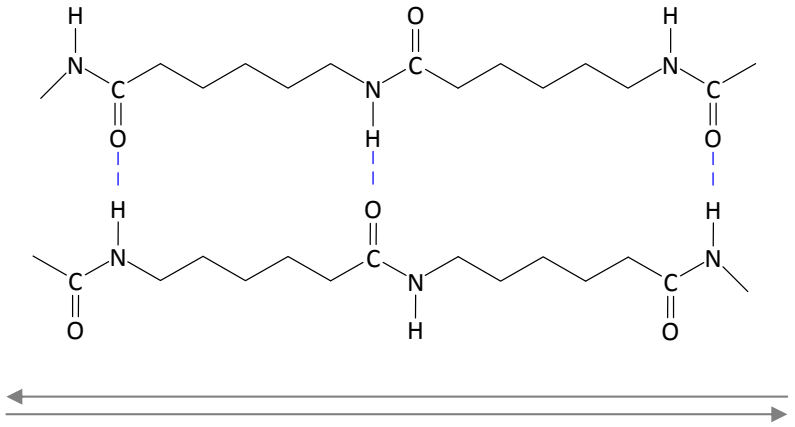

Figure 5.1 Repeat units of the antiparallel arrangement in polyamide 6 illustrating hydrogen bonds between all amide groups [2]

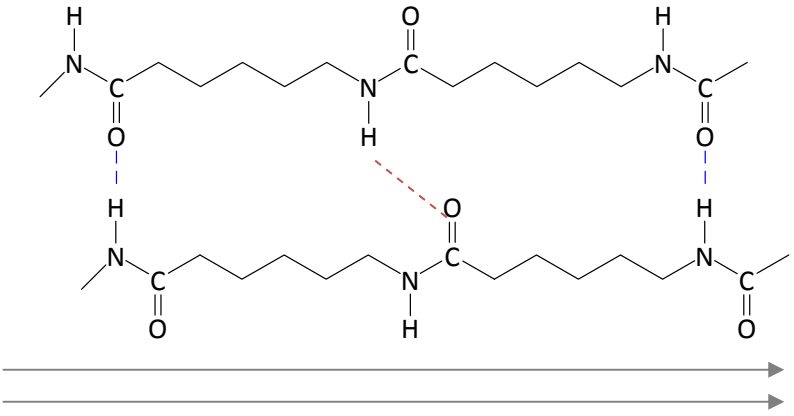

Figure 5.2 Repeat unit of the parallel arrangement in polyamide 6 illustrating the reduced hydrogen bonding between amide groups[2]

AABB polyamides, formed through the condensation reaction between dicarboxilic acids and diamides, form both parallel and antiparallel conformations (Figure 5.3). These are equivalent to each other due to the centre of symmetry [2].

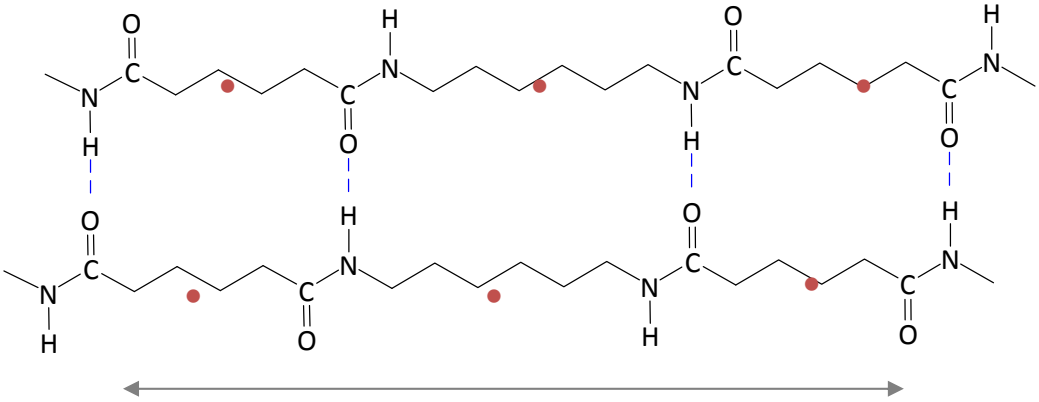

Figure 5.3 Repeat unit of polyamide 6,6 illustrating the centres of symmetry (red dots) [2]

5.1.2 Crystal Units

The resulting polymer chain sheets stack upon one another, forming crystal lattices dependent on the orientation of the amide linkages and producing ordered regions with anisotropic properties. Due to the directionality of the bonding within, and between, chain lengths there are two crystal structures which predominate. These are referred to as the α and γ structures.

The α structure relates to those polymers where the methyl groups are extended to a planar zigzag conformation [2-4]. For even-even polyamides the hydrogen bonded sheets contained in the *a-c* crystal faces are progressively displaced by one chain atom in the direction of *c*, where *c* is the chain axis (Figure 5.4). This ensures that the hydrogen bonds are in line with neighbouring functional groups without strain. The result is a 13° shear along axis *a* in all even-even polyamides [5]. In extruded polyamide fibres the *c* axis runs parallel to the direction of the fibre length.

These sheets are also displaced by three chain atoms in the *b* axis, thus forming a triclinic unit cell defined as three unequal axes which intersect at oblique angles (Figure 5.5) [6].

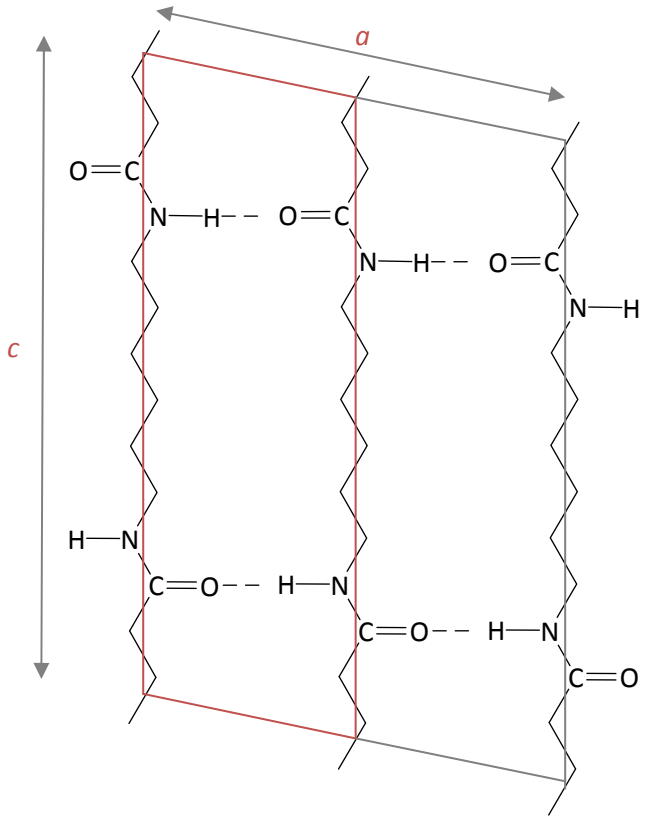

Figure 5.4 The progressive displacement of the polymer chains in the *c* axis of even-even polyamides [2]

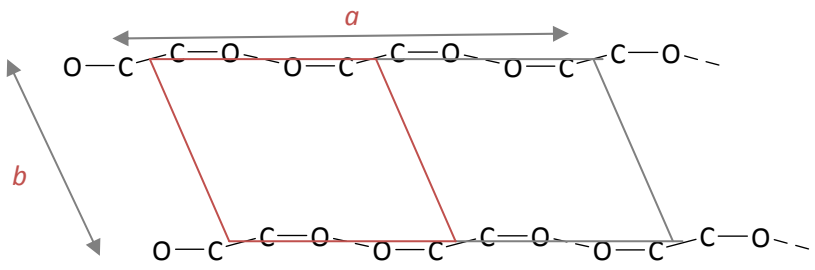

Figure 5.5 The displacement by three atoms in the *b* axis of even-even polyamides [2]

A second structure is also possible in even-even polyamides, termed the β-structure. In this conformation the sheets shear alternately, rather than form a progressive shear as shown in Figure 5.5 [5].

Even polyamides can crystallise into either the α or γ structures. The former generally predominates where the number of carbons along the polymer is equal to or less than seven and the latter when the carbons exceed seven. As found in the α structure for even-even polyamides, the polymer chains are in a fully extended conformation. However, rather than displacement in the same direction they are staggered up and down along the chain axis to bring the amide groups into line (denoted *b* in monoclinic structures) (Figure 5.6). This forms a monoclinic unit cell, such that the three unequal axes intersect with two oblique angles, perpendicular to the third (Figure 5.7). The unit cell contains two sheets corresponding to four chain segments [7].

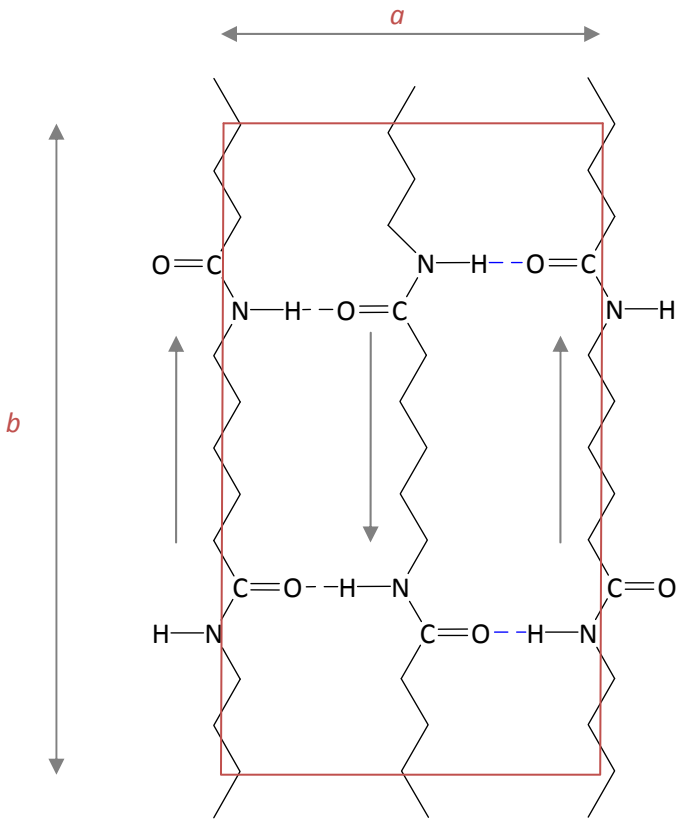

Figure 5.6 The staggered displacement of the polymer chains in the b axis of α-structure of even polyamides [2]

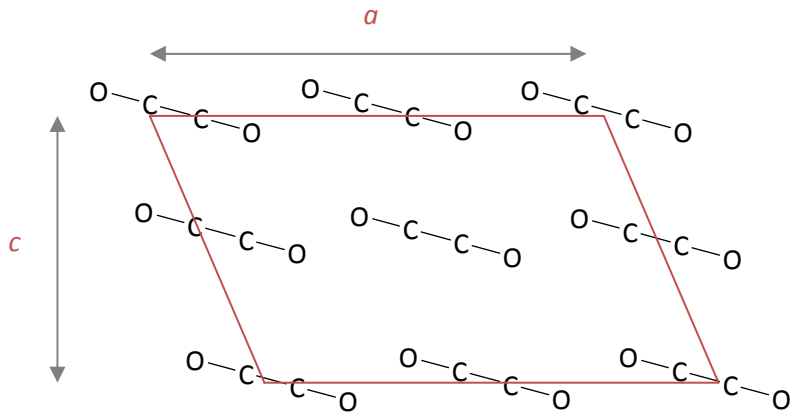

Figure 5.7 The two oblique angles in the *a* ,*c* plane of the α-structure of even polyamides [2]

The γ structure is the primary structure seen in even polyamides greater than seven, even-odd, odd-even and odd-odd polyamides [1, 7]. The chain axis is twisted out of plane in the γ structure to enable full hydrogen bonding (Figure 5.8). The amide groups are tilted, and as a consequence, the individual chain lengths are shorter than in the α structures [3]. Where both the α and γ forms are possible, the α form will predominate as it is the most thermodynamically stable at low temperatures [7].

The twist of the polymer chains produces a crystal packing of six chain lengths normal to the *c* axis, forming a hexagonal unit cell. The structure is known as pseudohexagonal, due to the symmetry restrictions imparted by the interchain bonds retaining their zig-zag conformations [2, 7].

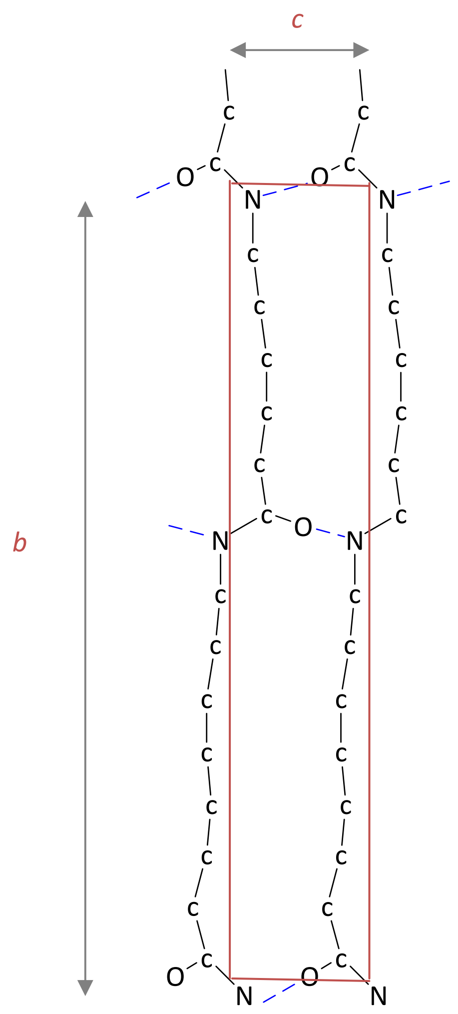

Figure 5.8 The tilting of the chain axis to form the γ structure in an even-odd polyamide

5.1.3 Thermal Behaviour of the Crystalline Region

The thermal behaviour of the crystalline region is characterised by its melting temperature (Tm) and the Brill transition (Tb).

On melting, complete breakdown of the ordered regions results. Due to the presence of the interchain hydrogen bonding, polyamides will melt at a higher temperature than polyolefin materials, for example [5]. A number of amide groups remain hydrogen bonded even in the polymer melt [4, 8].

Tm will increase with increasing hydrogen bond density since they impart mobility restrictions on the polymer chains. It therefore follows that the melting temperature of polyamides will decrease as the number of methylene groups (per amide group) increase.

For example, polyamide 2,20 has a melting temperature of 230°C compared to a melting temperature of 170°C for polyamide 12,20 [9]. The melting temperatures of a number of synthetic polymers used in fibre production are presented in Table 5.1.

Polymer	Melting temperature/°C
Polyamide 6	215
Polyamide 6,6	264
Polypropylene (isotactic)	135
Polypropylene (syndotactic)	170
Cellulose Triacetate	300

Table 5.1 The melting temperature of some synthetic polymers found in textile collections [10]

Before the melting temperature is reached and the crystal structure is broken down, the crystalline regions will undergo some structural changes, due to the mobility of the methylene groups. On increasing the temperature of polyamide 6,6 to the region of 175°C to 200°C it has been shown that it will pass through what is called the Brill transition (Tb) [2]. This transition is the point at which, on heating, the inter-chain distance and the inter-sheet distance are equal. X-ray diffraction studies have shown this as the merging of two separate diffraction signals into one signal [11]. The alteration in diffraction pattern is caused by the triclinic structure taking on a pseudohexagonal unit, similar to the one described above. These alterations have been shown to have a concurrent effect on the packing of the amorphous chain segments [7, 12].

As with the Tm, the temperature at which this occurs is dependent on the length of the polymer chains, with an increase in methylene concentration causing a decrease in the transition temperature [2]. Contrary to reported values for polyamide 6,6, Jones *et al* [5] reported the Brill transition of a number of aliphatic polyamides to occur in the region of 192-253°C, just before their corresponding melting temperatures.

5.1.4 Effect of Polymer Processing on the Crystalline Structure

The degree of crystallinity is dependent on the processing of the material. This governs the time available for crystals to form and for re-orientation of the chains, enabling inter-chain bonding. In polyamides the percentage crystallinity may fluctuate by as much as 40% [8]. Fibre formation of polyamides is generally via the process of melt spinning and extrusion through a die to give a constant cross-section. In order to improve mechanical properties

spinning is usually followed by fibre drawing. Depending on the conditions, this has the effect of increasing the percentage crystallinity, chain orientation and crystal size, as well as inducing some orientation of the amorphous regions.

Drawing of polymer fibres is normally carried out above the glass transition temperature as this allows for greater chain mobility and rearrangement (See Section 5.2) [13]. The draw ratio (DR) is a measure of the degree of extension of a fibre after polymer drawing. It is the ratio of the cross-sectional area of the undrawn fibre to that of the drawn fibre. Vasanthan *et al* [13] showed that the size of the crystallites in polyamide 6,6 fibres increased rapidly with an increase in DR from one to two, but this tailed off with higher draw ratios. It was also demonstrated that the degree of orientation developed more slowly in the amorphous regions than in the crystalline regions.

Murthy *et al* [14] have reported unprocessed polyamide 6 film to contain as little as 15% crystallinity, as determined by deuterium exchange studies and small-angle neutron scattering. In a separate study [15], the same co-workers applied polarized infrared spectroscopy and x-ray diffraction to monitor the changes in crystalinity during fibre processing. It was shown that there was an increase from 16% to 29% crystallinity on the annealing of polyamide 6 fibres.

5.2 Amorphous Structure

Aliphatic polyamides are semi-crystalline materials, where the regions outside of the crystal lattice show some short range order and intermolecular bonding, but are disordered over longer distances [15].The non-crystalline, amorphous regions are characterised by segmental motion affecting the final flexibility of the material.

The bulk amorphous region is characterised by a number of thermal transitions which are linked to local vibrations and rotations, and longer range chain mobility.

Fully crystalline materials or low molecular weight materials experience defined thermal transitions accompanied by a phase change from solid to liquid and liquid to gas. Whereas high molecular weight polymeric materials experience a number of second order transitions over discrete temperature ranges, which do not see a phase change (Figure 5.9). The secondary transitions are associated with main chain and side chain motions within the polymer matrix. The temperature at which these motions are free to occur are dependent on, and influenced by, a number of factors, which will be discussed more fully in Section

5.2.2. It will become clear that since they relate directly to conformational changes in the macromolecule, they will also have a significant effect on the physical properties of a material.

The primary relaxation for polyamides on raising the temperature is the α relaxation, known as the glass transition (occurring at Tg). This is the most important transition with respect to the physical behaviour of polymers. It covers a narrow range at which the non-crystalline regions move from a rigid, glassy state to a rubbery state caused by an increase in energy [16]. The glass transition temperature is a visco-elastic transition, governed by the amorphous regions, where free volume begins to increase resulting in increased molecular motion of the long chain segments and rupturing of the intermolecular bonds (see Figure 4.1) [17].

In highly oriented fibres this glass transition can occur at two temperatures, related to the presence of a rigid amorphous fraction connecting the bulk amorphous region with that of the crystalline regions, termed the interlamellar region. The bridges between the two bulk phases are known as tie molecules, and exhibit an intermediate orientation [18]. The process of heat setting, or annealing of fibres, has been shown to increase the crystallinity in these regions [17].

The significance of the glass transition temperature is related to the changes in physical properties experienced as a polymer moves from below to above it's Tg. Characteristic changes include a decrease in hardness and modulus, and an increase in volume and percent elongation at break [4]. It is these changes in the physical characteristics that are exploited to detect the temperature range of the transitions.

5.2.1 The Significance of Temperature

This thesis will primarily focus on the polyamide α transition, the glass transition temperature, as this has particular relevance to the pest control methods under study. In a study by Qiu *et al* [19] into the phase structures of polyamide 6,6 it was shown that as the temperature is increased towards the region of the glass transition the isotropic, amorphous regions experience increased molecular motions, from skeletal vibrations to larger amplitude rotations and oscillations. As a consequence of this, it can be expected that this will cause a concurrent alteration in the properties of the amorphous regions.

Table 5.2 shows the glass transition temperature values for a number of different aliphatic polyamides.

Polyamide	Glass Transition Temperature/°C
Polyamide 6	40
Polyamide 6,6	52
Polyamide 6,10	40
Polyamide 11	43
Polyamide 12	42

Table 5.2 Glass transition temperature of a number of aliphatic polyamides [20]

The raised temperature pest control treatments under investigation in this thesis apply temperatures up 58°C. Consequently, polyamide 6,6 would be taken 6°C above its glass transition and polyamide 6 raised 18°C above Tg. For the low temperature treatments at -30°C, polyamide 6,6 and polyamide 6 would be 82°C and 70°C below their Tg. In a study into the deterioration of polyamide 6,6, fishing nets Toivonen [21] states that at -40°C polyamide 6,6 fibres becomes brittle and lose their strength.
Thus, a consideration of the physical properties of polyamides above and below the glass transition becomes an important consideration when assessing the application of such treatments.

The shrinkage behaviour of unprocessed polyamide 6,6 and polyamide 6 fibres at various temperatures, ranging from 30°C to 190°C has been studied by Simal and Martin [22]. Interpolating between their data points to the temperature of interest, the polyamide 6,6 fibres showed a shrinkage of approximately 3% at 60°C, and 1% for the polyamide 6 fibres. At just ten degrees higher, the polyamide 6,6 fibre was shown to have shrunk by 4.5%, half of the final shrinkage value at 190°C. The authors related the increased shrinkage in polyamide 6,6 compared to polyamide 6, to the higher degree of chain mobility in the former caused by a lower hydrogen bond density.

The effect of temperature on the creep behaviour of magnetic tape substrates was illustrated by Higashioji and Bhushan [23]. Various polymer films were subject to dynamic mechanical analyses at a constant load with varying temperature and RH conditions. It was shown that the creep compliance increases with increasing temperature, caused by an increase in molecular motion. Comparative creep studies of increasing RH, at a constant

temperature of 55°C, illustrated the relationship between the plasticizing effect of water and increased compliance.

Zimmerman and Kohan [24] reported on the low temperature flextural modulus of polyamide 6,6 film. It was shown that with increasing moisture content there was an increase in the flextural modulus. At -50°C the modulus of dry polyamide 6,6 was 60 gigapascals (GPa) whereas the samples conditioned at 100% RH showed a modulus of approximately 80GPa. This increased stiffening with moisture content was attributed to the moisture acting as a bonding agent. This shows the opposite effect to that found at ambient temperatures, where moisture acts as a plasticizer, reducing polymer stiffness. This point was also raised in a second study by Toivonen *et al* [25] looking into the effects of freeze-thaw cycles on polyamide 6 fishing nets. They found that the tensile and flextural moduli increased at lowered temperatures in the presence of moisture. The ductility of the samples was reduced. It was proposed that the presence of moisture caused an increase in the internal voids and surface cracking, which in turn, increased brittle fracture. It should be noted that both of these studies focus on the low temperature behaviour of wet samples, rather than samples of intermediate moisture content.

5.2.2 Factors Affecting the Glass Transition Temperature

Due to the fact that the glass transition is a phenomenon relating to the amorphous regions of a polymer, changes in these regions will have a corresponding effect on the Tg. A few of these factors are considered below.

5.2.2.1 Crystalline Fraction

Although the glass transition is a phenomenon of the amorphous region of a polymer, Jin *et al* [26] propose that the crystalline region acts as cross-links, which impart physical restrictions on the non-crystalline regions, and affect the thermal and mechanical properties. Similarly, Zilberman *et al* [27] correlated the glass transition values of a number of polyamide 6 and 6,9 co-polymers with the degree of crystallinity. A linear relationship was shown to exist for the polymers containing 50% or more polyamide 6, suggesting restrictions in the amorphous mobility imparted by the crystal lattice. This relationship breaks down for the copolymer containing a greater percentage of polyamide 6,9.

5.2.2.2 Length of the Repeat Unit

Since the glass transition is related to the ability of polymer chains to rearrange and move, the presence of hydrogen bonds along the polymer backbone can be assumed to affect the transition. Botta and co workers [28] looked at the aliphatic polyamides, which included the secondary amines as the precursor monomers, to assess what effect the absence of hydrogen bonding would have on the Tg. They found that the glass transition was in the same temperature region as primary amine based aliphatic polyamides. This would suggest that the presence, or otherwise, of a bonding hydrogen does not affect the transition temperature.

Huang *et al* [9] characterised a series of long alkylene segmented polyamides by spectroscopic and thermal analyses. The focus was on the effect of increasing the methylene segment along the diamine part of the polymer chain, thus decreasing amide density. Their DSC heating curves showed a decrease in the Tm with increasing CH_2 units along the polymer backbone, attributed to a reduction in hydrogen bonds per unit length. The polyamide 2,20 experienced a double melting endotherm ascribed as an indication of its relatively low crystalline perfection. The results from the DMTA analyses placed the Tg of all of the samples under study between 42-50°C, with an inverse relationship between Tg and chain length. This study illustrated some of the key factors that relate structure with thermal behaviour.

There was shown to be a depression of the glass transition in polyamide 6 and 12 with increasing co-polymerisation with polyaniline in a study by Basheer *et al* [29]. This was attributed to the plasticisation of the matrix by residual water and due to hygroscopic salts remaining in the structure from the processing of the samples. However, Zilberman *et al* [30] attributes a decrease in Tg of co-polymers to the decrease in bonded amide groups. In their work, polyamide 6 was co-polymerised with the co-monomer polyamide 6,9 to varying degrees, to establish the effect of hydrogen bond concentration on glass transition. DSC and FTIR were used to measure the Tg, and the bonded and unbonded amide groups, respectively. The Tg of polyamide 6 was found to be higher than that of polyamide 6,9, and all co-polymers exhibited a reduced Tg below that of either homopolymer, with the minimum obtained for the sample containing almost equal weight of both monomers. The authors note that this is inconsistent with the literature, which suggests that the Tg of a miscible co-polymer is situated between the Tg of the individual homopolymers. A number

of methods were applied to determine the hydrogen bond content, based on spectroscopic data. Although there were variations in the absolute numbers derived, the general trend supported the idea that the irregular distribution of amide groups along the polymer backbone caused a decrease in hydrogen bonds. The findings showed that the Tg is positively correlated with the hydrogen bond concentration. The effect is much greater in polyamide 6 based polymers due to the higher bond density.

5.2.2.3 The Plasticisation Effect of Moisture

Moisture sorption is known to play a major role in the thermal and mechanical behaviour of polymers. This is of particular interest with regards to polyamides as they are known to hold up to 9% of their weight as water [31], owing to the high amide group concentration. Ellis [32] showed a 15°C reduction in the glass transition temperature of an amorphous polyamide by the addition of 1% water. This suggests that the reduction for a fully moisture laden sample would be significant.

Penetration of moisture has been shown to occur primarily in the amorphous regions, due to the reduced density and increased accessibility for small molecules [14]. Jin *et al* [26] have suggested that the diffusion of water is further restricted to the wholly amorphous regions, rather than the interlamellar regions of intermediate order. The penetration of moisture results in the interruption of the interchain hydrogen bonds, which in turn reduces the steric hindrance of the chains increasing mobility [4]. This has the effect of significantly reducing the Young's modulus, due to plasticization [31].

Men *et al* [33] studied the mechanical properties of moulded polyamide 6 and a co-polymer under dry and saturated conditions. They showed that the saturated samples at room temperature took on a rubbery characteristic in the stress strain curve (not showing a well defined yield point), which was similar to the behaviour of the dry samples at temperatures between 80 and 160°C. They interpreted this as illustrating that moisture imparts similar mobility to amorphous regions as raised temperatures. The same effect was shown to occur at lower stress in the copolymer samples. This is likely to be caused by the decrease in packing found within copolymer systems, causing an increase in the number of moisture sorption sites and greater mobility.

Park and co-workers [34] applied thermal analytical techniques to monitor the effect of moisture on a variety of homo and co-polymers based on two semi-aromatic polyamides.

The samples were allowed to equilibrate at ambient to illustrate the different moisture uptake of each sample. Three successive DSC heating scans were carried out between 30-280°C, where the samples were quenched from the high temperature and reheated. In the first scan two endotherms were seen, attributed to the expulsion of water and the glass transition respectively. During the second and third runs only one endotherm was experienced, at a higher temperature than in the initial scan. The differences in moisture content between the first and second scans was shown to be 2.8%. This gave an experimentally derived value of 11.4°C depression per 1% weight of moisture. They compared the experimental and calculated values for all of their samples, and found that all but one followed the trend of a decrease of 12-13°C for a corresponding increase of 1% wt in water.

In the same study the influence of water on the low temperature, secondary transitions was monitored using the peak maxima in tan δ from the phase angle (δ) calculated by a DMTA analyser using a temperature scan range of -150 up to 180°C. During the first scan the β transition was seen at -70°C and the Tg occurred at 154°C. The second scan showed an increase in both the β transition and the glass transition to -55°C and 160°C respectively, and the appearance of a weak band at -110°C. During the third scan the intensity of the β transition dropped considerably, occurring at -45°C, and a more intense peak assigned to the γ relaxation, appeared at -108°C. A fourth scan was carried out and it was shown that the β peak had completely disappeared and the Tg was consistent with that of the third scan, at 162°C. This latter point indicates that the sample was completely dry. These observations indicate that the lower temperature β and γ relaxations are moisture dependent, with the former relating to intermolecular hydrogen bonds between water and amide groups along the polymer chain, and the latter associated with the intra and inter-molecular hydrogen bonds between amide groups

A similar study was carried out by Undin *et al* [35] into the moisture effect on the secondary transitions in a semi-aromatic fibre. As Park *et al* reported, there was a significant increase in the Tg after vaporisation of moisture from the sample. They also confirmed the observation that the β relaxation completely disappeared on drying.

Wide angle x-ray diffraction studies on vacuum dried and moisture absorbed samples did not show any differences in the scattering properties, even though moisture was shown to increase the β relaxation temperature. This confirms the accepted theory that water resides in the amorphous regions of a polymer, as the diffraction patterns did not exhibit any alterations to the crystalline phase.

The interrelationship between moisture and the glass transition was investigated by Reimschuessel [36]. It was shown that the Tg of polyamide 6, in agreement with other hygroscopic polymers, reaches a lower limit when all available amide groups are hydrogen bonded with water. At this point there is complete interaction and the glass transition cannot be suppressed further by moisture.

5.3 Degradation

Although all polymers will undergo thermal degradation at high temperatures, under normal circumstances, photo-degradation is the primary route of deterioration in polyamide materials. Egerton and Shah [37] have shown that although temperatures above 40°C play a role in accelerating the deterioration of polyamides, relatively low temperatures do not cause a significant loss in tensile strength unless accompanied by photolytic action.

UV radiation at wavelengths below 290nm is implicated in the direct photolysis reactions of polymers, whereas wavelengths in the region of 290-400nm are thought to be primarily responsible for photo-oxidation.

Early work suggested that the photolytic breakdown of the polymer chain was initiated by direct chain scission of the amide group [38]:

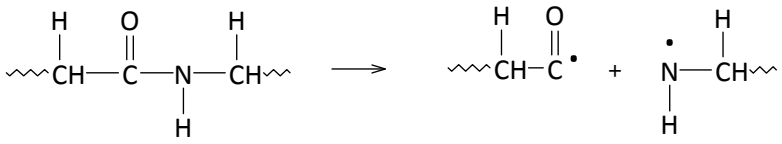

Figure 5.9 Direct photolysis of the amide group in aliphatic polyamides [39]

Kohan [2] states that model compounds of aliphatic polyamides do not absorb UV radiation below 300nm. However, significant UV absorption is seen in polyamides at these wavelengths, and it has been suggested that this is caused by the reactions of other species within the matrix formed during, or remaining after, manufacture [2]. Allen and Parkinson

[40, 41] have attributed these initiation reactions to the presence of α, β-unsaturated carbonyl groups, which show a peak maximum at 290nm. This absorption maximum was shown to decrease after exposure to wavelengths shorter than 300nm. The species was found to be consumed after initial radiation, under both oxygen and nitrogen, but was regenerated in the dark. The authors attributed the reversible photolysis behaviour to the breakdown of the polymer chain vicinal to the carbonyl group:

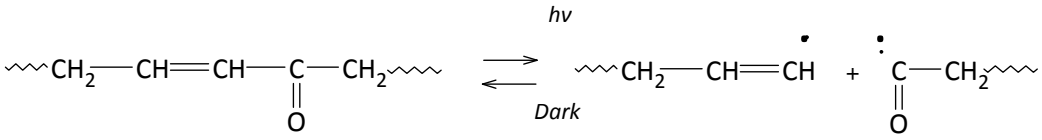

Figure 5.10 Photolysis initiation of α, β-unsaturated carbonyl [40]

The wavelengths between 290-400 nm, relating to photo-oxidation, are of primary interest in this work as these are the wavelengths contributing to photo-degradation during sunlight exposure [42]. Lock and Frank [43] quote the wavelength region between 270-340nm as the primary cause of photo-degradation in polyamide 6,6. The most commonly accepted route of photo-oxidation in aliphatic polyamides is initiated by a free radical, such as formed above in Figure 5.10. This radical abstracts a hydrogen atom from the methylene group vicinal to the nitrogen atom. This leaves a reactive site onto which oxygen attaches to form a peroxide. This then goes onto to degrade further, causing chain scission and cross linkages at terminating reaction sites [2, 39, 43].

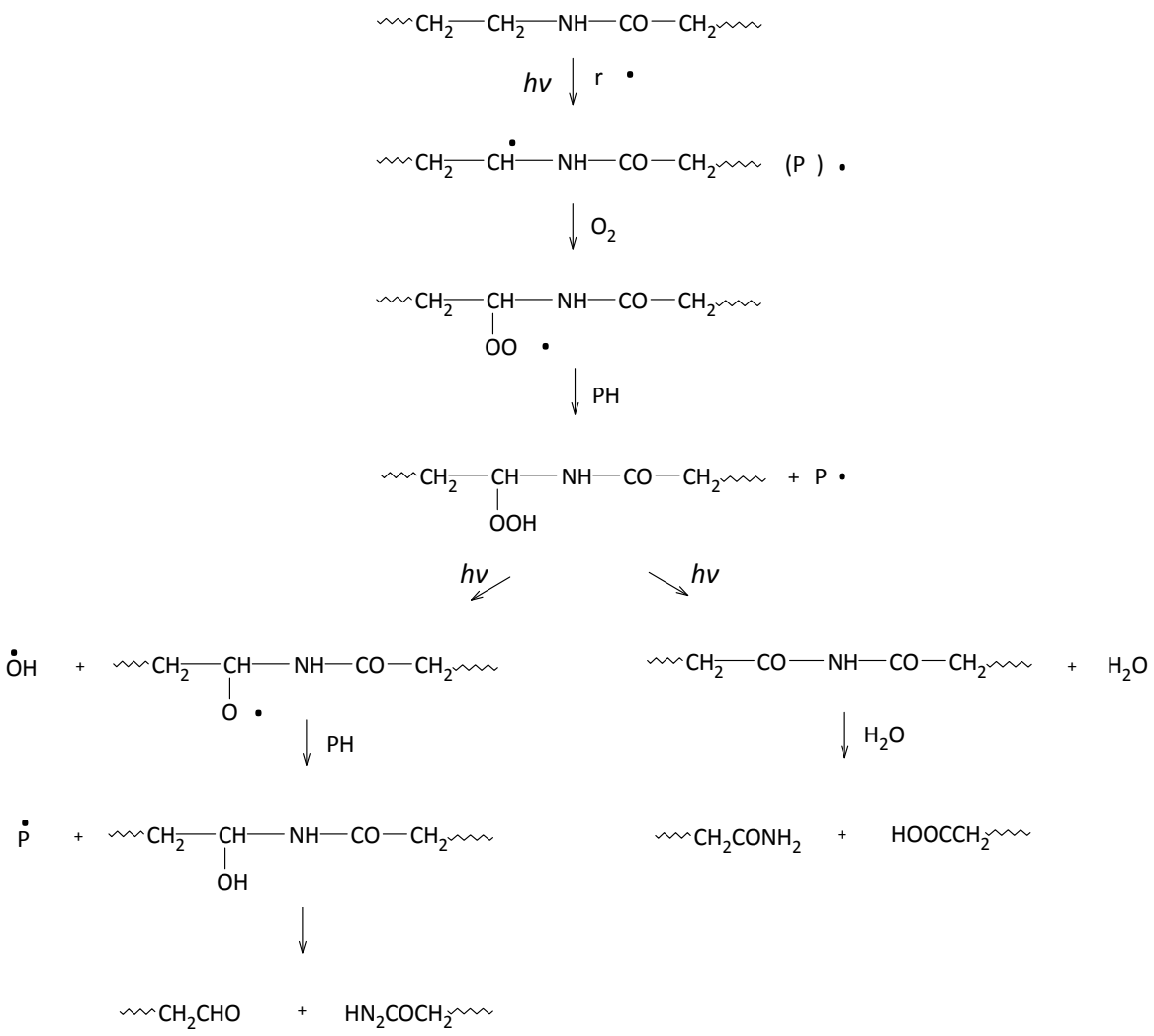

Figure 5.11 Routes of photo-oxidation in aliphatic polyamides [2]

The photo-degradation and break down of the polymer chains have implications for the strength and stability of polyamides, and therefore life expectancy and applications. Meenakumari *et al* [44] used the residual strength as a measure of serviceability in polyamide fishing twine. They showed that the fraction of retained strength was proportional to the length of exposure, for both natural and artificial UV ageing. In a similar study looking into the effect of natural sunlight on the physical strength of polyamide 6 multifilament and monofilament, Thomas and Hridayanathan [45] found that the breaking strength reduced linearly with increased exposure time. However, they did not find a correlation between the elongation at break and the length of exposure. It was found that the multifilament material was more susceptible to UV degradation than the

monofilaments. In addition, the maximum proportional loss of strength was seen in the thinnest samples. This is agreement with Singleton *et al* [46] who state that the degree of degradation is not only dependent on the compounds within the matrix, but also related to the surface to volume ratio. The dependence of the degree of degradation on fibre size has been attributed to the rate of oxygen diffusion into the bulk of the material [47].

Although not covered in detail, it is clear that the breakdown of the polymer chains during photo-degradation will not only have an effect on the mechanical behaviour of polyamides, but will also affect the thermal properties of the polymer too. As previously discussed in Section 5.2.2, it is the underlying structure that governs temperature dependent transitions, and any process that will reduce intermolecular bond and chain order will have a corresponding effect on the glass transition temperature.

5.4 Conclusions

Polyamides are synthetic polymers consisting of a highly oriented, rigid structure interspersed by flexible regions of reduced orientation.
The ordered crystalline regions are maintained by a high degree of crystal packing and intermolecular bonding, and are be characterised by high temperature melting and Brill transitions.
The lower ordered amorphous zones experience regional vibrations and chain mobility at relatively low temperatures, in the region known as the glass transition temperature.
This temperature is related directly to segmental motion and as such, governs the physical properties of the polymer. It is clear that any alterations to the chemical and physical structure will therefore influence the point of the transition between glassy and rubber states. Such factors include the introduction of small molecules, such as water, or the breakdown of the polymer chain during photo-degradation.

The different sub-classes of polyamide material have very similar chemical structures, e.g. differing by the number of methylene groups separating the amide linkages, and any processing additives. Nonetheless, their behaviour in terms of their response to pest treatment measures may differ significantly. Due to the similarity of the chemical structures, the ready differentiation of the various types, such as X,Y and Z, would prove problematic by near-infrared spectroscopy without the means of multivariate analyses.

This will be the focus of the following two Chapters, where the discrimination of the polyamide sub-classes by NIR spectroscopy, coupled with multivariate analyses, will be investigated to enable rapid, non-invasive identification.

5.5 References

1. Lewin, M. and E.M. Pearce, *Handbook of Fibre Chemistry*. 2nd ed. International Fibre Science and Technology Series, ed. M. Lewin. 1998, New York: Marcel Dekker Inc.
2. Kohan, M.I., *Nylon Plastics Handbook*. 1995, New York: Hanser Publishers.
3. Persyn, O., et al., *Structural Organization and Drawability in Polyamide Blends.* Polymer Engineering and Science, 2004. **44**(2): p. 261-271.
4. Murthy, N.S., *Hydrogen Bonding, Mobility, and Structural Transitions in Aliphatic Polyamides.* Journal of Polymer Science Part B: Polymer Physics, 2006. **44**(1763-1782).
5. Jones, N.A., et al., *Chain-folded Lamellar Crystals of Aliphatic Polyamides. Investigation of Nylon 4 8, 4 10, 4 12, 6 10, 6 12, 6 18 and 8 12.* Polymer, 1997. **38**(11): p. 2689-2699.
6. Cotterill, R., *The Cambridge Guide to the Material World*. 1986, Cambridge: Cambridge University Press.
7. Atkins, E.D.T., M.J. Hill, and K. Veluraja, *Structural and Morphological Investigations of Nylon 8 Chain-folded Lamellar Crystals.* Polymer, 1995. **36**(1): p. 35-42.
8. Brydson, J., *Plastics Materials*. 7th ed. 1999, Oxford: Butterworth-Heinemann.
9. Huang, Y., W. Li, and D. Yan, *Preparation and Characterization of a Series of Polyamides with Long Alkyene Segments: Nylon 12 20, 10 20, 8 20, 6 20, 4 20 and 2 20.* Polymer Bulletin, 2002. **49**: p. 111-118.
10. Shashoua, Y.R., *Conservation of Plastics: Materials Science, Degradation and Preservation*. 2008, London: Butterworth-Heinemann.
11. Jones, N.A., et al., *Chain-folded Lamellar Crystals of Aliphatic Polyamides. Investigation of Nylon 4 8, 4 10, 4 12, 6 10, 6 18 and 8 12.* Polymer, 1997. **38**(11): p. 2689-2699.
12. Feldman, A.Y., et al., *The Brill Transition in Transcrystalline Nylon 66.* Macromolecules, 2006. **39**: p. 4455-4459.
13. Vasanthan, N., S.B. Ruetsch, and D.R. Salem, *Structure Development of Polyamide-66 Fibres During Drawing and Their Microstructure Characterization.* Journal of Polymer Science Part B: Polymer Physics, 2002. **40**: p. 1940-1948.
14. Murthy, N.S., M.K. Akkapeddi, and W.J. Orts, *Analysis of Lamellar Structure in Semicrystalline Polymers by Studying the Absorption of Water and Ethylene Glycol in Nylons Using Small-Angle Neutron Scattering.* Macromolecules, 1998. **31**: p. 142-152.
15. Murthy, N.S., et al., *Drawing and Annealing of Nylon-6 Fibres: Studies of Crystal Growth, Orientation of Amorphous and Crystalline Domains and Their Influence on Properties.* Polymer, 1995. **36**(20): p. 3863-3873.
16. Brydson, J., *Plastic Materials*. 7th ed. 1999, Oxford: Butterworth-Heinemann.
17. Murthy, N.S., et al., *Drawing and Annealing of Nylon 6 Fibres: Studies of Crystal Growth, Orientation of Amorphous and Crystalline Domains and Their Influence on Properties.* Polymer, 1995. **36**(20): p. 3863-3873.

18. Vasanthan, N., S.B. Ruetsch, and D.R. Salem, *Structure Development of Polyamide 66 Fibers During Drawing and Their Microstucture Characterization.* Journal of Polymer Science Part B: Polymer Physics, 2002. **40**: p. 1940-1948.
19. Qiu, W., A. Habenschuss, and B. Wunderlich, *The Phase Structure of Nylon 66 as Studies by Temperature-modulated Calorimetry and Their Link to X-ray Structure and Molecular Motion.* Polymer, 2007: p. 1-10.
20. Gordon, G.A., *Glass Transitions in Nylons.* Journal of Polymer Science Part A-2, 1971. **9**: p. 1693-1702.
21. Toivonen, A.L., *Investigating the Effect of Cold Winter Conditions on Fishing Gear Materials.* Journal of the Textile Institute, 1992. **83 Part 1**: p. 163-177.
22. Simal, A.L. and A.R. Martin, *Structure of Heat-Treated Nylon 6 and 6.6 Fibres I. The Shrinkage Mechanism.* Journal of Applied Polymer Science, 1998. **68**: p. 441-452.
23. Higashioji, T. and B. Bhushan, *Creep and Shrinkage Behaviour of Improved Alternate Substrates for Magnetic Tape.* IEEE Transactions on Magnetics, 2001. **37**(4): p. 1612-1615.
24. Zimmerman, J. and M.I. Kohan, *Nylon - Selected Topics.* Journal of Polymer Science Part A: Polymer Chemistry, 2001. **39**: p. 2565-2570.
25. Toivonen, A.L., P. Jarvela, and P. Nousianinen, *The Effects of Cold Winter Conditions on Fishing Gear Materials Part II: Strength Examination of Freeze-thawed Polyamide and Polyethylene Multifilament Nettings.* Journal of the Textile Institute, 1996. **87 Part 1**(3): p. 572-585.
26. Jin, X., T.S. Ellis, and F.E. Karasz, *The Effect of Crystallinity and Crosslinking on the Depression of the Glass Transition Temperature in Nylon 6 by Water.* Journal of Polymer Science: Polymer Physics, 1984. **22**: p. 1701-1717.
27. Zilberman, M., A. Siegmann, and M. Narkis, *Structure and Properties of 6/6.9 Copolyamide Series I: Amorphous Phase.* Journal of Applied Polymer Science, 1996. **59**: p. 581-587.
28. Botta, De Candia, and Palumbo, *Glass Transition in Aliphatic Polyamides.* Journal of Polymer Science, 1985. **30**: p. 1669-1677.
29. Basheer, R.A., A.R. Hopkins, and P.G. Rasmussen, *Dependence of Transition Temperatures and Enthalpies of Fusion and Crystallization on Composition in Polyaniline/Nylon Blends.* Macromolecules, 1999. **32**: p. 4706-4712.
30. Zilberman, M., A. Siegmann, and M. Narkis, *Structure and Properties of 6/6.9 Copolyamide Series I. Amorphous Phase.* Journal of Applied Polymer Science, 1996. **59**: p. 581-587.
31. Vlasveld, D.P.N., et al., *Moisture Absorption in Polyamide-6 Silicate Nanocomposites and its Influence on the Mechanical Properties.* Polymer, 2005. **46**: p. 12567-12576.
32. Ellis, T.S., *Moisture Induced Plasticization of Amorphous Polyamides and Their Blends.* Journal of Applied Polymer Science, 1988. **36**: p. 451-466.
33. Men, Y., J. Rieger, and K. Hong, *Critical Strains in Tensile Deformed Polyamide 6 and 6/66 Copolymer.* Journal of Polymer Science Part B: Polymer Physics, 2005. **43**: p. 87-96.
34. Park, Y., et al., *Moisture Effects on the Glass Transition and the Low Temperature Relaxations in Semiaromatic Polyamides.* Journal of Polymer Science Part B: Polymer Physics, 1997. **35**(5): p. 807-815.
35. Uddin, A.J., et al., *Influence of Moisture on the Viscoelectric Relaxations in Long Aliphatic Chain Contained Semiaromatic Polyamide, (PA9-T) Fibre.* Journal of Polymer Science Part B: Polymer Physics, 2003. **41**: p. 2878-2891.

36. Reimschuessel, H.K., *Relationships on the Effects of Water on Glass Transition Temperature and Youngs Modulus of Nylon 6.* Journal of Polymer Science: Polymer Chemistry, 1978. **16**: p. 1229-1236.
37. Egerton, G.S. and K.M. Shah, *The Effect of Temperature on the Photochemical Degradation of Textile Materials.* Textile Research Journal, 1968. **February**: p. 130-135.
38. Do, C.H., et al., *FT-IR Spectroscopic Study on the Photo- and Photooxidative Degradation of Nylon.* Journal of Polymer Science Part A: Polymer Chemistry, 1987. **25**: p. 2301-2321.
39. Do, C.H., et al., *FT-IR Spectroscopic Study on the Photo- and Photo-oxidative Degradation of Nylons.* Journal of Polymer Science: Part A: Polymer Chemistry, 1987. **25**: p. 2301-2321.
40. Allen, N.S. and A. Parkinson, *Ultraviolet Derivative Absorption Spectra of Nylon 6,6: Effect of Photolysis Vs Photo-induced Oxidation.* Polymer Degradation and Stability, 1982. **4**: p. 239-244.
41. Allen, N.S., *A Study of the Light Absorption Properties of Polymer Films Using UV Derivative Spectroscopy.* Polymer Photochemistry, 1981. **1**: p. 43.
42. Hamid, S.H., ed, *Handbook of Polymer Degradation*. 2nd ed. 2000, New York: Marcel Dekker Inc.
43. Lock, L.M. and G.C. Frank, *A Study of Some Factors Affecting the Photodegradation of Textile Yarns Part II: Nylon 66 and Polyethylene Terephthalate Yarns.* Textile Research Journal, 1973. **September**: p. 502-512.
44. Meenakumari, B., K. Ravindran, and A.K. Kesavan Nair, *Effect of Sunlight and UV Radiation on Mechanical Strength Properties of Nylon Netting Twine.* Indian Journal of Textile Research, 1985. **10**(March): p. 15-18.
45. Thomas, S.N. and C. Hridayanathan, *The Effect of Natural Sunlight on the Strength of Polyamide 6 Multifilament and Monofilament Fishing Net Material.* Fisheries Research, 2006. **81**: p. 326-330.
46. Singleton, R.W., R.K. Kunkel, and B.S. Sprague, *Factors Influencing the Evaluation of Actinic Degradation of Fibers.* Textile Research Journal, 1965. **March**: p. 228-237.
47. Zimmerman, J., *Degradation and Crosslinking in Irradiated Polyamides and the Effect of Oxygen Diffusion.* Journal of Polymer Science 1960. **46**: p. 151-162.

Chapter 6: Multivariate Analysis and the Determination of the Experimental Protocols

The ability to classify the various types of synthetic polymers found in contemporary heritage collections is of prime importance. If deterioration is not to be exacerbated by the application of detrimental treatments or environments then an understanding of an artefacts constituents is vital.

It has already been shown that the use of near-infrared spectroscopy together with a comprehensive reference spectral library and appropriate spectral matching software can successfully resolve this problem when analysing materials of distinct classification and garments of simple construction. However, a more robust method is required when attempting to differentiate chemically similar polymers.

In the event of a pest infestation, such robust, non-invasive analysis would prove an invaluable tool for conservators, enabling vulnerable material to be readily identified prior to treatment. Case Study I, Chapter 2, illustrated the problem of misclassification of visually similar textiles. If an infestation were to have occurred, the garment could have been subject to thermal treatment since silk has been shown to be stable under such conditions. However, the dress may have been vulnerable to damage as it was actually found to be synthetic polyamide.

In this Chapter the background to multivariate analytical techniques for the problem of discrimination and classification will be discussed. Experimental focus will be given to the extraneous factors that influence the near-infrared spectrum, and as a consequence, the calibration models. The outcomes of these preliminary studies enabled the confident discrimination of natural and synthetic polyamide materials; namely, wool, silk and polyamide, as described in the next Chapter.

6.1 Multivariate Analysis

The purpose of multivariate analysis is to reduce large data sets, containing many variables, to a smaller set of components in order to enable the user to monitor patterns or highlight any co-dependant variables not readily seen in the raw data set. It extends the process of univariate and bivariate calibration, which ordinarily highlights any correlations to be found within a set of data, but is only easily applied within the dimensions of the Cartesian coordinate system. When there is one, two or three variables under study it is possible to plot data onto *xyz* axes and readily identify whether there are any patters or co-dependencies visible within the samples. For example it is possible to ask whether an increase in *x* has a corresponding increase or decrease in *y*. In the former situation the variables are said to be positively correlated and in the latter they are negatively correlated. If there is no change in *y* as *x* is increased then there is no relationship between these two variables.
As more variables are introduced then it becomes increasingly difficult to identify whether such patterns exist. Multivariate analysis provides a means of interpreting such complicated, multi-variable data.

Mulitvariate analysis (MVA) uses matrix algebra to study and find correlations across a multi-dimensional, multi-variable space. The initial data matrix is known as the *X* matrix and is made up of *n* rows and *p* columns [1]. In the case of NIR spectra, *n* are the number of recorded samples, expressed as intensity of absorbance at each wavenumber. The *p* values represent the number of variables, which are the wavenumbers (Figure 6.1).

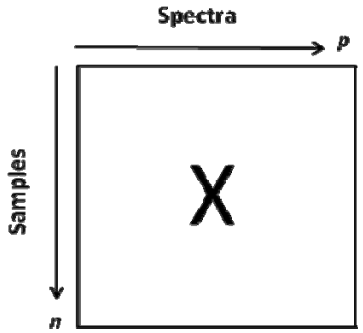

$$X = \begin{bmatrix} x_{11} & x_{12} & x_{13} & \ldots\ldots & x_{1p} \\ x_{21} & x_{22} & x_{23} & \ldots\ldots & x_{2p} \\ x_{31} & x_{32} & x_{33} & \ldots\ldots & x_{3p} \\ \vdots & & & & \\ x_{n1} & x_{n2} & x_{n3} & \ldots\ldots & x_{np} \end{bmatrix}$$

Figure 6.1 the X matrix made up of the row wise samples and column wise wavenumbers

For NIR spectroscopic data, the number of variables can be anywhere in the region of 2 000-12 000, corresponding to the number of recorded data points across the spectral region for each sample, and dependent on the spectral resolution. The use of multivariate calibrations allows spectroscopic changes to be monitored, which relate to changes in the sample sets. This is a particularly useful application when studying near-infrared spectra. As already discussed in Chapter 1, the origin of NIR spectra relate to overtone and combination vibrations. This causes the spectra to be characteristically complicated with many overlapping bands. The low visual resolution of the spectra inhibits ready interpretation of wavenumber shifts and changes in absorbance, as such variations may be related to a change in one or more factors.

There are a number of multivariate techniques that can be applied to the problem of calibrating large data sets, ranging from simple classification of samples into “groups”, to more complex linear regression methods for quantification problems. However, most of these are based on one underlying process, known as Principal Component Analysis (PCA) [2].

6.1.1 Correlation Matrix

Principal component analysis is a method used to reduce large amounts of data to a smaller, more manageable data set. It highlights the dependent variables and removes superfluous data, which can be classed as noise. This is usually done through the application of the NIPALS algorithm (nonlinear iterative partial least squares), which computes a new coordinate system using the X matrix.

Any correlations that exist in the data are highlighted, and are directly related to the co-variance and correlation matrices, which can be described through the n x p data set.

Details of the NIPALS algorithm are not provided here, but the reader is directed to the relevant literature [1, 2].

The variance and covaraiance of the data are calculated in the same manner as those applied in univariate analysis, only they are applied across the entire data set and used to construct the correlation matrix.

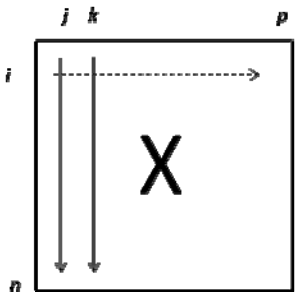

Figure 6.2 Components of the X matrix

The variance calculation is used to determine the variance of all the variables (*p*), and it is a measure of the distribution of intensities, amongst different samples, looking down each column (*j*) (Figure 6.2).

$$Stj^2 = \frac{1}{n-1}\sum_{i=1}^{n}(xij - \bar{x}j)^2$$

j = 1 ..... *p*

Figure 6.3 Variance calculation [2]

The co-variance is used to determine whether there is an association between adjacent *p* variables (wavenumbers). It is a measure of the spread looking down two wavenumber columns simultaneously (*j, k*).

$$\mathrm{Cov}(j,k) = \frac{1}{n-1}\sum_{i=1}^{n}(xij - \bar{x}j)(xik - \bar{x}k)$$

j, *k* = 1 ..... *p*

Figure 6.4 Covariance calculation [2]

Based on the above relationships, the correlation matrix is calculated. However, the data need to be normalised by use of the relevant standard deviations. This scales variables, or wavenumbers, so that factors such as sample concentration are accounted for. A measure of similarity or difference can then be found within the sample set. Normalisation is carried out by dividing the covariance values with the product of the corresponding deviations from the *j* and *k* columns.

$$r_{jk} = \frac{\mathrm{Cov}(j,k)}{StDev_j\, StDev_k}$$

Figure 6.5 Correlation calculation [2]

If *j* and *k* are the same, in this case the corresponding absorbance intensities, then dividing by two standard deviations that are the same will give a correlation of one.

$$R = \begin{bmatrix} 1 & r_{12} & r_{1p} \\ r_{12} & 1 & \vdots \\ r_{1p} & \cdots & 1 \end{bmatrix}$$

Figure 6.6 Correlation matrix [2]

The above calculations allow the relationships within the data set to be highlighted, before decomposition into the smaller matrices which will be discussed in the following section.

6.1.2 Principal Component Analysis

As already outlined, principal component analysis is used to reduce the original data to a small number of components by defining a new co-ordinate system. It does this by decomposing the X matrix into two smaller matrices and determining any correlations. These two components are known as the scores and loadings matrices, S and L^T respectively, and are determined through a process of iteration (Figure 6.7) [2].

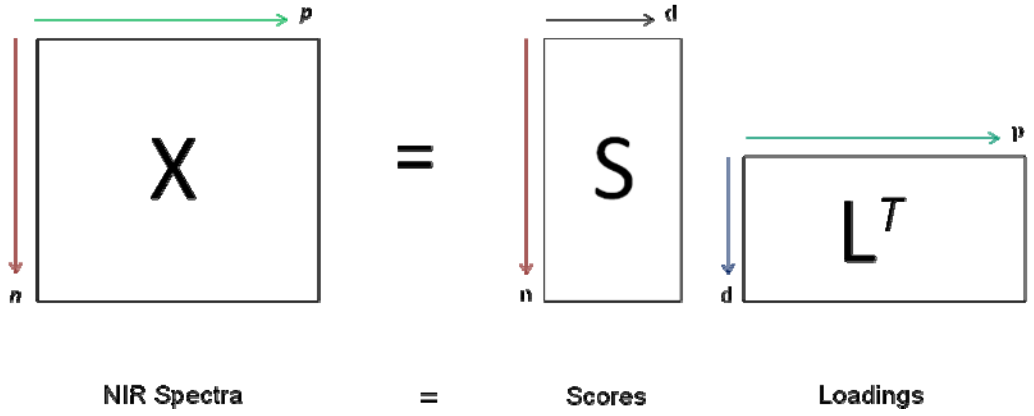

Figure 6.7 Scores and loadings matrices

Effectively, an approximation of the loadings matrix is first made, and along with the known X matrix, is used to calculate the scores matrix. This is then used to refine the loadings matrix along with X, until all of the data have been described. The appropriate relations are shown below.

$$X = SL^T$$

$$S = \frac{X}{L^T}$$

$$S = XL$$

Where L^T is a transpose matrix of S

Figure 6.8 Iterative approaches to calculating the scores matrix

The scores represent the distance of each sample from each principal component (PC) which is the new axes that describe the spread of the data along a given direction. The

first PC is the new axis that describes the greatest variance within the data. The second PC is orthogonal to the first and describes the second largest variance in the data. This pattern follows for all subsequent PC's until all of the data have been modelled.
The first principal component is calculated using the first column of the loadings matrix and all of the rows in the X matrix, as follows:

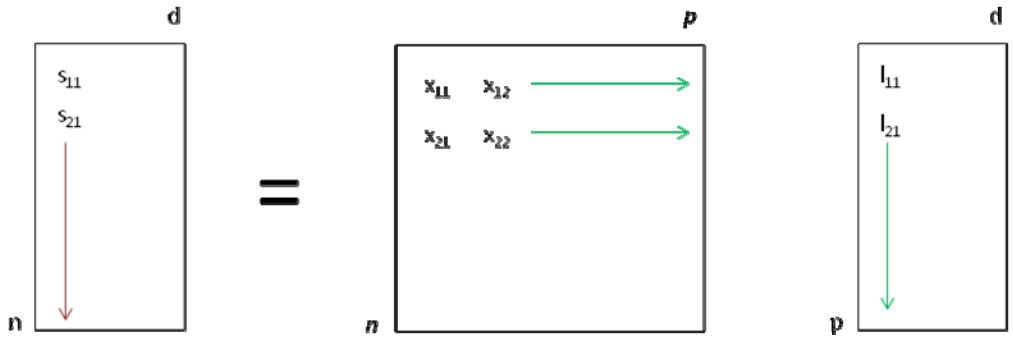

$$s_{11} = x_{11} l_{11} + x_{12} l_{21} + x_{1p} l_{p1}$$
$$s_{21} = x_{21} l_{11} + x_{22} l_{21} + x_{2p} l_{p1}$$

Figure 6.9 Calculation of the co-ordinates for the first principal component [2]

6.1.2.1 Scores and Loadings Plots

If the first principal component is represented in a two dimensional co-ordinate system, then the loadings represent the angle of the new PC from the original axes. This is illustrated in Figure 6.10. The two variables p1 and p2 are two wavenumbers from across the near-infrared spectrum. Each data point represents the intensity at each wavenumber (X1 for p1, X2 for p2) for each of the samples in the data set. The diagram is a schematic and not based on real data.

The first principal component, shown here in red, represents the maximum variance in the data and is fitted in a similar manner to finding the line of best fit in conventional calibration, by reducing the sum of the squares of the residuals. The next PC is orthogonal to the first, so would lie at 90 degrees to the red line.

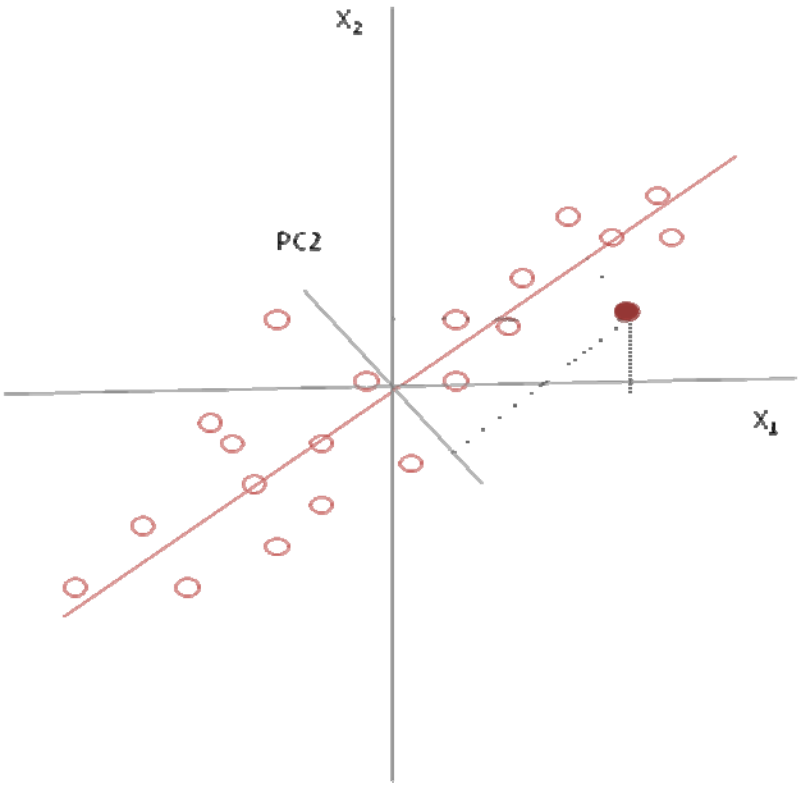

Figure 6.10 Illustration of the first two principal components relative to the original axes

The loadings represent the cosine of the angle between the new co-ordinate axis and the original co-ordinate axis. This gives an indication of the contribution that particular variable has to the PC of interest [1]. The closer the PC is to the original axis then the greater is the contribution that this variable makes to that component. If the first principal component is at right angles to a particular axis then that wavenumber contributes nothing:

$$\theta = 0, \ \cos\theta = 1$$

$$\theta = 90, \ \cos\theta = 0$$

$$\theta = 180, \ \cos\theta = -1$$

This will be discussed in more detail later, however the loadings plots enable the contributing wavelengths to be determined. This highlights which spectral regions are contributing to the calibration model. Thus enabling an assessment of whether regions of high noise are being modelled or those corresponding to true spectral information.

6.1.2.2 Outliers

An outlier is a sample that widely differs from the rest of the sample population. In the case of the work presented here, an outlier represents a sample with physical and chemical properties affecting the near-infrared spectrum, but not contributing the information of interest. A sample may be an outlier in a data set due to factors such as misclassification, differences in light scattering properties and effects of colour. Careful consideration is need before removing a sample from a data set. The raw spectra should be studied, determining whether obvious discrepancies exists between the remainder of the calibration set.

It can be seen in Figure 6.11 that the inclusion of an outlier (blue triangle) will have a skewing effect on the direction of the PC (blue), and subsequent, principal components. This will affect the overall description of the data and the interpretation of the relevant loadings plots.

Outlier detection is an important factor when building PCA models due to their effect on the overall description of the data. Consideration needs to be given as to whether a sample is a true outlier or whether it is just an extreme example within that group. If such a sample were to be removed from the calibration set purely because of its skewing effect on the data, then future samples with the same properties would not be accounted for and this would prevent classification.

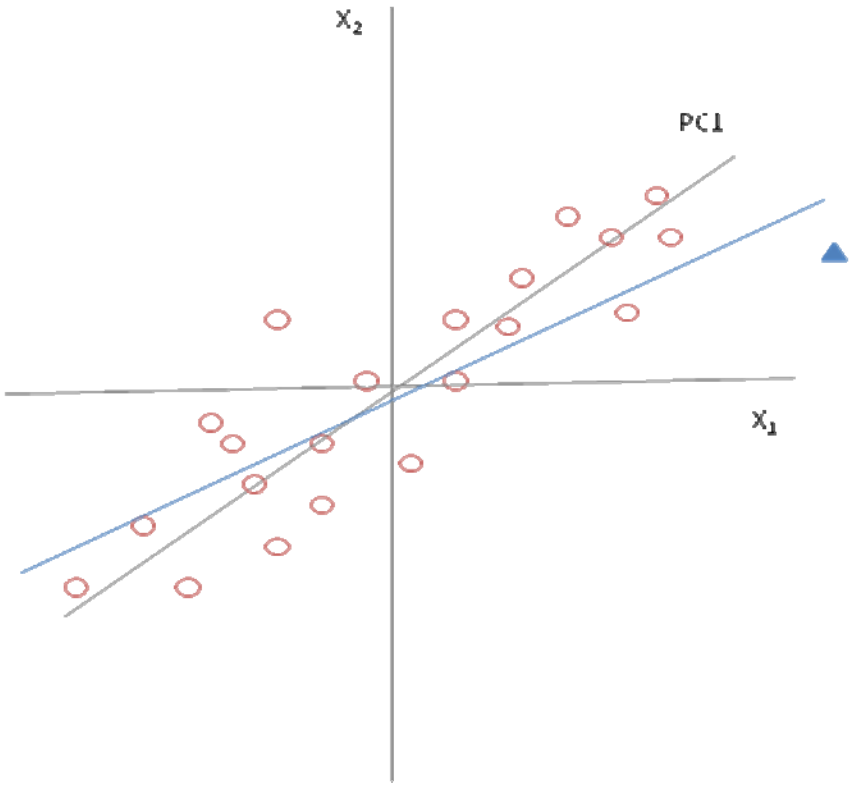

Figure 6.11 Illustration of the first principal component and the effect of an outlier

6.1.3 Pre-processing of the Raw Spectra

As the nature of the near-infrared spectra is influenced by physical scattering properties, in addition to low resolution bands, it is usually necessary to apply spectral pre-processing methods. This helps unify the data and ensure that any variability being modelled relates to that of interest. Such methods can include mean centring, smoothing methods and baseline corrections. The latter covers a number of methods, that can be applied to account for a constant off-set data or wavelength dependent scattering [3].

In all calibration models built during this work the initial analyses were carried out on the raw, unprocessed spectra. The reason for this was to help determine what regions of the spectrum were having the greatest effect on the spectrum, thus highlighting, for example, whether regions of high noise needed to be removed.

If two or more pre-processing methods are used in conjunction, then the order in which they are applied can be an important factor. On discussion with Professor T.

Fearn[I], Professor of Applied Statistics at University College London, it was suggested that as a general rule the standard normal variate method was usually applied before derivatives are used, but this is a process of trial and error and there is no one way of carrying out data processing.

The choice of pre-processing methods should be made with an understanding of the variability to be found in the data and the possible problems that may be encountered. However, it is acceptable to apply a number of relevant methods and study the results before the final analysis is carried out on the data [4].

A number of pre-processing methods, such as first and second derivative transformations, have already been covered in Section 2.3, Chapter 2, and will not be discussed here.

6.1.3.1 Mean Centring

Mean centring of the data is always applied before the PCA calibration. The process is a column wise transformation and it subtracts the mean of each variable (wavenumber) from the variable value for each sample. This effectively means that the focus is on the deviations from the mean, and studies the variance rather than the raw data. This is a similar process to that for the correlation matrix (Figure 6.5), but mean centring focuses on each column individually rather than comparing two columns consecutively.

6.1.3.2 Standard Normal Variate

The standard normal variate (SNV) transformation is a row wise function, which subtracts the mean of each individual spectrum from each value. Each value is then normalised by dividing with the standard deviation from the individual spectrum [5]. The SNV method is not a pre-requisite for multivariate analyses, but is often found to improve calibration by reducing the effects of shifting baselines caused by scattering.

6.1.4 Classification Methods

There are a number of classification methods available that can be applied to discriminate between groups of data. The simplest methods use averaged measures of distance, as already discussed in Chapter 3. These, however, can be problematic on two

[I] Private conversation with Professor T. Fearn, Department of Statistical Science, University College London, 14 April 2008.

counts. Firstly, they do not have the ability to reject a sample even when a true match is not present in the calibration set. Secondly, they do not provide a means of distinction between real data and noise[II], and therefore a correlation may be found, but not necessarily with the desired property of a material. The application of multivariate classification methods enables large amounts of data to be reduced, and patterns found, which can be related directly back to the underlying features that make up the different classes.

6.1.4.1 Soft Independent Modelling of Class Analogies

One of the most commonly applied multivariate classification methods is Soft Independent Modelling of Class Analogies (SIMCA), applied for the determination of groups within data. Examples include the identification of different species of oak coupled with NIR spectroscopy [6] and the determination of the presence of nitrogen containing nutrients within microalgal cells using Raman spectroscopy [7].

SIMCA is used to build separate principal component models for each known subclass. The PC dimensionality of each model can be visualised as individual, multidimensional boxes that contain each sample for that class. New samples are then categorized depending on their orientation in PC space with respect to the centre of the model and the distance from the model boundaries [8]. Figure 6.12 is a schematic of three principal component models, representing three different groups of samples. Unknowns will be classified as belonging to a group if their Euclidean distance is not significantly larger than the Euclidean distance of the class samples to the PC model [9].

[II] In the case of the work presented here, noise is defined as the spectral responses which do not relate directly to the chemical and physical properties of interest. These include factors such as high NIR absorbing species, such as colourants. These can cause increased absorption towards the longer wavenumber region of the spectrum, impacting on the decomposition of the calibration model. Other sources of 'noise' relate to the scattering properties of the sample, and instrument noise.

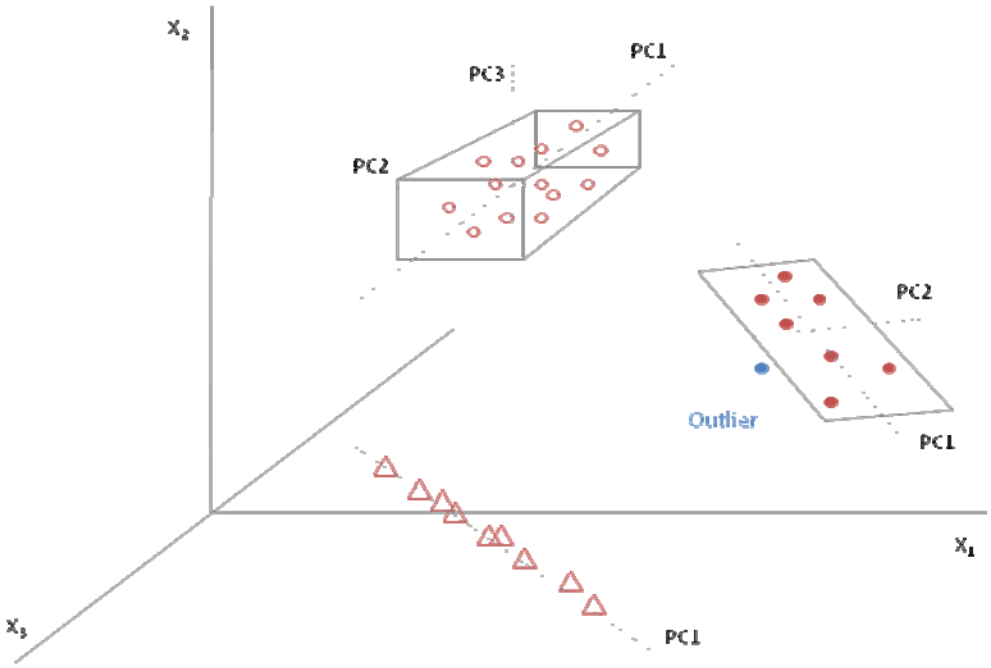

Figure 6.12 Schematic representation of three principal component models in three dimensional space [2]

The software allows for the statistical significance levels to be set to ensure that a level of certainty can be determined as to whether an object truly belongs to a particular group. An F-test is used, related to the deviations of the objects from the respective calibration models [9]. In the work presented here significance levels were set at 5%. This means that there is a 5% chance of a Type I error, ie a sample that truly belongs to a group being rejected as an outlier. The higher the significance level is set the stricter the model.

The SIMCA method allows an unknown sample to be compared to each class in turn and to determine whether it shows similar characteristics to one or more class, or whether it does not belong to any of the groups in question. This latter point is one of the strengths of the SIMCA method when compared to other classification methods that utilise measures of distance [10].

Depending on “across group” variability, different models may occupy similar regions in PC space. If the boundaries of two or more PCs overlap then there may be problems with classification, especially at the extremes. In such cases the sample may be

classified as belonging to more than one group, which in turn allows for possible anomalies to be detected [1].

6.1.4.2 Partial Least Squares Discriminant Analysis

The second method used to investigate the classification of polyamide material in this work is Partial Least Squares Discriminant Analysis (PLS-DA). The PLS method is a multidimensional regression method, which has typically been coupled with near-infrared spectroscopy and applied to quantitative applications. These applications include the quantification of copolymer concentration in the production of acrylic fibres [11], the determination of moisture content in human skin [12] and the determination of stresses in hanging silk textiles [13].

PLS has often been applied in cases where a spectroscopic technique is to be used in place of more time consuming, laboratory methods. This is done by formulating a calibration model using spectroscopic data and an independent response, such as tensile strength [13] or pH levels [14]. The resulting regression line is used to correlate changes in spectroscopic data back to the original property of interest.
In addition to quantitative determinations, the method has been shown to be applicable to problems of discrimination [15-17], and has therefore been investigated as a comparative method to SIMCA.

Partial Least Squares regression is based on an algorithm using two matrices. There is an X matrix, which is the same as that described in Section 6.1, and a Y matrix. The Y matrix contains independent responses, such as analyte concentrations or a physical property such as tensile strength, independently determined from the calibration samples. The Y matrix may be a *1*x*n* matrix (PLS1) or a larger *p*x*n* matrix (PLS2), depending on the problem (Figure 6.13).

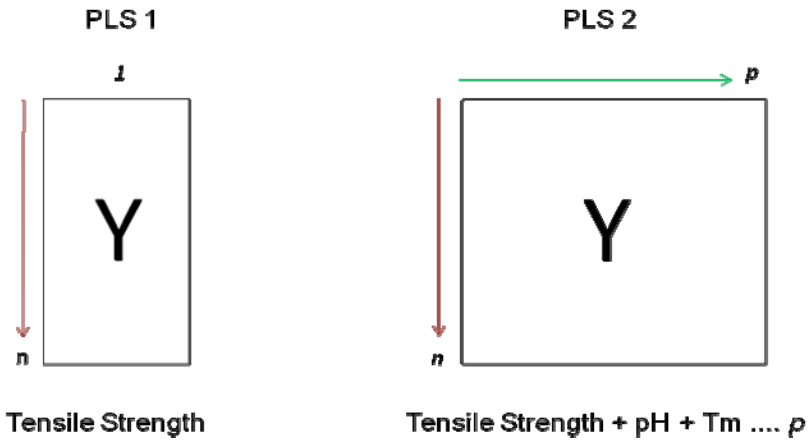

Figure 6.13 The Y matrix in PLS1 or PLS2 multivariate regression

Esbensen [1] describes the process as a two way principal component analysis.
The algorithm works by using the scores of the Y matrix (U) in the initial decomposition of the X matrix. So, whereas in Figure 6.8 the loadings are used to make an approximation of the scores before the iterative calculations continue:

$$S = XL$$

Figure 6.14 Iterative approaches to calculating the scores matrix in PCA

The Y matrix (U) replaces the original scores:

$$U = XL$$

Figure 6.15 Iterative approach to calculating the loadings matrix in PLS

This leads to a calculation of the X-loadings (L) that have been directly influenced by the Y matrix. These loadings are then used to calculate the actual scores for the X matrix (S). In turn, S is used to fully decompose the Y matrix. As before, this is an interative approach. By decomposing the two matrices together, factors that correlate with the information held in Y are highlighted.

In using PLS-DA a quantitative approach of analysis is being exploited for a qualitative problem of classification. The way in which PLS can be applied to the problem of discrimination is through the construction of a false Y matrix. This uses a binary system

for column wise variables, *J*, and each sample in the data set is assigned 0 or 1 depending on group membership [16]. Samples belonging to the class of interest are assigned one, all remaining samples from the other classes are assigned zero. A new Y matrix is constructed for each group.

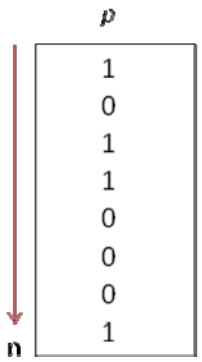

Figure 6.16 Pseudo Y matrix showing the sample classification using a binary system

6.1.5 Validation Method

Validation of the final models is an important step in determining how well the calibration will determine future unknown samples. There are a number of methods possible, such as leverage correction or the test set method. However, due to a limited number of samples available it was not possible to have a completely independent set of validation samples. Therefore the method employed throughout this work was a full cross-validation method.

The full cross-validation method applies the same samples used in the calibration to validate the model. One sample is left out of the calibration in succession and the model is calibrated. The sample which has been left out is then predicted using the calibration and the residuals determined. This is repeated for each sample in the calibration set. This method highlights possible outliers and enables the modelling power of the calibration to be assessed through the explained variance [18].

Cross validation allows a measure to be made of the residual variance between the actual and projected X-values. The cross validation process is repeated for each principal component in turn. The result is presented as the explained variance plot and is used to determine the number of principal components required to describe the data as fully as possible.

De Maessachalck et al [9] reported that the number of PCs calculated necessary to describe different dosage strengths of a set of tablets was larger than expected when accounting for the "within group" similarities. On discussion with Professor T Fearn[III], the over optimistic calculation of principal components was highlighted as a common problem within PCA. It was suggested to use fewer PCs than the software calculates to avoid overfitting of the models. The approach taken was to determine at which PC the explained variance values reached a plateau and use one fewer PC than this point.

6.2 Application to Polyamides

The software used for the following multivariate analysis was Camo Technologies Inc, The Unscrambler® version 9.7. This package allows for graphical representations of the scores and loadings plots to be made and classification of subsequent materials using the Soft Independent Modelling of Class Analogies application (SIMCA) or via Partial Least Squares Discriminant Analysis (PLS-DA).

For each individual sample three replicate NIR measurements were made, and averaged using Thermo Galactic Grams AI® version 7.1 software. If it is known that there is some variation across a sample it can be appropriate to leave individual spectra in as "pseudo" new data. However, this can be problematic when it comes to applying a cross validation method, as these measurements will be treated as new samples and fitted to the model as such, when they have actually already been represented in the calibration model[III]. This will result in an over optimistic correlation.

The first step in multivariate classification is to look at the full data set using principal component analysis, before applying the individual classification methods. This is to determine how the samples are clustered, and whether there is any inherent separation in the data relating to the different classes. It is during this step that the influential variables (wavenumbers) are highlighted and selected, pre-processing methods applied and any outliers are removed from the data. It is only after the data has been studied as a whole that the classification methods are applied.

[III] Private conversation with Professor T. Fearn, Department of Statistical Science, University College London, 14 April 2008.

The following sections will illustrate the application of the multivariate technique for classification and the steps taken to determine whether it is possible to distinguish the different polyamide classes. The initial step was to determine what additional factors other than the underlying chemistry of the samples may have an influence on the calibration models. These are presented in Section 6.2.1 below.
Once these had been determined Principal Component Analysis could be applied to discriminate the major polyamide groups; namely synthetic aliphatic polyamides (Nylon), silk and wool. Latterly, the discrimination of the subgroups of synthetic polyamides was investigated. A full discussion of these calibrations models will be presented in Chapter 7.

6.2.1 Extraneous Factors to be Considered Before Calibration

Near-infrared spectra are affected by factors other than the underlying chemical structure of a material (Section 2.5, Chapter 2 and Section 3.4, Chapter 3). As such, these needed to be accounted for before the final calibration could be made. This was to ensure that only the variations of interest were influencing the models, rather than other extraneous properties. NIR spectra were acquired using the experimental methodology set out in Section 3.1.1.2, Chapter 3.

6.2.1.1 Probe vs Integrating Sphere

The physical difference between the fibre optic probe and integrating sphere accessories have already been discussed in Section 2.2, Chapter 2. Since the optical probe is known to collect a degree of specularly reflected light, in addition to diffusely reflected light, there may be small variations in the resulting spectrum when compared to those collected using the integrating sphere. Although these differences did not have a detrimental effect on the identification of distinctly different materials, they may, however, be an important factor when only minor spectral changes are likely to be experienced between the sub-classes of the polyamide material. In order to test this, a selection of reference materials were analysed using both the fibre optic probe and the integrating sphere and principal component analysis applied to the data set. This was to determine whether each sample pair occupied the same PC space, highlighting whether the two techniques were interchangeable.

6.2.1.2 Effect of Physical Form

The diffusely scattered light dominating the near-infrared spectrum means that the surface properties of a material will affect the way in which the radiation is reflected back from the surface. As already shown to be the case when studying highly reflective surfaces in the shoe collection at The Victoria and Albert Museum (Section 3.4.3, Chapter 3), refractive properties can influence the spectrum. Therefore, the spectral variations between solid and extruded reference samples have been investigated, to determine whether materials of differing physical form require separate PCA models.

6.2.1.3 Effect of Colour

As was previously shown in Section 2.5.2.8, Chapter 2, the near-infrared spectrum is influenced by absorption from coloured species as wavenumbers increase. Consequently, colour may have been an important factor in the successful discrimination of the polymer sub-classes and thus warranted further investigation. To determine this, the spectra from the same polyamide 6,6 netting, dyed using a variety of colours, were collected. These were then studied using PCA to study what effect colour may be expected to have on subsequent analyses.

6.2.2 Preliminary Calibrations to Determine the Influence of the Extraneous Factors

6.2.2.1 Probe vs. Integrating Sphere

In order to determine whether spectra collected with the probe (P) and the integrating (IS) sphere are interchangeable with respect to PCA, reference spectra from 44 samples were collected using both accessories. To ensure that the effects being studied were only related to the method of analysis, all spectra were collected using the same experimental parameters and only solid synthetic polyamides (polyamide 6, polyamide 11, polyamide 12, polyamide 6,6, and two aromatic polyamides) were analysed.

Figure 6.17 shows the scores plots for the first two principal components calculated from the unprocessed spectra. It is clear that although many of the duplicate samples occupy similar regions in space, there are rather more sample analyses by the probe that are clustered away from the majority of the data. This indicates that there may be a problem when interchanging between the two accessories.

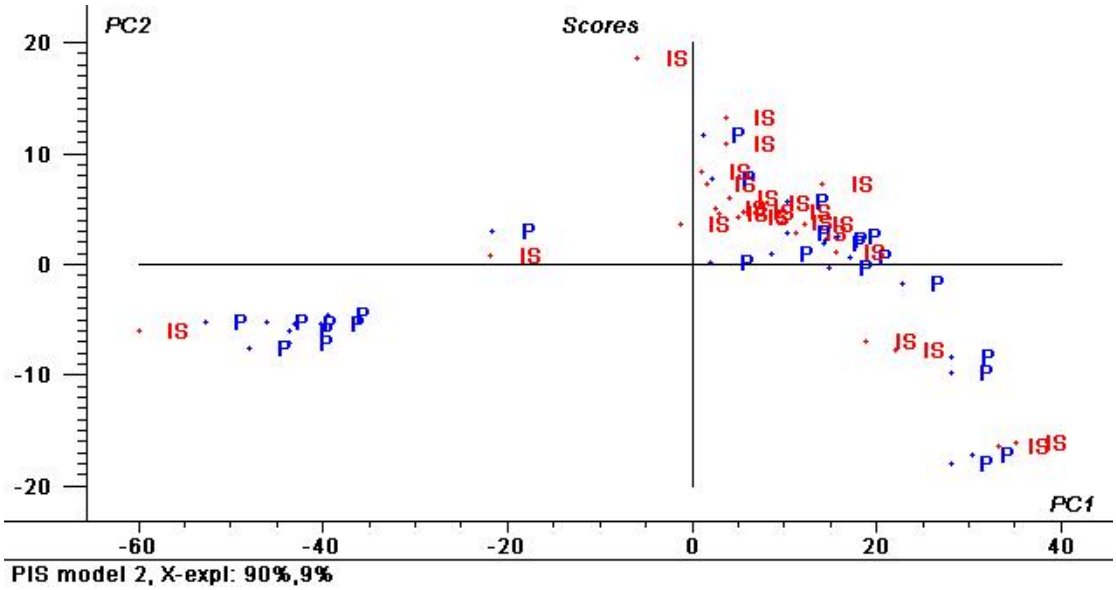

Figure 6.17 Raw data scores plot for the first and second principal components before spectral processing. Data were collected with the NIRA integrating sphere (IS) and the fibre optic probe (P).

To test whether this effect could be removed, the data were processed as before, using the second derivative Norris gap function and limiting the wavelength range, in an attempt to reduce the scattering effects of the samples and identify whether the samples could be brought closer together.

Figure 6.18 shows the subsequent scores plot for the first two principal components. Although the samples appear to be more evenly spread, when viewed with their corresponding sample description (Figure 6.19) it is clear that each paired sample occupies a different region in space. For example, the polyamide 6 samples analysed using the probe are seen in the bottom left quartile of the scores plots in Figure 6.18 and Figure 6.19. The same samples analyses using the integrating sphere accessory are found to the centre right of the same scores plots.

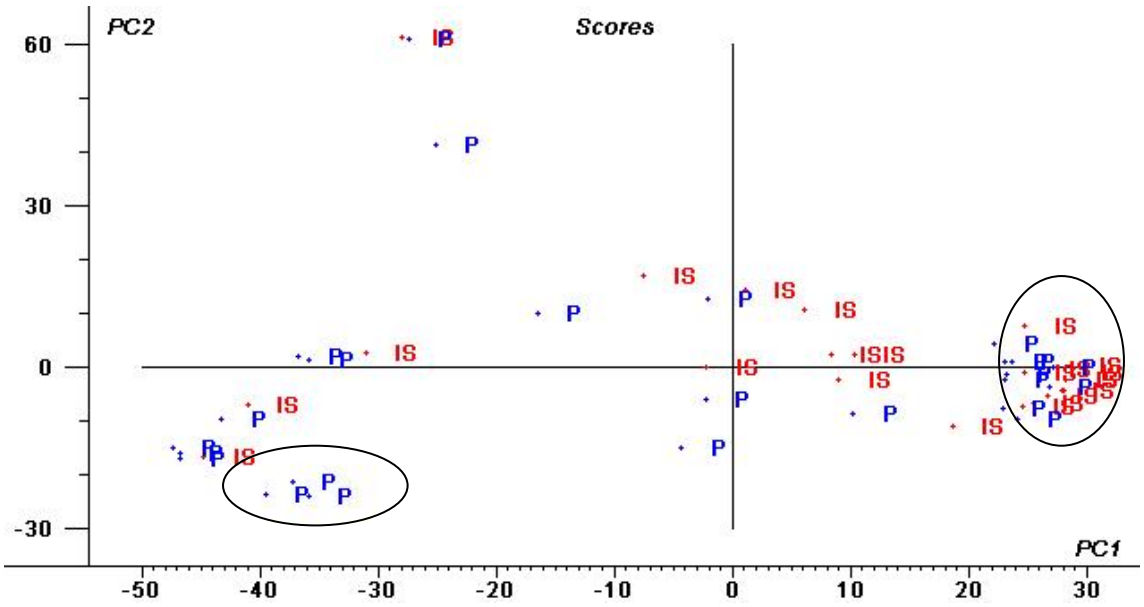

Figure 6.18 Scores plot for the first and second principal components after processing with second derivatives Norris gap function. Envelopes are drawn around the data points for the polyamide 6 samples

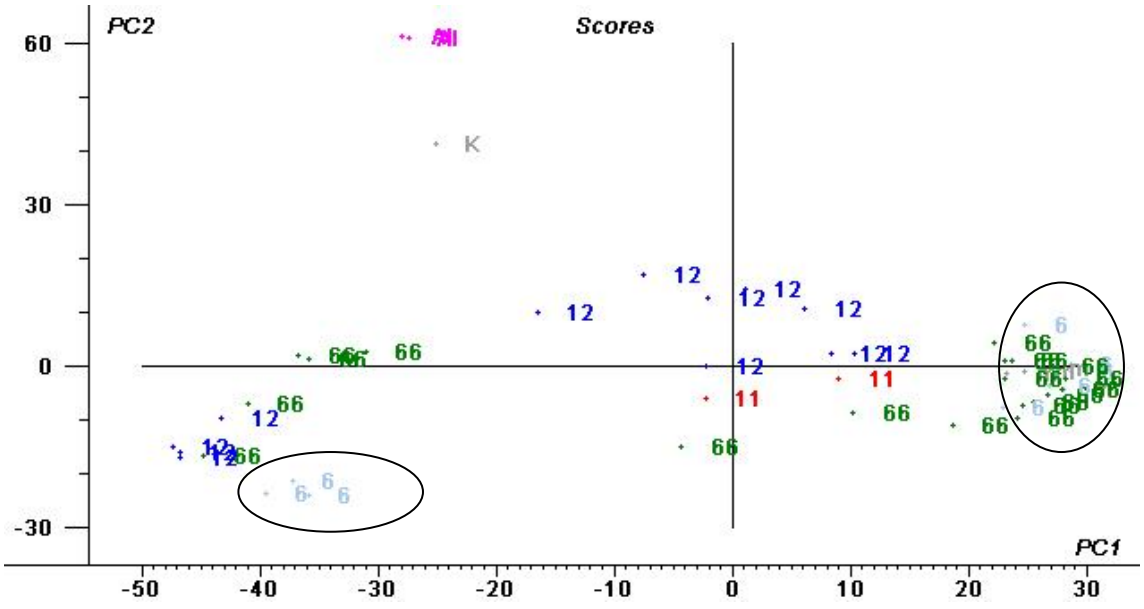

Figure 6.19 Scores plot for the first and second principal components plotted as their subclass assignments. The data points are marked with the polyamide sample type.

It can be concluded that the sampling method used does produce different results, which may hinder correct classification when only minor variations are likely to be seen

between the subclasses. Such factors need to be reduced, and therefore two separate models are required for application with the two methods of sampling. In the work presented here, only models built using the optical probe have been studied as this is the most applicable sampling method for “collections care” applications.

6.2.2.2 Effect of Physical Form

Due to the differences in physical scattering properties of the solid (S) and extruded (Ex) material, it was deemed necessary to identify whether materials of different forms would require separate PCA models.

Figure 6.20 shows the scores plot for the first two principal components. It is quite apparent that there are two distinct clusters relating to the physical nature of the samples. Many of the samples used to build the model have subclasses represented in each form. This ensures that the separation seen is not due to the underlying chemical structure, but rather is caused by the physical form itself.

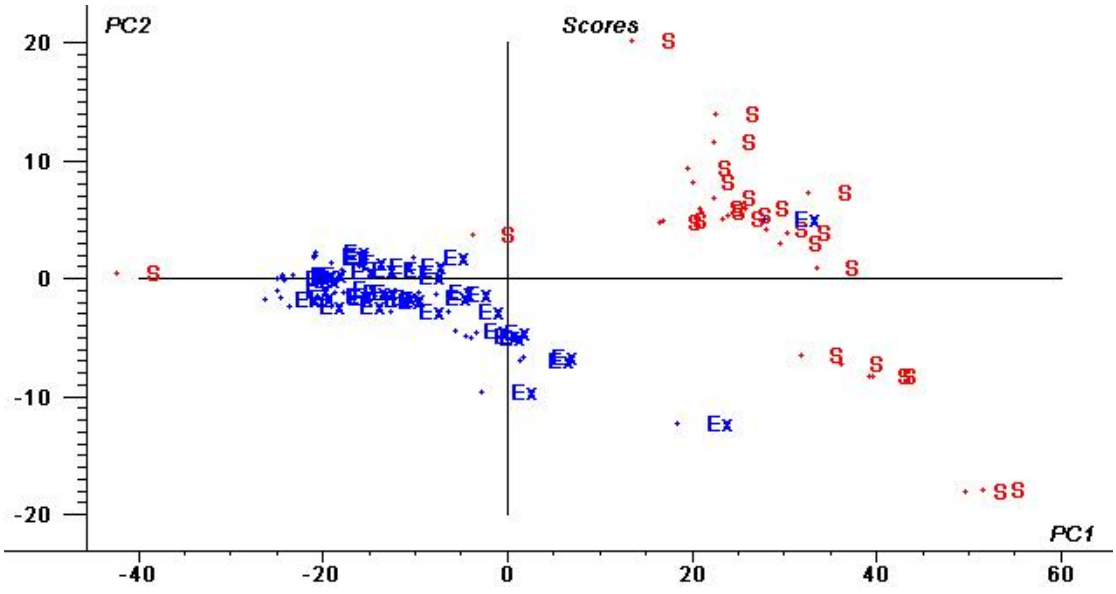

Figure 6.20 Raw data scores plot for the first and second principal components before spectral processing. Samples were either solid (S) or extruded (Ex).

As the differences in the two material types are due to scattering effects relating to the surface characteristics and crystal structure, the spectra were pre-processed to ascertain whether these variations could be minimised.

Figure 6.21 shows the first two principal components after spectral processing with second derivative Norris gap function and by limiting the spectral region investigated. The plot shows that the two groups have been brought closer together, but the separation is still pronounced whilst the spread of the solid material has been reduced.

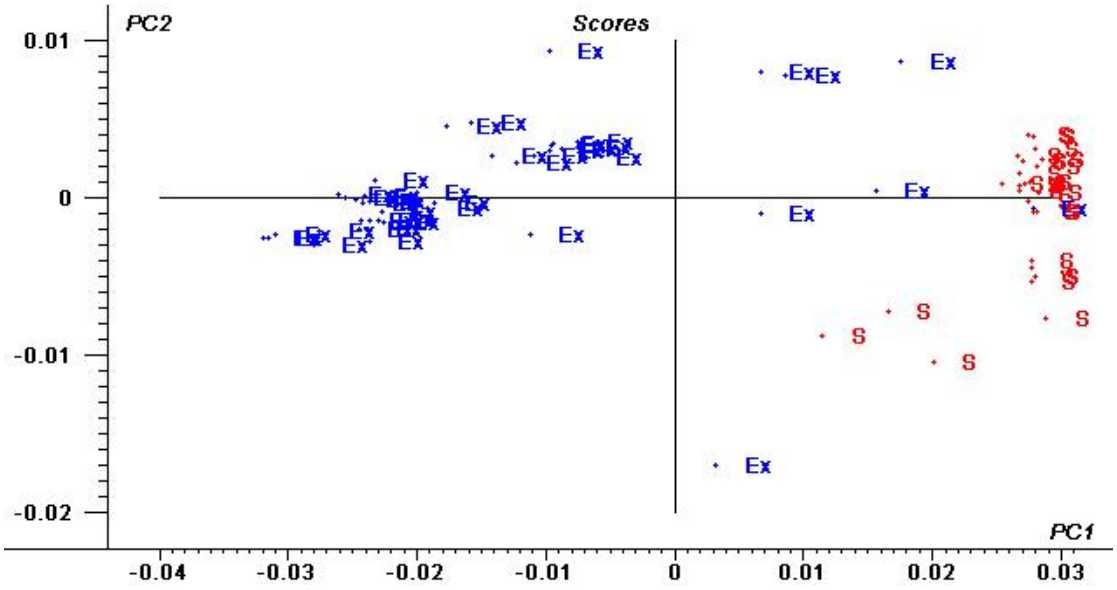

Figure 6.21 Second derivative data scores plot for the first and second principal components after processing with second derivatives Norris gap function

The results clearly indicate that polyamides that have been processed through different routes cannot be readily modelled together. Successful classification of the subclasses requires separate models to be formed. At the point of application this would not pose a problem as it will always be apparent which model to apply.

6.2.2.3 Effect of Colour

As presented in the earlier Section 2.4.2.8, Chapter 2, colour is seen to have an effect on the near-infrared spectrum as the wavenumber increases towards the visible region of the spectrum. It is therefore important to understand what impact this may have on future analyses and principal component space and to account for it in the calibration. Sixty four samples of polyamide 6,6 conservation netting were analysed, subsequent to being dyed using a range of Lanaset® conservation grade dyes (red, orange, yellow, green, blue). These were applied in a pH neutral dye bath at raised temperatures, following the method outlined in Section 8.1.1, Chapter 8. Differences in the chemical

structures of the dyes were not taken into account, but may have an influence on the NIR spectra.

When the first and third principal components are plotted against each other there appears to be some general clustering of data for samples of the same colour (Figure 6.22) . These are not tightly grouped, probably due to the combinations of dyes present in some of the samples.

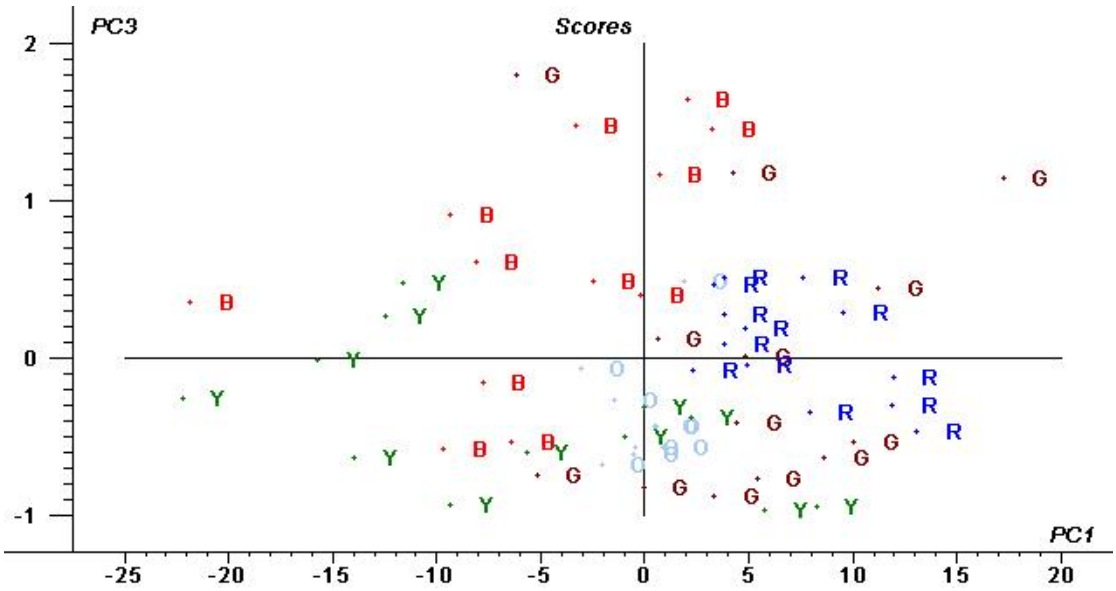

Figure 6.22 Raw data scores plot for the first and third principal components before spectral processing. Samples were dyed red (R), orange (O), yellow (Y), green (G) or blue (B).

The corresponding loadings plots are shown in Figures 6.23 and 6.24. The first PC holds the majority of the information and relates directly to the underlying chemistry of the samples. It should be noted that on comparison with the near-infrared spectrum of polyamide (Appendix 1) the resulting pattern appears to be inverted. This is reported to be due to an artefact of how the algorithm starts and is a common occurrence. It does not affect the subsequent analyses, as distance measure usually rely on the absolute values or squares [19]. This loadings plot also shows that there is a raising baseline running from low wavenumbers to high wavenumbers (inverted), which indicates that there are wavelength dependent scattering effects. These need to be accounted for through pre-processing.

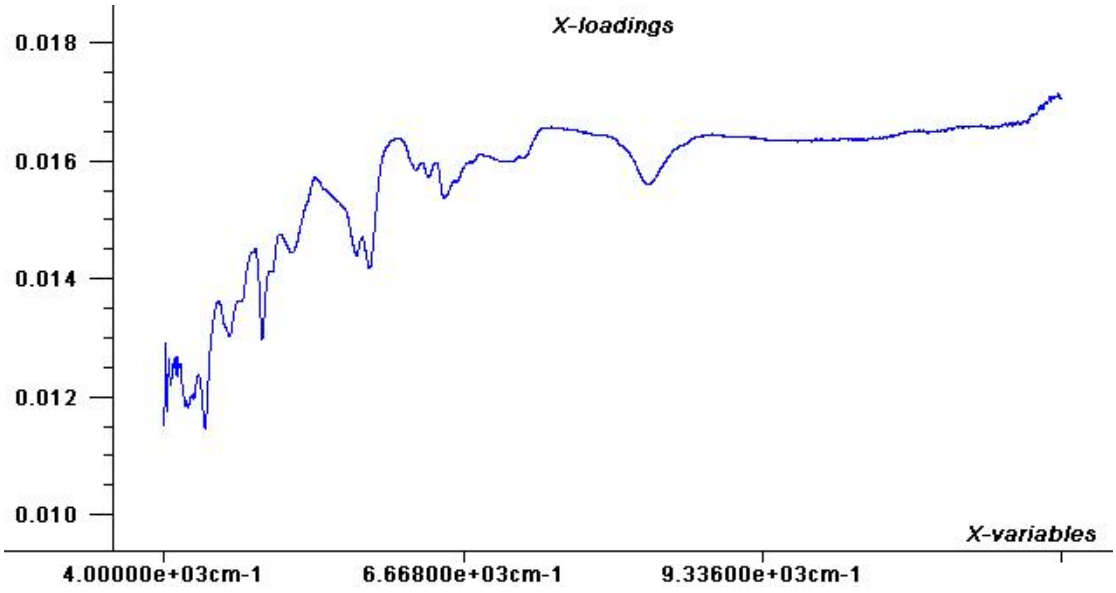

Figure 6.23 Loadings plot for the first principal component before spectral processing

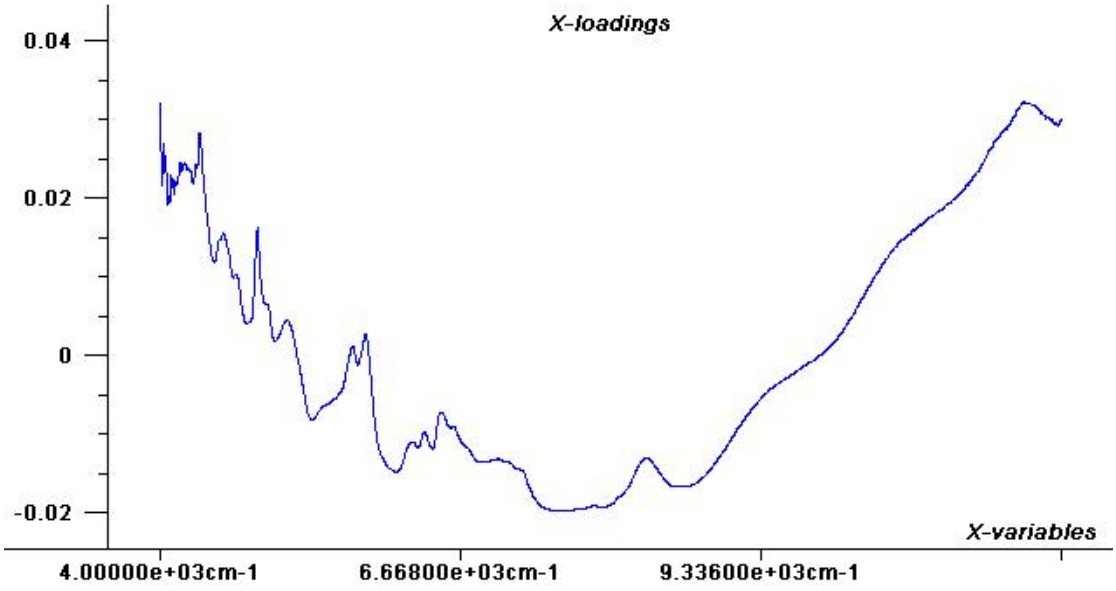

Figure 6.24 Loadings plot for the third principal component before spectral processing

The loadings plot for PC3 (Figure 6.24) shows that there is a large contribution from to the high wavenumber variables; a region previously shown to be that most affected by colour. This, to a significant extent, accounts for the general clustering of the samples into their respective groups.

The data were transformed using the standard normal variate (SNV) function to determine whether this would reduce any scattering effects. The wavelength region between 8 600–12 000 cm^{-1} was removed as this corresponded to the region where the baseline was seen to significantly increase in the loadings plot for the third PC (Figure 6.24).

The explained variance tails off at five PCs and therefore four PCs have been used to describe 89% of the validation samples (Figure 6.25). When the first two principal components are plotted against each other (Figure 6.26) the general clustering of the coloured groups tend to have been reduced.

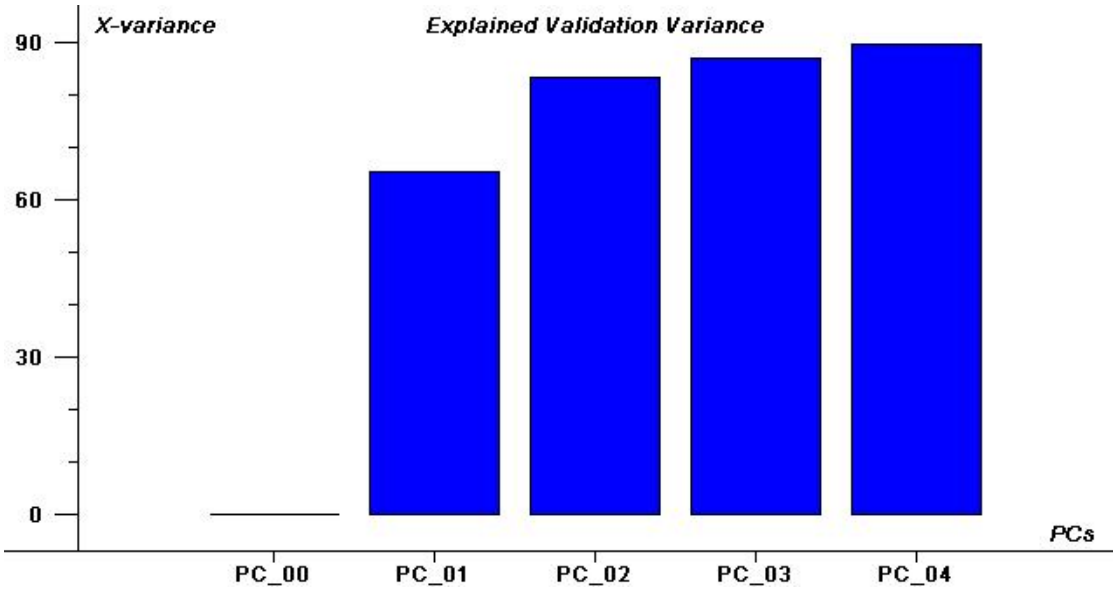

Figure 6.25 Explained variance plot for the description of coloured polyamide 6,6

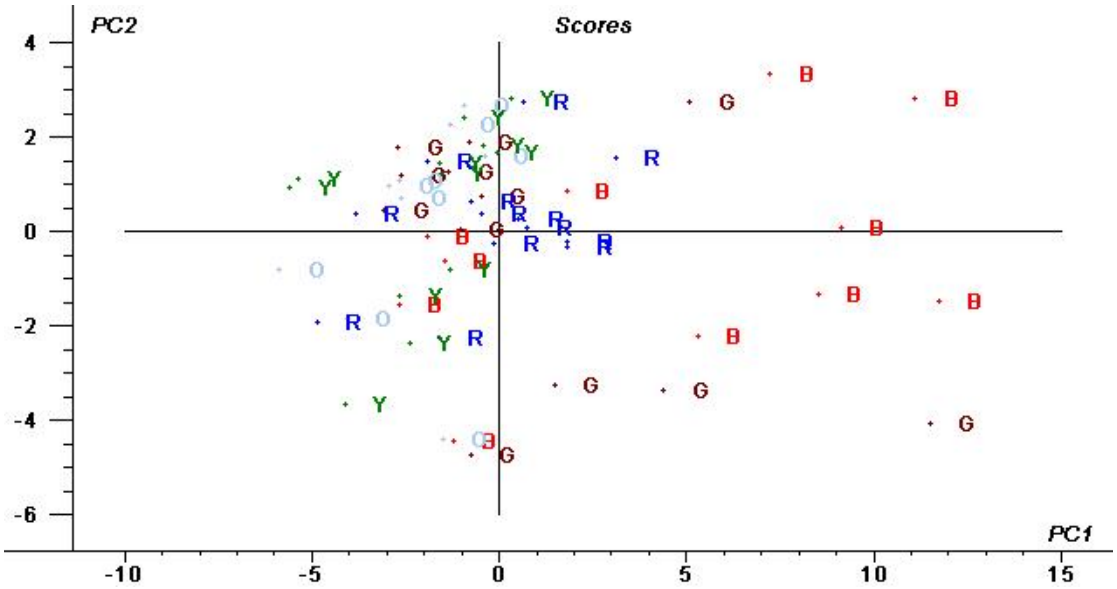

Figure 6.26 Scores plot for the first and second principal components after processing with standard normal variate function

When PC3 is plotted against the first and second principal components, there are clearly three outliers being described by this axis (Figure 6.27 and Figure 6.28). On inspection of the corresponding spectra they do not show any obvious variations from the remainder of the samples. Although it is not clear why these samples are outliers, it was deemed appropriate to remove them from the calculation before studying the effects of derivatives.

Removing those samples increased the explained variance for the validation to 92%.

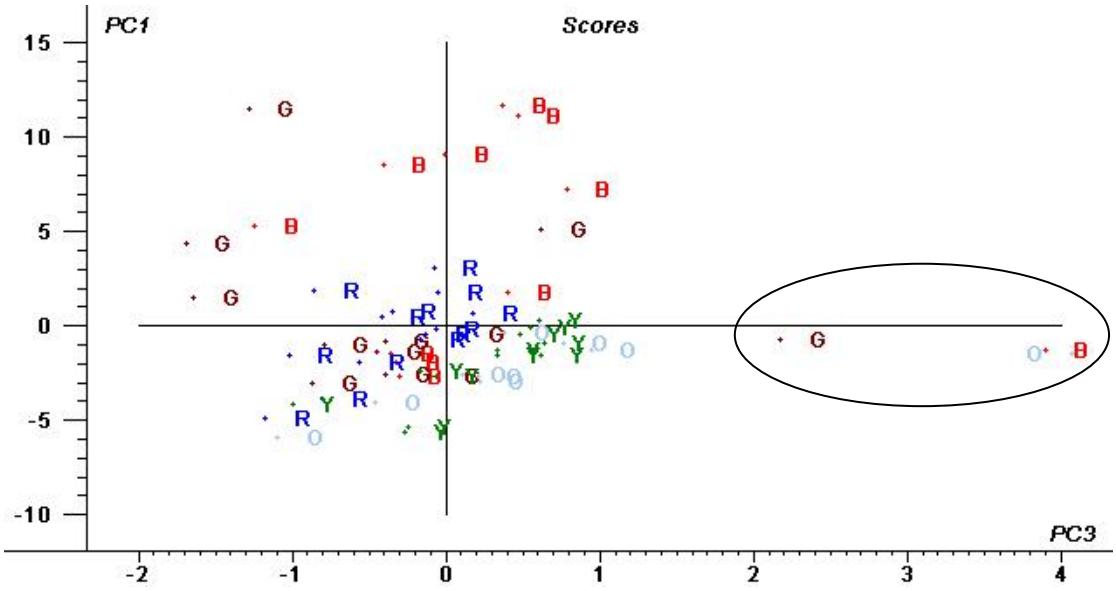

Figure 6.27 Scores plot for the first and third principal components showing the outliers in the third PC projection. Envelopes are drawn around the three outliers

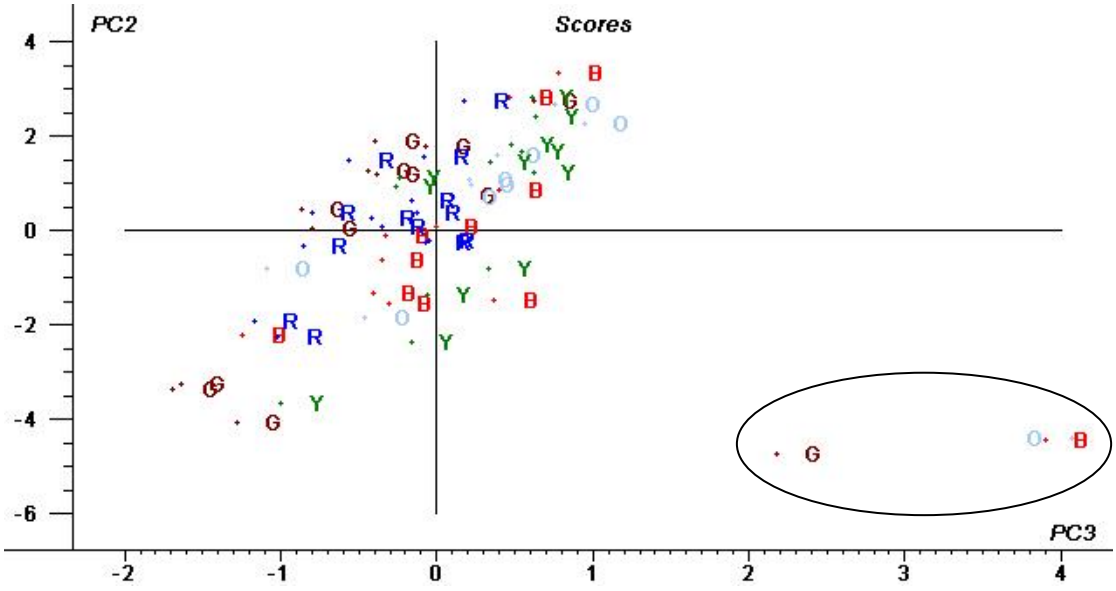

Figure 6.28 Scores plot for the second and third principal components showing the outliers in the third PC projection. Envelopes are drawn around the three outliers

The spectra were processed using the second derivative Norris gap function and PCA applied as before. The scores plots do not show any inherent clustering of the coloured

samples. However, the explained variance for the validation has dropped down to 80% for ten principal components, in comparison to 92% for four principal components after SNV transformation (Figure 6.29). In this case, therefore, the SNV pre-process method enabled a more robust method of calibration.

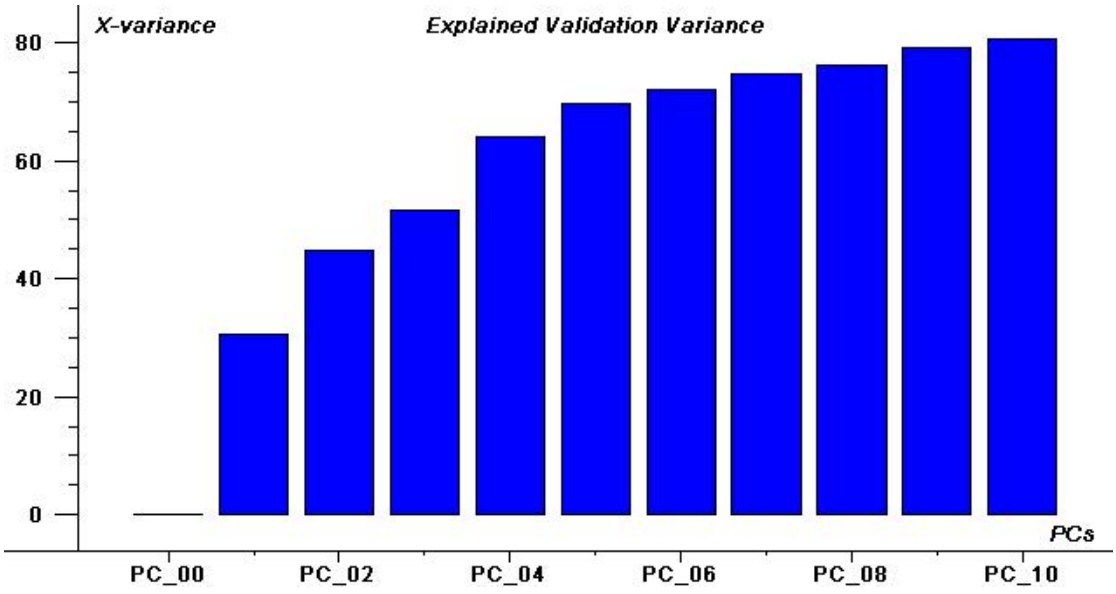

Figure 6.29 Explained variance plot for the first ten principal components after processing with second derivate Norris gap functions

It does appear that colour will have an effect on the overall description of the samples, however the samples used prevented a quantitative approach, as many were dyed with more than one dye stuff to form different shades. The application of the SNV function and reducing the spectral region did successfully reduce the sample variations. Conversely, for the problem at hand the second derivatives tended to reduce the overall description of the data.

6.3 Conclusions

It has been illustrated that the application of multivariate analysis to the problem of classification cannot be carried out without careful consideration of extraneous influential factors. It is clear that the sampling method as well as the physical and

chemical nature of a material will have an effect on the resulting calibration unless these are accounted for.

This preliminary work proved necessary to ensure that such effects would be minimized, enabling confidence in the subsequent discrimination analyses. For the work presented in the following chapter, all spectra were acquired using the fibre optic probe. The results showed clear differences in PC space between those samples analyses using the probe and by the integrating sphere. For monitoring of the small spectral changes expected with subclass discrimination, the sampling method requires consistency. For 'collection care' applications the probe provides the most flexibility. The differences that the physical form of the polyamides had on the principal component analyses illustrated the need to model extruded and solid material separately. The presence of colouring agents in the polyamide fibres caused a degree of clustering, but the application of pre-processing methods successfully enabled this to be reduced. Differences in the chemical structures of the dyes were not taken into account.

6. 4 References

1. Esbensen, K.H., *Multivariate Data Analysis: In Practice*. 5th ed. 2002, Esbjerg: Camo.
2. Otto, M., *Chemometrics: Statistics and Computer Application in Analytical Chemistry*. 1999, Frieberg: Wiley-VCH.
3. Haines, E.S., *The Application of Chemometric Techniques to Spectroscopic Data*. 1997, University of Hull.
4. 1, et al., *Chemometrics: A Practical Guide*. 1998, Chichester: Wiley-Interscience Publications.
5. Dhanoa, M.S., et al., *The Link Between Multiplicative Scatter Correction (MSC) and Standard Normal Variate (SNV) Transformations of NIR spectra.* Journal of Near Infrared Spectroscopy, 1994. **2**: p. 43-47.
6. Adedipe, O.E., et al., *Classification of Red Oak (Quercus Rubra) and White Oak (Quercus Alba) Wood using a Near Infrared Spectrometer and Soft Independent Modelling of Class Analogies.* Journal of Near Infrared Spectroscopy, 2008. **16**: p. 49-57.
7. Heraud, O., et al., *Effects of Pre-processing of Raman Spectra on in vivo Classification of Nutrient Status of Microalgal Cells.* Journal of Chemometrics, 2006. **20**: p. 193-197.
8. Beebe, K.R., R.J. Pell, and M.B. Seasholtz, *Chemometrics: A Practical Guide*. 1998, Chichester: John Wiley & Sons Inc.
9. De Maesschalck, R., et al., *Decision Criteria for Soft Independent Modelling of Class Analogy Applied to Near Infrared Data.* Chemometrics and Intelligent Laboratory Systems, 1999. **47**: p. 65-77.

10. Fearn, T., *On SIMCA and Measuring Distances.* Near Infrared News, 2007. **18**(6): p. 12-13.
11. Blanco, M., et al., *Calibration in Non-linear Near Infrared Reflectance Spectroscopy: A Comparison of Several Methods.* Analytica Chimica Acta, 1999. **384**: p. 207-214.
12. Woo, Y.A., et al., *Development of a Method for the Determination of Human Skin Moisture Using a Portable Near-infrared System.* Analytical Chemistry, 2001. **73**: p. 4964-4971.
13. Richardson, E. and G. Garside. *The Use of Near Infrared Spectroscopy as a Diagnostic Tool for Historic Silk Artefacts*. in *IRUG 8*. 2009. Vienna: e-Preservation Science.
14. Trafela, T., et al., *Nondestructive Analysis and Dating of Historical Paper Based on IR Spectroscopy and Chemometric Data Evaluation.* Analytical Chemistry, 2007. **79**: p. 6319-6323.
15. Barker, M. and W. Rayens, *Partial Least Squares for Discrimination.* Journal of Chemometrics, 2003. **17**: p. 166-173.
16. Indahl, U. and T. Naes, *A Variable Selection Strategy of Supervised Classification with Continuous Data.* Journal of Chemometrics, 2004. **18**: p. 53-61.
17. Castillo, R., et al., *Multivariate Strategies for Classification of Eucalypus Globulus Genotypes Using Carbohydrate Content and NIR Spectra for Evaluation of Their Cold Resistance.* Journal of Chemometrics, 2008. **22**: p. 268-280.
18. Flaten, G.R., B. Grung, and O.M. Kvalheim, *A Method for Validation of Reference Sets in SIMCA Modelling.* Chemometrics and Intelligent Laboratory Systems, 2004. **72**: p. 101-109.
19. Fearn, T., *Assigning Signs to Principal Components.* Near Infrared News, 2008. **19**(2): p. 16-17.

Chapter 7: The Application of Multivariate Analysis for the Discrimination of Polyamide Sub-classes

In the previous chapter, a discussion was given on some of the key theoretical aspects of multivariate analyses. Particular focus was given to the discrimination methods to be applied for the identification of polyamide sub-classes. The preliminary experimental section gave an indication of the types of issues to be born in mind during the multivariate calibration steps.

The following chapter will present the application of the multivariate analysis methods, namely SIMCA and PLS-DA, for the discrimination of the sub-classes of polyamides.

The initial step was to determine the appropriate protocol for distinguishing synthetic polyamide from two natural polyamides fibres, silk and wool. In the latter part of this chapter, the focus is given to the process of discriminating three forms of synthetic polyamide; polyamide 6, polyamide 6,6 and polyamide 12.

7.1 Discrimination of Synthetic Polyamides, Silk and Wool

The discrimination of chemically and physically similar material is of great importance for collection care. The case study in Section 3.2.2, Chapter 3, emphasised this, and highlighted the problem of discriminating synthetic polyamide and the natural polyamide silk. The details of the structure of silk will not be covered here. However, it is sufficient to say that both of these polymers are characterised by an extended chain conformation interspersed by amide groups. These similarities, along with the polymer processing of synthetic polyamide, means that both of these fibres exhibit similar characteristics. Therefore, the discrimination of these two fibres will be investigated in this section. For completeness, the discrimination of wool, the other major natural polyamide material found in textile collections, is also included. The polymer chains of wool are again characterised by the presence of the amide linkages, but the chains take on a helical form rather than an extended conformation. Although wool is generally readily identified visually, it was deemed appropriate to include it in the calibration model due to the underlying chemical relationships.

NIR spectra were recorded for 48 polyamide samples, 29 silk samples and 38 wool samples, using the standard protocol (Section 3.1.1.2, Chapter 3) and the probe attachment. The data were then subjected to multivariate analysis. The samples used were textile reference samples, both dyed and undyed. The NIR spectra and sample details can be found on the accompanying CD-ROM.

Figure 7.1 shows three reference NIR absorbance spectra of polyamide 6,6, silk and wool, stacked vertically for clarity.

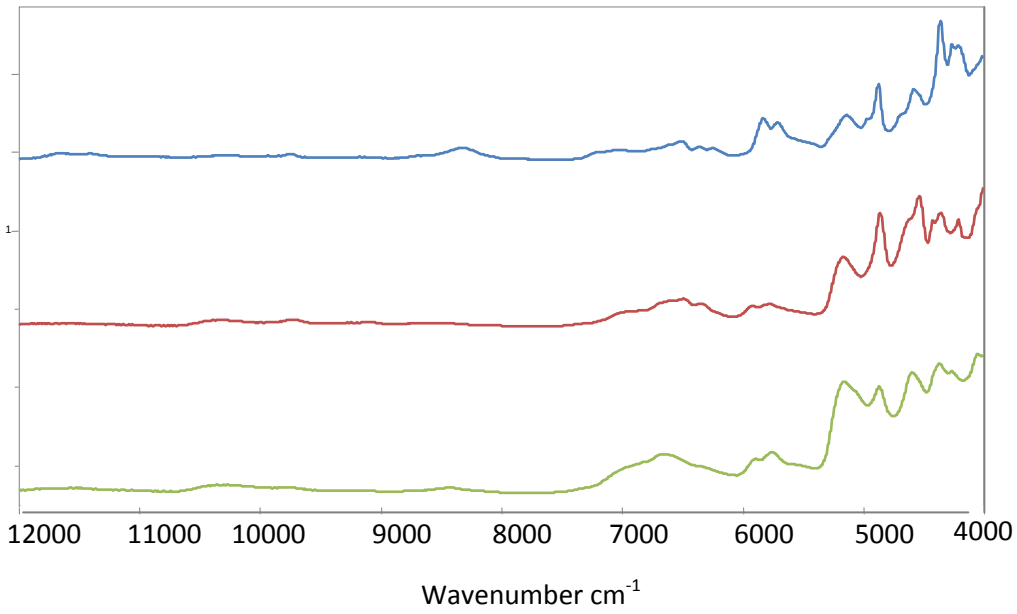

Figure 7.1 Offset raw near-infrared absorbance spectra of reference synthetic polyamide 6,6 (blue), silk (red) and wool (green)

The first step in any multivariate analysis is to look at the raw data to see whether there are any inherent patterns in the data set and identify what factors might be influencing the calibration model.

An initial principal component analysis (PCA) was carried out on unprocessed, raw spectra. This gave an overview of the distribution of the samples in PC space. Figure 7.2 shows the scores plot for the first two principal components. In the scores plots the crosshairs represent the two principal components with the samples scattered about these new axes. The numerical outputs indicate the coordinates of each sample from these two PCs. For example, the silk sample highlighted to the right of the plot lies in close proximity to PC1, but is a long distance from PC2. It can therefore be said that PC2 does not describe this sample.

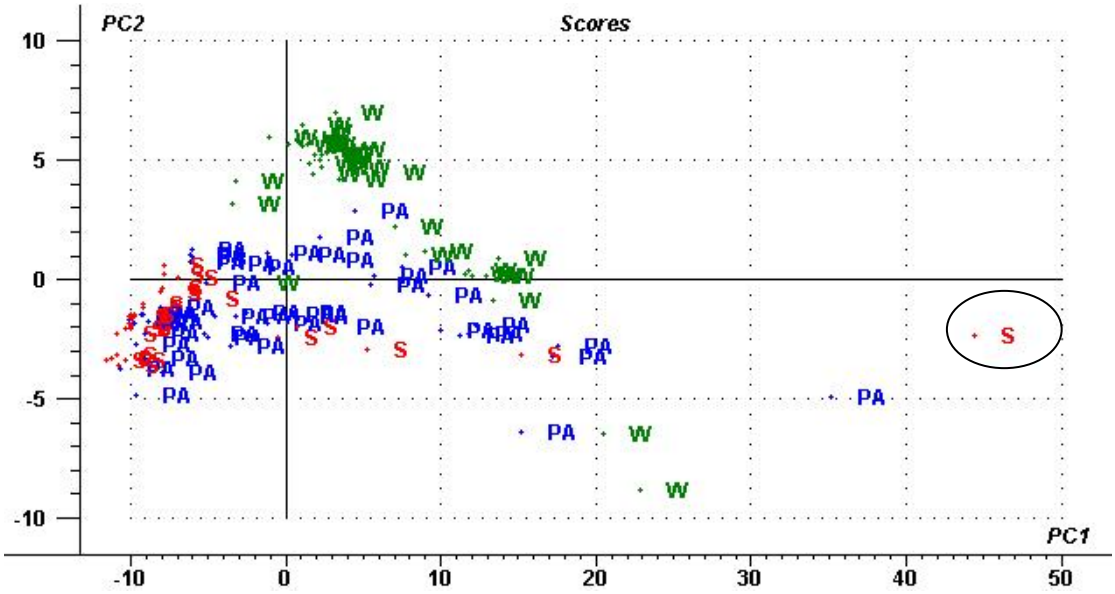

Figure 7.2 Raw data scores plot of the first two principal components for the discrimination of polyamide (PA), silk (S) and wool (W)

It can be seen that there is a general pattern with the grouping of the different fibres, but they are not highly resolved clusters and require greater separation. The total number of samples left in the calibration after outlier removal (Section 6.1.2.2, Chapter 6) was 44 polyamide, 28 silk and 35 wool.

The corresponding loadings plot for the first principal component is shown in Figure 7.3 The X axis corresponds to the variables in the data matrix, which are the wavenumbers. The Y axis is the distance of the new PC from the original coordinates. The closer the loadings are to the origin the less that particular wavenumber contributes to the corresponding PC. Generally, the first principal component loadings plot resembles the raw NIR spectra. This is because the first principal component describes the largest spread of the data and therefore most of the wavenumbers contribute to a greater or lesser extent.

It can be seen from the plot below that the high wavenumber region of the spectrum (7 500-12 000cm^{-1}) has a large influence on the first PC. Since this area is known to be affected by noise and highly coloured material (Section 2.5.2.8, Chapter 2) the decision was made to remove this region from the calibration to ensure that the model is not finding an erroneous correlation.

It is also possible to see that there is a contribution from the lower wavenumber region. This region related to the first overtone and combination vibrations and relates directly to

the underlying structure of the materials of interest (Appendix 1). It is possible to see that this whole region is influenced by a sloping baseline. This is a possible indication of the need for spectral pre-processing.

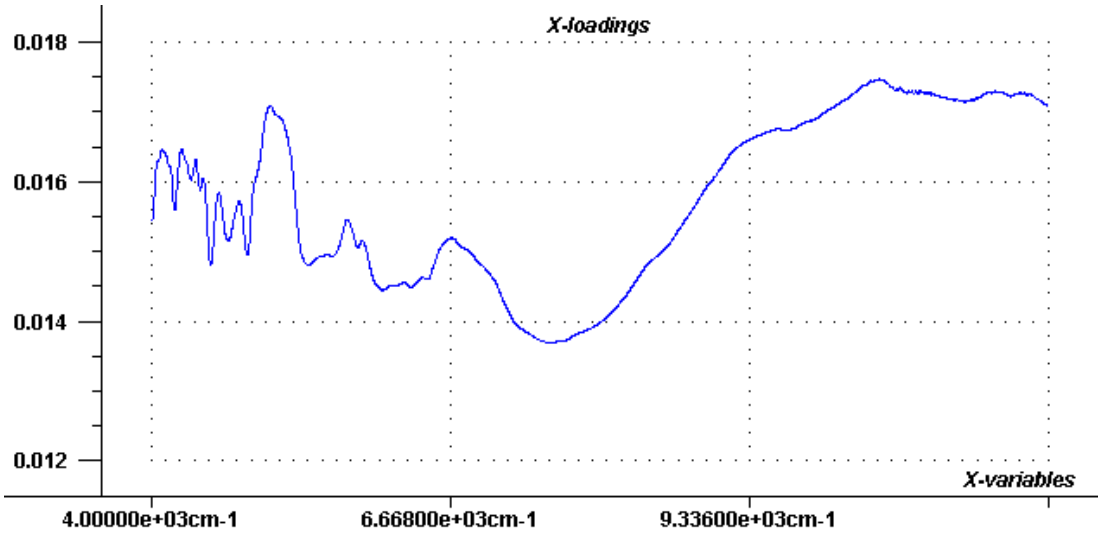

Figure 7.3 Raw data loadings plot for the first principal component for the discrimination of polyamide, silk and wool

The spectra were processed using a second derivative Norris gap function and the region limited to 4 000-7 000 cm^{-1}. The subsequent scores plot (Figure 7.4) now shows that the three classes of polyamide occupy distinctly different regions of PC space. This indicates that classification of these classes will be possible without any further spectral processing being required. The first principal component describes the synthetic polyamides (PA), whist the second principal component allows the two natural polyamides to be resolved (S and W). The overall spread of the synthetic polyamides is greater because the samples within this group vary in chemical structure and there is more than one type of sub-class being modelled.

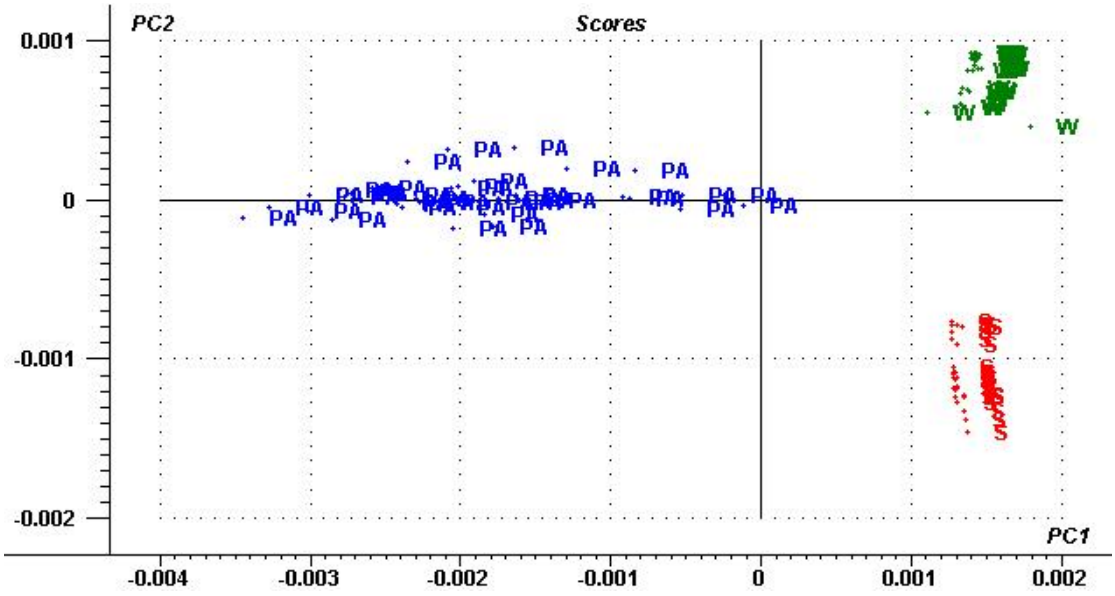

Figure 7.4 Second derivative processed data scores plot of the first two principal components for the discrimination of polyamide (PA), silk (S) and wool (W)

Figure 7.5 shows the explained variance plot for the validation of the model. It can be seen from this plot that the explained variance in the validation samples (Full Cross Validation) does not increase significantly after the fourth principal component. At PC4, 97.8% of the variance in the data set has been accounted for.

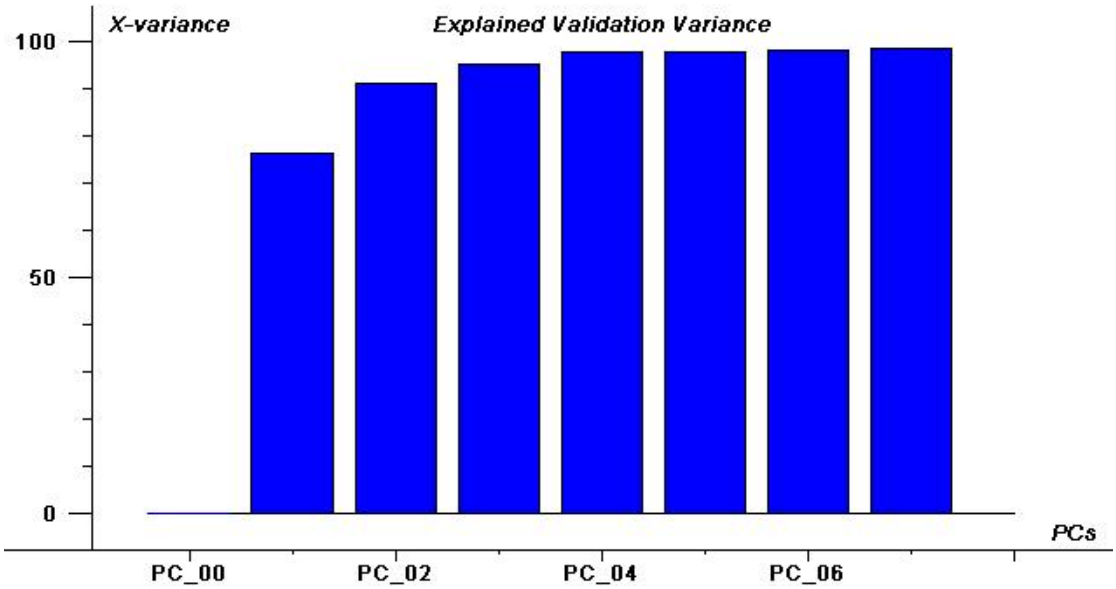

Figure 7.5 Explained variance plot for the first seven principal components for the discrimination of polyamide, silk and wool

7.1.1 Soft Independent Modelling of Class Analogies Results for Synthetic Polyamide, Silk and Wool

After the processing method and spectral region had been determined three separate PCA models were built for the application of the Soft Independent Modelling of Class Analogies (SIMCA) method. The parameters for each of the individual principal component SIMCA model are shown in Table 7.1. The number of PC's used in each calibration was determined as the point prior to which the explained variance reached a plateau (Section 6.1.5, Chapter 6).

Class	Pre-processing	Spectral Region	Number of PCs	Explained Variance/%
Polyamide	2nd Derivative	4000-7000	3	98
Silk	2nd Derivative	4000-7000	2	99
Wool	2nd Derivative	4000-7000	3	86

Table 7.1 The individual PCA parameters for the for the process of SIMCA classification of polyamide, silk and wool

Once the individual PCA models have been built, the first validation step that is taken is to reintroduce all of the samples that were used to build the models and check to see if they are correctly classified. On reintroduction of the training samples there were no samples misclassified and there were seven samples not assigned to any group. All of the unidentified samples were seen at the extremes of the PC score space plots. On inspection of the spectra there were spectral features that differed greatly from the other samples. These samples were left in the calibration because they were representative reference samples and therefore deemed valid samples.

The fact that there were no "false positive" classifications (Type II error) indicates that the models are highly resolved. A Type II error relates to a sample being classified as belonging to a particular group in error. This is illustrated by the model distance plots shown in Figures 7.6 to Figure 7.8.

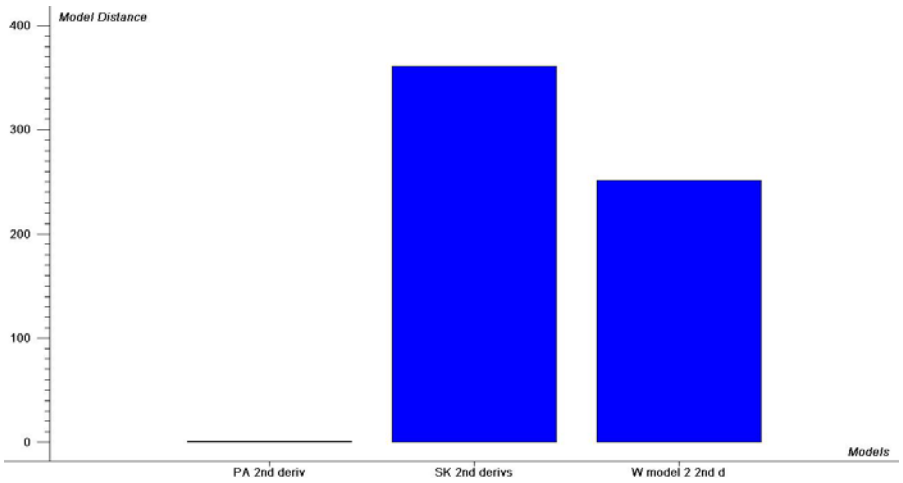

Figure 7.6 The distance in PC space of the silk and wool calibration models from the polyamide model

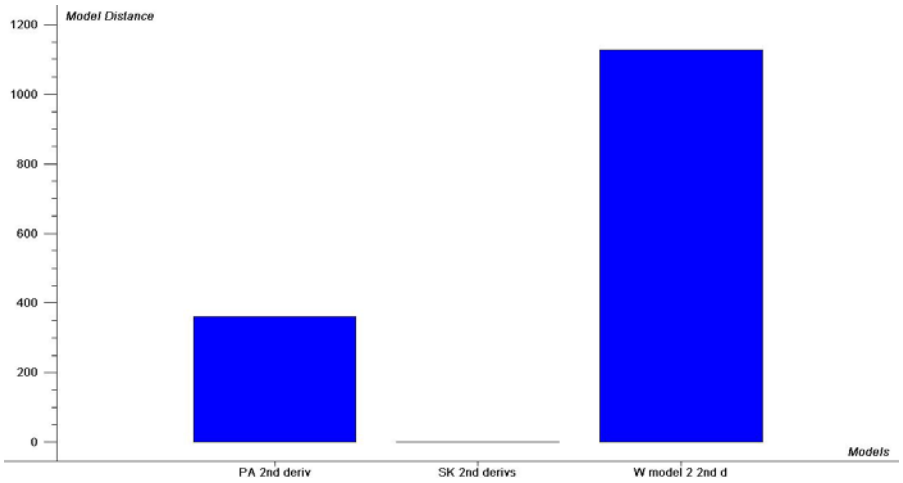

Figure 7.7 The distance in PC space of the polyamide and wool calibration models from the silk model

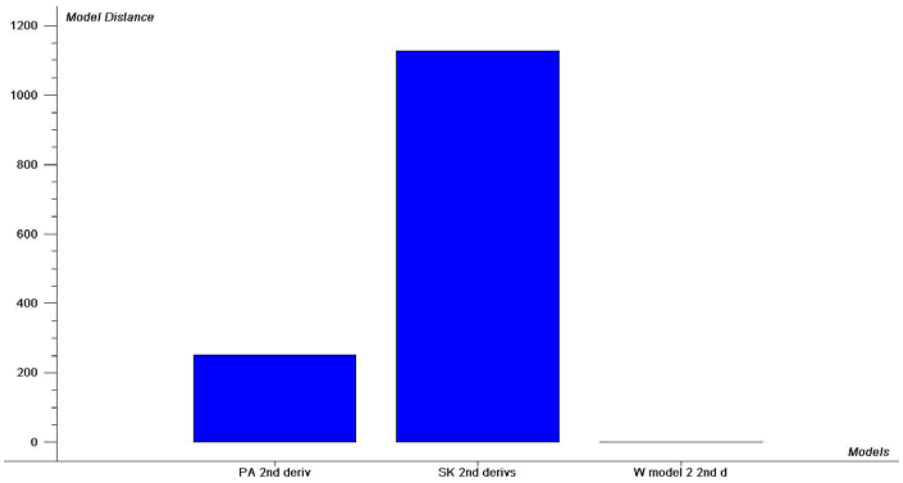

Figure 7.8 The distance in PC space of the polyamide and silk calibration models from the wool model

The model distance plot is used to determine how different each model is with respect to PC space. Therefore, it gives an indication of how successful the classification is likely to be. If the boundaries of two models are close to each other then there is an increased risk that an unknown sample may be classified as belonging to the wrong group (Type II error). The model distances are determined by fitting the respective samples to the model itself and then fitting the same samples to the comparator model. The total residual standard deviations are used as a measure of difference [1]. As a consequence, the distance of a model to itself is 1, and therefore all other models need to be greater than one for successful model separation. Values greater than three are said to provide robust differentiation [1, 2]. The greater the model distances from each other the lower the chance that a Type II error will occur. In the present case the model distances range from 200-1 200, indicating very robust differentiation.

7.1.2 Partial Least Squares Discriminant Analysis Results for Synthetic Polyamide, Silk and Wool

The same sample set, pre-processing and spectral parameters were used for the Partial Least Squares Discriminant Analysis (PLS-DA) model to ensure that the results were comparable with those from the SIMCA calibration.

As previously described in Section 6.1.4.2, Chapter 6, the PLS-DA method requires a pseudo-Y matrix to be constructed for each individual class using a binary system. For example, in order to determine whether an unknown sample belongs to the silk group, all of the calibration samples of silk are assigned the number one. All other samples in the

calibration set i.e. polyamide and wool, are assigned as zero. The PLS-DS method is then applied to the data set, regressing the X matrix (spectra) against the pseudo-Y matrix (binary matrix).

Figure 7.9 shows the scores plot for the first two principal components. It can be seen that the different classes of samples take on similar clusters in space, after the inclusion of the Y matrix, to the score plot from the SIMCA calibration (Figure 7.4). The explained variance for the validation is 97.9% for three principal components, indicating that the data are well described.

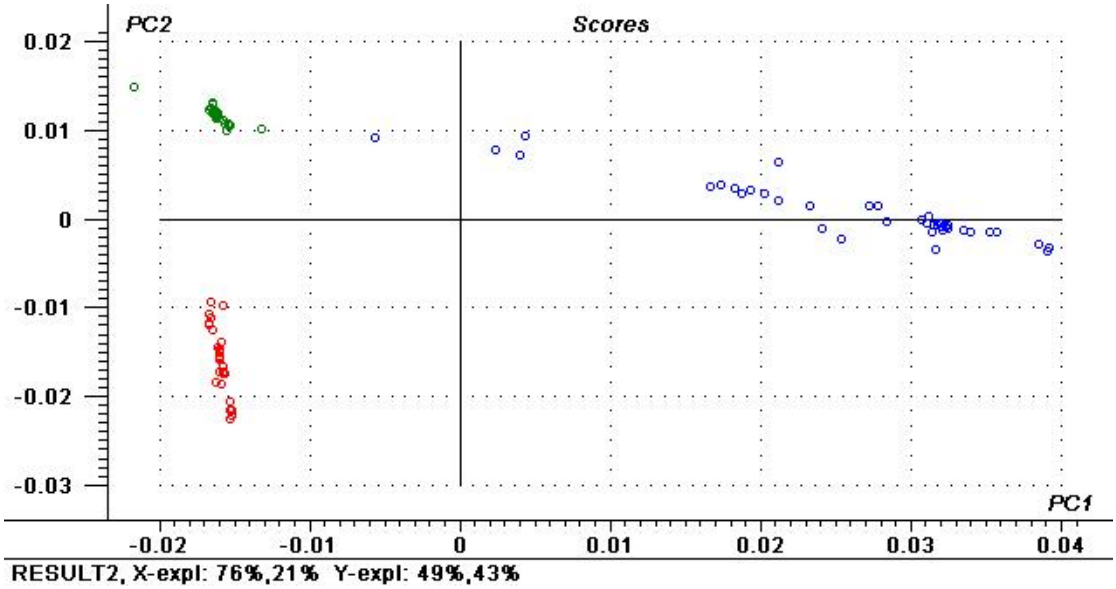

Figure 7.9 Second derivative processed data scores plot of the first two principal components for the discrimination of polyamide (blue), silk (red) and wool (green)

Each sample is removed one at a time and predicted against each calibration model, being given a value between one and zero, depending on whether they are identified as belonging to the group or not belonging, respectively. The results of these predictions are represented graphically as a regression line.

Figure 7.10 to 7.12 show the predicted versus measured regression lines for the three groups, which is effectively the calibration line for the data. The black line is the target line and the blue line is the actual measured line. Although there is some deviation about the predicted values, the samples are well described.

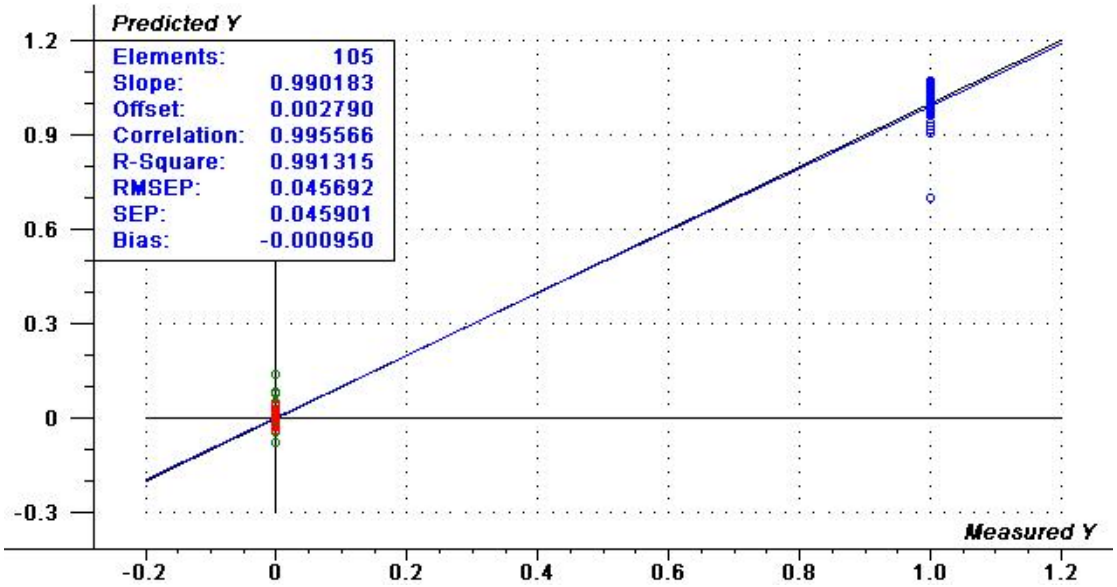

Figure 7.10 Predicted versus measured regression line for PLS-DA of polyamides (blue) regressed against silk (red) and wool (green)

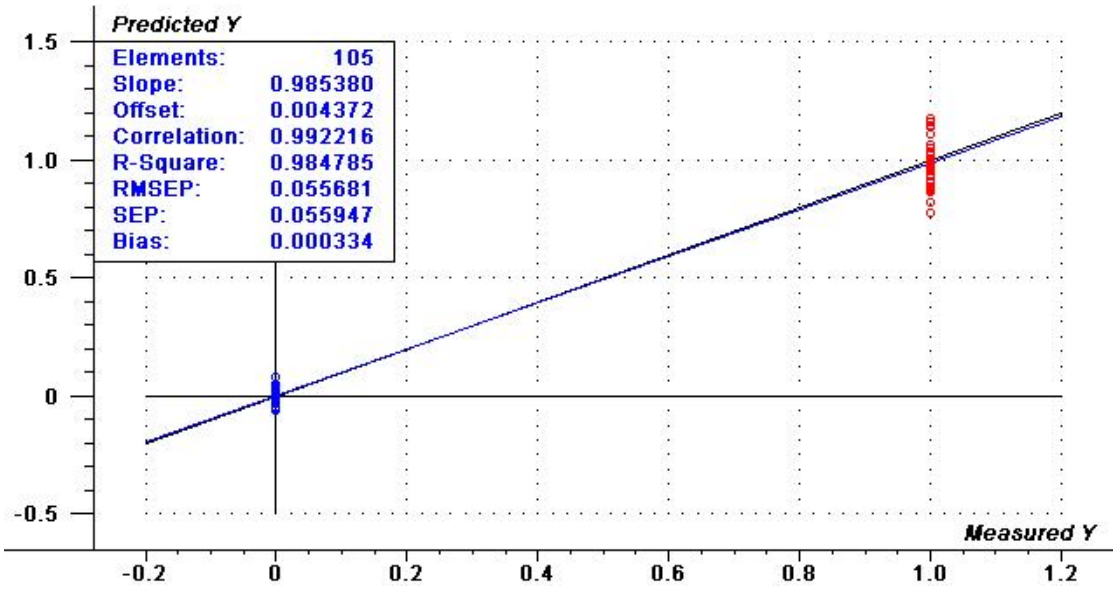

Figure 7.11 Predicted versus measured regression line for PLS-DA of silk (red) regressed against polyamide (blue) and wool (green)

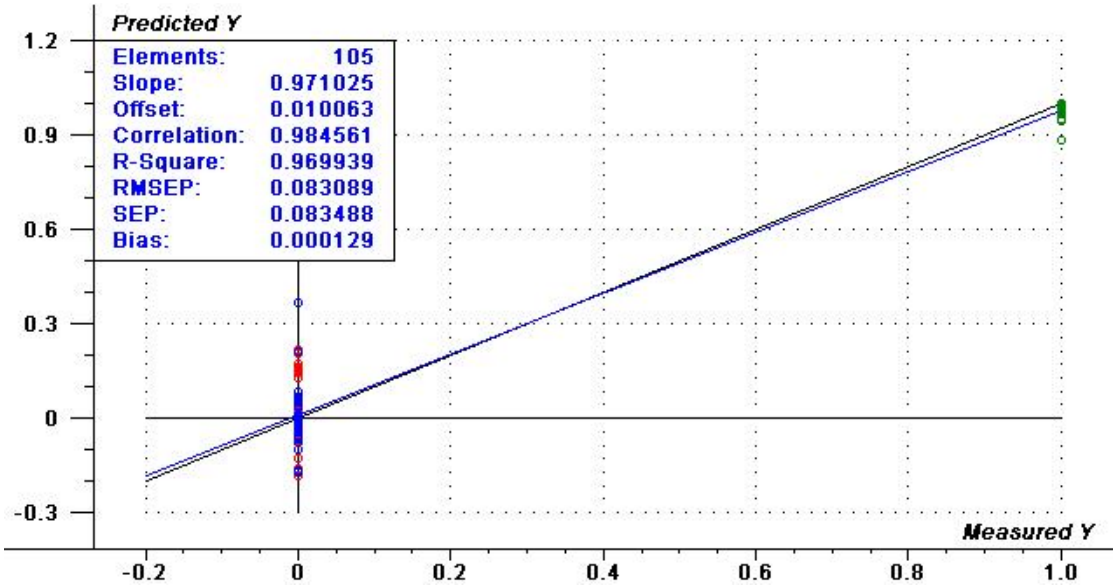

Figure 7.12 Predicted versus measured regression line for PLS-DA of wool (green) regressed against silk (red) and polyamide (blue)

The Root Mean Squared Standard Error of Prediction (RMSEP) provides a method of monitoring the error in the validation method [2]. This is the square root of the residual variance between the predicted and the measured *y* value (zero or one), given by:

$$\mathrm{RMSEP} = \sqrt{\sum_{t=1}^{n} \frac{(\hat{y}_t - y_{t,ref})^2}{n}}$$

Figure 7.13 Root Mean Squared Standard Error of Prediction [2]

The calibration is optimised when the RMSEP is at its lowest (similar to what is found by reducing the sum of the squares of the deviations in more conventional linear regression methods). This therefore, can be used to determine the optimum number of principal components needed to describe the data. The results for each group are presented in Table 7.2.

Class	RMSEP	Number of PCs
Polyamide	0.04	3
Silk	0.06	3
Wool	0.08	3

Table 7.2 Calibration results for the PLS-DA classification of polyamide, silk and wool

Once the calibration models had been formed, the reference samples were reintroduced as validation samples to determine whether they were correctly classified. In order to classify the "validation" samples it was necessary to set boundaries for whether a sample belonged to one group or another. Therefore, classification boundaries were arbitrarily set at plus or minus 0.5 from the relevant Y matrix assignment. For example, if a sample was being compared against the polyamide calibration model, and predicted as having a value equal to or greater than 0.5, then it would be assigned as polyamide. However, if the sample was predicted as having a value less than 0.5 then it would be outside of the group boundaries and not classified as belonging to the group.

The results of the three classifications are shown in Figure 7.14 to 7.16. On reintroduction of the calibration data samples there were no samples misclassified or without assignment to a group. For the synthetic polyamide and silk regression models, there were no samples classified close to the boundary, so all samples were well resolved (0.5 boundary shown as dashed line). There were, however, three samples very close to the 0.5 boundary when predicted against the wool model, as seen in Figure 7.16 (one wool sample and two synthetic polyamide samples). These samples were at the extremes of each principal component cluster and therefore deviate from the overall description of their group.

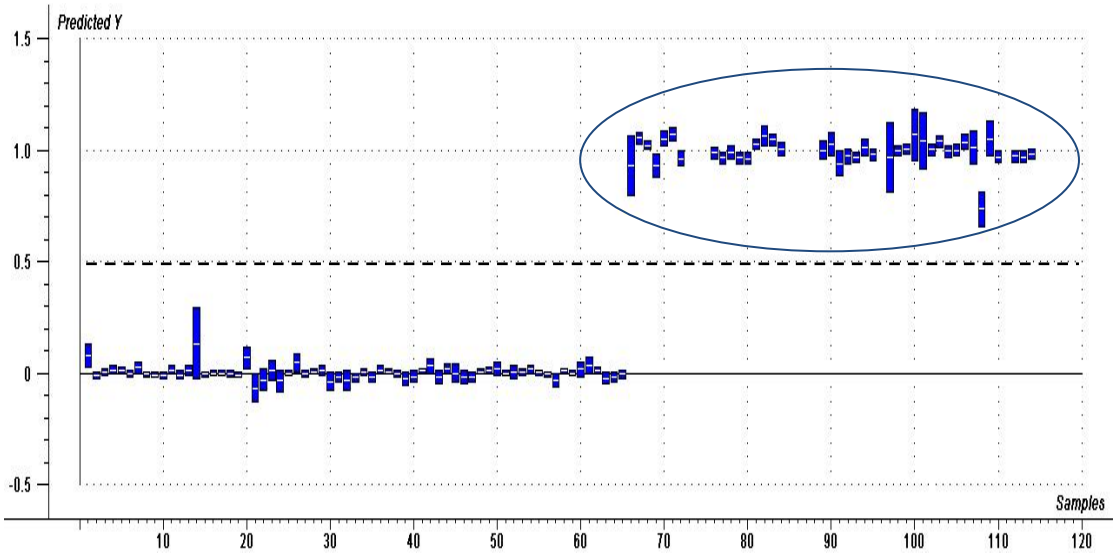

Figure 7.14 Classification of the calibration samples against the polyamide PLS-DA calibration model (PA samples circled)

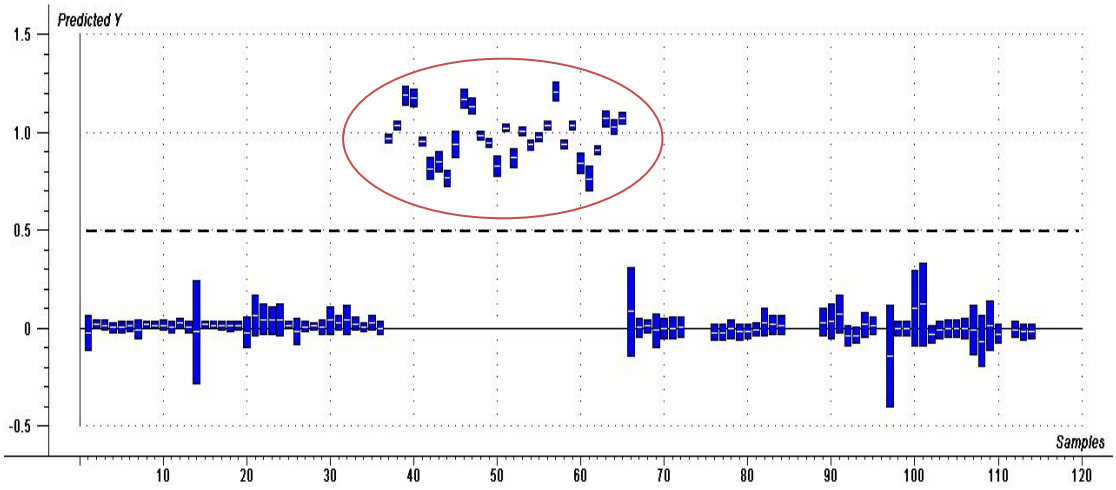

Figure 7.15 Classification of the calibration samples against the silk PLS-DA calibration model (silk samples circled)

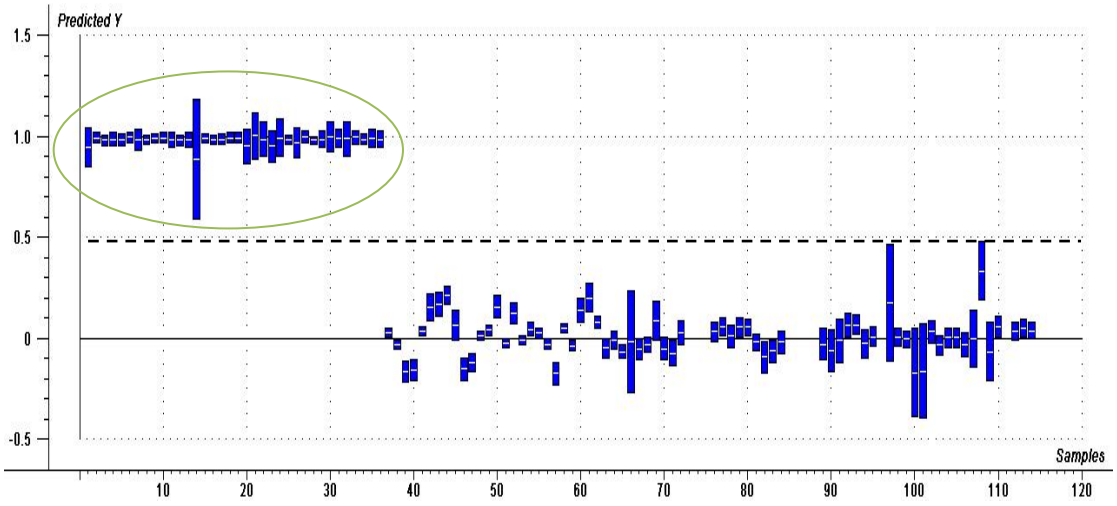

Figure 7.16 Classification of the calibration samples against the wool PLS-DA calibration model (wool samples circled)

Figure 7.17 shows a graph illustrating the percentage success rate for the SIMCA and PLS-DA methods on correct, unambiguous classification for the calibration set. It can be seen that the PLS-DA method has performed slightly better in this situation.

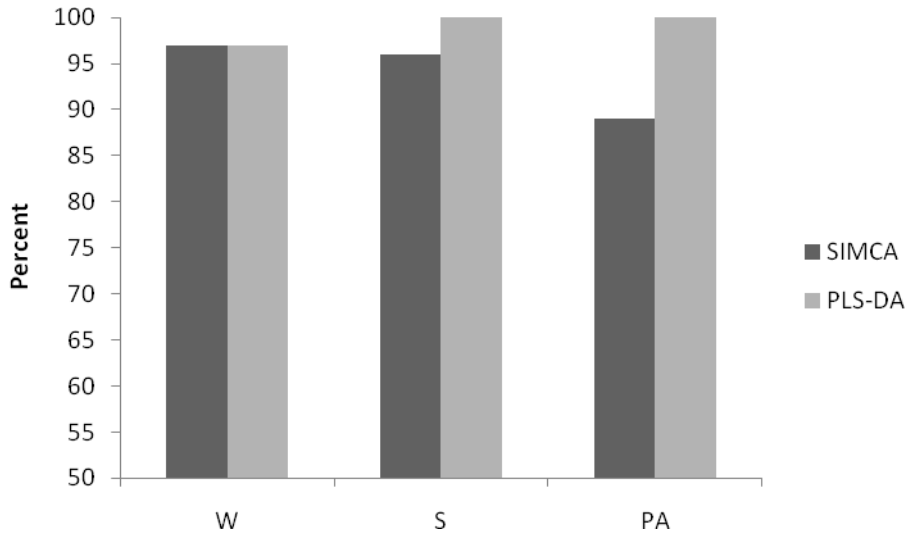

Figure 7.17 Percentage of correct, unambiguous assignments for the two classification methods

In order to test the application of the SIMCA and PLS-DA calibration models, two museum textile samples of known construction were analysed. The results are presented in the following two sections.

7.1.3 Case Study I: Parachute 'Silk' Slip

In Section 3.2.2, Chapter 3, the results of a site visit to Hampshire County Council Museums and Archives Service were presented. During the visit a garment that had been catalogued as silk was found to be made of polyamide after near-infrared analyses. Since this represents the types of classification problem curators and conservators face it was deemed an appropriate case study to test against the discrimination models.

7.1.3.1 Classification of the Parachute 'Silk' Slip by SIMCA

Using the software, the near-infrared spectra of the miscatalogued sample was compared to the three individual PCA calibration models discussed in Section 7.1.1. The SIMCA method correctly classified the sample as a polyamide and not as silk.

The plot shown in Figure 7.18 is known as a Cooman's plot. This plot is one of a number of plots generated by the software to visualise where an unknown sample is positioned in PC space when compared to the SIMCA calibration models.

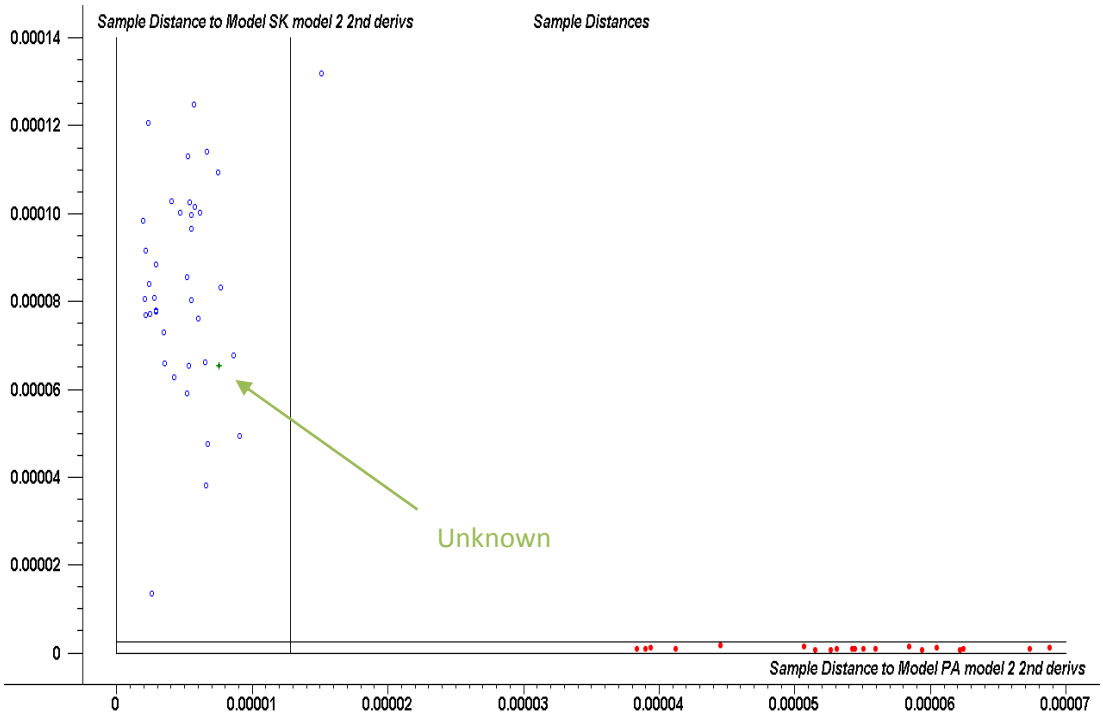

Figure 7.18 SIMCA Cooman's plot showing the orthogonal distance of the parachute 'silk' slip (green) from the polyamide model (blue) and silk model (red)

This represents the orthogonal residual distance of the unknown sample (green) from the centre of the silk model and polyamide model. The x and y axes can be considered to represent the first principal component axes for the silk and polyamide models, respectively. Samples that fall within the boundaries parallel to these axes belong to the corresponding models. If the sample does not belong to either model then it will appear in the upper right quadrant of the plot. Significance levels are set to 5% of the total residual variance. This means that there is a 5% chance that a sample that truly belongs to a group will be classified as not belonging.

It can be seen that on comparison of the unknown to the relevant models the sample falls well within the orthogonal boundary of the polyamide model and a long distance from the boundary of the silk model. This result is in keeping with the earlier findings.

7.1.3.2 Classification of the Parachute 'Silk' Slip by PLS-DA

The software enables the classification of unknown samples against the PLS-DA calibration models. The unknown sample is compared to each regression model individually. A sample predicted to have a value of one belongs to the class of interest, with a value of zero

indicating that the sample does not belong to that class. The boundaries for classification is the midpoint (0.5). The results for the misclassified slip are presented in Table 7.3.

Class	Predicted	Deviation
Polyamide	0.98	0.07
Silk	-0.02	0.12
Wool	0.05	0.14

Table 7.3 PLS-DA classification of Parachute 'Silk' Slip

It is clear from the results that when the sample was compared to the polyamide calibration model it was classified correctly as belonging to that group. On comparison with the silk and wool models it was not classified, illustrating that the calibration was successful.

7.1.4 Case StudyII: Schiaparelli Thai Silk Under Dress

The dress pictured in Figure 7.19 was recently displayed in the Couture exhibition at The Victoria and Albert Museum. In its original inventory the fuchsia pink under dress had been catalogued as Thai silk. During preparation for the exhibition analyses were carried out to determine the identity of the different components. FTIR-ATR was carried out at the Museum[I] and the warp and weft directions of the fabric were found to be different – one being silk the other being polyamide. These analyses were repeated and confirmed the results obtained by the Museum (spectra shown in Appendix 2). This dress proved a suitable case study to validate the differentiation capabilities of the SIMCA and PLS-DA classification models.

[I] Analyses carried out by Brenda Keneghan, Polymer Scientist, Science Section, Victoria and Albert Museum, as part of the preparations for the Couture exhibition at the museum in September 2007.

Figure 7.19 Image of the Thai silk under dress (V&A T.397-1974) (Copyright V&A)

7.1.4.1 Classification of the Schiaparelli Thai Silk Under Dress by SIMCA

The SIMCA method did not classify the sample as belong to either the silk or the polyamide groups. The silk vs polyamide Cooman's plot is shown in Figure 7.20, illustrating the orthogonal distance of the unknown sample from the respective models. Samples that fall within the boundaries belong to the corresponding models. The unknown sample is within the boundaries for the polyamide class, and positioned very close to that of the silk calibration model. However, it is clear that the unknown sample is placed a long distance along the length of the respective principal components. The sample is a long way from the length wise projections, and might therefore explain why the sample was not identified as belonging to either class.

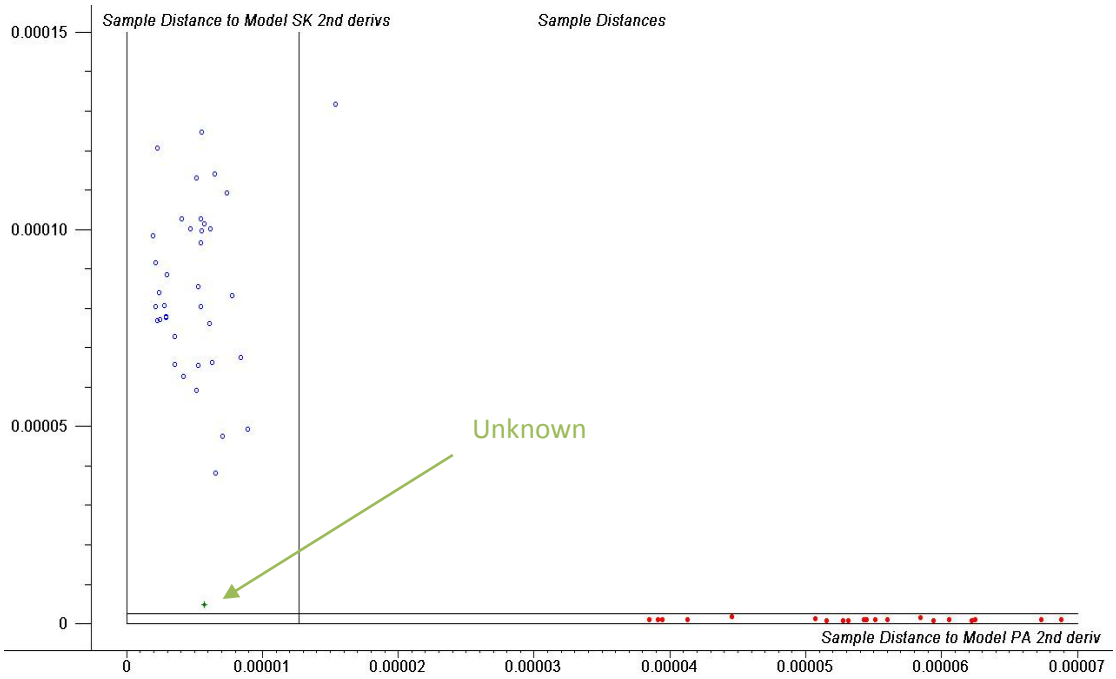

Figure 7.20 SIMCA Cooman's plot showing the orthogonal distance of the Schiaparelli dress (green) from the polyamide model (blue) and silk model (red)

7.1.4.2 Classification of the Schiaparelli Thai Silk Under Dress by PLS-DA

The results for the PLS-DA classification of the Schiaparelli sample are presented in Table 7.4.

Class	Predicted	Deviation
Polyamide	0.27	0.18
Silk	0.15	0.3
Wool	0.73	0.3

Table 7.4 PLS-DA classification of Schiaparelli dress

The FTIR-ATR analyses showed that the woven under skirt was a warp/weft textile blend, consisting of a silk component and polyamide component. However, on regression against the three calibration models the sample was actually classified as wool. As with the SIMCA method, this illustrates that for this particular sample it is not possible to distinguish the two textile components.

7.1.5 Conclusions

The results show that for the partial least squares discriminant analysis method provided a more robust method of differentiation of synthetic polyamide, silk and wool, in comparison to the SIMCA method. The reasons for this lie in the fact that the calibration model uses the known Y values (binary Y matrix) in the decomposition of the X matrix. The Y matrix is directly influencing the calibration.

For the cross validation method using the calibration samples the models were shown to be robust, with no Type II errors occurring. However, the samples at the extremes of each model were not successfully classified, due to their distance from the model centres and the significance limits set to 5%. Although the significance levels can be reduced, it was deemed appropriate to set them at 5% because it is always preferable to reject an object that truly belongs to a group than to run the risk of a false positive classification.

The two case studies highlighted the types of problems that are likely to be found in textile collections and illustrated the applicability of the classification methods. However, the results of the SIMCA analyses did not prove conclusive in the case of the blended fabric. This result suggests that a quantitative approach to blended fabrics may be necessary, rather than projecting the two materials onto two separate calibration models. A traditional PLS method should enable both components to be identified if coupled with the relevant blended fabric calibration samples.

7.2 Discrimination of Synthetic Polyamide Sub-classes

Due to the limited number of samples available for each subclass of synthetic polyamide, only models built on NIR spectral data for solid polyamide 6,6 (9 samples), 6 (6 samples) and 12 (7 samples) were studied. The nature of the multidimensional analysis requires that there are three or more samples for each group. Therefore, solid polyamide samples were studied as there were insufficient extruded polyamide samples in each class to ensure a successful calibration. This is one of the limitations of the work presented here. While the small sample set prevents unequivocal statements to be made, nonetheless the outcomes should indicate the potential of the approach for discrimination between the classes.

In a similar manner to the differentiation of the synthetic and natural polyamides, the initial step was to run a PC analysis on the raw spectra for the three synthetic polyamide subclasses to identify whether there was any inherent clustering.

The first two principal components are plotted in Figure 7.21. There does appear to be a separation of the samples, but the data for the polyamide 6 and 12 samples are interspersed. The corresponding loadings plots for PC1 shows there is a significant raising baseline affecting the data (Figure 7.22). For PC2, the high wavelength region shows an inverse relationship to the low wavenumber region, indicated by the positioning on either side of the dashed zero line (Figure 7.23). This is in keeping with the idea of a relative decrease in signal, relating to the peaks of interest, as the contribution from noise increases. As before, this longer wavenumber region was removed in further analyses. The influence of the raising baseline indicates that the spectra require pre-processing in order to reduce wavelength dependent scattering effects.

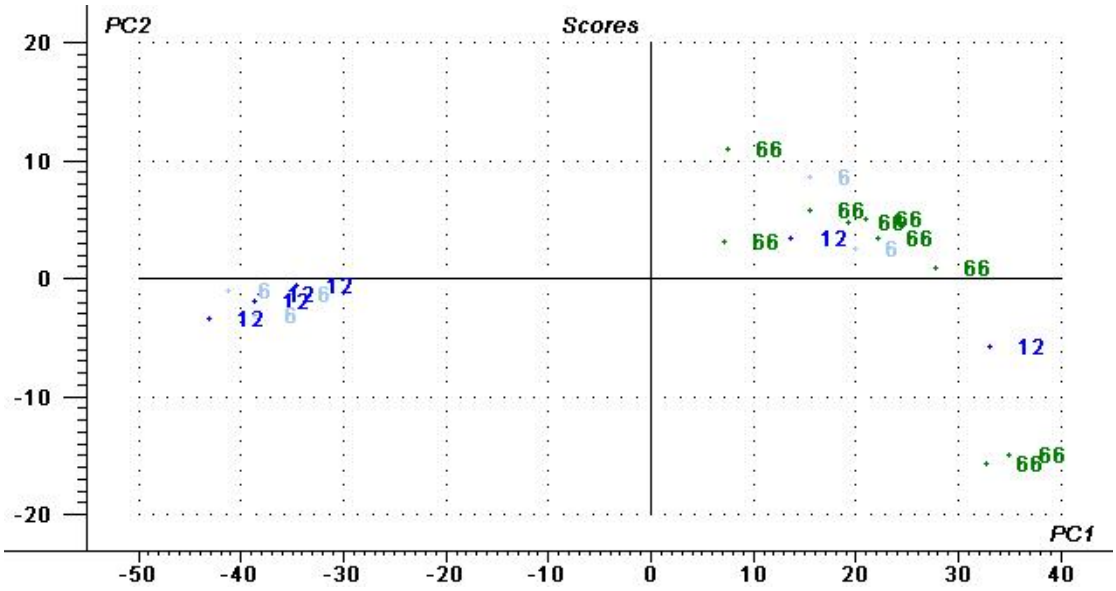

Figure 7.21 Raw data scores plot of the first two principal components for the discrimination of polyamide 6 (pale blue), polyamide 6,6 (green) and polyamide 12 (dark blue)

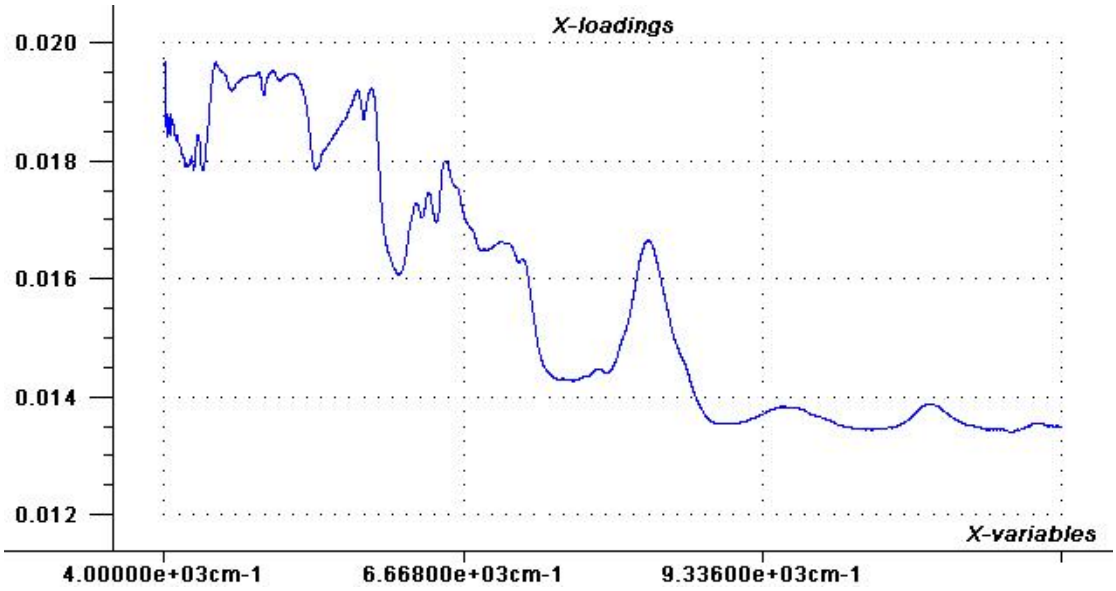

Figure 7.22 Raw data loadings plot of the first principal component for the discrimination of polyamide 6, polyamide 6,6 and polyamide 12

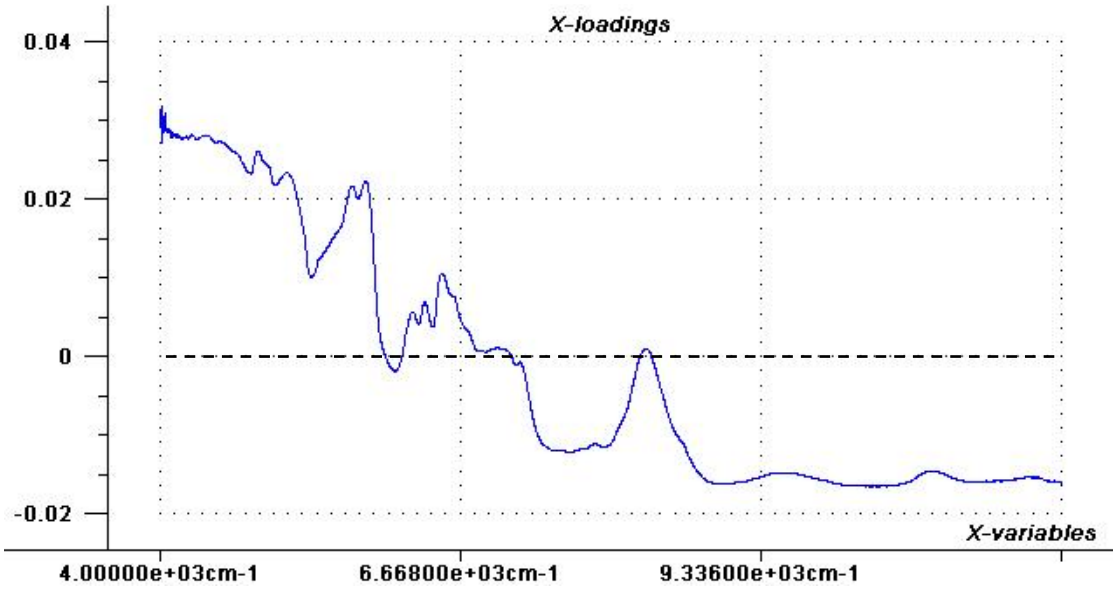

Figure 7.23 Raw data loadings plot of the second principal component for the discrimination of polyamide 6, polyamide 6,6 and polyamide 12

Figure 7.24 shows the resulting scores plot after removal of the higher wavenumber region (8 500-12 000cm^{-1}) and processing with the SNV function. There appear to be two outliers to the left of the plot. On inspection of the spectra (Figure 7.25) it is clear that there is a high degree of scattering and noise present, which have reduced the spectral features in

the region of interest. Both of these samples are carbon fibre reinforced samples, and strongly absorbing towards the visible region of the spectrum, having very different properties to the remainder of the group. Since it is unlikely that such material would be present in the types of collections of interest it was deemed appropriate to remove these samples from the calibration as they were causing a skew effect on the remainder of the model.

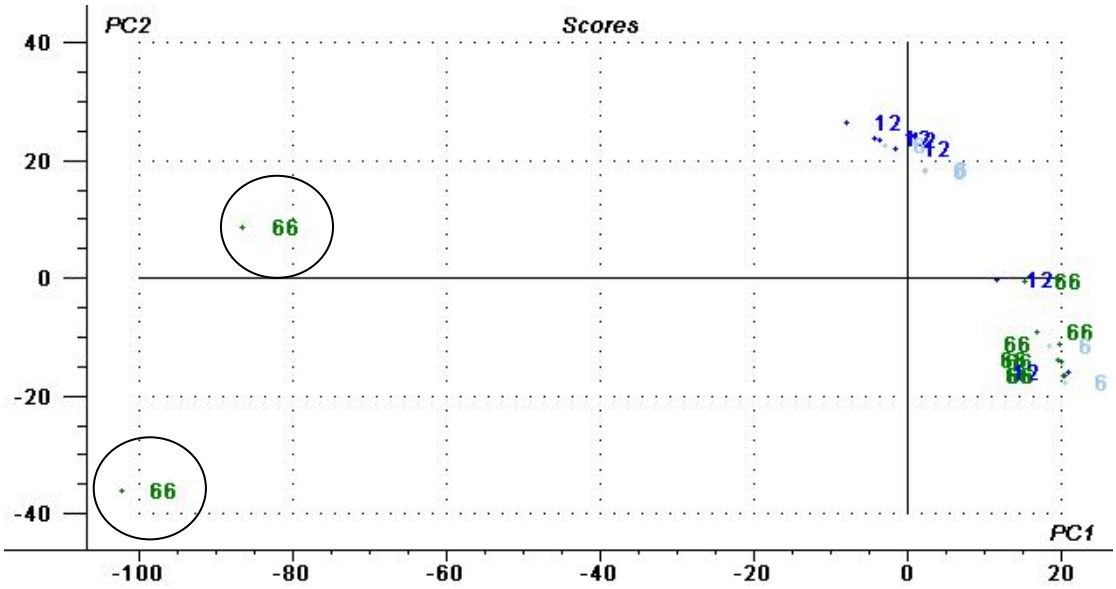

Figure 7.24 SNV processed data scores plot of the first two principal components for the discrimination of polyamide 6 (pale blue), polyamide 6,6 (green) and polyamide 12 (dark blue)

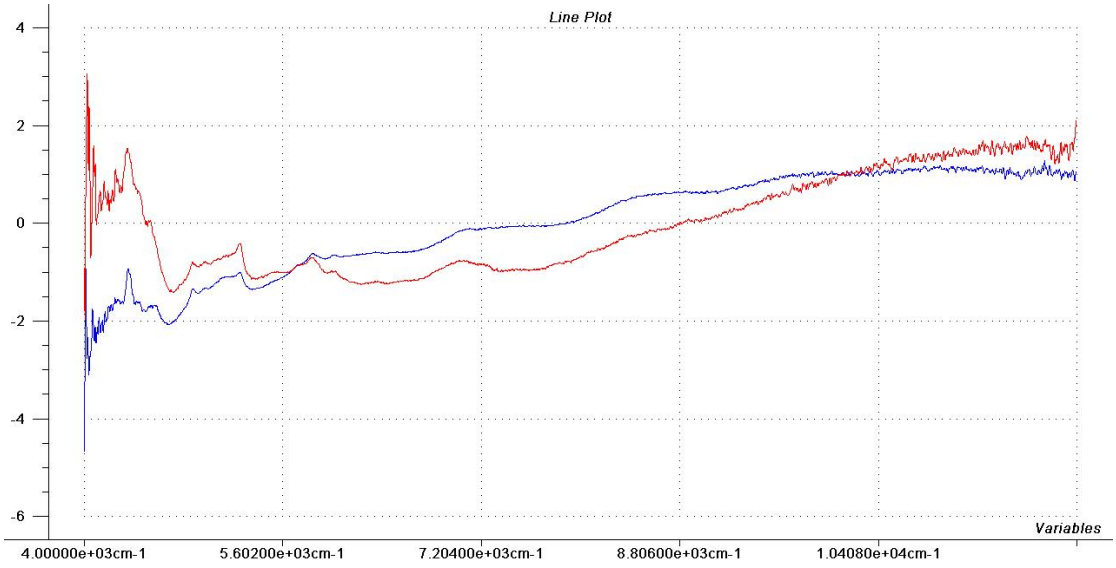

Figure 7.25 SNV processed near-infrared spectra of the two polyamide 6,6 outliers

The resulting scores plot after outlier removal is presented below:

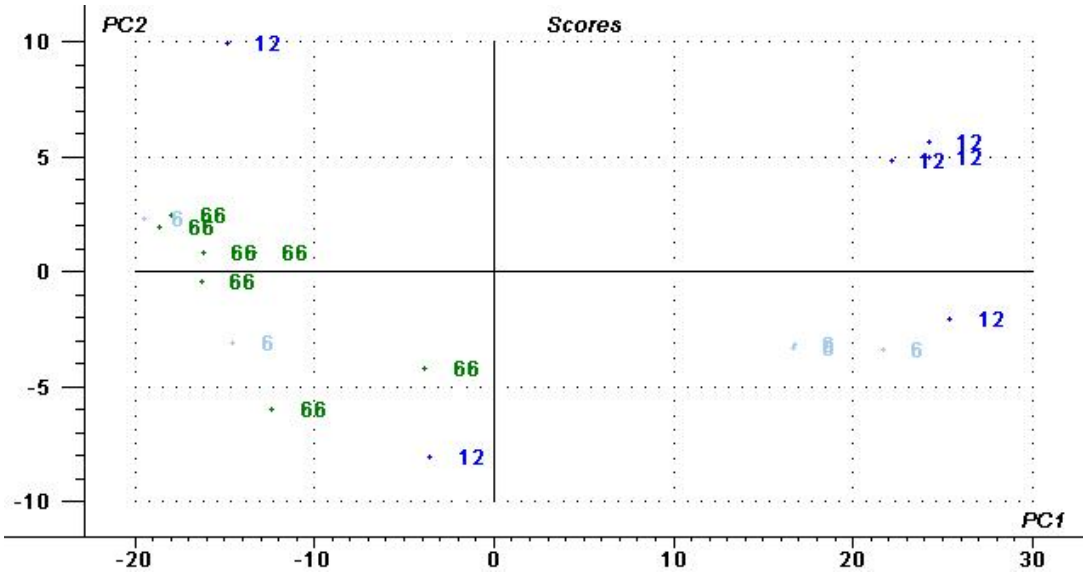

Figure 7.26 SNV processed data scores plot of the first two principal components for the discrimination of polyamide 6 (pale blue), polyamide 6,6 (green) and polyamide 12 (dark blue) after outlier removal

The loadings plot for the first PC shows that there is an inverse relationship between the region of most of interest and the low wavenumber region (Figure 7.27). It was therefore decided to remove the region between 4 000 – 4 420 cm^{-1}.

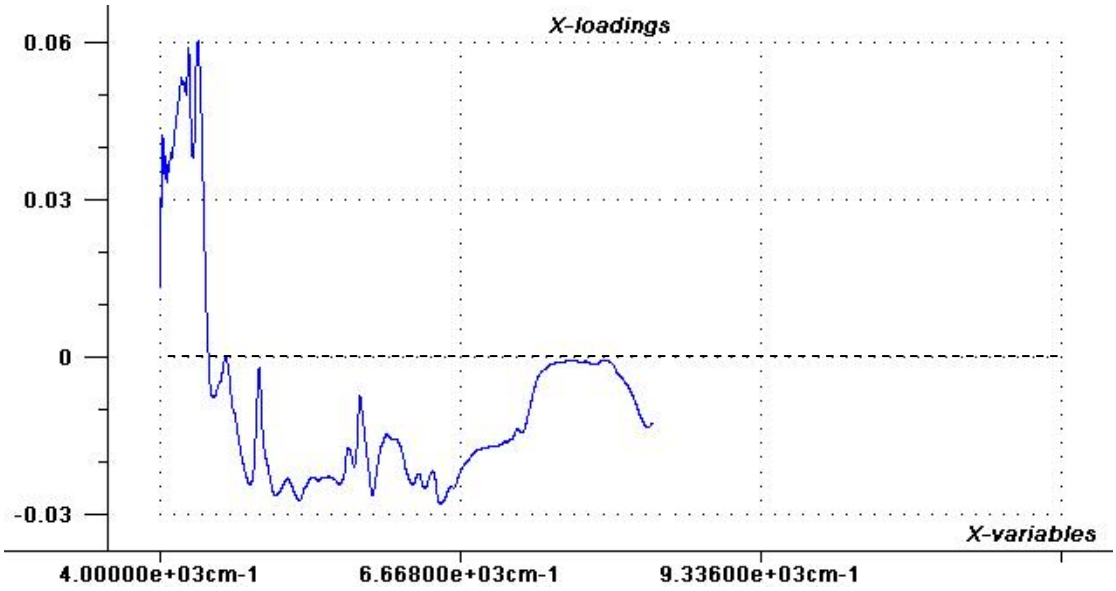

Figure 7.27 SNV processed data loadings plot of the first principal component for the discrimination of polyamide 6, polyamide 6,6 and polyamide 12

Reducing the region at the low wavelength range did not significantly altered the PC space distribution, but did increase the separation of the polyamide 6 and 12 points (Figure 7.28).

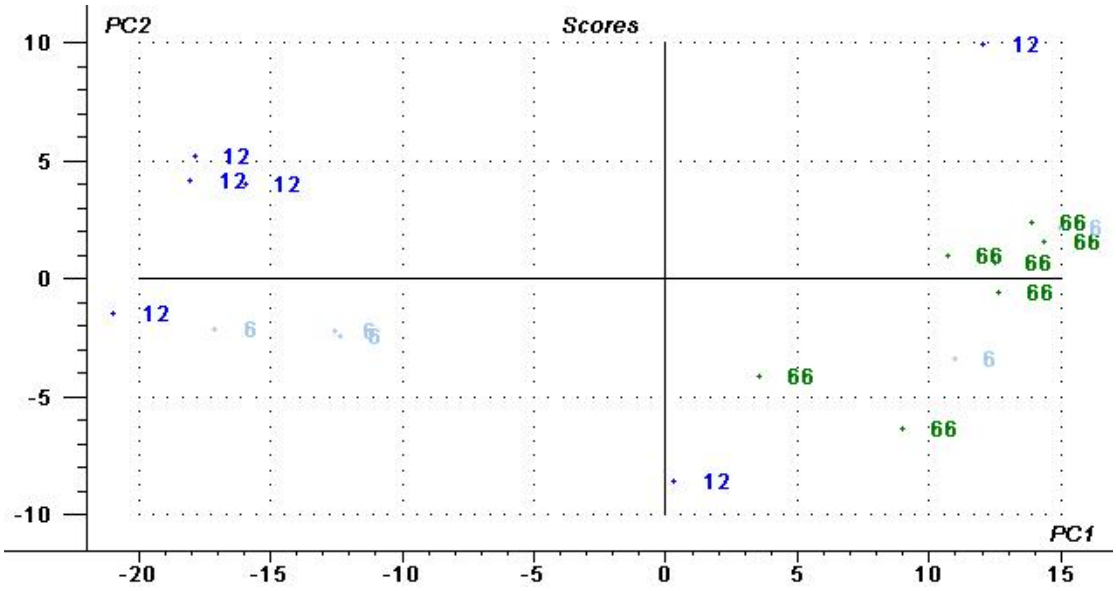

Figure 7.28 SNV processed data scores plot of the first two principal components for the discrimination of polyamide 6 (pale blue), polyamide 6,6 (green) and polyamide 12 (dark blue) after removal of the region between 4 000 – 4 420 cm^{-1}

The explained variance was found to tail off at five principal components and therefore four PCs were used, describing 95.8% of the data. The explained variance plot showed that the percentage explained information levelled off between PC1 and PC2, but there was a large jump at PC3 to 92%. This indicates that the third principal component is important and is shown plotted against the first PC in Figure 7.29.

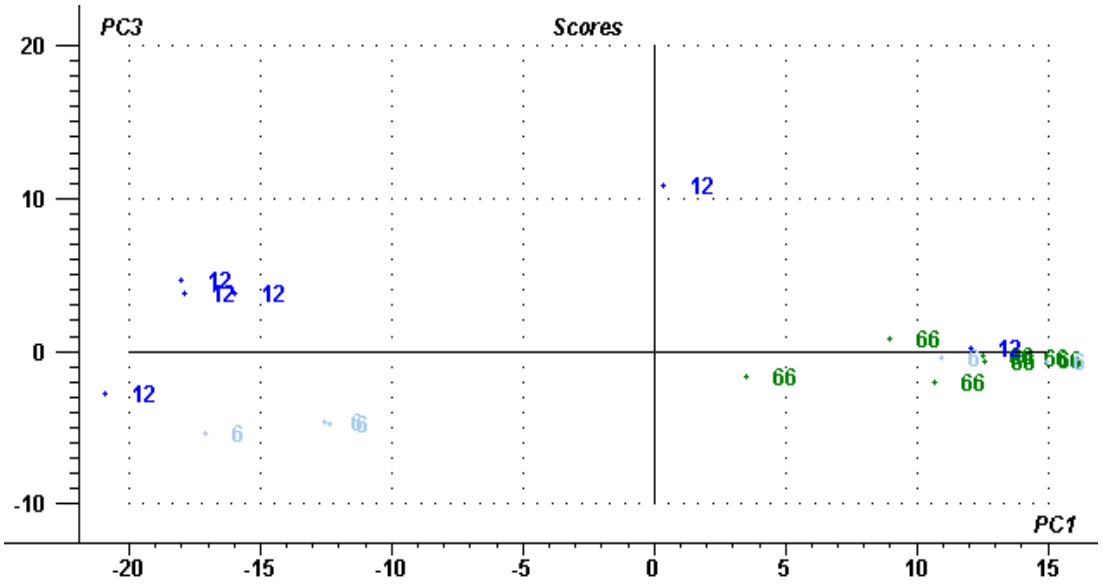

Figure 7.29 SNV processed data scores plot of the first and third principal components for the discrimination of polyamide 6 (pale blue), polyamide 6,6 (green) and polyamide 12 (dark blue). The analysis was restricted to the region 4 420 – 8 500 cm^{-1}.

On studying the loadings plot for PC3 (Figure 7.30), there are predominant peaks at 5 654, 5 782 and 8 224 cm^{-1}. These wavenumber regions have been attributed to the CH_2 second overtone symmetric stretch, CH_2 second overtone asymmetric stretch and a CH_2 third overtone stretch, respectively, in polyamide 11 [3].

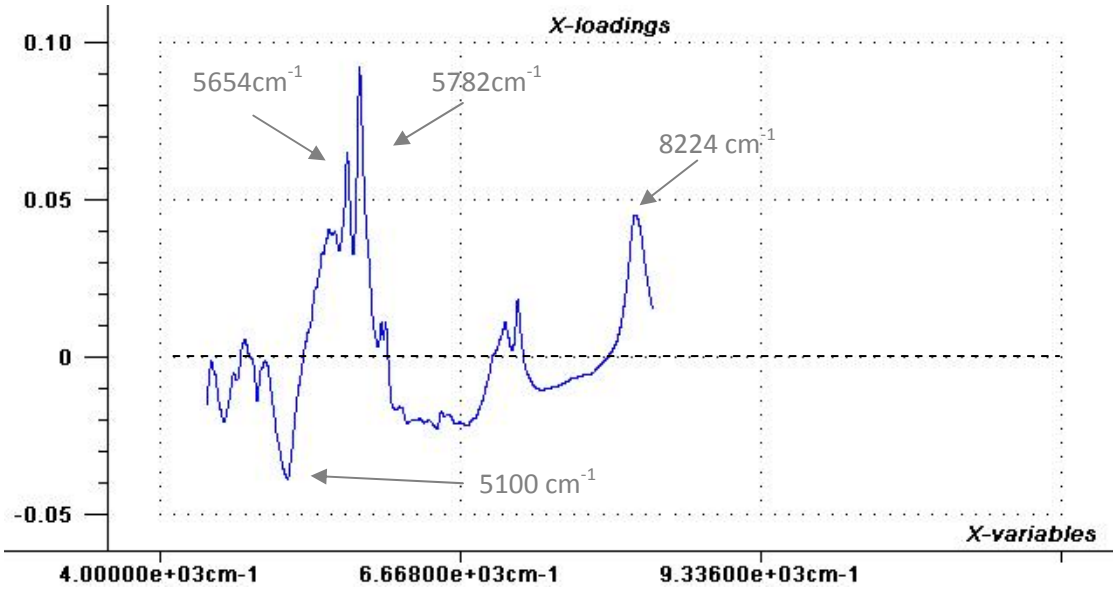

Figure 7.30 SNV processed data loadings plot of the third principal component for the discrimination of polyamide 6, polyamide 6,6 and polyamide 12.

For PC1, the loadings plot in Figure 7.31 also shows contributions from the above variables, in addition to 4 828 and 5 092 cm^{-1}, which were assigned to *v*(NH)as + Amide II, and *v*(NH)as + Amide I, respectively, in the same work. This indicates that the appropriate bands are being modelled

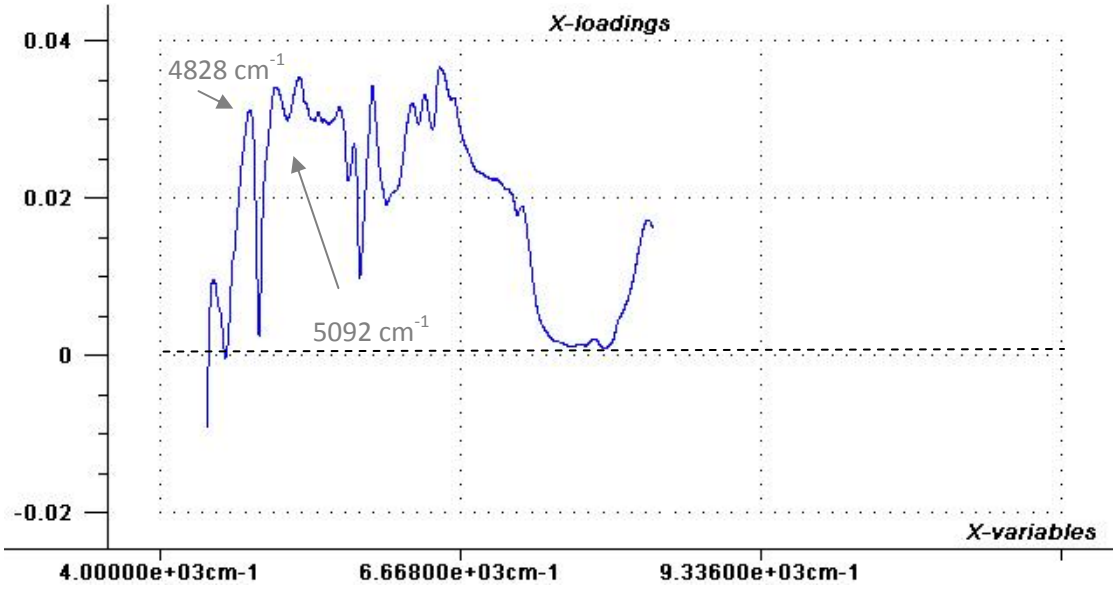

Figure 7.31 SNV processed data loadings plot of the first principal component for the discrimination of polyamide 6, polyamide 6,6 and Polyamide 12.

In Figure 7.30, the PC3 loadings plot also shows an inverse relationship between 5 100 cm^{-1} (Amide I) and the vibrational bands associated with the CH_2 stretching modes. As the carbon chains increase, there is a relative decrease in the number of amide bonds.

For comparison, the spectra were processed using the first and second derivatives to determine whether these would improve the separation of the classes. The first derivative scores plot for the first two principal components are shown in Figure 7.32. Polyamide 6,6 and 12 are now well separated, but polyamide 6 samples are still distributed amongst the two other groups. The explained variance dropped to 88.6% for three PC's.

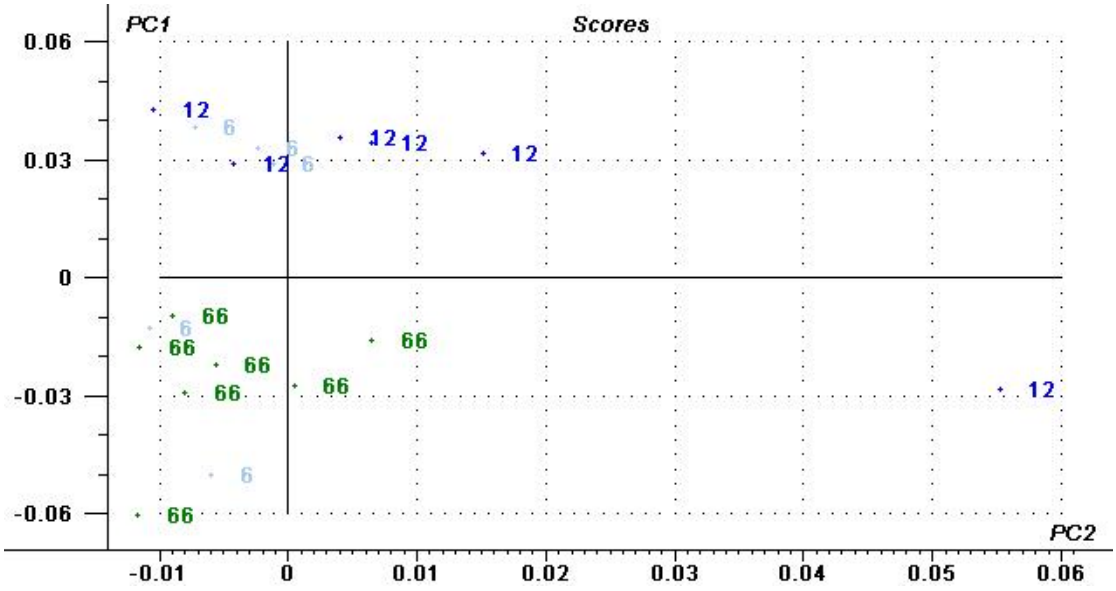

Figure 7.32 First derivative processed data scores plot of the first and third principal components for the discrimination of polyamide 6 (pale blue), polyamide 6,6 (green) and polyamide 12 (dark blue)

On applying the second derivative the clusters were not greatly affected and the explained variance dropped down to 84.5%.

On comparison of the three different spectral processing methods (Figure 7.33) it is apparent that there is a deterioration in the explained variance for the validation method when the spectra are processed with derivatives. Therefore, it was decided that the SIMCA and PLS-DA models would be built using spectra that had been pre-processed using the

standard normal variate function, as this provided the highest measure of prediction using the full cross validation method.

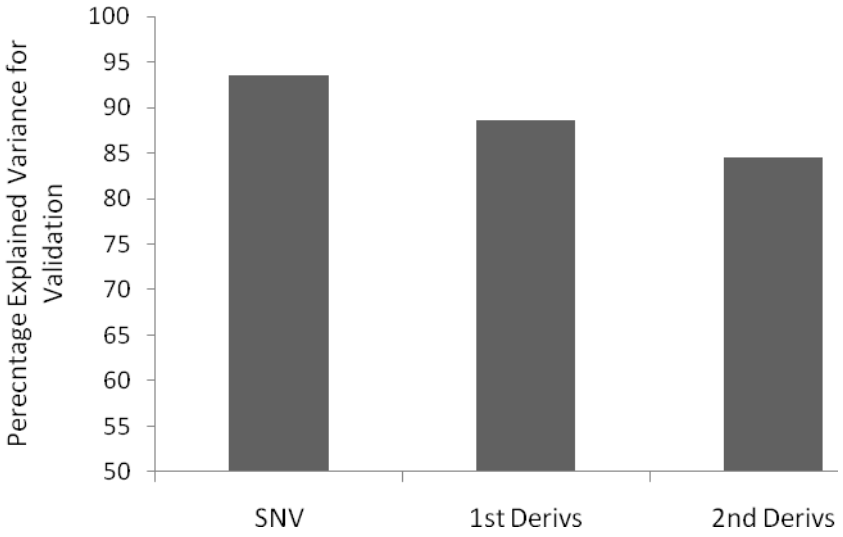

Figure 7.33 Percentage explained variance for model validation after different data processing methods

7.2.1 Soft Independent Modelling of Class Analogies Results for Synthetic Polyamide Sub-classes

Three separate PCA models were built using the parameters shown in Table 7.5 for the SIMCA method.

Subclass	Pre-processing	Spectral Region cm^{-1}	Number of PCs	Explained Variance %
Polyamide 6	SNV	4 420-8 500	3	96
Polyamide 66	SNV	4 420-8 500	4	91
Polyamide 12	SNV	4 420-8 500	4	76

Table 7.5 Individual PCA parameters for the for the process of SIMCA classification of polyamide 6, polyamide 6,6 and polyamide 12

On reintroduction of the samples back into the SIMCA models, all of the polyamide 12 samples were correctly classified, but one was also ambiguously classified as belonging to the polyamide 6 group. This sample was a transparent, amorphous polyamide and may represent an outlier to the others within that class . All of the polyamide 6,6 samples were classified as belonging to the correct group, but were also classified in the polyamide 6

group. Three out of the five polyamide 6 samples were classified as belonging to polyamide 6 and 6,6 groups.
The high level of cross classification between the polyamide 6 and polyamide 6,6 groups indicates that it may not be possible with this technique to distinguish these subclasses from one another. It does however, appear that the polyamide 12 samples occupy different regions in PC space, and can be resolved from the other two groups.

The model distance between polyamide 6 and polyamide 6,6 was only nine. The rule of thumb for robust classification is that a model distance of three is the minimum required to separate samples – this is very close to the limit and may explain the problems encountered with the classification. For the polyamide 12 calibration model there is a distance of 1 236 from the polyamide 6,6 model and 44 from the polyamide 6 model. This correlates with the classification results. None of the polyamide 12 samples were classified as polyamide 6,6, due to the large model distance. There was one sample classified as belonging to both polyamide 12 and polyamide 6 groups caused by the relatively small distance of the models.

7.2.2 PLS-DA Results for Synthetic Polyamide Subclasses

The data were processed in the same manner as applied for the SIMCA classification and the spectral region was reduced to 4 420-8 500cm^{-1}.

Figure 7.34 shows the scores plot for the first two principal components. It is clear that there is some degree of separation of the polyamide 12 samples from the other two groups. However, the inclusion of the Y variables has not enabled a clear separation of the polyamide 6 samples from the polyamide 6,6 samples. The explained variance for the validation is only 58.5% for three PC's, indicating that the data are poorly described.

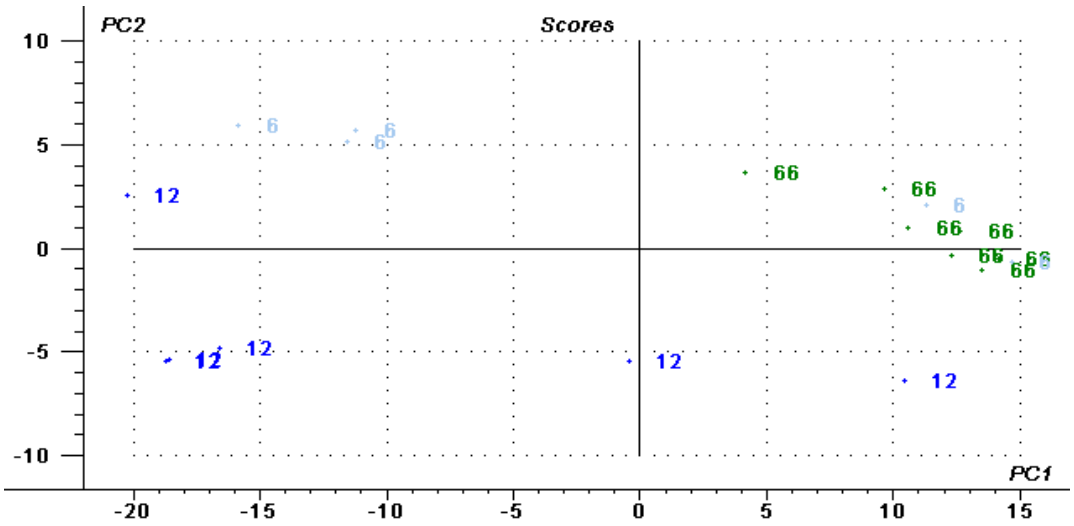

Figure 7.34 SNV processed data scores plot for the first two principal components for the PLS-DA discrimination of polyamide 6, polyamide 6,6 and polyamide 12.

The cross validation results are presented below as the predicted versus measured plots (Figures 7.35 to 7.37). The reader is reminded that each sample is removed from each of the three calibration models and re-introduced as a new sample for prediction. If the sample belongs to the group then it is assigned one and if it does not belong to the group it is assigned zero. In the case of the regression line, for successful prediction the slope will be near one and the line will intercept close to zero. The black line is the target and the blue line the measured line.

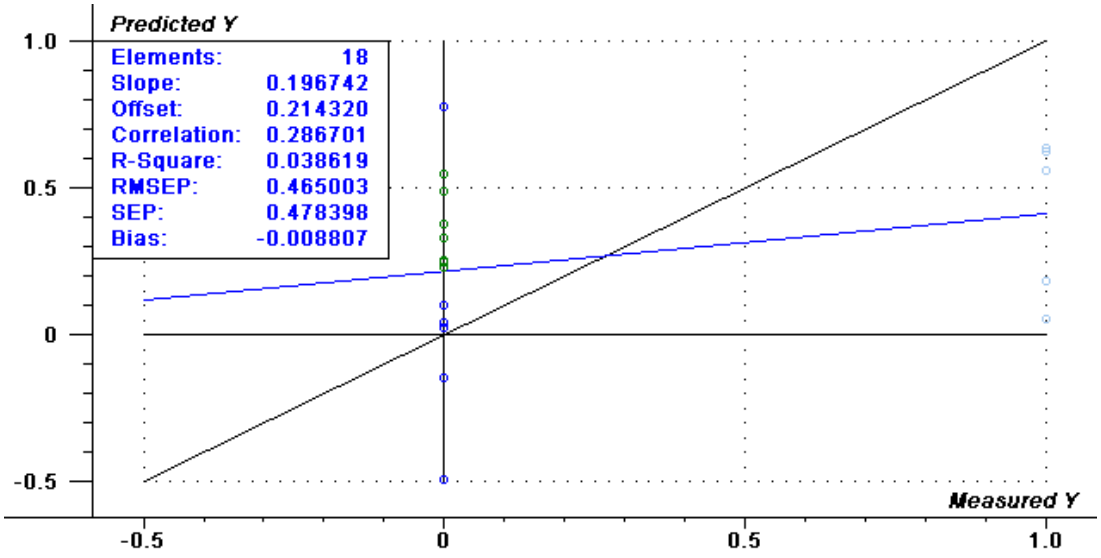

7.35 Predicted versus measured regression line for PLS-DA of polyamide 6 (light dark) against polyamide 12 (dark blue) and polyamide 6,6 (green)

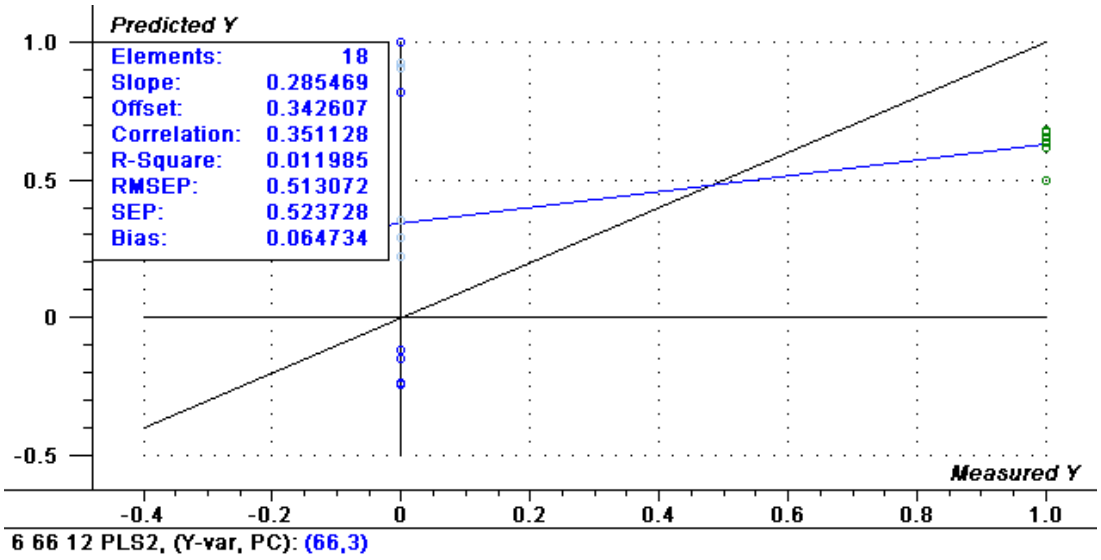

7.36 Predicted versus measured regression line for PLS-DA of polyamide 6,6 (green) against polyamide 6 (light blue) and polyamide 12 (dark blue)

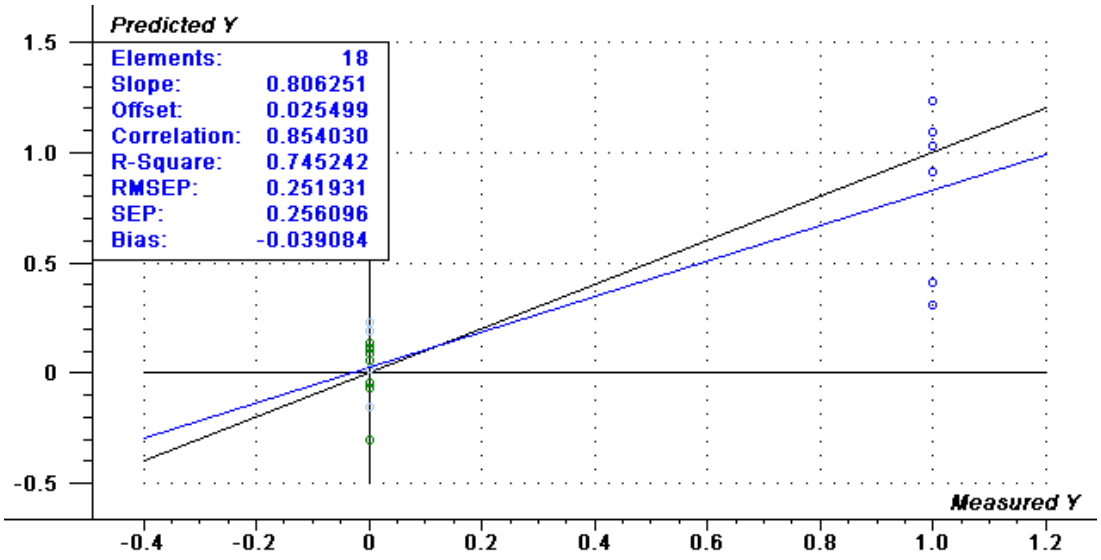

Figure 7.37 Predicted versus measured regression line for PLS-DA of polyamide 12 (dark blue) against polyamide 6 (light blue) and polyamide 6,6 (green)

The three regression lines confirm the trend seen in the scores plots for the first two principal components. For the validation process, it does not appear possible with this data set to distinguish polyamide 6 and polyamide 6,6. However, although there is some

deviation about the predicted values it is possible to distinguish polyamide 12 from the other two classes of polyamide.

Due to problems with the Unscrambler software, it was not possible to reintroduce the reference samples as an independent validation step to assess the success rate of classification, as previously illustrated (Section 7.1.2). The prediction model was built twice on two separate computers, but this did not circumvent the problem.

7.2.3 Conclusions

The results indicated that it is possible to distinguish polyamide 12 from the polyamide 6 and polyamide 6,6 classes. However, for both the SIMCA and PLS-DA methodologies the discrimination of the polyamide 6 and polyamide 6,6 proved problematic. The differences in the chemical structure of these two sub-classes of polyamide are small (Section 5.1.1, Chapter 5). However, the polyamide 12 samples have a reduced amide density and an increase in methylene groups along the polymer chain on comparison to the other two classes. Thus, the vibrational intensities of the absorption bands will differ, resulting in separation in PC space.

7.3 Conclusions

Confident discrimination of visually, chemically and physically similar materials is of prime importance when faced with the application of remedial conservation treatments. Although showing similar spectral features, it has been shown that polyamide, silk and wool can be readily separated in principal component space after the application of second derivative pre-processing. During the validation step it was shown that the PLS-DA method performed slightly better than the SIMCA method when comparing the percentage success rate of unambiguous classification. This is because the method uses the classification assignments in the Y matrix in the decomposition of the X matrix. The calibration models were tested against two samples representative of the types of problems likely to be encountered in contemporary textile collections. Namely, a misclassified fabric and a textile blend. In the first case, both discrimination methods were able to successfully classify the sample. For the second case, neither the SIMCA nor the PLS-DA methods successfully identified the sample as belonging to either the silk or polyamide classes. This indicated that in order to distinguish two or more components a quantitative PLS approach may be required.

Due to sample availability, classification models for polyamide sub-class discrimination was carried out on a limited test set. Therefore, the calibrations can only serve as an indication of the possibilities for sub-class identification. It was shown that, with the application of SNV pre-processing, it is possible to separate polyamide 12 from both polyamide 6 and polyamide 6,6 in PC space. On studying the loadings plots, it was apparent that the spectral regions influencing the calibration related directly to the length of the methylene chain and the amide density. Validation of the SIMCA method by sample re-introduction showed that the polyamide 12 samples could be successfully classified, but it was not possible to distinguish the polyamide 6 and polyamide 6,6 groups from each other. This was due to the small model distance between these two groups. The limited separation in PC space is due to the similarities in the chemical structures. By comparison the polyamide 12 model distance was much greater, owing to the fact that polyamide 12 has a methylene chain length twice that of polyamide 6 and only half of its amide density. The outcome suggests that while it may be difficult to unambiguously identify synthetic polyamide subclasses which have the same methylene to amide ratio, sub-classes with different ratios may be discriminated by multivariate analysis of their NIR spectra.

7.4 References

1. Adedipe, O.E., et al., *Classification of Red Oak (Quercus Rubra) and White Oak (Quercus Alba) Wood using a Near Infreared Spectrometer and Soft Independent Modelling of Class Analogies.* Journal of Near Infrared Spectroscopy, 2008. **16**: p. 49-57.
2. Esbensen, K.H., *Multivariate Data Analysis: In Practice*. 5th ed. 2002, Esbjerg: Camo.
3. Siesler, H.W., *Applications to Polymers and Textiles*, in *Near-Infrared Spectroscopy: Principles, Instrumentation, Applications*, H.W. Siesler, et al., Editors. 2005, Wiley-VCH: Weinheim. p. 213-246.

Chapter 8: Sample Preparation, Artificial Ageing and Pest Eradication Treatments

The intrinsic value, rarity and historical importance of materials held within museum and heritage collections means that the removal of even very small samples for analyses is often prohibited. In any case, for larger scale destructive testing and analysis the use of the original material becomes unacceptable. Therefore the investigation of models subjected to accelerated ageing becomes a prerequisite for many heritage science studies. Typically, a control set of samples are compared against a set of samples that have been subjected to a variety of different environments known to induce a particular set of degradative processes. Somewhat extreme conditions are applied in order to force the reaction processes forward at a faster rate than would normally occur during long-term natural ageing. These types of studies usually allow the stability of a material to be assessed, providing an insight into possible behaviour during a particular application [1].

Such an approach was applied here, affording a better understanding of the physical and chemical effects of ageing on polyamides, besides providing model aged specimens for further testing.

8.1 Sample Preparation

The test material used throughout the artificial ageing and subsequent treatments was a polyamide 6,6 ISO Single Adjacent Fabric made in accordance with ISO Section F03 [2]. This fabric is a standard polyamide textile used for colour fast testing within the dye industry. It was not possible to establish from the manufacturers whether any other chemicals were added during the manufacture of the textile. Any additives could affect the material's properties. For example, titanium dioxide is often added to polyamides as a delustrant, but has been shown to act as a photosensitiser, shifting UV absorption to longer wavelengths [3, 4].

The fabric was an undyed, plain-weave structure, with 20 warps and 20 wefts per cm^2, weighing 125g/m^2. The warps were double Z-plied yarns and the wefts single yarns[I]. Supplied by Testfabrics Inc., it was received after being washed and scoured in an alkaline bath. This process is used by manufacturers to remove oils and starches that have been deposited on the textile during fibre extrusion and subsequent weaving on the loom[II]. The thermal history and processing of the as received sample is not known.

Although constituting an important part of heritage collections, there has been limited detailed work within the field of conservation into the stability of aged polyamides. One of the few studies has been completed recently, investigating the effects of dyes on the photostability of polyamide 6,6 support netting [5, 6]. In their work Sinha *et al* describe the significant alterations in the tensile behaviour of dyed and undyed netting when exposed to wavelengths of 300-800nm at ambient conditions. The UV-visible spectra of undyed samples suggested the appearance of carbonyl compounds attributed to the photooxidation of the polyamide chains. They also found that the presence of a dye enhanced degradation, with the type of dye having a significant effect on the degree of deterioration. SEM analysis showed clear surface alterations, with the appearance of cracks along the fibre axis, possibly due to the rupturing of the chain lengths. Studies of the crystal structure by DSC and XRF presented slight increase in crystallinity, which was more predominant in the dyed samples.

Since the purpose of this study was to provide an overview of how new and aged polyamides from collections may behave during pest control treatments, it was decided that in addition to investigating the stability of 'as received' undyed material, it would also be beneficial to determine whether the presence of dyes was likely to alter the behaviour of the polyamide. The method of dyeing synthetic textiles requires a number of chemical additives and relatively high solution temperatures, there was concern that these factors in themselves would make it difficult to determine the effect of the dye alone. To overcome this complicating issue it was deemed necessary to have a third set of samples that had been taken through the dyeing procedure, but without the addition of the dye. This would enable conclusions to be drawn about the differences that may be expected between dyed

[I] A double Z-plied yarn refers to an assembly of two previously twisted yarns, with a right handed twist. The twist is determined by looking down the length of the yarn, and the progression of the twist away from the observer describing the direction. The two types of yarn twists are Z and S, referring the to the central diagonal sections of each letter.
[II] Personal conversation with Shawn Meeks, Test Fabrics Inc., 6 December 2007

and undyed material, and also provide a means of assessing the effect of the textile processing itself. These samples from the third set will be referred to as 'Treated' from this point on.

For the dyed material, a Lanaset Acid Red dye was applied[III], following a modified method as stated in ISO 105 Section F03, which is applied routinely at the Textile Conservation Centre. The treated samples were processed using the same method as for the dyed samples, however the dye powder itself was excluded.

8.1.1 Sample Dye Methodology

Deionised water in a beaker was heated to 50°C, at which point the polyamide fabric was immersed (fabric to water ratio 176:5280 g:cm^3) and allowed to wet out for 10 minutes. The fabric was removed and all additives, excluding the dye, were added and thoroughly dispersed in the solution. The pH was monitored using a Hanna HI9024C pH meter, and maintained at approximately pH7 by the addition of either acetic acid or saturated sodium acetate solution. The fabric was then returned to the bath for a further ten minutes. The fabric was removed again whilst the dye liquor was added (final dye to liquor ratio 7:8800 g:cm^3), and again returned to the solution. The temperature was raised to 95°C over a period of 60 minutes, during which time the temperature was held at 75°C for 20 minutes. The dye to liquor ratio was maintained throughout the process by the addition of water up to the starting level. The solution was cooled to 70°C for ten minutes and then maintained at this temperature for a further 15 minutes, at which point the fabric was removed and thoroughly rinsed in hot water. Finally the sample was submerged in a 1% solution of formic acid (fabric to solution ratio 176:1.76 g:cm^3) for 10 mins and then rinsed in deionised water until there was no further dye bleeding.

8.2 Artificial Ageing

The nature of museum and heritage objects means it is often difficult to acquire samples to enable representative analysis and testing. It is therefore necessary to artificially age model material, using conditions that can be related to the environments in which the objects are kept. Light, heat and humidity are the common factors that promote natural ageing [7]. By subjecting a material to extremes of these factors, accelerated ageing can provide

[III] Acid red dye was chosen as it was shown to induce intermediate degradation behaviour in the work carried out by Sinha [5].

information about the principal causes of deterioration. Some caution is required in the interpretation of the results however, due to the varying and competing reactions that may occur at extremes.

To provide degraded test material to assess the likely behaviour of aged artefacts, artificial ageing can be carried out under a variety of environmental conditions, in which one or more factors are taken to extremes simultaneously or sequentially.

8.2.1 UV/Visible Light Ageing

UV degradation is known to be a major contributing factor in the working life of polyamide material. Preliminary experiments confirmed that there was a significant drop in tensile strength after light exposure. One set of model aged specimens was therefore generated by exposing the polyamide samples to high intensity light, with a spectral distribution of 300-800nm. These would subsequently enable the stability of aged polyamide 6,6 subjected to pest eradication treatments to be determined.

8.2.1.1 Light Ageing Methodology

Each sample was exposed to artificial sunlight using a Q-Sun Xenon test chamber Xe-1 fitted with a Xenon arc lamp. A daylight filter was fitted between the source and the samples and irradiance was set at 0.68 W/m^2 (340nm). This produced a spectral power distribution equivalent to summer sunlight, with a total dose of 40 MJ/m^2 over one day. The samples were aged for 168 hours, which equates to around 20 days of outdoor exposure. Preliminary experiments (not presented) illustrated that this length of exposure would provide a material exhibiting half of its original tensile strength. A chiller unit was used to maintain the chamber at room temperature (23°C ±3) to avoid heat ageing of the samples. The relative humidity within the chamber was not controlled, though the RH of the room was 50% ±4.

The chamber comprises a flat bed, which could accommodate six polyamide samples each measuring 8x10 cm (Figure 8.1). The samples were held in place by glass tipped pins and the bed inserted into the chamber at 20 cm below the source. The samples were exchanged with each other daily to ensure an even exposure and to prevent differential ageing.

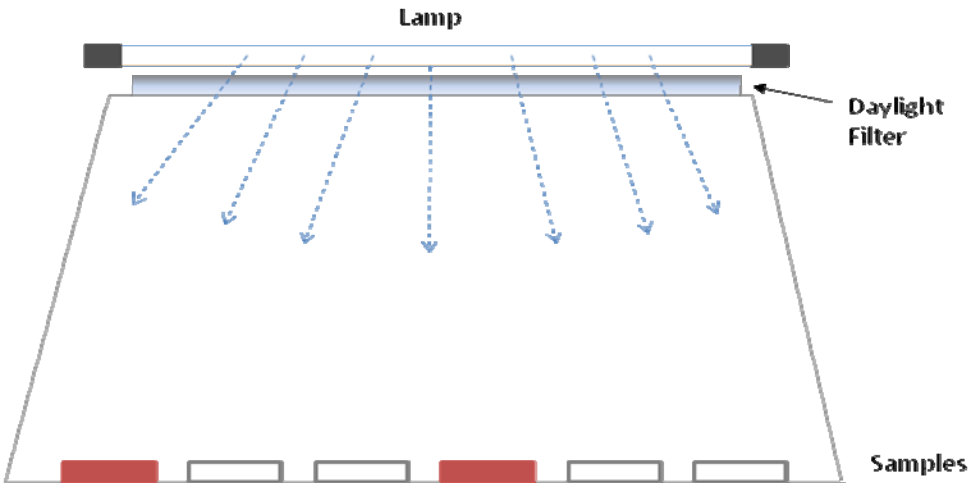

Figure 8.1 Schematic of the inside of the Q-Sun Xenon Test Xe-1 chamber

8.2.2 Heat Ageing

In order to emulate a material that has been subjected to normal use (ie sunlight exposure) and then kept in a controlled museum environment for some years (without UV exposure), pre-irradiated polyamide 6,6 was further artificially aged at a raised temperature of 80°C for 28 days, maintaining a constant RH of 50%. This provided a further degraded specimen for the investigation of pest control methods. The primary aim was to enable links to be drawn between the behaviour of the test material, when subject to the eradication treatments, and the way in which naturally aged material may behave.

The use of artificial ageing relies on tentative assumptions, in an attempt to correlate the behaviour of artificially aged samples with that of naturally aged material. It has been suggested that an increase in 5-10°C doubles the deterioration rate of an organic material [8]. If this principle is applied, the reaction rates presented in Table 8.1 could be expected:

Artificial Ageing Temperature/°C	Reaction Rate at 5°C	Reaction Rate at 10°C
30	x 4	x 2
40	x16	x 4
50	x 64	x 8
60	x 256	x 16
70	x 1024	x 32
80	x 4096	x 64

Table 8.1 Increased reaction rates with increasing temperature

These reaction rates do not take into account additional factors that may occur at raised temperatures. The complex nature of organic materials means that there are many possible reaction routes. As the temperature is raised it cannot be assumed that each series of reaction will occur at the same relative rate. Reactions which were predominant at ambient temperatures may be superseded by other competing reactions at elevated temperatures. This is especially true when working above the glass transition temperature of a material. Since the glass transition temperature of polyamide 6,6 is known to be in the region of 45-55°C, ageing at 80°C will enhance freedom of movement of the chains within the amorphous regions which could promote degradation pathways that would not necessarily have been effective during 20 years of natural ageing. This needs to be borne in mind when extrapolating the results to the behaviour of museum artefacts.

Table 8.2 lists the samples that were prepared together with their treatments and artificial ageing regimes.

Sample label	Sample Treatment	Light Ageing Regime	Heat Ageing Regime
Con Au	Undyed	N/A	N/A
Con At	Treated	N/A	N/A
Con Ad	Dyed	N/A	N/A
Con Bu	Undyed	UV aged for 168hrs	N/A
Con Bt	Treated	UV aged at 168hrs	N/A
Con Bd	Dyed	UV aged for 168hrs	N/A
Con Cu	Undyed	UV aged for 168hrs	80°C 50% RH for 28 days
Con Ct	Treated	UV aged for 168hrs	80°C 50% RH for 28 days
Con Cd	Dyed	UV aged for 168hrs	80°C 50% RH for 28 days

Table 8.2 Ageing regimes relating to each sample (N/A = not applicable)

8.2.2.1 Heat Ageing Methodology

Each sample was curled around the inside of a glass hybridisation tube. A glass vial containing 5 cm^3 of a saturated solution of sodium bromide over 1 g of solid NaBr was placed at the bottom of the hybridisation tube (to maintain a relative humidity of 51.4% ±1.5 [9]). The vial was plugged loosely with glass wool to prevent the salt from migrating onto the sample. The tube was then tightly sealed with a screw top having an underlying PTFE coated silicone rubber septum, and placed into an oven (Figure 8.2).

Two ovens (Heraeus Instruments) were used, a Laboratory Air Circulation Oven model UT 6 P and an Air-Circulation Drying Oven model UT 6060. The tubes were rotated in the ovens every other day to avoid temperature variations causing differential ageing, and where the saturated salt solution appeared to have reduced it was topped up.

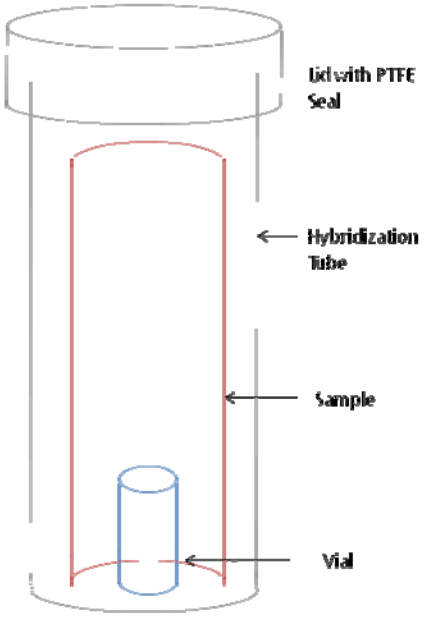

Figure 8.2 Schematic of a hybridization tube containing a sample and vial

8.3 Pest Eradication Treatments

As discussed in Chapter 4, the application of pest eradication treatments to synthetic material is of growing concern to keepers of contemporary collections. The stability of polyamide 6,6 textiles was investigated by treatment of samples in situ using the Thermo Lignum treatment and a chest freezer at The Victoria and Albert Museum. Samples were subjected to the relevant temperatures unloaded and loaded to ascertain whether textiles could be treated whist hanging from their display supports.

In addition to the raised and lowered temperatures, a control set of sample were also prepared. Again these were also in their unloaded and loaded state and were maintained at room temperature within a humidity glove box at 50% RH ±2.

8.3.1 The Thermo Lignum® Process

The Thermo Lignum® WARMAIR process uses a large walk-in sealed chamber (Figure 8.3) where the temperature and relative humidity are controlled.

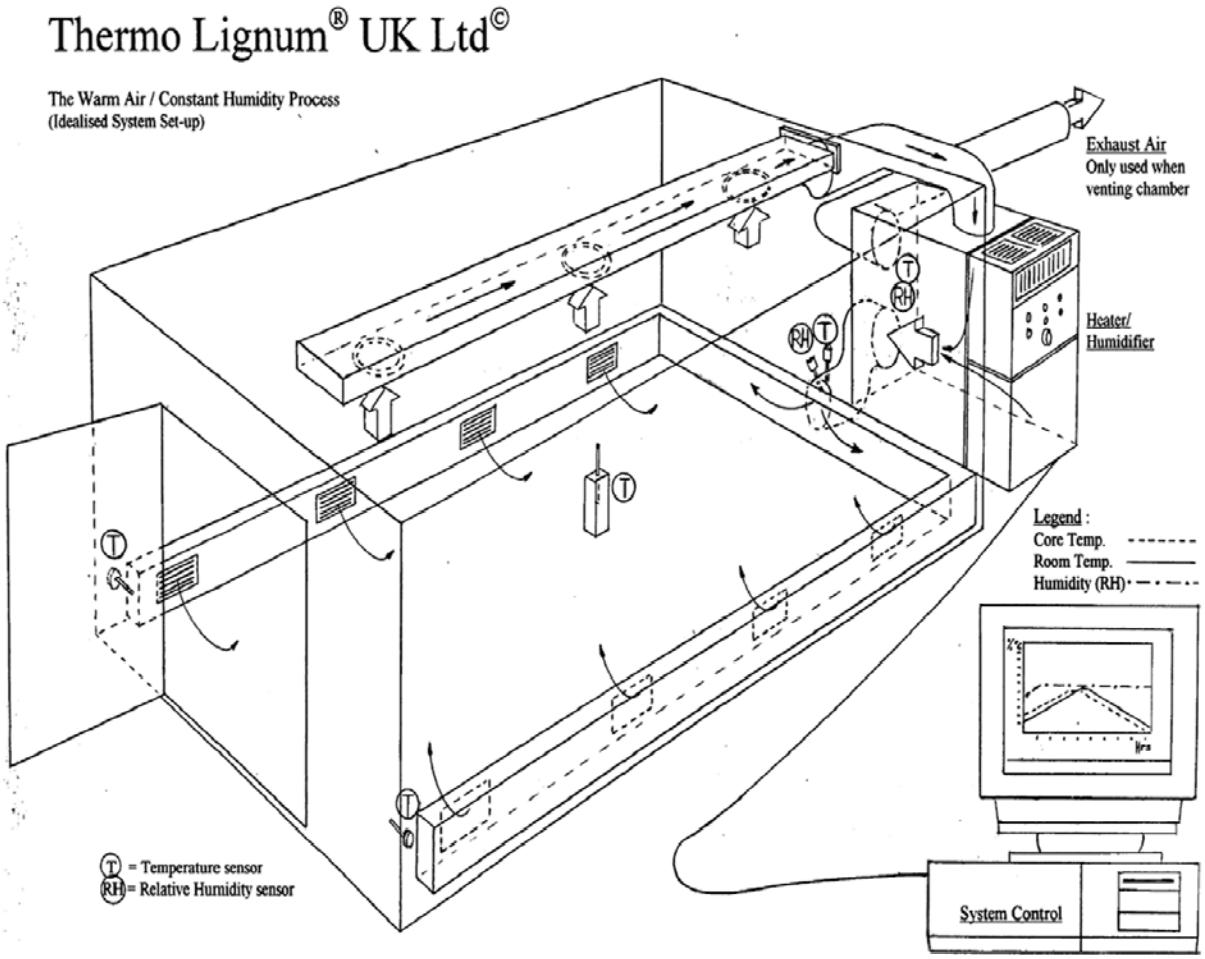

Figure 8.3 Thermo Lignum® WARMAIR chamber sketch (Copyright Thermo Lignum®)

Warm air and moisture are pumped in via floor level air vents. There are a number of temperature sensors situated throughout the chamber, with an additional temperature probe/protimeter that is inserted into the centre of a wooden block. This is used to represent an organic object and is required to ensure that the core temperature reaches the required 55°C to kill all insect species that are encountered in heritage settings. This means that there is a temperature difference (ΔT) between the core and the chamber. In order to maintain constant moisture content of the wood (8.5%) whilst increasing the temperature the chamber conditions are modified accordingly.

8.3.1.1 Heating Cycle

During the heating and cooling there is a temperature lag where ΔT = 8°C as the chamber temperature increases and decreases at a faster rate than the large wooden block (Figure 8.4). The chamber is heated until it reached 58°C at which point it is maintained constant until the wooden block reaches 55°C, ΔT = 3°C. The core temperature is then maintained at 55°C for 30 minutes, which results in a chamber temperature of 58°C for 120 minutes. For the duration of the cycle (approximately 14 hours) the temperature is above 50°C for between four and six hours.

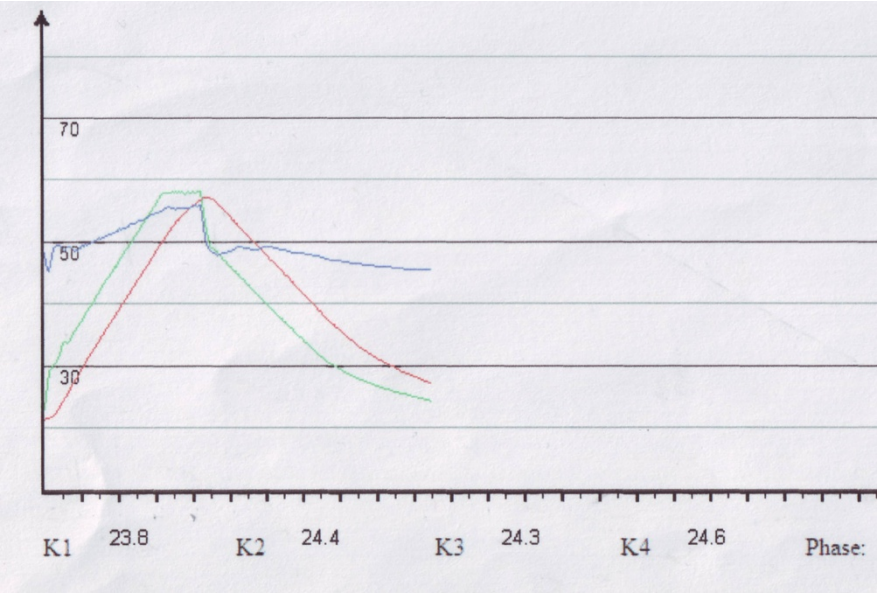

Figure 8.4 Temperature and humidity profile generated by the Thermo Lignum® software, chamber temperature (green), core temperature (red) and chamber humidity (blue). The Y axis is both temperature and humidity and the X axis is the treatment phase (time/days)

During the treatment of the polyamide samples no other objects were placed within the heating chamber ensuring good air flow. The samples, both unloaded and loaded, were placed in the centre of the chamber on a raised shelf (Figure 8.5).The unloaded samples were laid flat in the bottom of archival cardboard boxes without lids. The loaded samples were allowed to hang freely from wooden frames, as will be discussed further in Section 9.5, Chapter 9.

Figure 8.5 Samples in place on a raised shelf in the centre of the Thermo Lignum® chamber

8.3.2 The Freezing Process

The freezing of organic artefacts is routinely carried out within heritage institutions as a rapid and easily accessible method of pest eradication. Low temperature chest freezers without a defrost cycle are employed, ensuring a constant temperature is maintained. At -20°C the artefacts are required to be treated for 21 days to ensure total mortality. At -30°C treatment is carried out for 72 hours. For the work carried out here a chest freezer at The Victoria and Albert Museum was used, which is maintained at temperatures of -30°C ±1. Due to the risk of condensation forming on the surface of an object as it is brought back up to room temperature objects are wrapped in low density polyethylene.

8.3.2.1 Cooling Cycle

The unloaded samples were prepared by wrapping in polyethylene, carefully removing as much air as possible, and sealed using parcel tape (Figure 8.6). The samples were then carefully placed into the freezer, ensuring they were flat and not load bearing.

Figure 8.6 Unloaded samples before treatment, wrapped in low density polyethylene and sealed using parcel tape

It was not possible to closely wrap the loaded samples in polyethylene, due to the fact that they were suspended from frames. In this case the central sections of the samples were wrapped in acid free tissue paper and every three samples double sealed in polyethylene bags (Figure 8.7). The frame was then sealed in a larger polyethylene bag before placing into the base of the freezer(Figure 8.8).

The samples were treated for 72 hours, after which time they were removed from the freezer and allowed to acclimatise at room temperature. After four hours the loaded samples were unwrapped and removed from their frames for transport. The unloaded samples remained wrapped for 24 hours.

Figure 8.7 Loaded samples suspended from frames before treatment, with the central sections wrapped in acid free tissue, then double wrapped in low density polyethylene bags

Figure 8.8 Samples being placed into the freezer

8.4 References

1. Feller, R.L., *Accelerated Ageing: Photochemical and Thermal Aspects*. Research in Conservation, ed. D. Berland. 1994, Los Angeles: Getty Conservation Institute.
2. Institution, B.S., *Textiles - Tests for Colour Fastness*. 2001. BS ISO 105: Part F03: 2001: London: British Standards Institution.
3. Taylor, H.A., W.C. Tincher, and W.F. Hammer, *Photodegradation of Nylon 66 by TiO2.* Journal of Applied Polymer Science, 1970. **14**: p. 141-146.
4. Lock, L.M. and G.C. Frank, *A Study of Some Factors Affecting the Photodegradation of Textile Yarns Part II: Nylon 66 and Polyethylene Terephthalate Yarns.* Textile Research Journal, 1973. **September**: p. 502-512.
5. Sinha, M.K., *An Investigation of Photodegradation of a Support Netting Used in the Conservation of Historic Textiles*. 2006, Heriott-Watt: Edinburgh.
6. Sinha, M.K., R.M. Christies, and R. Shamey. *The Effect of Acid Dyes on the Photodegradation of Knitted Nylon Conservation Support Net*. in *AHRC Research Centre for Textile Conservation and Textile Studies Second Annual Conference: The Future of the 20th Century - Collecting, Interpreting and Conserving Modern Materials*. 2005. Winchester, UK: Archetype Publishers.
7. Erhardt, D. and M.F. Mecklenburg. *Accelerated Vs Natural Aging: Effect of Ageing Conditions on the Aging Process of Cellulose*. in *Materials Research Society Symposium Proceedings* 1995. Pittsburgh: Materials Research Society.
8. Michalski, S. *Double the Life for Each Five-degree Drop, More Than Double the Life for Each Halving of Relative Humidity*. in *Preprints of the 13th Triennial Meeting of the ICOM Committee for Conservation*. 2000. Rio de Janeiro: James & James.
9. Greenspan, L., *Humidity Fixed Points of Binary Saturated Aqueous Solutions.* Journal of Research of the National Bureau of Standards - A. Physics and Chemistry, 1977. **81A**(1): p. 89-96.

Chapter 9: Experimental Techniques and Protocols

The techniques employed within this study were chosen to focus on the underlying structural changes of the polyamide material. That is, to monitor any alterations in the amorphous and crystalline phases of the polymer. As already highlighted, it is these regions that govern the thermal response of polymers and therefore are deemed the most important factors in determining the stability under thermal pest control treatments.

Alongside the experimental parameters employed for each analytical technique, this chapter will focus on the key features that may be expected during the interpretation of the data.

The experimental techniques used to characterise the structural, chemical and mechanical character of the polyamide under study were Fourier transform Infrared Spectroscopy (FT-IR), Mechanical Testing, Differential Scanning Calorimetry (DSC) and creep experiments using a Dynamic Mechanical Thermal Analyser (DMTA).

9.1 Fourier-transform Infrared Spectroscopy (FT-IR)

9.1.1 Experimental Overview

The underlying principles of infrared spectroscopy have already been outlined during the discussion on Vibrational Spectroscopy in Heritage (Section 1.1, Chapter 1) and Infrared Spectroscopy (Section 2.1, Chapter 2).

Mid-infrared spectroscopy is concerned with the application of radiation of lower energies than those applied in near infrared spectroscopy; namely 4 000-700 cm^{-1}. This longer wavelength radiation provides information on lower frequency, fundamental molecular vibrations. As a consequence this region of the spectrum can afford detail on the structure and bonding in molecular species.

As previously outlined (Section 1.1, Chapter 1) there are a number of sampling techniques available for application with FTIR.

Attenuated Total Reflectance (ATR) relies on the phenomenon of the evanescent wave. When electromagnetic radiation penetrates a crystal of high density, such as diamond or germanium, internal refraction can occur at the internal surface if the angle with the

interface is sufficiently acute. At the point of reflectance an electronic field, known as an evanescent wave, is produced and extends beyond the crystal into the less dense material. If a sample is placed in direct contact with the crystal the evanescent wave will be absorbed by the sample (Figure 9.1). This results in attenuation of the beam at specific absorption wavelengths [1].

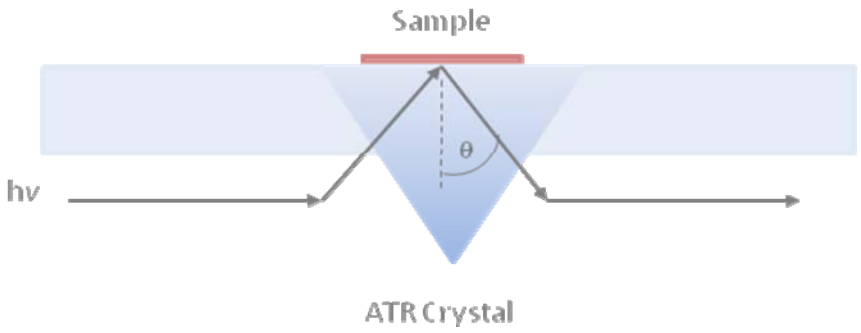

Figure 9.1 Schematic of an attenuated total reflectance sampling crystal

The depth of penetration of the radiation into the sample, d_p, is typically of the order of magnitude of the wavelength of the incident radiation, but is also dependent on the refractive indices of the crystal window and the sample itself, and the angle of incidence:

$$d_p = \frac{\lambda}{2\pi n_c \sqrt{\sin^2\theta - \left(\frac{n_s}{n_c}\right)^2}}$$

Eq. 9.i [2-4]

dp = depth of penetration

λ = wavelength of incident radiation

n_c = refractive index of the crystal

n_s = refractive index of the sample

θ = angle of incidence

The varying depths of infrared penetration into a polyamide sample are presented in Figure 9.2, where the refractive indices of the crystal (n_c) and polyamide (n_s) are 2.4 and 1.57, respectively. This illustrates that at longer wavenumbers the depth of penetration into a sample will be lower than at lower wavenumber.

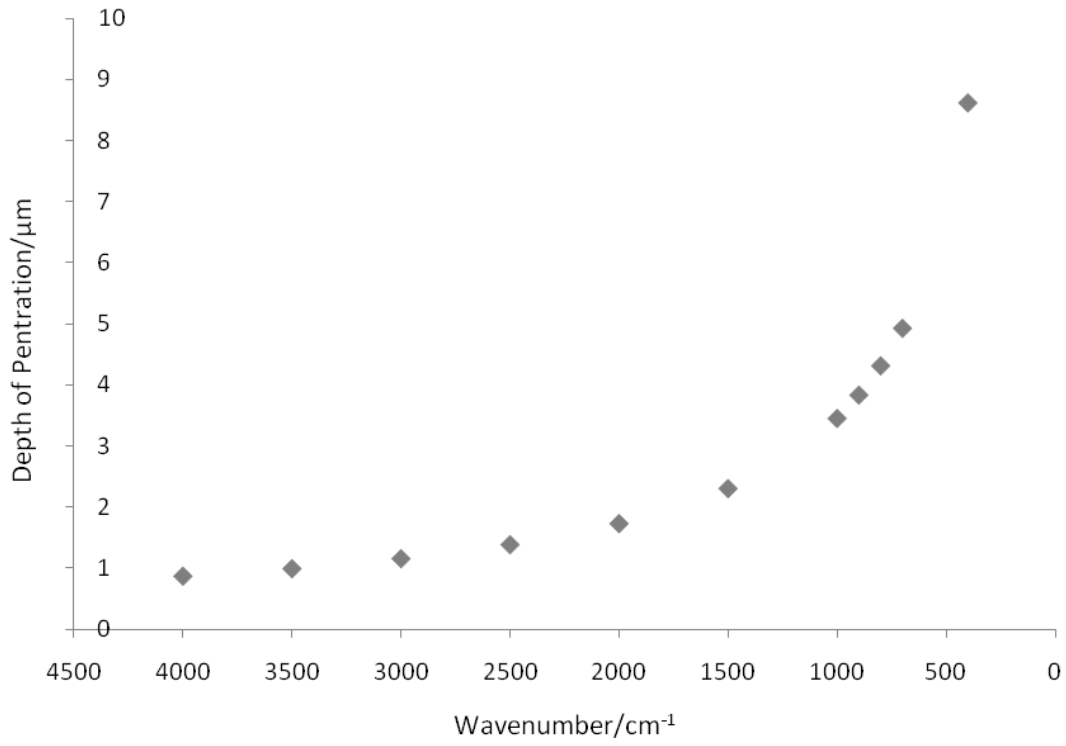

Figure 9.2 Depth of penetration into a polyamide sample using an ATR accessory

The primary advantage of the ATR technique is its ready application. The nature of the sampling technique requires minimum sample preparation and enables the sample to be retained after analysis. One of the drawbacks to FTIR-ATR and the application to heritage material is the invasive nature of the technique. This is due to the need for good contact to be made between the crystal and sample, caused by the short sampling capabilities of the evanescent wave. Here, this is not of concern as the samples under study are not conservation materials and do not pose a problem for invasive analyses.

The directionality of the incident beam means that it is inherently partially polarized. It is key to ensure that when studying fibres and textiles which may contain oriented material they are placed on the sample cell in a consistent orientation. The polarized, directional nature of the beam and orientation of molecular bonds can be exploited to allow polarised-ATR experiments, to elucidate information on the crystal structure of a material.

9.1.2 Experimental Methodology

In this study mid-infrared analysis was carried out using a Perkin Elmer Spectrum One Fourier transform infrared spectrometer, using a Universal attenuated total reflectance accessory (ATR) with a diamond/ zinc selenide crystal. A scan range of 4 000-700cm^{-1} was

employed, with a wavenumber resolution of 4cm^{-1} and scan accumulation of 32. These parameters were chosen because they have previously been applied successfully for the investigation of textiles within the department [5, 6].
For the work carried out here, both normal FTIR-ATR and Polarized ATR (Pol ATR) were employed.

9.1.2.1 Fractional Crystallinity by FTIR-ATR

Besides assessing chemical changes, FTIR-ATR may be used to monitor alterations in the crystallinity of the polyamide following a method described by Vasanthan *et al* [7, 8]. In this method the deconvoluted bands at 934cm^{-1} and 924cm^{-1} were used to determine the amorphous and crystalline fractions of the polyamide 6,6 samples. In similar work, Goncalves *et al* [9] used the reference band at 930 cm^{-1}, assigned to Amide IV, to normalize their spectra. Their paper investigated the effects of moisture degradation on polyamide material and they used this peak as it represents the crystalline phase, and therefore precluded moisture penetration.

Due to the fact that these bands overlap, they were separated using the peak fitting function in Grams AI software. A baseline was applied between 860-960cm^{-1} (Figure 9.3), peaks fitted to the Voigt peak function, with sensitivity set to medium and the maximum number of peaks set to three. This was the set of parameters used in the method being followed [7]. For the two absorbance bands of interest the sampling depths are 4.03µm and 4.06µm, showing that the spectral information is derived from the same regions of the samples.

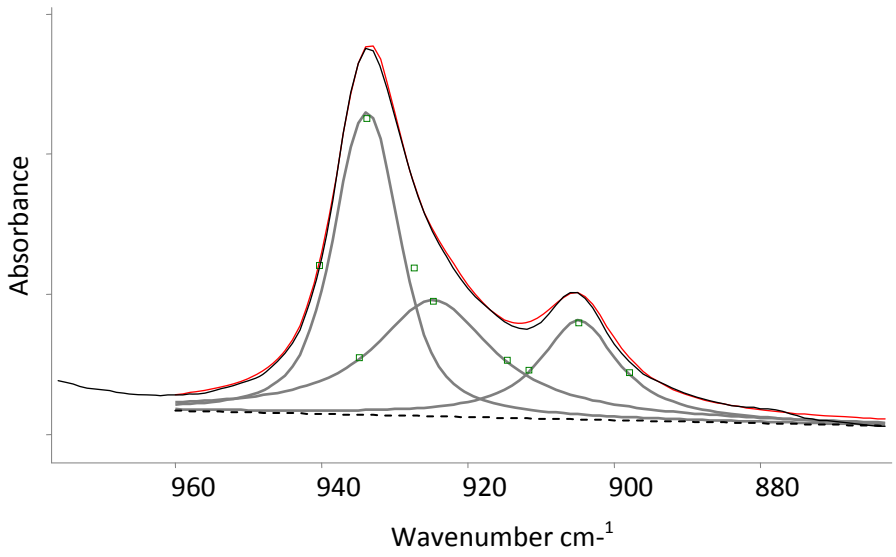

Figure 9.3 Deconvolved peaks for polyamide 6,6 FT-IR absorbance spectrum between 960 cm^{-1} and 860 cm^{-1} (grey), baseline (dashed), original trace (black) and fitted trace (red

The absorbance intensities for both of these peaks were subsequently normalised against the height of the peak at 1 630cm^{-1} (Amide I), which was shown to be unaffected by heat treatment [7]. The peak height at 1 630 cm^{-1} was determined using the software's peak integration function, with a two point baseline set to 1 701-1 587 cm^{-1} and forcing the data points to the curve.

The two intensity ratios, I_{1631}/I_{925} and $I_{934}/I_{925,}$ were plotted against each other. The slope of this regression line (P1) was then used to calculate the percentage crystallinity of the samples, by multiplying with the crystalline absorbance ratio I_{934}/I_{1631}:

$$\text{Fractional Crystallinity} = P1 \times (I_{934}/I_{1631})$$

Eq. 9.ii

The numerical output represents the crystalline fraction of the samples assuming a two phase model, following the equation:

$$P1 \times (I_{934}/I_{1631}) + P2 \times (I_{925}/I_{1631}) = 1$$

Eq. 9.iii

A full discussion of the methodology along with the results are given in Section 10.1.1.3, Chapter 10.

9.1.2.2 Degree of Anisotropy by Polarized ATR

Polarized ATR (Pol ATR) experiments were employed to monitor alterations in the anisotropy of the polymer chains. This provides an indication of the overall order of the structure, highlighting alterations in orientation, chain break down and regions of surface fracture.

A polariser is placed between the source and the ATR crystal, and set to 0° (Figure 9.4). This is so that the electric vector is in the plane of the sample interface, and nominally oriented from front to back of the spectrometer ($E_{\perp}$). The fibre was rotated between 0 and 90 degrees, where 0° refers to the fibre axis oriented with the electric vector, front to back across the ATR crystal (Figure 9.5).

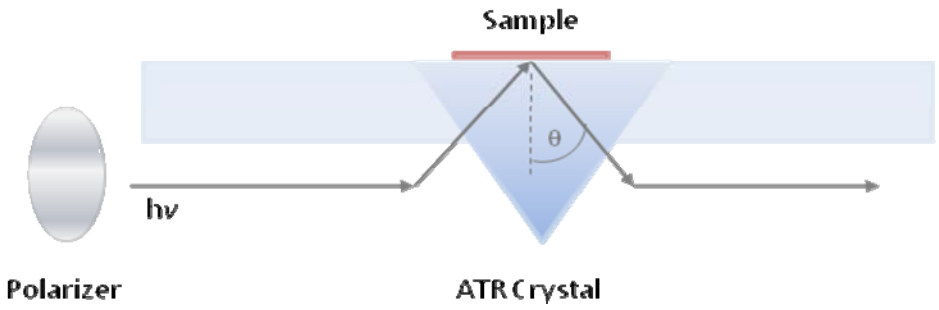

Figure 9.4 Schematic of the polarizer and attenuated total reflectance sampling crystal [5]

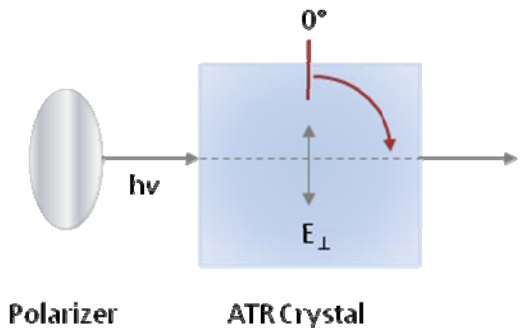

Figure 9.5 Birds eye schematic of the polarizer and attenuated total reflectance crystal, showing the direction of the electric vector and the fibre orientation at 0 degrees [5]

Dichroic and non-dichroic bands were determined by comparison of spectra taken with the fibres at 0 and 90 degrees. The absorbance intensities of the dichroic bands were normalised against non-dichroic bands as an internal reference to account for variations in depth of penetration.
Details of the dichroic and non-dichroic bands are provided in Section 10.1.1.2, Chapter 10, along with a full discussion of their application for monitoring orientational alterations in the polyamide 6,6 yarns.

9.2 Mechanical Analysis

9.2.1 Experimental Overview

Mechanical testing is used to give an overview of the physical properties and characteristics of a material and to enable changes to be monitored over time. The work presented here focuses on the tensile properties of the samples through tension tests, before and after treatment.

9.2.2 Experimental Methodology

Mechanical testing was carried out using an Instron 5544 tensile tester, with Bluehill software version 1.4, data acquisition every 100ms and when the load changed by one Newton or greater.

Tensile testing was carried out following a modified strip test method, BS EN ISO 13934-1:1999 [10]. This method was deemed the most appropriate method for identifying changes in strength due to treatments. This test applies a constant extension rate to the sample and records the maximum load achieved at the point of rupture (N), the total tensile extension (mm), and the energy required to take the sample to failure (J).

During the course of the experiments temperature and relative humidity fluctuations averaged 21°C ±1 and 50% ±4, respectively. These variations were beyond the control of the experimental setup, but could have influenced the tensile behaviour of the samples [11].

9.2.2.1 Test Strips

The polyamide 6,6 textile samples were prepared by cutting test strips measuring 20 warp yarns wide, corresponding to approximately 10mm in width[I]. For each sample, seven repeat tests were carried out to account for variability in the textile material, enabling a mean and standard deviation to be calculated. Samples were held in rubber faced jaws, any that broke close to the jaws were removed from the analysis.

It is clear from Figure 9.6 that the yarns in the warp direction are more than twice as strong as those running in the weft direction. As previously discussed in Section 8.1, Chapter 8, the warp yarns were double Z-plied yarns and the wefts single yarns. It follows that the weft yarns will be weaker as there are fewer fibres in a bundle.

Figure 9.6 also shows that the tensile properties of the textile are directly proportional to the width of the sample.

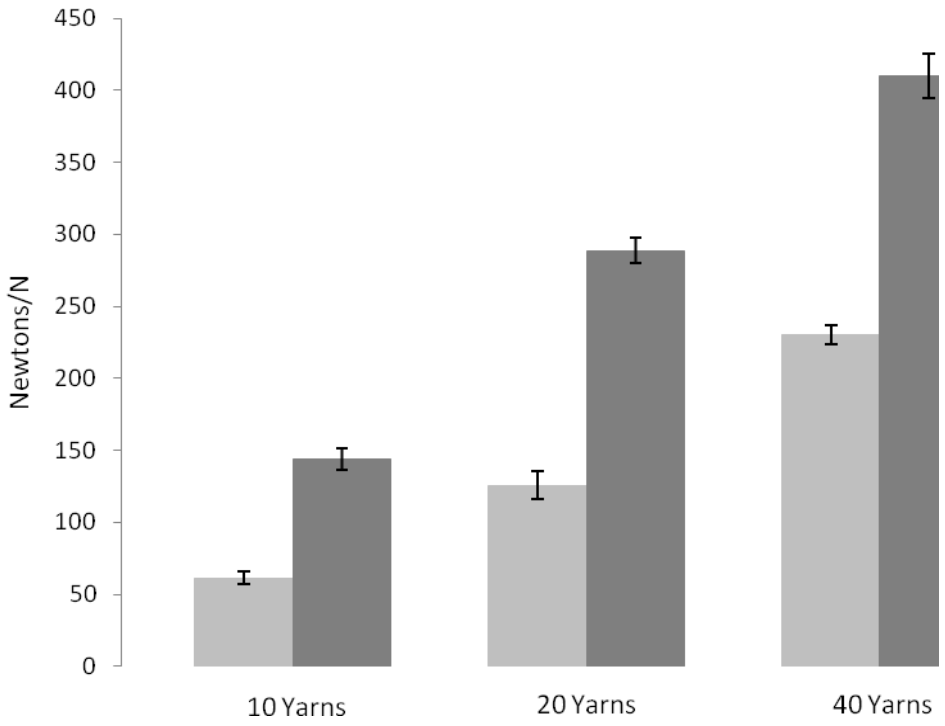

Figure 9.6 Comparison of the tensile strength of the weft yarns (pale grey) vs warp yarns (dark grey), and the proportional strength of textile strips of different widths. Error bars show standard deviations

[I] This sample size was chosen due to the amount of textile available to carry out each set of analyses. In preparing each sample the number of warp yarns were counted to ensure consistency throughout the tensile analyses.

When cutting the textile samples, each “within group” repeat strip was cut adjacent to the next, rather than from the same length (Figure 9.7) This ensured that there were no repeat samples containing the same warp threads, which were the threads of interest in this work [12].

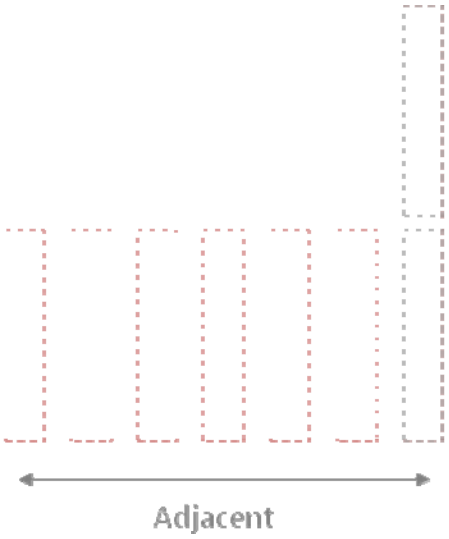

Figure 9.7 Tensile strips cut from adjacent fabric (red) rather than from the same length of fabric (grey)

9.2.2.2 Gauge Length

The gauge length refers to the initial distance apart of the tensile jaws, and is effectively the length of the sample before extension. It is required that this distance is constant to enable comparisons to be made between elongation measurements, but it can also have an effect on the other tensile properties of the material. It can be seen from Figure 9.8 that increasing the gauge length causes a drop in the maximum load at break. This is because a longer sample length will contain a greater number of fibre ends, which are weak spots within a textile material. The larger the gauge length the more representative in relation to a hanging garment. It is clear that there is a significant difference between the gauge lengths of 60mm and 80mm compared the tests carried out at 100mm. However, as was the case when determining the width of the samples, the amount of sample available for testing limited the gauge length of 80mm.

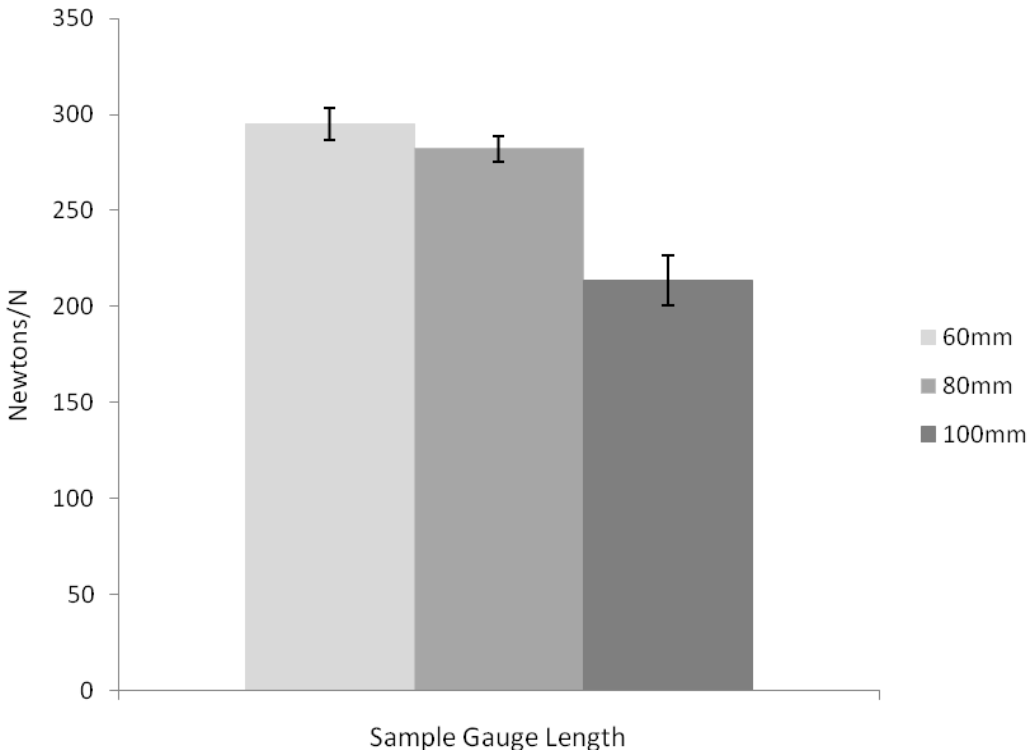

Figure 9.8 Comparison of the tensile strength with different gauge lengths. Error bars show standard deviations

6.2.2.3 Extension rate

To identify the effects of varying the extension rate on the tensile properties, samples measuring 20 yarns wide with a gauge length of 80 mm were subjected to tensile extension at rates of 1, 2, 5, 10 and 20 mm/min. In keeping with the literature [12, 13], it was found that increasing the extension rate caused an increase in the breaking load (Figure 9.9) whilst causing a decrease in extension. The extension rate was set at 10mm/min to enable a compromise between the length of each experiment and for consistency.

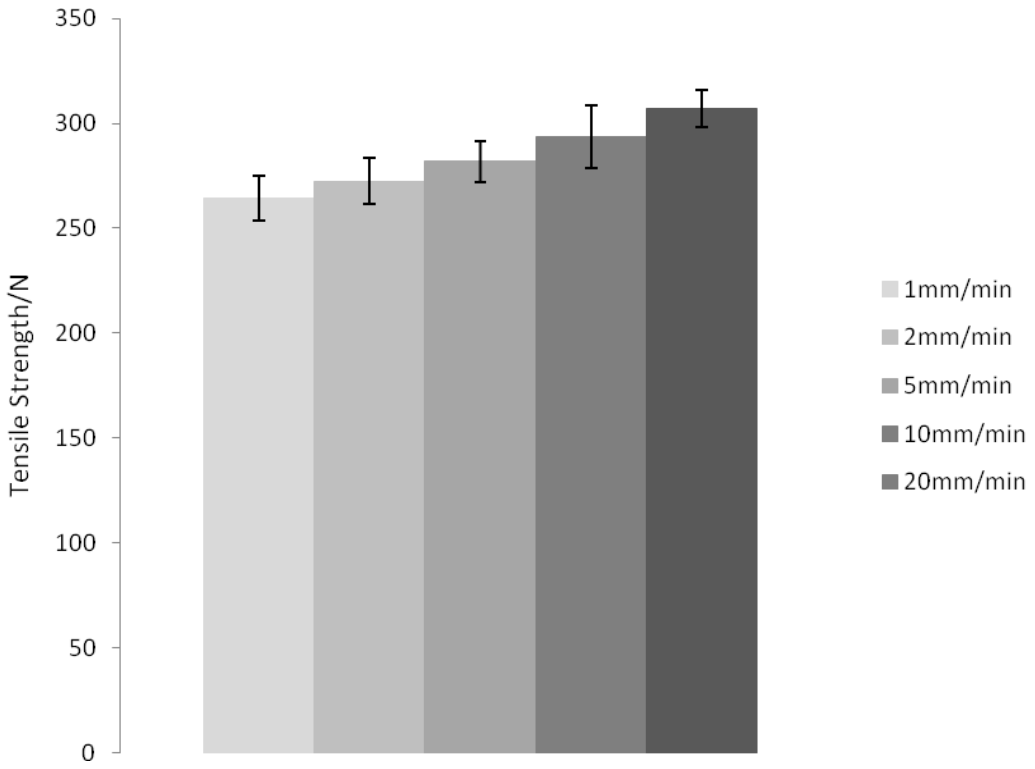

Figure 9.9 Comparison of the tensile strength using different cross head speeds. Error bars show standard deviations

6.2.2.4 Initial Extension and Preload

Due to the weave and yarn twist during the initial part of the tensile test the sample experienced an extension before the yarns experienced a significant load. This "de-slackening" effect has an effect on the initial starting length and impacts on the calculation of the percentage strain. To account for this the initial displacement needed to be calculated and removed from each extension value.

This was done by determining the slope between two low level loads on the Y axis (1.0 and 1.5 N) and extrapolation (Figure 9.10).

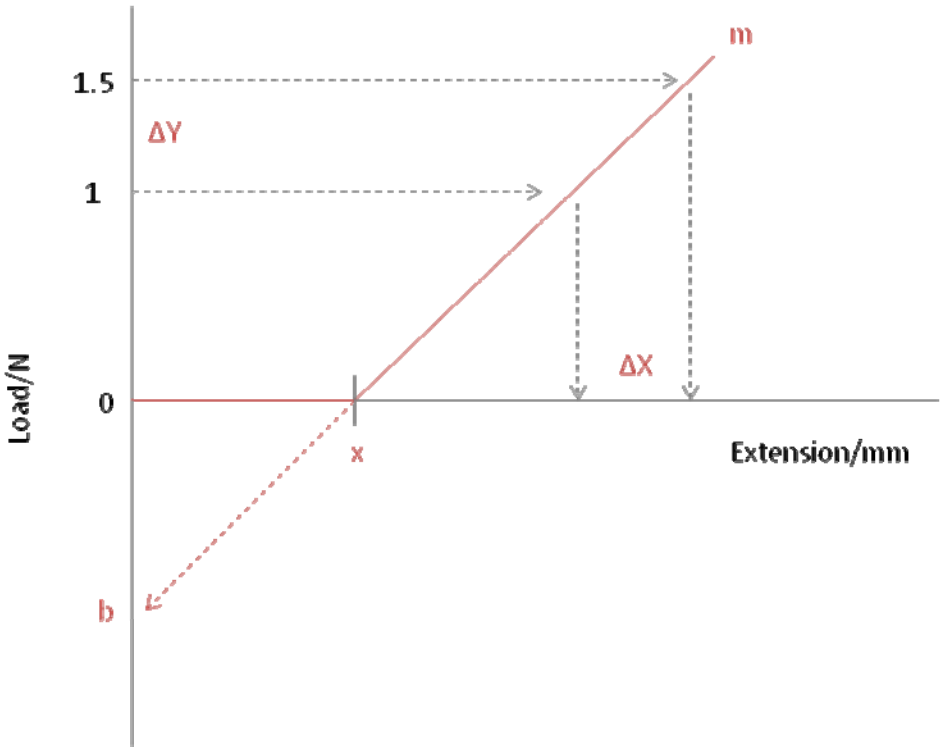

Figure 9.10 Schematic showing a theoretical tensile curve (red) and extrapolation of the slope back to the intercept, illustrating how the initial "de-slackening" was accounted for when determining the percentage strain in the tensile tests

9.2.3 Key Features

There are a number of pieces of information that can be derived from a load extension curve, such as that presented in Figure 9.11.

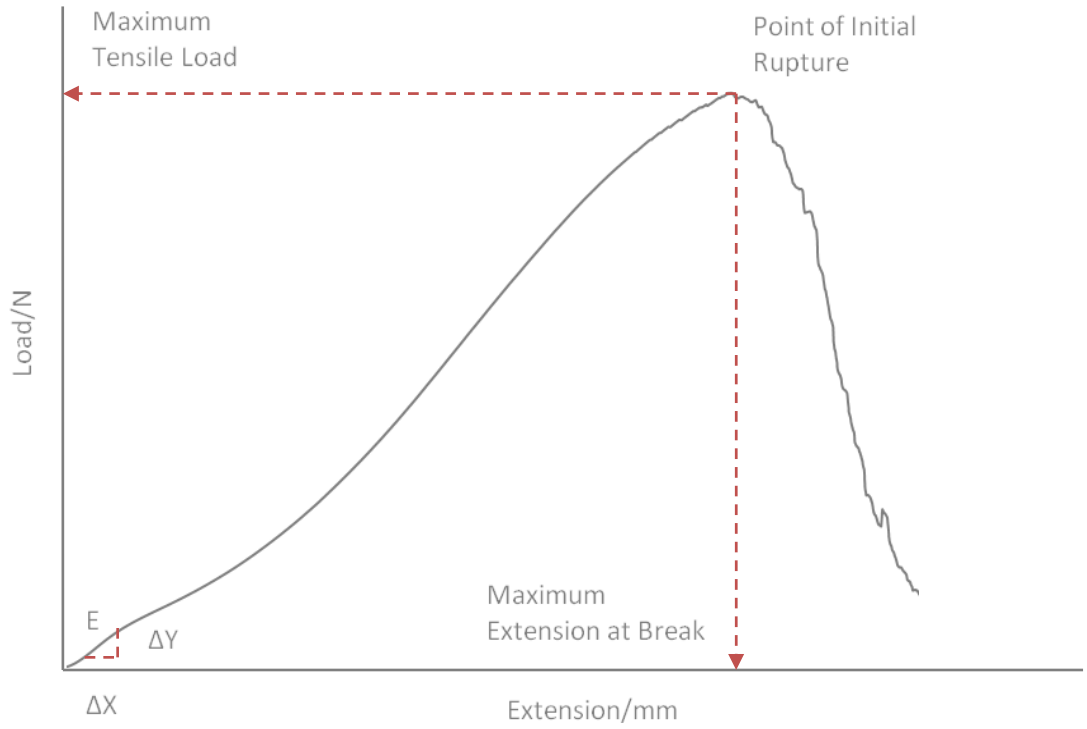

Figure 9.11 Load extension curve of an unaged polyamide 6,6 fabric strip, illustrating some of the key features derived from a tensile test

The initial slope is referred to as the Young's modulus (E) and is determined as:

$$E = \frac{\Delta Y}{\Delta X}$$

Eq. 9.iv

In the work presented here the two X coordinates were nominally taken as 1mm and 3mm, where ΔX = 2.

The tensile strength of a specimen is the maximum tensile load experienced by the sample before it fails, and is measured in Newtons (N). Although the extension of the sample may continue beyond the initial point of rupture as the sample has not fully separated, the tensile strength will be presented as the breaking load.

The elongation of a specimen is the change in length between the start of the test and point of initial rupture. The relationship between initial length and the extension is often expressed as a fraction, giving the engineering strain. Here, strain will be presented as a percentage of the extension with an initial gauge length of 80mm.

9.3 Differential Scanning Calorimetry (DSC)

9.3.1 Experimental Overview

Differential scanning calorimetry (DSC) is one of a number of thermal analysis techniques that can be employed to monitor the thermal transitions discussed previously in Section 5.1 and 5.2, Chapter 5.

DSC was employed in this thesis because it is able to provide information on the glass transition and melting temperature of the polyamide material. DSC provides a measure of the heat flow into the sample as the temperature is raised and lowered, and thus provides information of thermal transitions. Accurately weighed samples are presented into the instrument (Figure 9.12). The difference in heat flow between an empty, control crucible and that of the sample and crucible is determined, normalised by the starting weight.

Figure 9.12 Image of the DSC cell showing the sample cell without cover and the control cell with cover

Two different DSC methods are available. The first is a heat flux DSC, which records the temperature difference between the sample and control crucible as they are both heated at the same rate using one furnace. The temperature difference in the sample is caused by change in heat capacity and enthalpy of the specimen under investigation.

The second type is a power compensated DSC, which monitors the difference in power as the temperature of the sample and the reference are kept the same using different heating furnaces (Figure 9.13). It is the energy difference that is a measure of the change in heat capacity and enthalpy [14]. A power compensated differential scanning calorimeter was used in this work.

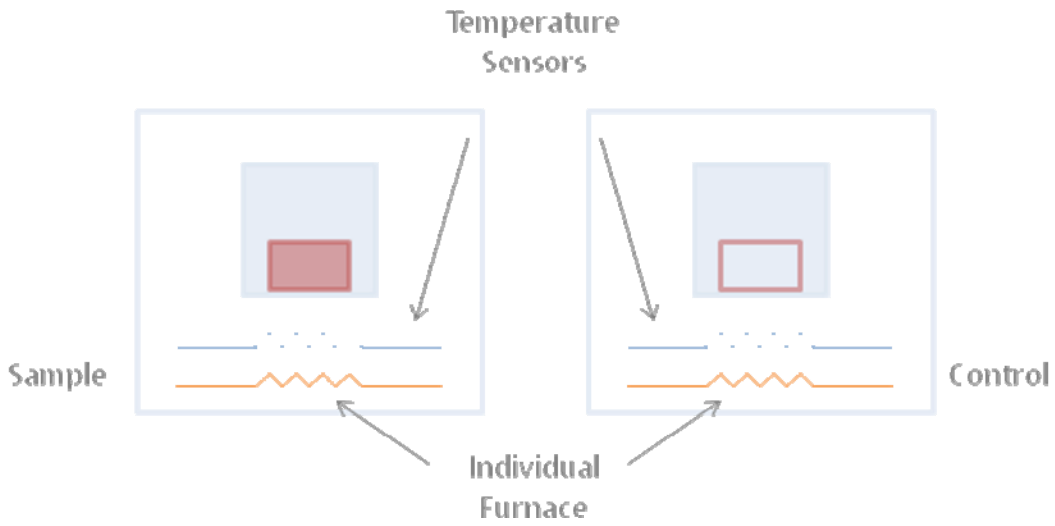

Figure 9.13 Schematic of a power compensated differential scanning calorimetry sample cell [14]

9.3.2 Experimental Methodology

Differential scanning calorimetry was carried out using a Perkin Elmer Power Compensated Pyris 1 DSC controlled using Pyris software and coupled with a Perkin Elmer CCA7 temperature controller.

The cell and furnace was purged with oxygen free nitrogen line at a flow rate of 30ml/min, and the samples heated from -35°C to 300°C at a rate of 20°C per minute. Liquid nitrogen was used to reduce the sample cell to sub-zero temperatures.

As is the case with all analyses, it is advantageous to carry out replicate analyses in order to determine the significance of any results. Due to limitations of access, it was not possible to run repeat analyses. This means that quoted temperature values are given with caution. However, all data presented result from DSC analyses carried out on a single day, thus minimising the variations between samples.

9.3.2.1 Determination of the Baseline

The initial step in DSC is to determine a baseline of the instrument, also known as a zero line. This is used as a background curve and is subtracted from all subsequent sample heating curves [14].

An empty crucible was put into the sample cell, whist the empty control crucible was placed in the control cell. The DSC was taken down to -30°C and the heating run started at a rate of 20°C/min. The resulting heating curve (Figure 9.14) was then subtracted from all sample heating curves presented.

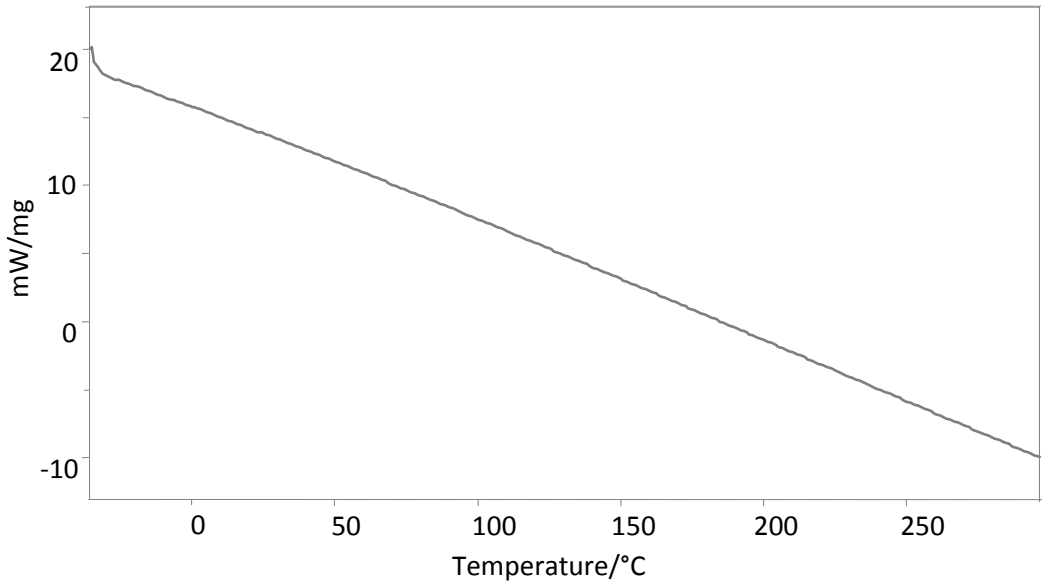

Figure 9.14 DSC baseline curve

9.3.2.2 Sample Preparation

The fabric samples were prepared in rectangular pieces measuring 7x7 yarns each, in order to reduce the amount of variability in contact between the sample and crucible, causing inhomogeneous heat transfer.

The copper crucible was accurately weighed three times, with and without the sample, using a Sartorius microbalance. The average weight of the sample, minus that of the empty crucible, input into the DSC software for normalisation. This ensures that each heating curve is normalised by the software to account for variations in weight, giving a Y axis of mW/mg. Samples averaged an approximate mass of 2mg.

9.3.2.3 Sample Heating Run

Once the sample was prepared and the weight input into the software, the crucible was placed into the sample cell; and the reference crucible put in place in the control cell. The DSC cell was then taken down to -35°C using liquid nitrogen and then heated to 300°C at a rate of 20°C/min. The baseline curve was then subtracted from the resulting sample heating curve.

9.3.3 Key Features

Figure 9.15 illustrates the key thermal features that may be present during the heating run of polyamide 6,6 using DSC.

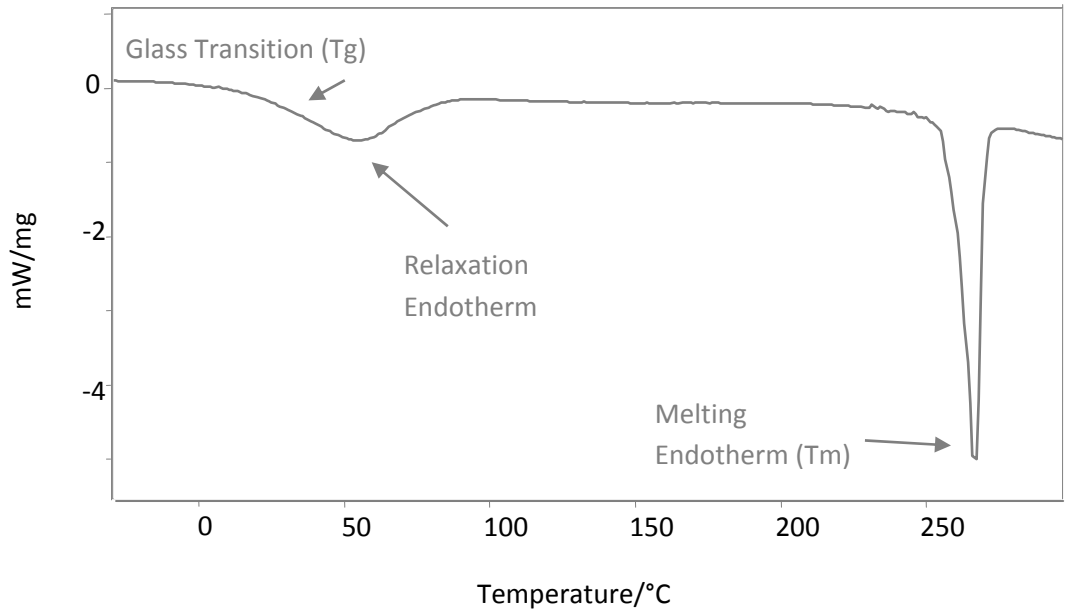

Figure 9.15 DSC heating curve for a polyamide 6,6 sample, illustrating some of the key thermal features

9.3.3.1 Glass Transition Temperature

Due to the fact that the glass transition temperature does not occur at a single point, it can be interpreted in various ways. In the work presented here, any values for Tg quoted refer to the mid-point of the transition. That is, the temperature at which one half of the change in the heat capacity has occurred (ΔCp).

Determination of the mid-point was made by calculating the second derivative of the heating curves. This readily highlighted the change in the tangent and therefore the point

at which the curve passes though zero. The second derivative was calculated using the Norris gap function, as described in Section 2.3.2, Chapter 2, with a gap of 19.
As will be discussed in Section 10.2.1, Chapter 10, the determination of the glass transition mid-point was influenced by the presence of a relaxation endotherm. This endotherm occurs when internal stresses remain in oriented fibres as a result of processing.

9.3.3.2 Melting Endotherm and the Calculation of the Fractional Crystallinity
In addition to the determination of the glass transition temperature, the heating curves also provide information on the crystallinity of the samples. Assuming a two phase morphology, the percent crystallinity can be determined by the heat of melting:

$$\% \text{ Crystallinity} = \frac{[\Delta Hm]}{\Delta Hm^{\circ}} \times 100$$

Eq. 9.v

Where ΔHm° is the heat of melting of a 100% crystalline reference of the same material, and ΔHm refers to the sample of interest, in J/g. The literature values for the heat of fusion of a 100% crystalline polyamide 6,6 differ widely, from anywhere between 191 J/g [15] to 255 J/g [16]. For the work presented here the value was taken as 196 J/g, as is quoted in the Polymer Handbook by Brandrup *et al* [17].

ΔHm was determined by integration of the area under the Tm curve. This was carried out using the integration function in Grams AI software and drawing a linear baseline from 240-275°C. In order to calculate the heat of melting for each sample the area under the curve needed converting from W into J/s. This was done by converting the temperature scale to a time scale to determine the amount of energy per second.

$$\text{Measured Area (Tm)} = \text{Temperature Range} \times W$$

Eq. 9.vi

Where the temperature range is given as:

$$\text{Temperature Range} = \text{Heating Rate} \times \text{Time}$$

Eq. 9.vii

Therefore:

$$\text{Measured Area (Tm)} = \text{Heating Rate} \times \text{Time} \times W$$

Eq. 9.viii

$$\text{Measured Area (Tm)} = \text{Heating Rate} \times \text{Time} \times \frac{J}{\text{Time}}$$

Eq. 9.ix

$$\text{Measured Area (Tm)} = \text{Heating Rate} \times J$$

Eq. 9.x

$$\frac{\text{Measured Area (Tm)}}{\text{Heating Rate}} = J$$

Eq. 9.xi

The heating rate was 20°C per minute, which equates to 0.33°C per second. Therefore, all of the measured areas under the melting endotherm were divided by 0.33 to give energy in terms of J/g. This value was then used to calculate the crystalline fraction using Eq. 9.v.

9.4 Creep Experiments using a Dynamic Mechanical Thermal Analyser (DMTA)

9.4.1 Experimental Overview

Dynamic Mechanical Thermal Analysis (DMTA) was employed to monitor the creep and creep recovery behaviour of the samples at isothermal temperatures with a static load. During a creep experiment a stress is applied to the sample and held constant, whilst the resultant deformation is measured as a function of time at a given temperature. After a specified time the load is removed and recovery, or reversal, of the displacement is measured.

9.4.1.1 Choice of Static Load

In order to test the creep and recovery stability of the polyamide textile at raised and lowered temperatures, a static load needed to be applied to the test samples. An approximation was made that represented the maximum load likely to be experienced by a heavily beaded garment. It was calculated that a one metre length of fabric measuring 10

yarns wide (test strip size) could accommodate 250 evenly spaced glass beads. With each bead weighing 0.15g, this gave a total mass of 37.5g.

As this mass would be acting on the textile in a vertical state, this weight needed to be converted to units of force. The mass of 1kg in a vacuum falls freely at a rate of acceleration of 9.8m/s^2, and the force acting on the mass is 9.8N, so for a mass of 37.5g the force is given by:

$$\frac{37.5}{1000} \times 9.8 = 0.38N$$

Eq. 9.xii

Giving a value of 0.38N for the force experienced by the uppermost fibres of a metre length textile. For simplicity, it was decided to round the load up to 0.5N.

At this point it is necessary to state that the creep experiments do not take into account additional factors, such as friction, which may be experienced when garments are draped over a manikin. These additional forces are not thought to contribute a significant amount to the total loading and will not be covered in this research.

9.4.2 Experimental Methodology

The creep analyses were carried out using a TA Instruments DMA Q800 analyser fitted with a film tension clamp [II] and purged with compressed air (Figure 9.16). The instrument was controlled using the TA Instruments QAdvantage Software.

[II] All creep experiments were carried out using the DMTA at the Department of Physics, University of Surrey.

Figure 9.16 Image of the TA Instruments DMA Q800 analyser fitted with a film tension clamp

The initial intention of this work was to mimic the procedure of raising and lowering the temperature whilst the static load remained in place, as would be the case during pest control treatments. However, because the technique is isothermal, a trial run showed that it was not possible to bring the sample back to room temperature whilst maintaining the applied load. Therefore, a standard creep/recovery method was adopted.

9.4.2.1 Determination of the Applied Stress

The applied stress, in MPa, required calculating to take into account the cross sectional area of the sample held in the tension clamps. It was important to determine the cross sectional area of the warp yarns to ensure the correct stress was applied. If the textile strip had been treated as a film, then the total area would have been too great, and the calculated force would have been too low. With this in mind the individual yarns were accounted for to ensure the correct stress was applied. The average diameter of a yarn was found to be 0.456mm ±0.03, measured using a Zeiss Axiolab Pol Microscope with a x20

objective and using Image-Pro Plus version 5.0 software, and averaging the values for six yarns.

$$\text{Cross Sectional Area of Yarn} = \frac{\pi (0.456 \times 10^{-3})^2}{4}$$

Eq. 9.xiii

The stress is force divided by the cross sectional area of each yarn, so for a total of 10 yarns:

$$\text{Stress} = \frac{\text{Total Load Applied}}{\text{Total Area of Yarns}}$$

$$\text{Stress} = \frac{(0.5 \times 4)}{10 \times \pi \ (0.456 \times 10^{-3})^2} = 0.31 \ \pm 0.02 \ \text{MPa}$$

Eq. 9.xiv

9.4.2.2 Temperature and Stress Profile

A sample measuring 10 yarns wide was introduced into the sample cell and attached to the tension clamps with a gauge length in the region of 16mm[III] (Figure 9.17). A preload of 0.001N was applied to the sample to ensure the sample was fully elongated in the clamp, thus allowing for changes in length to be monitored.

[III] The initial gauge length varied when the lower section of the sample was clamped into place. Once the clamp was in place the instrument then determined the actual gauge length with the software subsequently accounting for this during the calculation of the percentage strain.

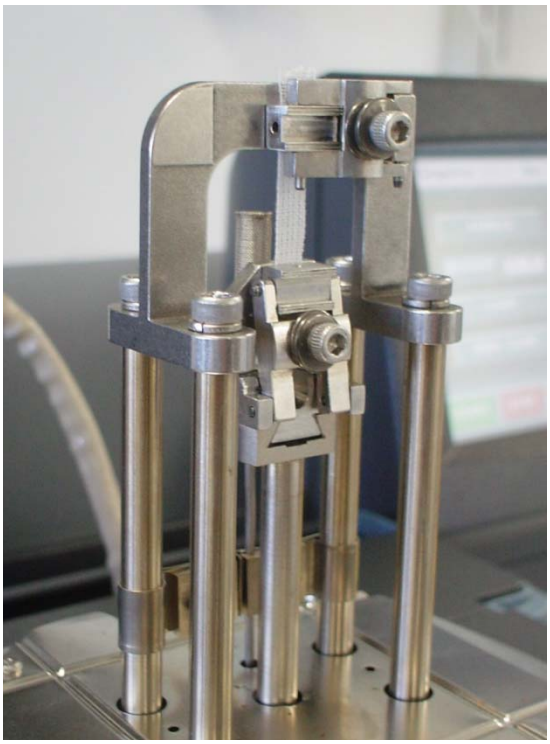

Figure 9.17 Image of a sample held between the DMTA film tension clamps

The sample was placed in the tension clamp, and subjected to the small preload. The DMTA cell was then taken to the temperature of interest and allowed to equilibrate for 5 minutes before the programmed stress was applied. Due to limited access to the equipment it was not possible to run the experiments for the same length of time as the thermal pest control treatments. Thus, the samples remained subject to the applied load for 150 minutes and were then allowed to relax for 300 minutes on removal of the load. Isothermal conditions were maintained throughout the experiment.

During these experiments it was not possible to control the relative humidity as the temperature was altered. This is one of the limitations of these creep experiments on polyamide material. The raised temperature process employed by Thermo Lignum®, and discussed fully in Section 8.3.1, Chapter 8, maintains a constant RH within the treatment chamber as the temperature is increased. This is to prevent dimensional changes caused by the loss or gain of moisture. Therefore, any discussion relating to the creep experiments needs to consider the additional role that moisture may play in the material's behaviour, which may or may not be present in the pest control treatments.

9.4.3 Key Features

There are a number of pieces of information that can be derived from creep experiments carried out using a DMTA, but focus here will be given to the time dependant strain behaviour presented as a creep/recovery curve (Figure 9.18).

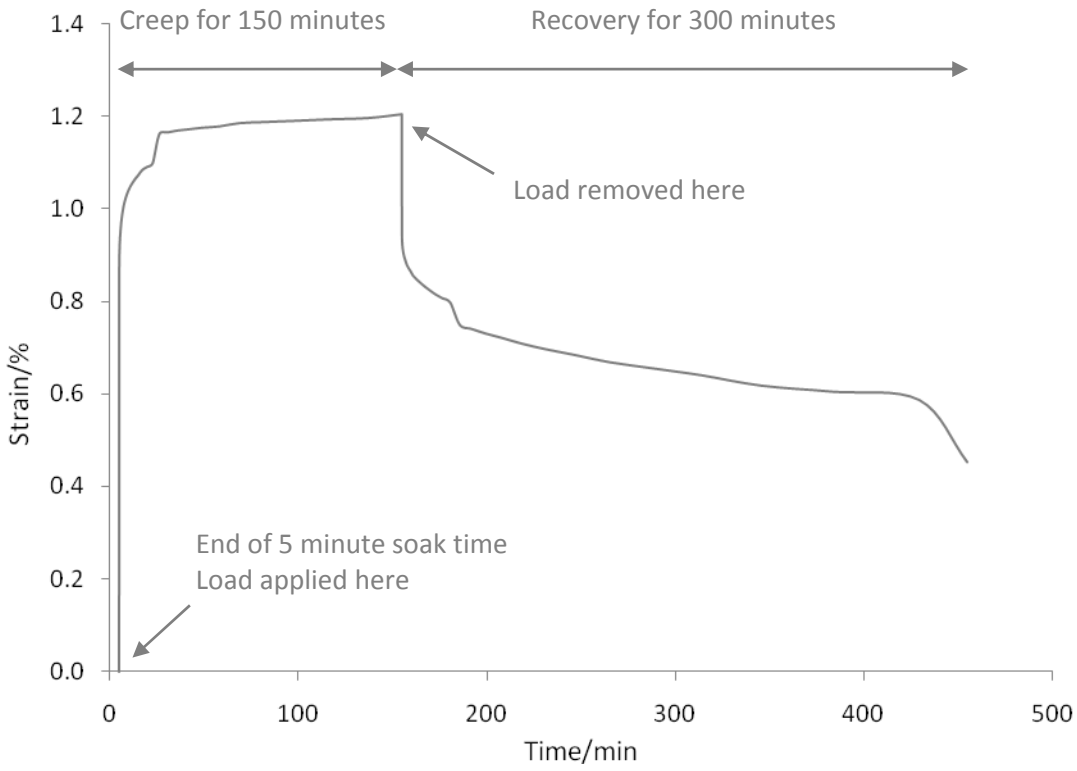

Figure 9.18 DTMA creep/recovery curve for a polyamide 6,6 sample, illustrating some of the key temperature features

During the first five minutes of the experiment the sample chamber equilibrates at temperature, after which time the load is applied and the sample undergoes an instantaneous displacement, or positive strain. As will be shown in the following chapters, the creep section of the curve may exhibit different behaviours. After 150 minutes the load is removed, and the sample will reverse the instantaneous displacement, seen as a rapid negative strain. During the remainder of the recovery time (300 minutes) the creep behaviour will be reversed to a greater or lesser extent, depending on the (partial) elastic recovery of the sample. The test ends at 455minutes when the sample is brought back to ambient temperatures.

9.5 *in situ* Loaded Samples

In addition to the creep sample analyses carried out using the DMTA, a set of samples were also subject to a load and treated *in situ* within the Thermo Lignum® chamber (Figure 9.19), in a freezer and at room temperature (control). This was carried out to monitor how loaded material behaved during the real treatments, and allowed comparisons to be made between the loaded and unloaded samples.

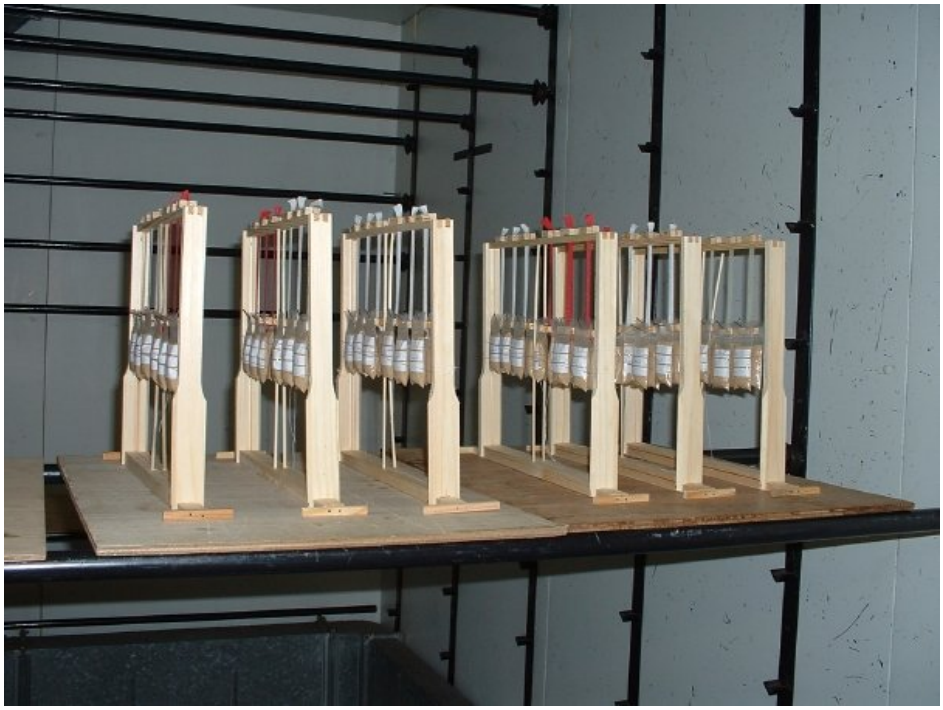

Figure 9.19 Image of the *in situ* loaded samples hanging from wooden frames before treatment in the Thermo Lignum® chamber

Textile strips measuring 20 yarns wide were suspended from wooden frames and a load of 50g applied directly to the bottom of each sample (Figure 9.20).

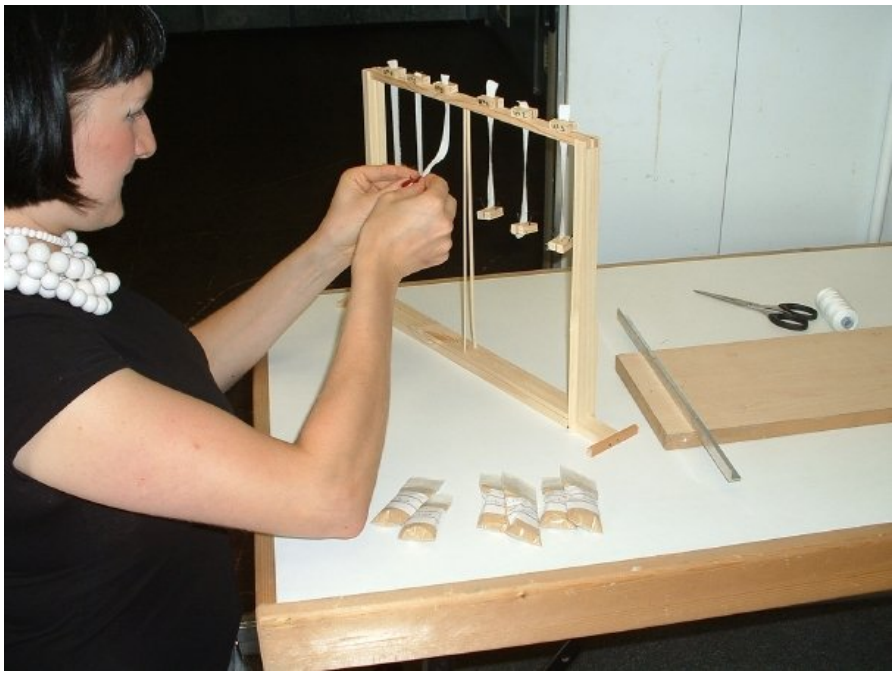

Figure 9.20 Image of samples being suspended from the wooden frames, before the sand bags were attached to the bottom

In order to suspend the textile from the frame, and attach the load onto the sample, small blocks of wood were adhered to either end of the strips (Figure 9.21 and 9.22). The upper pieces were supported between two wooden struts enabling the samples to hang freely. A nail was hammered into both sides of the lower blocks, from which two sandbags weighing 25g each were suspended.

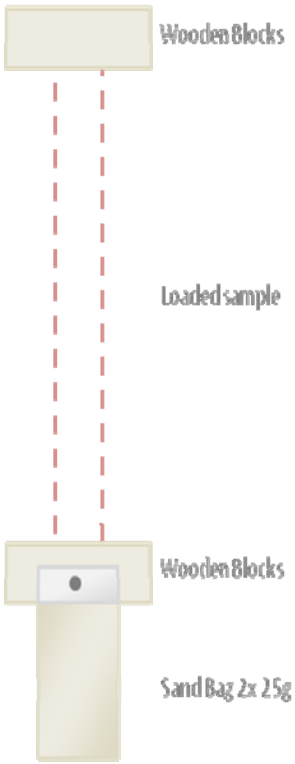

Figure 9.21 Schematic of the upper and lower blocks adhered to the sample, with a sandbag suspended from a lower nail

Figure 9.22 Image of six *in situ* loaded samples suspended from a wooden frame with the sandbags in place

One of the initial intension had been to monitor the displacement in the samples by taking digital images before and after treatment, keeping a camera at a set distance and focal length. However, during trials it became apparent that the pixel resolution on the resulting image was not sufficient to enable small dimensional changes to be monitored. Thus the displacement *in situ* could not be monitored. Nonetheless, the loaded samples could provide useful information on the behaviour of these samples under the said conditions by carrying out subsequent analyses to monitor permanent chemical or physical changes.

9.5 References

1. Skoog, D.A., F.J. Holler, and T.A. Nieman, *Principles of Instrumental Analysis*. 5th ed. 1998: Thompson Learning Inc. .
2. Harrick, N.J., *Internal Reflection Spectroscopy*. 1967, New York: John Wiley & Sons, Inc.
3. Gunzler, H. and H.U. Gremlich, *IR Spectroscopy: An Introduction*. 2002, Weinheim: Wiley-VCH.
4. Garside, P., *Investigations of Analytical Techniques for the Characterisation of Natural Textile Fibres Towards Informed Conservation*, in *Department of Chemistry*. 2002, University of Southampton: Southampton.
5. Garside, P., S. Lahlil, and P. Wyeth, *Characterisation of Historic Silk by Polarised ATR FT-IR Spectroscopy for Informed Conservation.* Applied Spectroscopy, 2005. **59**(10): p. 1242-1247.
6. Garside, P. and P. Wyeth, *Identification of Cellulosic Fibres by FTIR Spectroscopy: Thread and Single Fibre Analysis by Attenuated Total Reflectance.* Studies in Conservation, 2003. **48**(3): p. 269-275.
7. Vasanthan, N. and D.R. Salem, *Structural Characterisation of Heat Set and Drawn Polyamide 66 Fibres by FTIR Spectroscopy.* Materials Research and Innovation, 2001. **4**: p. 155-160.
8. Vasanthan, N., S.B. Ruetsch, and D.R. Salem, *Structure Development of Polyamide-66 Fibres During Drawing and Their Microstructure Characterization.* Journal of Polymer Science Part B: Polymer Physics, 2002. **40**: p. 1940-1948.
9. Goncalves, E.S., L. Poulsen, and P.R. Ogilby, *Mechanism of the Temperature-dependent degradation of Polyamide 66 Films Exposed to Water.* Polymer Degradation and Stability, 2007. **92**: p. 1977-1985.
10. Institute, B.S., *Textiles - Tensile Properties of Fabrics Part I: Determination of Maximum Force and Elongation at Maximum Force Using the Strip Method.* British Standards Institution, 1999. **BS EN ISO 13934-1:1999**.
11. Institute, B.S., *Textiles - Standard Atmospheres for Conditioning and Testing* British Standards Institute, 1992. **BS EN 20139:1992 ISO 139:1973**.
12. Saville, B.P., *Physical Testing of Textiles*. 2000, Cambridge: Woodhead Publishing Ltd.
13. Marcellan, A., et al., *A Multi-scale Analysis of the Microstructure and the Tensile Mechanical Behaviour of Polyamide 66 Fibre.* Polymer, 2006. **47**: p. 367-378.
14. Hohne, G., W. Hemminger, and H.-J. Flammersheim, *Differential Scanning Calorimetry: An Introduction for Practitioners*. 1996, Heidelberg: Springer-Verlag.

15. Simal, A.L. and A.R. Martin, *Structure of Heat-Treated Nylon 6 and 6.6 Fibres I: The Shrinkage Mechanism.* Journal of Applied Polymer Science, 1998. **68**: p. 441-452.
16. Sinha, M.K., *An Investigation of Photodegradation of a Support Netting Used in the Conservation of Historic Textiles* 2006, Heriott-Watt: Edinburgh.
17. Brandrup, J., E.H. Immergut, and E.A. Grulke, *Polymer Handbook*. 4th ed. Vol. 1. 1999, New York: Wiley.

Chapter 10: Unloaded and Loaded Control Samples

As set out in the preceding chapters, the treatment of synthetic polyamides by raised and lowered temperatures is of concern to the conservation profession. The alterations in the physical properties at the two temperature ranges of interest warrant further investigation. Although the thermal behaviour of polyamides is well documented, the literature is primarily focused on engineering polymers and the working properties of new material. However, in the case of heritage objects, the condition of an object is often in a state of deterioration. In addition, many of these materials have intrinsic or historical value, which means longevity is key. Therefore, any preventative or interventive conservation treatments should avoid exacerbating degradative processes.

It is for these reasons that the effects of raised and lowered temperature pest control treatments have been investigated, with the results of this work being presented in the following two chapters. Vibrational spectroscopy, thermal analysis and mechanical testing have been employed to investigate the possible chemical and physical alterations in a polyamide 6,6 fabric subject to these treatments.

The first half of this Chapter will focus on the characterisation of the control polyamide 6,6, before and after artificial ageing. This will provide an understanding of the starting material, enabling subsequent interpretation of the materials behaviour following exposure to pest control measures. In the latter half of the Chapter results will be presented relating to the control material after the application of a load. As outlined in previous chapters, the effect of thermal treatments whilst a textile is hanging under its own weight will be investigated. To enable this assessment, the control samples were subject to *in situ* loading and creep/recovery loading using DMTA. In this section the results and discussion will be presented for the tests carried out at ambient temperatures, providing a baseline from which to compare the later treatments presented in the following chapter.

10.1 Unloaded Control Samples

The following section contains the results and discussion relating to the control polyamide material, before and after artificial ageing. The specimens investigated were the unaged and artificially aged undyed, treated and dyed polyamide 6,6 fabrics discussed in Chapter 8. The table below presents the assignments given to the different ageing regimes.

Sample	Sample Treatment
Con Au	Unaged, Undyed
Con At	Unaged, Treated
Con Ad	Unaged, Dyed
Con Bu	UV Aged, Undyed
Con Bt	UV Aged, Treated
Con Bd	UV Aged, Dyed
Con Cu	UV + Heat Aged, Undyed
Con Ct	UV + Heat Aged, Treated
Con Cd	UV + Heat Aged, Dyed

Table 10.1 Control sample assignments and their corresponding treatments

10.1.1 Unloaded Control Sample Results and Discussion

10.1.1.1 Tensile properties

Figure 10.1 shows the seven repeat tensile tests carried out on undyed, unaged polyamide (Con Au), illustrating the consistent behaviour of the material. The remainder of the tensile data presented relate to the average of seven repeat tensile tests, and will be accompanied by their standard deviations. Where samples broke close to the jaw of the mechanical tester, these data were discarded.

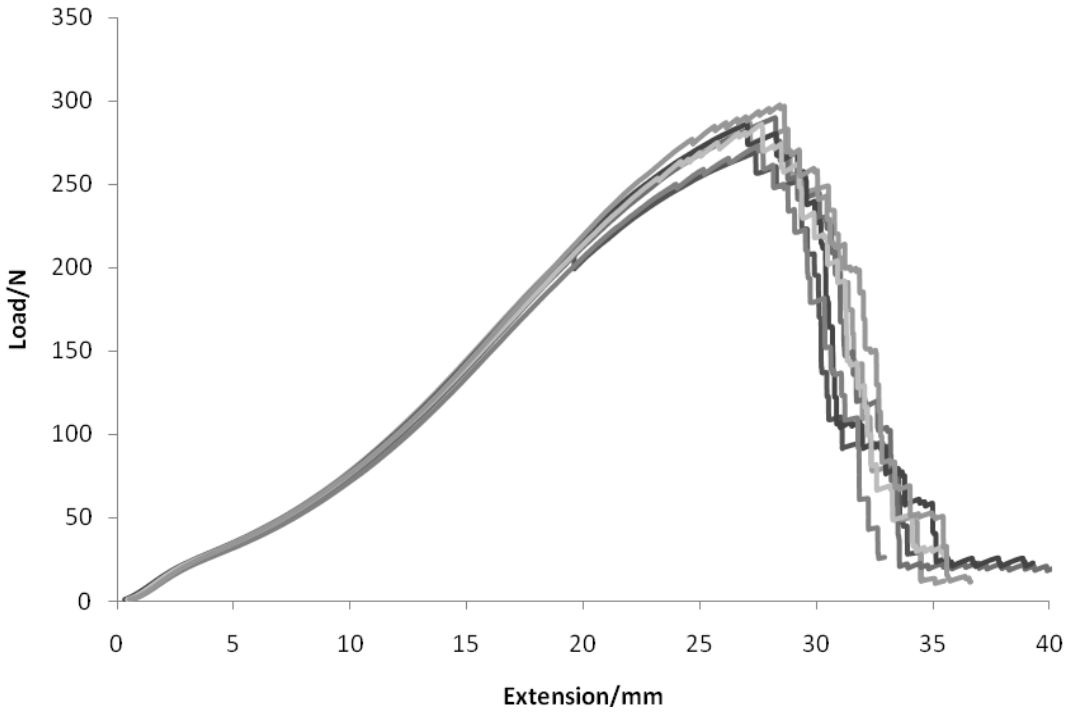

Figure 10.1 Seven tensile repeat tests on Con Au illustrating the consistent behaviour of the samples

Sample	Breaking Load/N	Strain/%	Energy at Maximum Load/J	Young's Modulus
Con Au	286.7 ±7.8	34.6 ±0.7	3.7 ±0.2	8.3±0.2
Con At	291.2 ±11.3	42.8 ±1.8	4.3 ±0.4	3.7±0.4
Con Ad	289.9 ±10.5	43.2 ±1.4	4.3 ±0.4	3.8±0.2
Con Bu	184.9 ±11.6	23.0 ±0.7	1.4 ±0.1	8.9±0.2
Con Bt	209.0 ±9.6	30.7 ±1.2	1.9 ±0.2	3.7±0.1
Con Bd	168.4 ±4.4	26.2 ±0.4	1.3 ±0.1	4.4±0.2
Con Cu	144.1 ±3.8	19.5 ±0.6	1.0 ±0	7.6±0.1
Con Ct	177.8 ±14.4	27.6 ±1.4	1.5 ±0.2	4.0±0.2
Con Cd	153.5 ±6.3	23.4 ±0.2	1.1 ±0.1	5.2±0.3

Table 10.2 Tensile properties of control samples (averages of up to 7 replicates)

Figure 10.2 show the breaking loads for each of the various control samples. Within the experimental error, there is no difference in strength amongst the Con A set. There has been a significant decrease in strength, up to 50%, for all Con B and Con C samples, with Con C showing the greatest deterioration. The effect of pre-treatment seems to be to

reduce the proportional loss in breaking strength (Con Bt and Con Ct), whilst prior processing with the dye re-establishes the drop in performance (Con Bd and Con Cd).

The same general trends are seen in the strain data, with ageing affecting a distinct drop in this measure of performance (Figure 10.3). In contrast to the tenacity, prior processing appears to increase the extension significantly, by around 40% (Con At and Ad), although the trends amongst the aged sets are very similar.

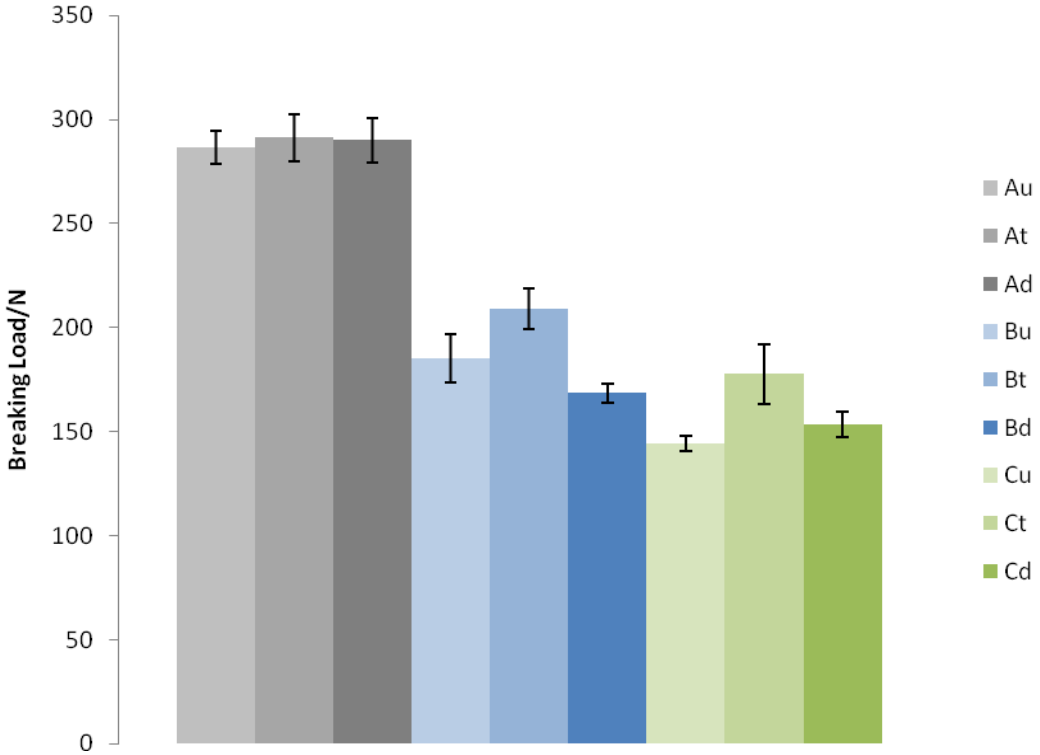

Figure 10.2 Breaking loads for the control samples. Error bars show standard deviations

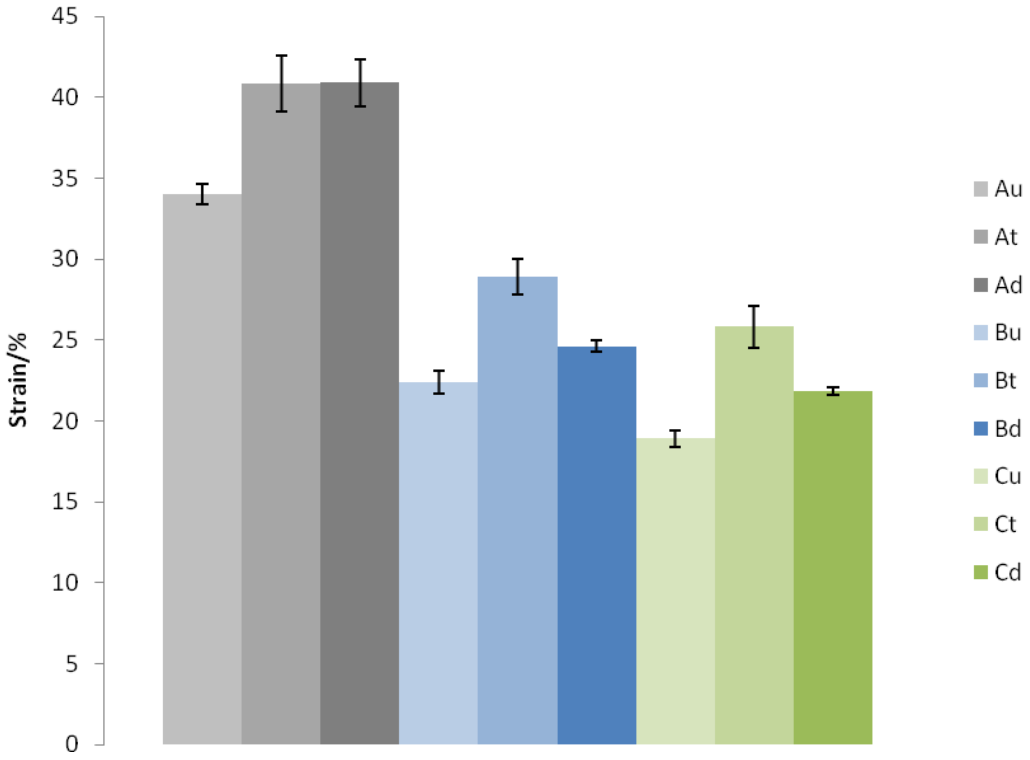

Figure 10.3 Percentage strain for the control samples. Error bars show standard deviations

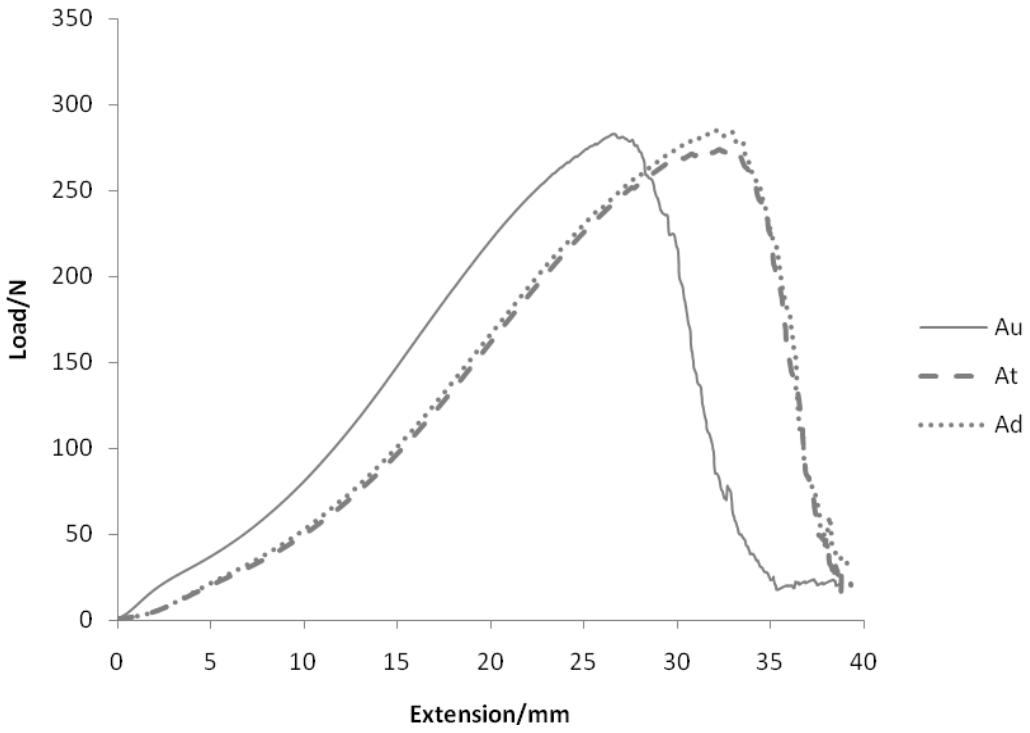

Figure 10.4 Averaged Force vs Elongation Curve for Con A specimens, resulting from the average of seven repeat measurements for Con Au, At and Ad (Gauge length of 80mm)

Figure 10.4 shows the averaged force elongation curves for the Con A samples, undyed, treated and dyed. The tensile curves follow the same characteristic shape to those presented by Marchellan *et al* [1], in their study of the tensile behaviour of polyamide 6,6 fibres. In their work, looking into the micromechanisms of deformation, they suggest that at small levels of extension (the equivalent of 0-3mm for the current specimens) the isotropic amorphous regions become extended and start to align along the polymer axis. The behaviour at this point is almost linear with respect to force and elongation, as the unbound chains begin to be drawn. The crystalline regions remain unloaded at this point [2]. The modulus of the treated and dyed samples are lower than for the undyed samples. This behaviour corresponds with the increased percentage strain of these two samples (Table 10.2).

In the region between 6 -19% strain (5-15mm, Figure 10.4), the ease of movement drops off a little, but there is still increased mobility as the oriented amorphous regions are brought closer together and begin to become aligned, in a pseudo crystalline manner.

At loads above about 75N (Figure 10.4) the crystalline domains begin to take the applied stress as the carbon-carbon bonds begin to extend. This is seen as an increase in the hardening rate as the load is increased, caused by the mobility restrictions imparted by the inter-molecular bonding. The final stage of deformation is seen at an extension in the region of 23mm, where the crystal chains slide past each other until rupture.

Con B specimens show a different behaviour to the unaged textile (Figure 10.5). In the first section of the curve it is still possible to see the extension of the isotropic amorphous regions and the modulus is not significantly different (Table 10.2). The curves differ towards the point of rupture, where the sample breaks before deformation of the crystalline regions can occur. This may suggest that the effect of UV ageing has introduced internal restrictions into the system, in the form of cross-links, preventing the ordered regions of the polymer from moving freely [3].

Con Bt and Con Bd follow the same path, but the treated sample is somewhat more ductile than the dyed sample. This suggests that the additives may have acted as UV stabilisers and prevented some deterioration.

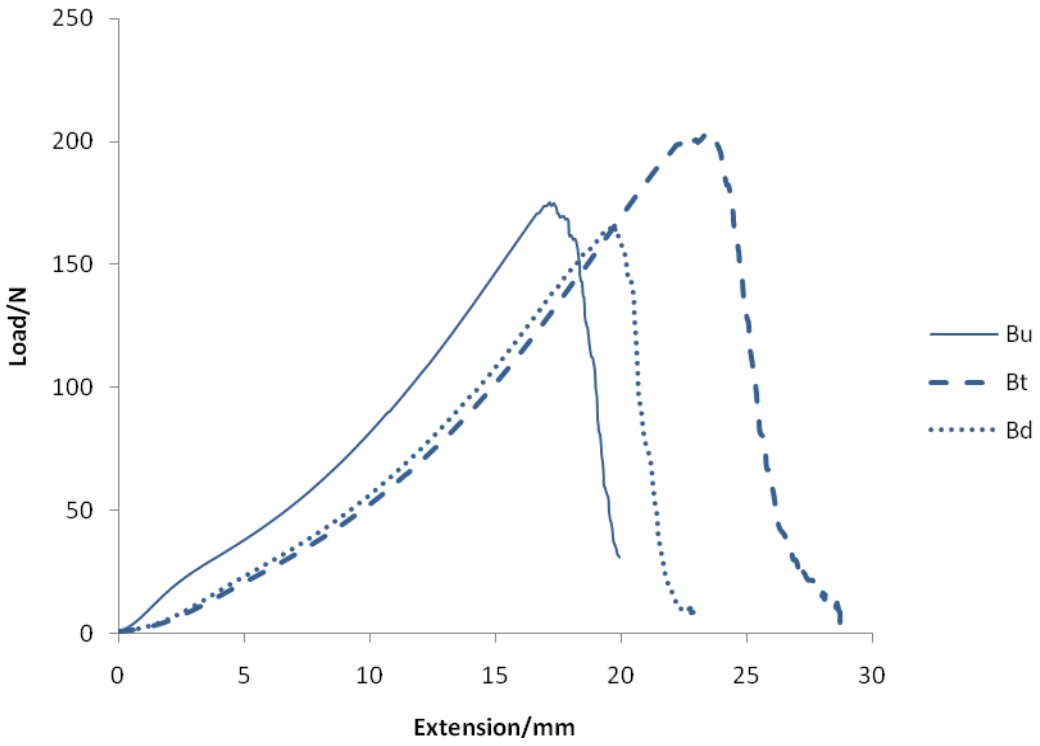

Figure 10.5 Averaged Force vs Elongation Curve for Con B, resulting from the average of six repeat measurements for Con Bu, and seven repeat measurements for Con Bt and Bd (Gauge length of 80mm)

Similar behaviour is seen in the Con C samples (Figure 10.6). The steep shape towards the end of the curve suggests that the extended C-C chains are taking the applied stress and that the crystals are resticted from slipping past each other, resulting in a brittle material. The energy requried to break the samples is approximatly one third of that required for the unaged material (Table 10.2). Again, the undyed material is showing a less ductile behaviour than the treated and dyed samples.

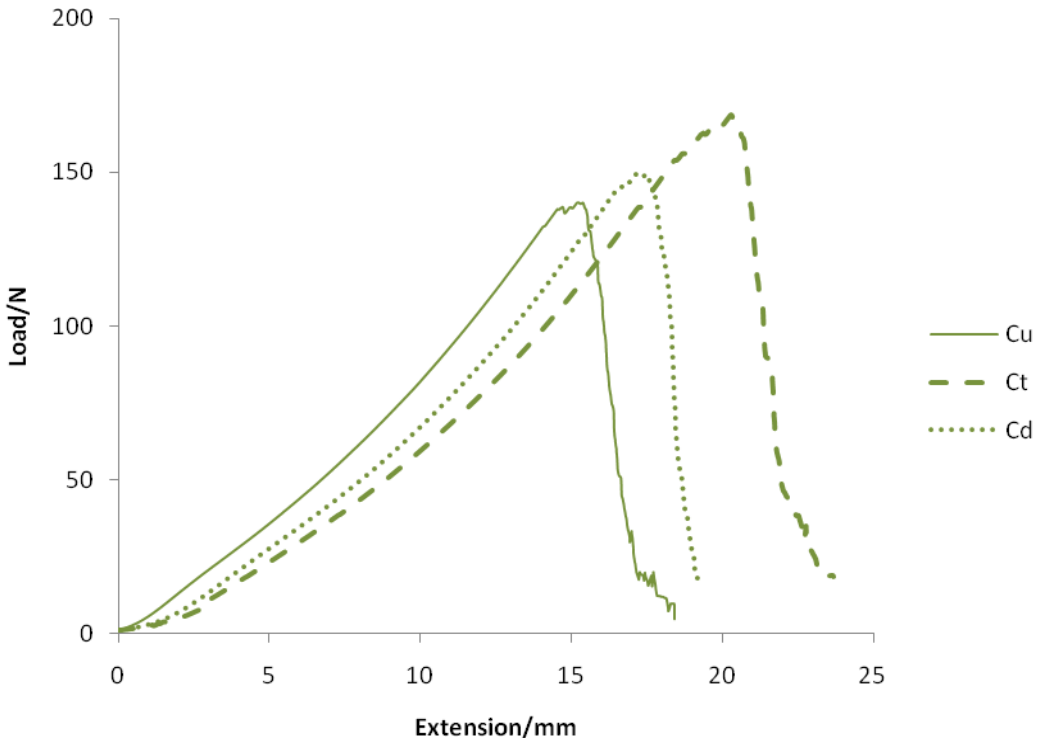

Figure 10.6 Averaged Force vs Elongation Curve for Con C, resulting from the average of seven repeat measurements for Con Cu, Ct and Cd (Gauge length of 80mm)

10.1.1.2 Polymer Ordering as Determined by Polarized FTIR-ATR

Figure 10.7 below shows the FTIR-ATR spectrum of the as received material, Con Au. Characteristic polyamide band assignments are given in Table 10.3.

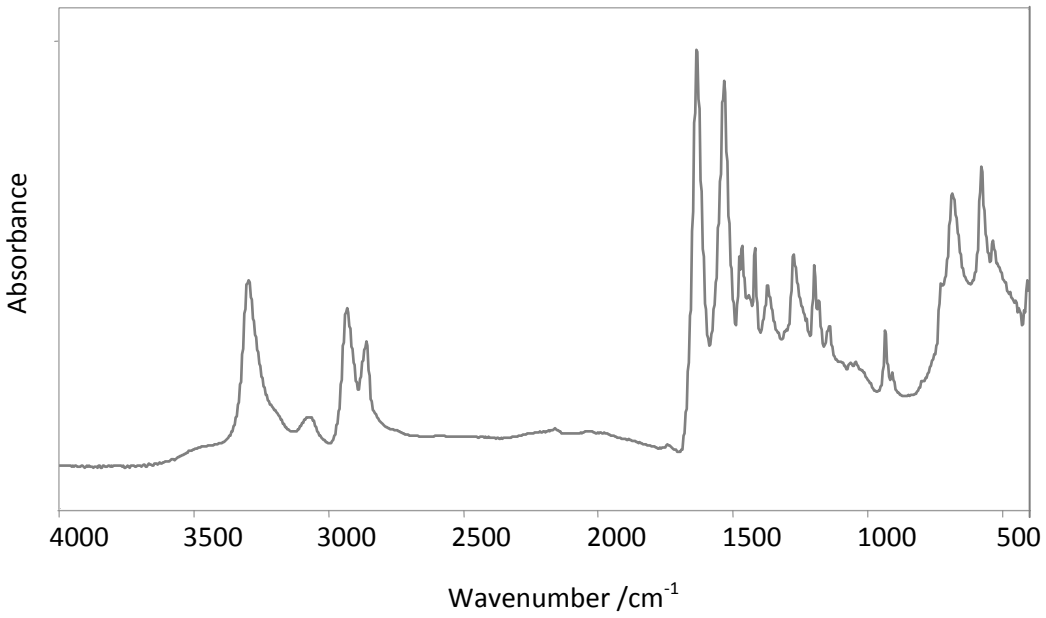

Figure 10.7 Non-polarized FTIR-ATR Spectrum of the polyamide 6,6 Reference

Wavenumber/cm^{-1}	**Assignment**
3 299	N-H stretch (hydrogen bonded)
3 065	N-H in-plane bend (overtone)
2 934	CH_2 stretch
2 858	CH_2 stretch
1 631	Amide I: C=O stretch, N-H bend
1 530	Amide II: C-N stretch, N-H bend
1 271	Amide III: C-N stretch, C-NH bend
934	Amide IV: C-C stretch, O-CN bend (crystalline) [4]
925	Amide IV: C-C stretch, O-CN bend (amorphous) [4]
727	CH_2 wag
683	Amide V: N-H out-of-plane bend
578	Amide VI: C=O out-of-plane bend

Table 10.3 Characteristic FTIR-ATR band assignments for polyamide 6,6 [5]

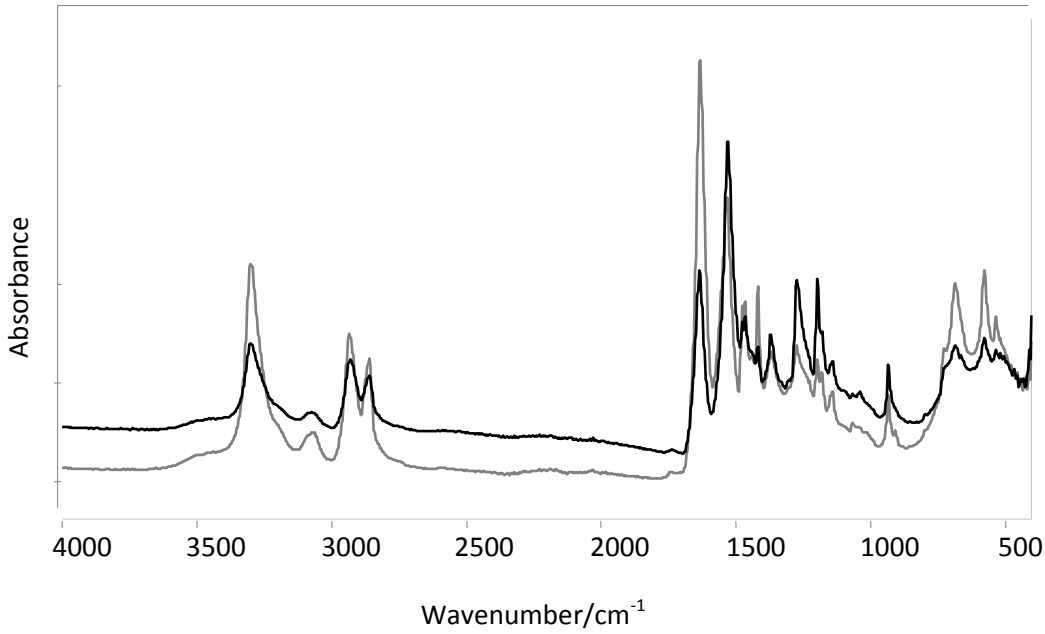

Figure 10.8 Polarized FTIR-ATR spectra of polyamide 6,6, 0° (black) and 90° (grey)

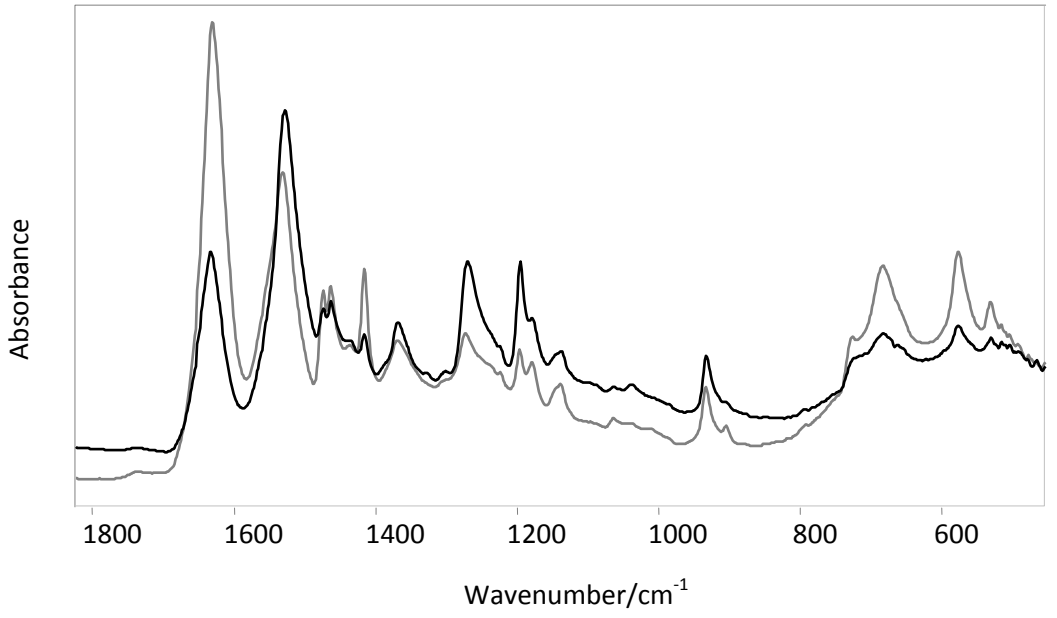

Figure 10.9 Expanded region of polarized FTIR-ATR spectra of polyamide 6,6, 0° (black) and 90° (grey)

Figure 10.8 shows the overlaid polarized spectra of the same sample. Curve 0° (black) refers to the fibres aligned front to back across the ATR window (and aligned with the infrared beam electric vector), and curve 90° (grey) with the fibres running from left to right. There are a number of bands which are dichroic, and were therefore investigated to see whether they would provide an indication of order within the samples. The Amide I at 1 631cm^{-1} (C=O stretch, N-H bend) is a perpendicular band, showing greater intensity when the sample fibres are aligned at 90° to the electric vector. Whilst the Amide II at 1 530cm^{-1} (C-N stretch, N-H bend) is a parallel band, showing opposite behaviour. This indicates that the carbon-carbon chains are aligned along the fibre axis, with the hydrogen bonded amine/carbonyl groups perpendicular to this.

It was necessary to normalise each band with an internal reference to account for alterations in sampling coverage of the ATR element caused by rotating the fibre through 90°. The reference peaks were chosen because they were non-dichroic for the two fibre alignments. Local baselines were applied and the peaks ratioed against adjacent reference bands, assuming similar depths of penetration (Table10.4):

Dichroic Peak	**Orientation**	**Reference Peak**	**Baseline**
1196cm^{-1}	Parallel	1179cm^{-1}	1211-1159cm^{-1}
1416cm^{-1}	Perpendicular	1369cm^{-1}	1585-1316cm^{-1}
1631cm^{-1}	Perpendicular	1530cm^{-1}	1698-961cm^{-1}

Table 10.4 Primary dichroic bands for polyamide 6,6 and baseline parameters

The dichroism, D (= $A_{\Pi}/A_{\perp}$), for the above bands was calculated as the ratio of the 0 and 90 absorptions, after they have been ratioed against the internal reference. For parallel bands the apparent dichroism, D, would be seen to decrease as the ordered arrangement becomes more disoriented and random. For the perpendicular bands the apparent D value should be seen to increase.

Table 10.5 shows the D values for the three ratios of interest. For a completely disordered system there would be no difference between the fibre orientations and the D values would approach 1. It is clear, that for all of the samples the spectra show evidence of an ordered polymer arrangement. In taking the errors into account for Con A, the effect of treating the sample appears not to have altered the degree of ordering (Con At). However, Con Ad may exhibit slightly increased order, although the changes are close to the standard experimental error.

Although the errors in some cases are again high in relation to the differences, looking at the trends across all three ratios does suggest a pattern of marginally increased ordering in all Con C samples compared to the unaged Con A samples. For example, when comparing Con Cu with Con Au there is a slight increase in D_{1196}, from 1.89 to 1.94, and a decrease in both D_{1416} and D_{1631}, from 0.34 to 0.30 and 0.38 to 0.33 respectively. Whilst there is an apparent increase in order for all the Con C samples, the trends amongst them are similar to those seen for the Con A set. In contrast, the effect of light ageing alone appears to show an increased ordering in the treated samples (Con Bt) and a decrease in ordering in the dyed samples (Con Bd).

Sample	**Ratio 0/90 D_{1196}**	**Ratio 0/90 D_{1416}**	**Ratio 0/90 D_{1631}**
Con Au	1.89 ±0.06	0.34 ±0.01	0.38 ±0.03
Con At	1.74 ±0.15	0.35 ±0.05	0.42 ±0.05
Con Ad	1.95 ±0.02	0.30 ±0.02	0.34 ±0.03
Con Bu	1.70 ±0.12	0.34 ±0.02	0.41 ±0.01
Con Bt	1.91 ±0.02	0.27 ±0.01	0.32
Con Bd	1.81 ±0.03	0.33	0.37 ±0.01
Con Cu	1.94 ±0.03	0.30 ±0.02	0.33 ±0.02
Con Ct	1.88 ±0.04	0.30 ±0.03	0.36±0.04
Con Cd	1.97 ±0.09	0.27 ±0.01	0.34 ±0.02

Figure 10.5 Dichroic ratios for the control samples (averages of 3 replicates)

10.1.1.3 Degree of Polymer Ordering as Determined by FTIR-ATR

Standard FTIR-ATR spectroscopy was used to examine the degree of crystallinity of the samples, according to the method of Vasanthan *et al* [6]. In their paper, FTIR calculated crystallinity was regressed against percentage crystallinity determined by density measurements. The two results were in good agreement and provided a means of validating the method. However, their results did show a percentage crystallinity discrepancy of plus 7% in the FTIR measurements, seen as an offset intercept on the regression line. The difference between FTIR and DSC data was attributed to an oriented amorphous phase contributing to the crystalline peak at 934cm^{-1}.

The bands at 934 and 925 cm^{-1}, assigned to Amide IV vibrations (Table 10. 3), were used to monitor the crystalline and amorphous regions, respectively. It should be noted that these two marker absorptions are in close proximity, and therefore the difference in ATR sampling depth between the two is only small, 4.03µm and 4.06µm respectively. Individual band intensities were determined following deconvolution of the absorbance envelope from 860 to 960 cm^{-1} (Figure 10.10). These were normalised against the peak at 1 631cm^{-1}, attributed to the Amide I vibration. The latter was used as an internal reference as it has been shown to be unaffected by changes caused by heat treatment [6].

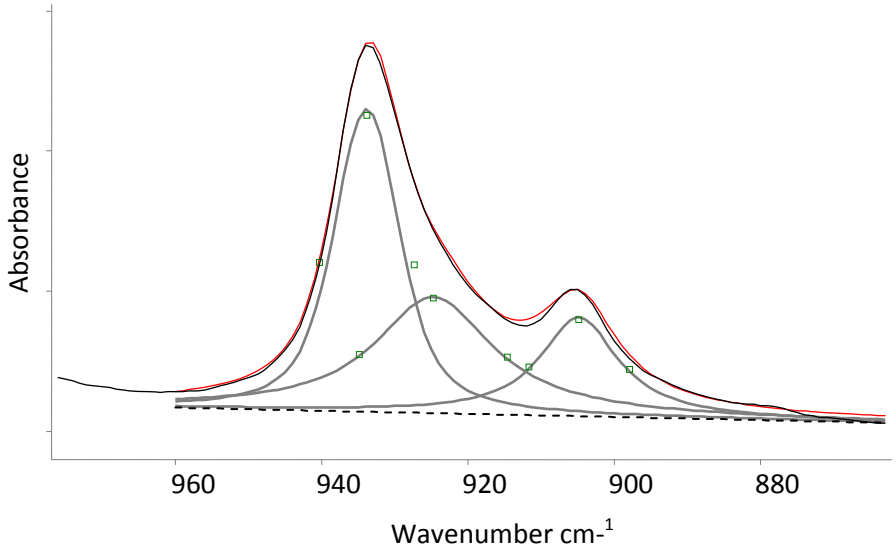

Figure10.10 Deconvolved peaks between 960 cm^{-1} and 860 cm^{-1} (grey), baseline (dashed), original trace (black) and fitted trace (red)

The subsequent calculation assumes a simple two phase model[I]:

crystalline volume fraction + amorphous volume fraction = 1

so P1 x I(crystalline band)+ P2 x I(amorphous band) = 1

and P1 x I_{934}/I_{925} + P2 = I_{1631}/I_{925}

[I] Original equation in Vasanthan *et al* [6] written in error, but used correctly. Therefore the equation has been re-arranged.

Where P1 and P2 are particular constants for the crystalline and amorphous phases, respectively. The constants are combinations of the proportions of the phases, the densities of the phases, the depth of sampling and the spectral molar absorbances. The intensity ratio I_{1631}/I_{925} is plotted against I_{934}/I_{925} in Figure 10.11.
This plot contains the global population of samples in this study. That is to say, all of the control material and all of the test samples discussed in later sections.

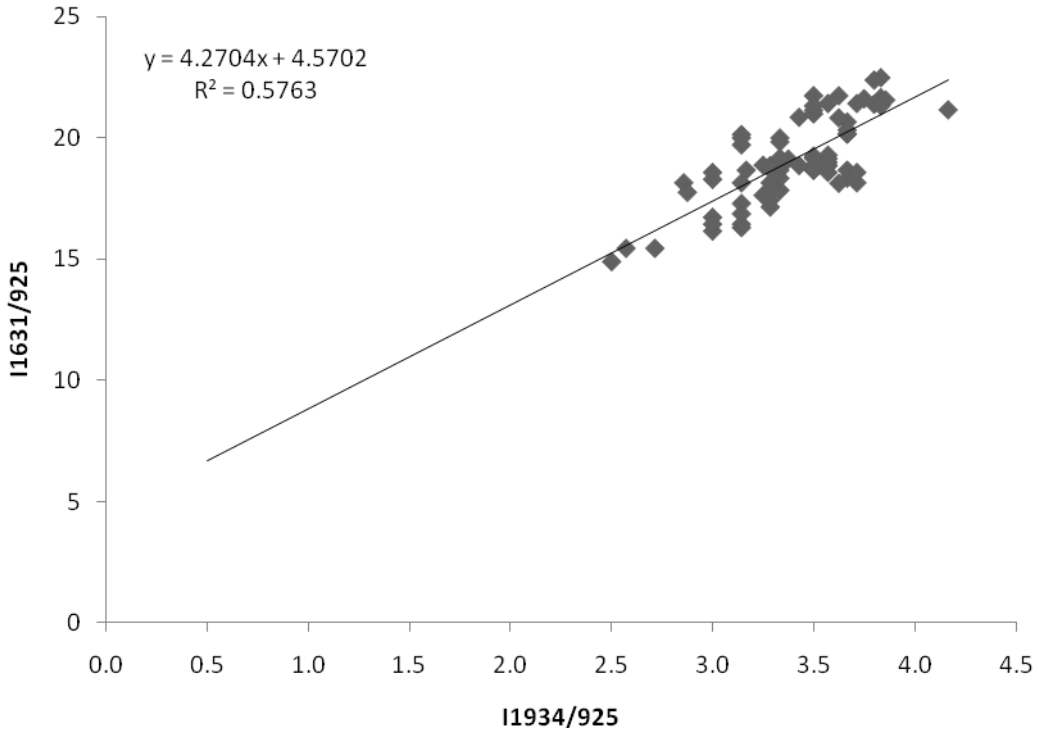

Figure 10.11 A plot of the Absorbance Ratios I1631/I925 vs I934/I925

From this it is possible to determine P1 and P2, the slope and intercept respectively. These were found to be 4.3 ±0.43 and 4.6 ±0.49 for the control samples Con Au,t,d, Bu,t,d and Cu,t,d. Three individual repeat measurements were used for each sample. The errors in the slope and the intercept were found using the method presented in Appendix 3. The slope of the regression line (P1) is then used to calculate the fractional crystallinity of the samples, by multiplying with the crystalline absorbance ratio $I_{934}/_{I1631}$:

$$\text{Fractional crystallinity} = 4.3 \times (I_{934}/I_{1631})$$

The values obtained using the above method are presented in Table 10.6, along with the percentage volume crystallinty as calculated by FTIR.

Sample repeat	I_{1631}	I_{934}/I_{1631}	I_{925}/I_{1631}	I_{1631}/I_{925}	I_{934}/I_{925}	P1(I_{934}/I_{1631})	% Crystallinity FTIR
Con Au [1]	0.14	0.17	0.04	22.50	3.83	0.73	**73**
Con Au [2]	0.14	0.19	0.05	19.29	3.57	0.79	**79**
Con Au [3]	0.13	0.20	0.05	21.17	4.17	0.85	**85**
Con At [1]	0.13	0.19	0.05	18.86	3.57	0.81	**81**
Con At [2]	0.12	0.19	0.06	17.14	3.29	0.82	**82**
Con At [3]	0.13	0.18	0.05	21.67	3.83	0.76	**76**
Con Ad [1]	0.13	0.18	0.06	17.86	3.29	0.79	**79**
Con Ad [2]	0.11	0.19	0.06	16.29	3.14	0.83	**83**
Con Ad [3]	0.13	0.17	0.05	21.00	3.50	0.72	**72**
Con Bu [1]	0.15	0.17	0.05	18.88	3.25	0.74	**74**
Con Bu [2]	0.12	0.18	0.05	20.17	3.67	0.78	**78**
Con Bu [3]	0.11	0.17	0.06	15.43	2.57	0.72	**72**
Con Bt [1]	0.11	0.19	0.05	18.83	3.50	0.80	**80**
Con Bt [2]	0.12	0.18	0.06	16.71	3.00	0.77	**77**
Con Bt [3]	0.14	0.16	0.05	20.00	3.14	0.68	**68**
Con Bd [1]	0.11	0.19	0.05	18.67	3.50	0.81	**81**
Con Bd [2]	0.12	0.19	0.06	16.43	3.14	0.82	**82**
Con Bd [3]	0.12	0.17	0.07	14.88	2.50	0.72	**72**
Con Cu [1]	0.13	0.18	0.06	18.14	3.29	0.78	**78**
Con Cu [2]	0.12	0.18	0.06	17.29	3.14	0.78	**78**
Con Cu [3]	0.13	0.19	0.05	19.00	3.57	0.81	**81**
Con Ct [1]	0.11	0.20	0.05	18.33	3.67	0.86	**86**
Con Ct [2]	0.11	0.19	0.06	17.83	3.33	0.80	**80**
Con Ct [3]	0.12	0.19	0.06	16.86	3.14	0.80	**80**
Con Cd [1]	0.11	0.20	0.05	18.67	3.67	0.84	**84**
Con Cd [2]	0.11	0.19	0.05	18.67	3.33	0.81	**81**
Con Cd [3]	0.11	0.19	0.06	16.14	3.14	0.80	**80**

Table 10.6 FTIR-ATR intensity ratios and calculated crystallinity for the control samples

The error in the crystallinity values is ± 1

It is clear that the scatter within each set of samples is high, therefore preventing general patterns to be determined. The variations relate to the normalised peak ratios, and are likely to result from the deconvolution function used to determine the peak intensities.
In addition, comparison with the literature values for polyamide 6,6 fibres shows the percentage crystallinities to be high, where the literature quotes values in the region of 42-58% [7-9].

There are a number of factors which need to be taken into account when interpreting the deviations from those previously found.
In the first instance, the size of the error in the slope will impact on the calculated crystallinity values (Figure 10.11). Thus, by including the full sample population in the data set the resulting error is reduced.
Another factor may lie in the contribution from the oriented amorphous regions. As derived from the Pol ATR results presented in Table 10.5, the polymer chains in the yarn are highly oriented. Therefore the oriented rigid phase may cause an increase in the crystalline vibration at 934cm^{-1}, as postulated by Vasanthan *et al* [6]. Using temperature modulated calorimetry, Qui *et al* [10] investigate the phase structure of polyamide 6,6 fibres. They found that the change in the heat capacity at the glass transition temperature was less than half of that expected for the 28% crystalline sample. They attributed this discrepancy to a rigid amorphous phase of about 36%, illustrating the possible impact it may have on both the characterisation of the crystalline and amorphous phases.
Finally, one of the most important factors relates to the sampling depth of the FTIR-ATR technique. The depth of penetration was shown to be in the region of a few microns when using the attenuated total reflectance accessory (Section 9.1.2.1, Chapter 9). This is governed by the refractive index of the crystal, the refractive index of the sample and the angle of incidence. The average diameter of the polyamdie 6,6 fibres was 32µm ±2, illustrating that the ATR technique would only interrogate the uppermost surface of the sample.

Although presented as an elegant method of determining the crystalline fraction of polyamide 6,6 fibres in the work by Vasanthan *et al* [6], the results presented here have shown that for this set of samples the technique is not sufficiently sensitive to distinguish any minor changes that may have occurred. It appears that the proportion of ordered material is similar for all of the samples.

10.1.2 Unloaded Control Sample Conclusion

UV irradiation effected a 30-40% drop in tenacity of PA 6,6, with subsequent thermal treatment reducing the performance by a further 10%. While untreated and dyed specimens showed similar changes, pre-treatment appeared to moderate the effects of ageing with these samples changing the least. The same general trends are seen in the strain data. The overall pattern of behaviour shows that the effect of UV light ageing is one of chain scission, with subsequent heat treatment increasing this effect. Detailed analysis of the stress versus strain plots further suggests that UV ageing produces a brittle, cross-linked material, though processing without dye may offer some protection.

While the proportion of ordered polymer seems to remain much the same, with any subtle differences undifferentiated by FTIR-ATR, there do seem to be some minor changes in polymer orientation amongst the samples. Whilst the light aged samples show varying effects, light plus heat ageing seems to result in slightly enhanced orientation along the fibre axis.

Due to equipment constraints, it was not possible to take all of the control samples through to the next stage of testing and analysis. Therefore, the decision was made to focus on the two extremes of conditions, Con Au and Con Cu. This ensured the best case and worst case scenario was determined when subjecting polyamide 6,6 to pest control treatments.

10.2 Loaded Control Samples

As discussed in Chapter 9 some of the samples were subjected to loading, both *in situ* and during the DMTA creep tests, to simulate the behaviour of a garment hanging under its own weight during pest control treatment. In order to assess whether there is an effect on subjecting a loaded textile to varying temperatures, the consequence of loading under ambient conditions first needed to be determined. The discussion below compares the results from the unloaded, undyed samples Con A and Con C, with their equivalents after loading *in situ* and after DMTA creep/recovery experiments. Table 10.7 presents the assignments given to each sample.

Sample	Sample Treatment
Con A	Unaged
Con AL	Unaged + load *in situ*
Con A – DMTA	Unaged + creep/recovery in DMTA
Con C	UV + heat aged
Con CL	UV + heat aged + load *in situ*
Con C – DMTA	UV + heat aged + creep/recovery in DMTA

Table 10.7 Loaded control sample assignments and their corresponding treatments. All samples are in their unprocessed state

10.2.1 Loaded Control Sample Results

Table 10.8 contains the polarized ATR D values calculated for the loaded control samples. The application of the load has caused an apparent slight decrease in the fibre alignment. While the changes are near the experimental error, the results are generally consistent across the D ratios; with the decreases in D_{1196} there are corresponding increases in D_{1416} and D_{1631}.

Sample	Ratio 0/90 D_{1196}	Ratio 0/90 D_{1416}	Ratio 0/90 D_{1631}
Con A	1.89 ±0.06	0.34 ±0.01	0.38 ±0.03
Con AL	1.78 ±0.02	0.40 ±0.03	0.46 ±0.05
Con A – DMTA	1.87 ±0.32	0.33 ±0.06	0.39 ±0.07
Con C	1.94 ±0.03	0.30 ±0.02	0.33 ±0.02
Con CL	1.74 ±0.17	0.35 ±0.06	0.39 ±0.05
Con C – DMTA	1.49 ±0.08	0.46 ±0.08	0.43 ±0.09

Table 10.8 Dichroic ratios for the loaded control samples

The restricted access to the DSC equipment prevented repeat analyses, therefore it was only possible to carry out repeat tests for one sample (Con C). Nonetheless, on inspection of the three repeat curves (Figure 10.12) it is clear that the sample and equipment were behaving in a consistent manner. In order to reduce the variability in the data, all thermal analyses presented were carried out on the same day.

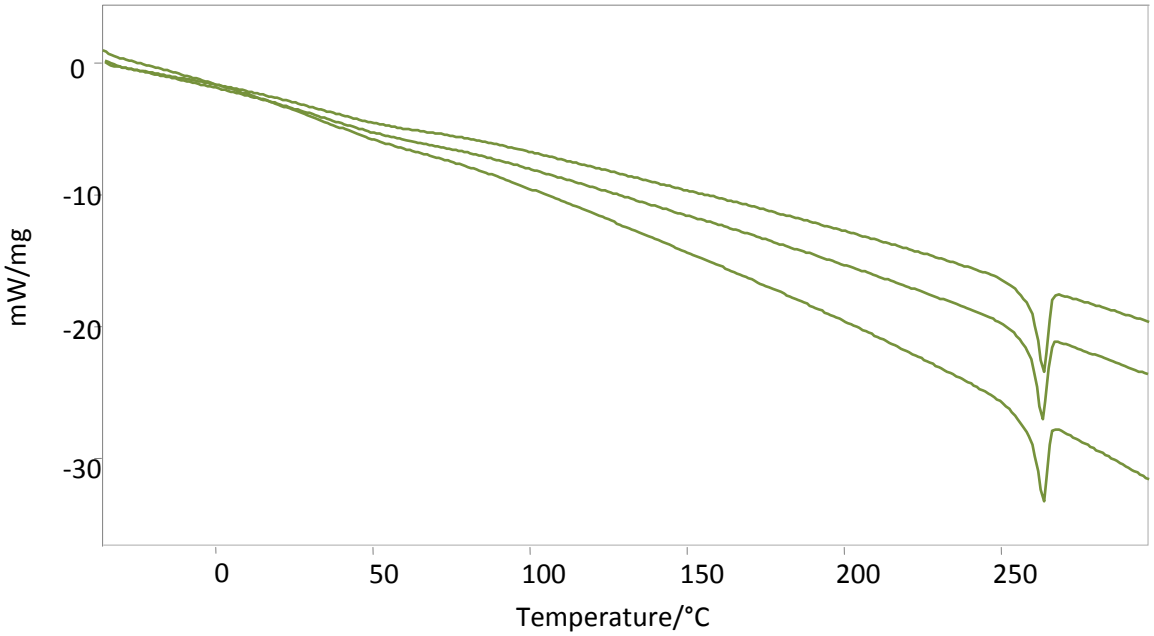

Figure 10.12 Three repeat DSC heating curves for Con C

The percentage crystallinity is calculated by integrating the area under the Tm endotherm, following the method described in Section 9.3.3.2, Chapter 9.
Below are the values for the percentage crystallinity (Table 10.9) and the melting temperature (Table 10.10) derived from the three replicate tests of Con C.

Sample repeat	Integrated Area	Mean	Max Variance	Heating Rate	Time Interval/Jg	% Crystallinity
Con C [1]	33.7	33.6	0.5	0.33	102	51.9 ±0.8
Con C [2]	33.1					
Con C [3]	34.1					

Table10.9 Calculated percentage crystallinity for Con C as determined by integration of the melting temperature endotherm

Sample repeat	Tm/ °C	Mean/ °C	Max Variance/°C
Con C [1]	263.1	263.2	0.2
Con C [2]	263.4		
Con C [3]	263.2		

Table 10.10 Melting temperature for Con C as determined by DSC

It is expected that the scatter within the calculated crystallinity for the other samples will be similar.

The glass transition temperature was taken as the point of maximum slope in the heat capacity step. Therefore, it can be determined by the zero line after calculating the second derivative of the heating curve (Figure10.13), as outlined in Chapter 9. Repeat values for the mean and maximum variance for the transition in Con C are presented in Table 10.11.

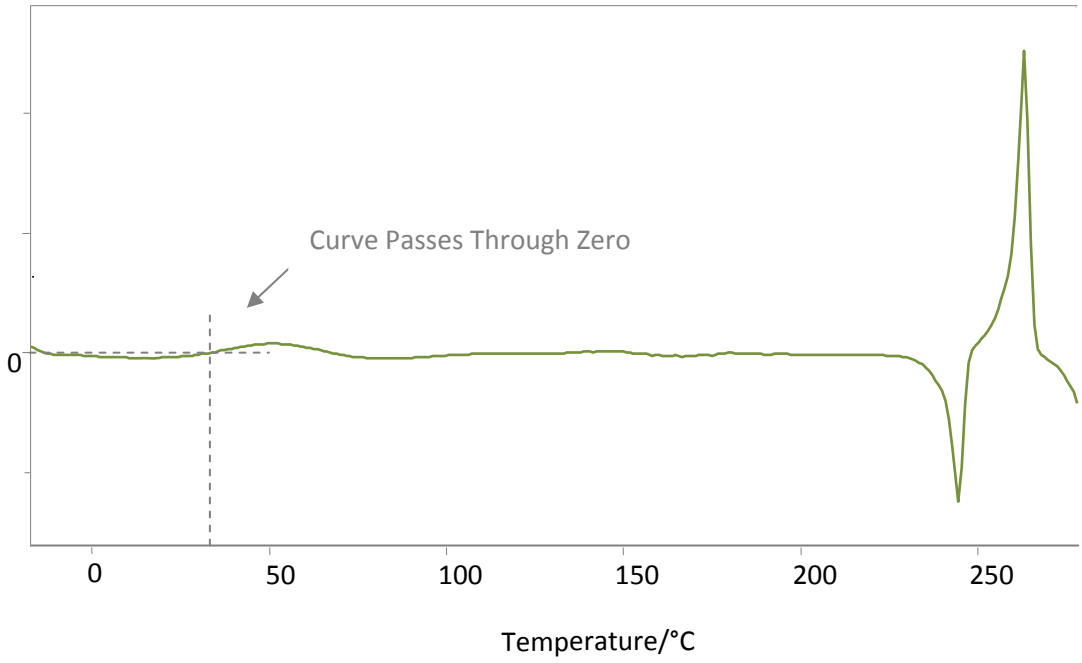

Figure 10.13 Second derivative DSC heating curve resulting from the average of three repeat measurements for Con C

Sample repeat	Tg/ °C	Mean/ °C	Max Variance/°C
Con C [1]	32.6	33.2	0.6
Con C [2]	33.6		
Con C [3]	33.4		

Table10.11 Glass transition temperature for Con C as determined by DSC

On review of the data relating to the thermal analyses of Con C, it is shown that the material and equipment were both behaving in a consistent manner. However, in view of the lack of replicate testing, the quantitive determinations are presented with caution, with the focus being given to relative values.

Presented in Table 10.12 are the calculated values of the DSC derived crystallinity and the temperatures of melting and the glass transition for the loaded control samples.

Sample	Crystallinity/%	Variance/%	Tm/°C	Variance/°C	Tg/ °C	Variance/ °C
Con A	54.7		266.8		35.3	
Con AL	58.1		264.1		33.9	
Con A DMTA	57.2		264.2		35.7	
Con C	51.9	0.8	263.2	0.2	33.2	0.6
Con CL	54.3		265		32.7	
Con C DMTA	56.3		265		31.6	

Table 10.12 Percentage crystallinity and thermal transitions for the loaded control samples as determined by DSC

Table 10.12 shows the percentage crystallinity, calculated using DSC, for Con A and Con C. It appears that within the expected experimental error, Con A and Con C may exhibit a small difference in crystallinity. The suggested decrease in crystallinity in Con C ties in satisfactorily with the results presented in Section 10.1, with ageing induced polymer chain scission. Loading seems consistently to raise the crystallinity by a small amount.
This is contrary to the PoI ATR results, which indicate a slight reduction in order. However, it should be noted that the DSC method is a bulk analysis, whereas the ATR method is a surface sensitive technique, which also probes the crystalline fringes. The characteristics of the samples may exhibit structural variations at different sampling volumes.

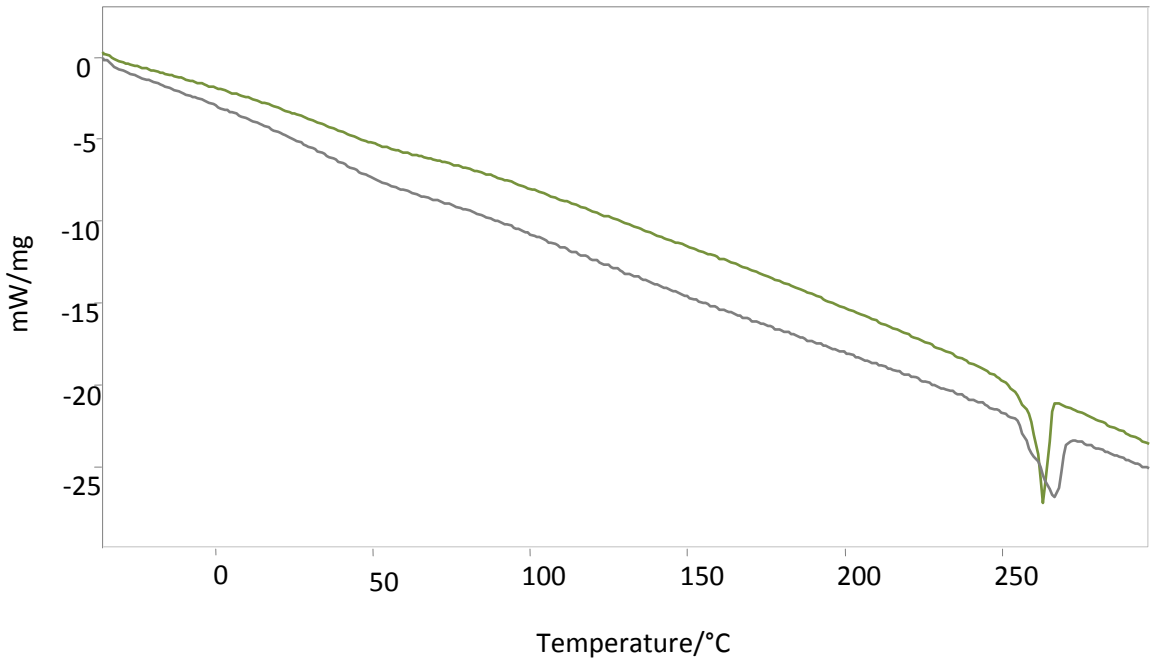

Figure 10.14 DSC heating curves for Con A (grey)and Con C (green)

The DSC heating curves for the unaged and aged samples show distinctly different melting endotherms, as shown in Figure 10.14. Con A shows a broad, ill-defined trough with evidence of a shoulder at 259°C and a trough minimum at 267°C. In contrast, Con C exhibits a much sharper trough and the shoulder is no longer present. The trough minimum is at 263°C ±0.2.

Simal and Martin [11] suggest that the presence of a double endotherm in polyamide 6,6 fibres relates to differences in size and perfection of the crystalline regions. In their work they show that on increasing the temperature above 70°C, the growth and perfection of the crystallites increased. This latter point may suggest why the endotherm for Con C is a more highly resolved peak. Thanki *et al* [12] also showed a similar double melting peak, which was attributed to the melting of the bulk crystal structure at the higher temperature, and melting of the smaller crystallites, which occurs at a lower temperature. It should be remembered that caution is needed in the quantitative interpretation of the curves because there are no replicates.

In all cases, the glass transition temperature is lower than those quoted in the literature for polyamide 6,6 fibres, with values ranging from anywhere in the region of between 40°C to 115°C [11, 13, 14].

There are a number of factors that could account for such discrepancies, such as differences in the thermal history of the fibres, polymer processing, and the use of different experimental methods for determination of the transition. However, in the case presented here the glass transition may appear low due to problems with determining the true mid-point of the heat capacity inflection. Towards the end of the step in the baseline there is a clear relaxation trough in the DSC heating curve (Figure 10.15) [15]. This endothermic trough is caused by the relaxation of molecules under internal stress, caused by the mechanical processing of the fibres [16, 17]. In the region of the glass transition the molecules are capable of mobility, and as a consequence, energy is absorbed during dissipation of stresses through their rearrangement.
The presence of this relaxation affects the determination of the glass transition temperature, when the Tg is taken as half the step height. It is clear that the endotherm will shift the position of the final baseline and therefore the centre of the transition.

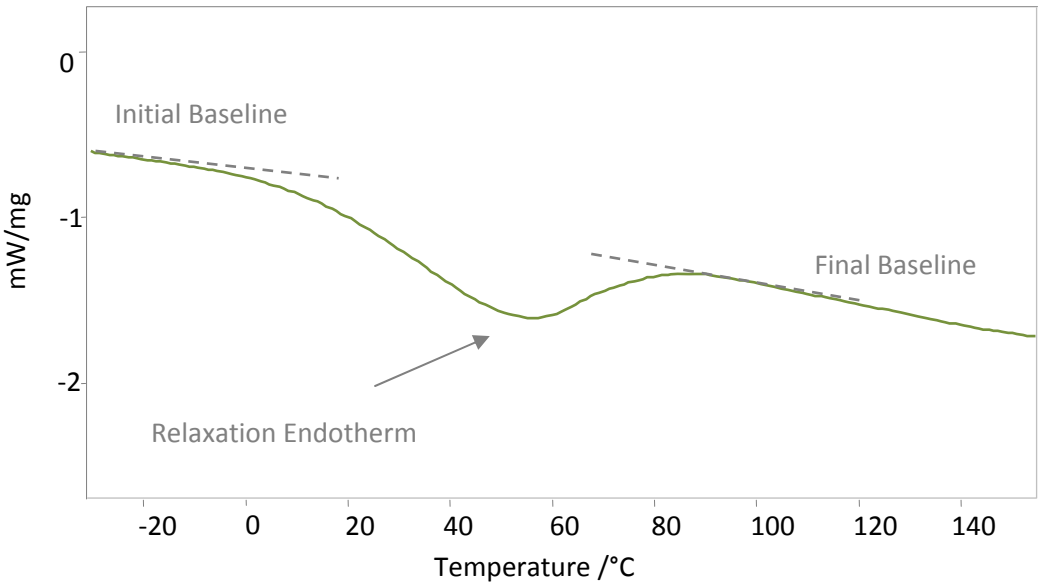

Figure 10.15 Expanded region of the DSC heating curve (-25-140°C) for Con C-DMTA, showing the position of the endothermic trough superimposed on to the glass transition

The glass transition temperature is shown to decrease a little, by 2°C**,** from unaged to light aged material. This again could suggest some structural rearrangement on ageing, and in this case slightly increased freedom within the amorphous region, which fits the theory of chain scission on UV irradiation, as indicated by the increase in anisotropy and embrittlement of the polyamide. However, the differences between Con A and Con C are small in comparison to the temperature range over which the Tg occurs and may not be significant.

On the application of a load, the percentage crystallinity appears to increase in both the unaged and aged material. This is most likely due to the drawing of the polymer chain and an increase in lateral packing in the amorphous regions. This effect appears to be greater for the unaged material, Con A.

Figure 10.16 shows the DSC heating curves for the unloaded and loaded samples for Con A. The difference in the apparent heat capacities of the samples is clear, as evidenced by the general slopes of the plots. This is also shown to be the case for Con C samples (Figure 10.17). The energy required to maintain a constant temperature between the sample and the reference crucible is greater in the samples that have not been subjected to deformation. Little reference to such differences has been found in the standard literature. Bershtein and Egarov [18] state that the slope of the curve is dependent on the thermal pre-history of a sample. Variations in the baseline have also been attributed to differences in the mass of the measuring crucibles, relative to the baseline scan, and to changes in the heat transfer between the sample and crucible [19]. However, in the present case these variations are consistent with the application of a small static load, and would appear to be somehow connected to this factor. It will be shown in the following chapter that this effect is also present in the test specimens in addition to the control material presented here. The reasons for this difference have not been reconciled, but the implications suggest that the more crystalline materials show a decrease in the apparent heat capacity. Carrying out mechanical work on the material causes rearrangement of the non-ordered regions, thus reducing the energy required to maintain the sample at a constant temperature during the heating ramp.

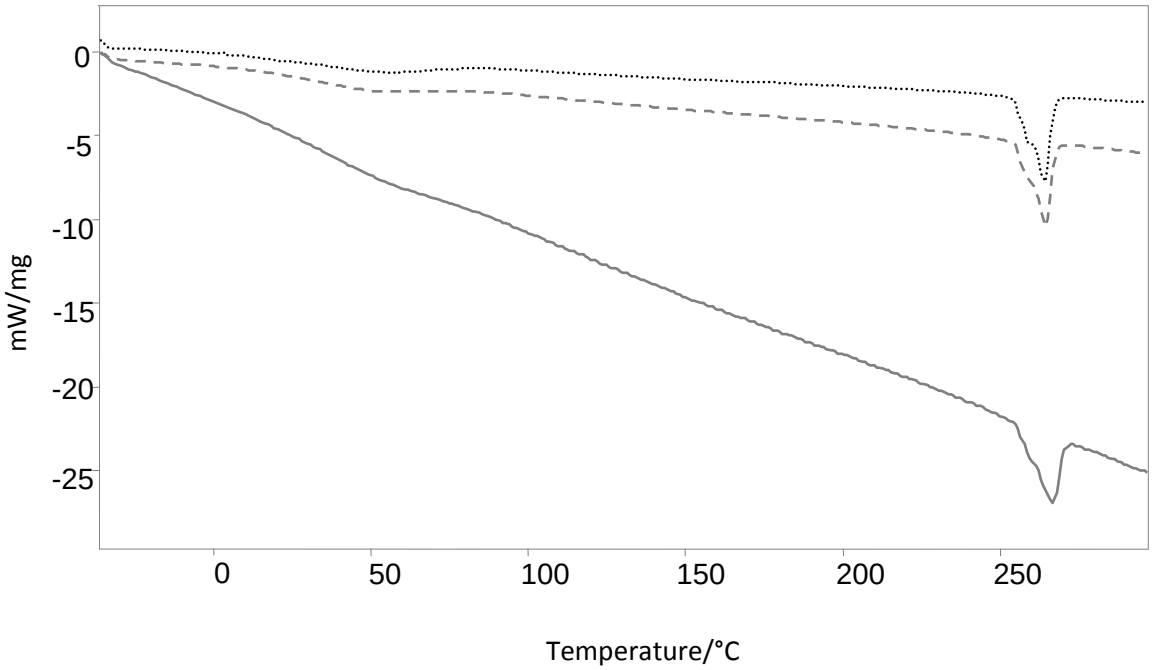

Figure 10.16 DSC Curves for Con A Unloaded (solid line), Loaded (dashed line) and after creep/recovery in the DMTA (dotted line)

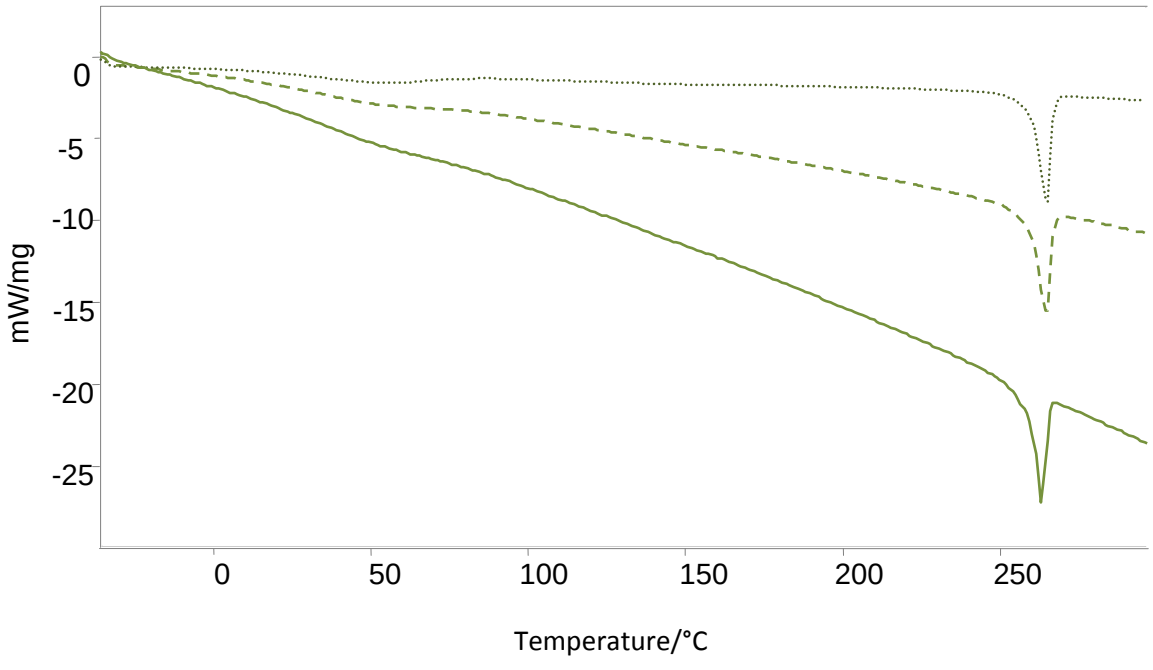

Figure 10.17 DSC Curves for Con C Unloaded (solid line), Loaded (dashed line) and after creep/recovery in the DMTA (dotted line)

On inspection of the DMTA creep/recovery data (Figure 10.18), both the unaged and aged material show similar behaviour. It is clear that the application of a small static load (0.31 MPa) onto the sample at ambient temperatures causes progressive contraction in the sample after the initial instantaneous elongation in the elastic region. The contraction is more exaggerated in the aged material than the unaged sample. After 150 minutes the static load was removed and the sample allowed to recover. Immediately after the load is removed the strain is rapidly reduced. This is followed by a continuing gradual contraction of the sample. At the end of the experiment (450 minutes) both samples are shorter than their initial length.

It is important to note that for this set of data it is the creep section of the DMTA curves that is of primary interest. This is the region representing the behaviour of a beaded garment hanging under its own weight and the final strain before the load is removed represents the displacement that would be seen in the yarns of a beaded dress at ambient temperatures. The final strains for Con A DMTA and Con C DMTA are 0.48% and 0.07% respectively. Con A-DMTA and Con C-DMTA represent the unaged and aged samples at room temperature, and should be regarded as the baseline for comparison with those samples treated at raised and lowered temperatures, to be presented in Chapter 11.

This data serves to support the *in situ* data, but it should be borne in mind that the load has been applied to the fabric subsequent to ageing. In the case of a real garment, any adornments would have been applied to a new garment, with the ageing process taking place thereafter.

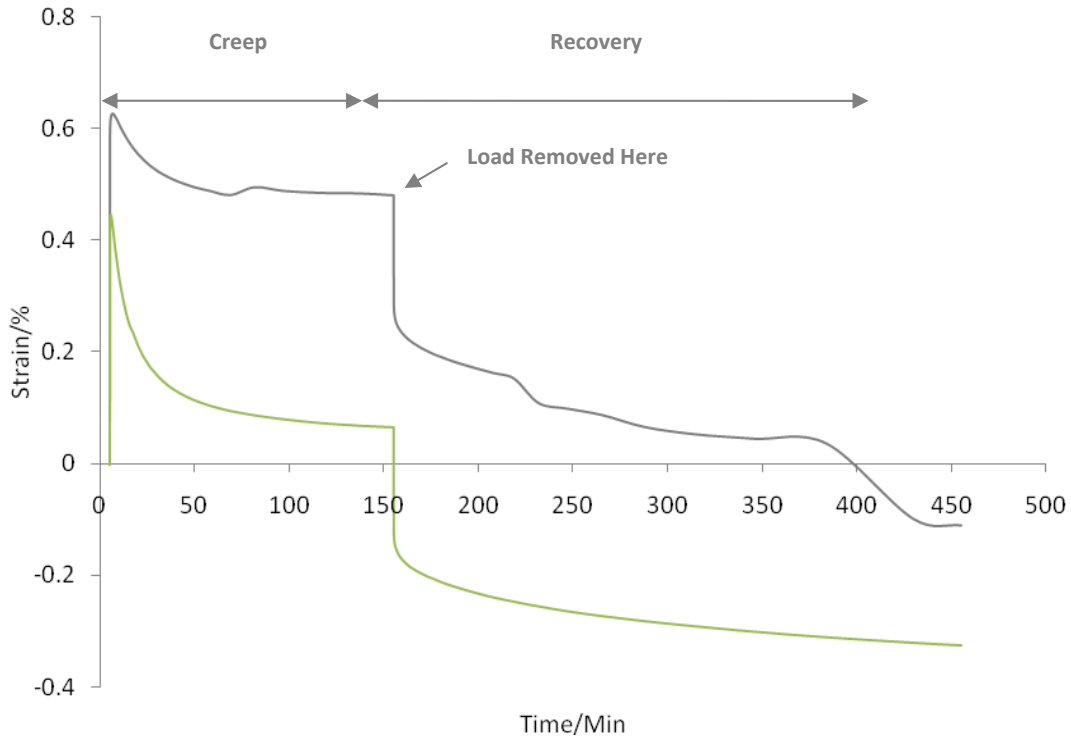

Figure 10.18 DMTA creep/recovery curves for Con A DMTA (grey) and Con C DMTA (green) at room temperature stressed with 0.31 MPa

10.2.2 Loaded Control Sample Summary Discussion

A summary of the results is presented in Table 10.13.

Sample	Ratio 0/90 D_{1196}	Ratio 0/90 D_{1416}	Ratio 0/90 D_{1691}	Crystallinity /%	Tm/°C	Tg/°C	Initial Strain/%	Final Loaded Strain/%
Con A	1.89 ±0.06	0.34 ±0.01	0.38 ±0.03	54.7	266.8	35.3		
Con AL	1.78 ±0.02	0.40 ±0.03	0.46 ±0.05	58.1	264.1	33.9		
Con A - DMTA	1.87 ±0.32	0.33 ±0.06	0.39 ±0.07	57.2	264.2	35.7	0.63	0.48
Con C	1.94 ±0.03	0.30 ±0.02	0.33 ±0.02	51.9	263.2	33.2		
Con CL	1.74 ±0.17	0.35 ±0.06	0.39 ±0.05	54.3	265	32.7		
Con C - DMTA	1.49 ±0.08	0.46 ±0.08	0.43 ±0.09	56.3	265	31.6	0.45	0.07

Table 10.13 Summery of the results for the loaded control samples

The Pol ATR data show there is a decrease in anisotropy upon loading of the samples. This is more exaggerated in the aged samples. The reasons for this are unclear. On the application of a load it is expected that the degree of directionality would increase, as the polymer chains are drawn longitudinally. The decrease in ordering is accompanied by an increase in percentage crystallinity, as calculated by integrating the area under the DSC melting endotherm. The slight increase in crystallinity is in keeping with the drawing of a polymer under uniaxal load. As the length of the *c* axis increases there will be a corresponding decrease in the width, along axis *a*. This will bring the polymer chains closer together allowing intermolecular bonding to increase.
The anomaly between these two results may lie in the fact that the ATR sampling technique is surface sensitive (4 microns in the region of interest). In comparison, the DSC technique provides information on the bulk properties of the material. The results therefore suggest that the application of a load has induced, or propagated already existing, surface defects.

On inspection of the DSC melting endotherm it is clear that the unaged and aged materials exhibit distinctly different melting behaviour. For Con A, the broader trough with a shoulder suggests a material with crystallites of inhomogenous size and perfection, which melt over a wider range of temperatures. Such behaviour is similar to that seen in low purity compounds, where differences in crystal structure result in poorly resolved fusion curves [20]. The effect of UV and subsequent heat ageing (Con C) has been to induce crystal homogeneity through rearrangement whilst held above the glass transition temperature.

The calculated values for the glass transition temperature were found to be somewhat lower than those quoted in the standard literature. This was due to the presence of an endothermic trough towards the end of the step change in the heat capacity. This is attributed to the relaxation of the polymer chains remaining under internal stress after fibre processing. On taking the samples to above their glass transition temperatures the molecules have increased energy and movement and rearrange into a state of equilibrium [16].

The creep/recovery data show a surprising behaviour for both the unaged and aged material, Con A DMTA and Con C DMTA respectively. Both samples after the initial displacement of the yarns are seen to contract on the application of the load. The reasons for this are not certain, and could be related to a change in the woven structure of the

fabric. However, coupled with the apparent increase in crystallinity determined by DSC, it is possible that there is some strain induced crystallisation occurring in the samples.
The initial extension and drawing of the polymer chains causes an alignment of the amorphous regions. This in turn would bring the amide groups into close proximity with each other, enabling inter-chain bonding. If the density of the crystalline phase is taken to be 1.24g/cm^3, and the amorphous phase 1.09g/cm^3 [21], then it is clear that increased crystallinity will induce an increase in density of the polyamide fibres. Murthy *et al* [22] showed that there is a density increase, alongside increased crystallinity, on the cold drawing of polyamide 6 fibres. Increased density will be accompanied by a decrease in volume. The new, ordered crystal structures would occupy a reduced space and would therefore be seen as a contraction in the sample. It is proposed that this is the mechanism occurring in the creep/recovery experiments at room temperature.
This effect is greater in the aged samples, Con C DMTA, and is related to the difference in starting material. The aged control material Con C it thought to have undergone chain scission reactions along the polymer chain. This would increase the number of reaction sites available for cross-linking and bridging or oriented chains.

The mechanism is corroborated by the behaviour in the recovery section of the curves. If the contraction is due to an increase in crystallinity then this would not be reversed by the removal of the load. At the end of the recovery period the overall strain is shown to be negative, meaning that the sample is smaller than the initial length of the sample. Since the initial contraction is greater in the aged sample compared to the unaged sample, the final negative strain is also greater in the aged sample.
In assessing the effects of raised and lowered temperature treatments on garments, the length of the sample at the end of the creep section of the curve will be regarded as the starting length of the sample. It should be noted, that this does not, however, take into account relaxation effects, which would occur under load over time.

10.2.3 Loaded Control Sample Conclusions

The Pol ATR data show there is a decrease in isotropy on applying a load to both the unaged and aged material. This is accompanied by an increase in the percentage crystallinity. These two opposing results suggest two mechanisms may be occurring at different sampling depths; load induced crazing at the surface of the samples and strain

induced crystallinity in the bulk of the material. The contraction in the creep/recovery curves appear to confirm this last mechanism.
Although the determination of the glass transition temperature proved problematic, it was shown that the transition occurred over the temperature region of interest when studying the effects of elevated temperature treatments.

10.3 Conclusions

The Pol ATR data and tensile tests indicate that the "as received", undyed material has a directionally ordered arrangement with reproducible tensile properties. The pre-treatments of the samples have produced a material with differing properties. The treatment and dye processes have induced plasticisation, causing an increase in percentage strain without altering the breaking strength. Neither treatment appears to have had a significant effect on the orientational properties of the polymer chains.
Subsequent artificial ageing has provided material with varying degrees of deterioration. The light ageing process has induced chain scission reactions, resulting in a significant reduction in tensile properties. The decrease in breaking strength and percentage strain is accompanied by an increase in anisotropy, supporting the theory of chain scission.
The tensile properties for the three samples aged using both UV and heat have experienced a reduction of approximately 50% of their original values. Again, this is attributed to chain scission. The orientation of the polymer chains in the upper layers of the fibres exhibit a small increase in order, as shown by Pol ATR. This may suggest the formation of cross-links between points of rupture, accelerated by the application of raised temperatures.
Due to equipment constraints, the sample set was reduced, focusing on the two specimens representing the extremes of conditions. That is the unaged, undyed material Con A, and the UV and heat aged material Con C.
To enable the stability of the test material to be determined when subjected to pest control treatments, the control material first required characterisation at ambient temperatures. The unaged and artificially aged samples were subjected to loading *in situ* and during creep/recovery tests using DMTA at room temperature. This was to provide a baseline from which to compare the behaviour of the samples at raised and lowered temperatures, to be presented in Chapter 11.

Determination of standard errors was not possible for the thermal analyses due to limited instrument access. However, for one sample (Con C) repeat measurements were possible. These indicated that the material and instrument were behaving in a reproducible manner. The melting endotherm of the DSC heating curve indicated that the aged material has increased crystal size and perfection. This was seen as a sharpening of the trough at the melting temperature.

The percentage crystallinity, as determined by integration under the Tm curve, indicated a small increase in crystallinity in all loaded samples, both *in situ* and during creep/recovery experiments. However, this was accompanied by a reduction in directionality, determined by Pol ATR. This difference may be attributed to the sampling volumes of the analyses. The DSC provides information on the bulk characteristics of the samples, whereas the ATR sampling method gives surface sensitive information. The results suggest that loading may cause the propagation of surface defects, inducing local rupture. The effect was more pronounced in the aged material.

The determination of the glass transition temperature proved problematic due to the presence of a relaxation endotherm towards the end of the heat capacity change. This caused the calculation of the glass transition to be considerably lower than that reported in the literature for polyamide 6,6. However, the relative temperatures did not suggest any significant variations with the expected experimental error.

It is important to note that when investigating raised temperature treatments, the Tg was shown to be occurring over the critical region of interest. This may pose important implications for the materials stability.

The creep/recovery experiments were used to monitor the physical deformation behaviour of the samples under load at room temperature. Both the unaged and aged material showed similar behaviour. The samples experienced contraction after the initial displacement of the yarns. This was attributed to strain induced crystallisation. On removal of the load the samples did not recover fully, with their final length being shorter than their starting length. Coupled with an increase in percentage crystallinity, this served to support the theory of strain induced crystallinity.

10.4 References

1. Marcellan, A., et al., *A Multi-scale Analysis of the Microstructure and the Tensile Mechanical Behaviour of Polyamide 66 Fibre.* Polymer, 2006. **47**: p. 367-378.
2. Nielsen, L.E. and R.F. Landel, *Mechanical Properties of Polymers and Composites*. 2nd ed. 1994, New York: Marcel Dekker.
3. Lock, L.M. and G.C. Frank, *A Study of Some Factors Affecting the Photodegradation of Textile Yarns Part II: Nylon 66 and Polyethylene Terephthalate Yarns.* Textile Research Journal, 1973. **September**: p. 502-512.
4. Vasanthan, N., S.B. Ruetsch, and D.R. Salem, *Structure Development of Polyamide 66 Fibers During Drawing and Their Microstucture Characterization.* Journal of Polymer Science Part B: Polymer Physics, 2002. **40**: p. 1940-1948.
5. Huang, Y., W. Li, and D. Yan, *Preparation and Characterization of a Series of Polyamides with Long Alkyene Segments: Nylon 12 20, 10 20, 8 20, 6 20, 4 20 and 2 20.* Polymer Bulletin, 2002. **49**: p. 111-118.
6. Vasanthan, N. and D.R. Salem, *Structural Characterisation of Heat Set and Drawn Polyamide 66 Fibres by FTIR Spectroscopy.* Materials Research and Innovation, 2001. **4**: p. 155-160.
7. Murthy, N.S., et al., *Drawing and Annealing of Nylon-6 Fibres: Studies of Crystal Growth, Orientation of Amorphous and Crystalline Domains and Their Influence on Properties.* Polymer, 1995. **36**(20): p. 3863-3873.
8. Domingues, Q.M.S., R.J.I.N. Gomes, and J.A. Martins, *Dyeing of PA 6.6 Fibres: Effect of Solvent and Temperature on Thermal Properties.* Journal of Thermal Analysis amd Calorimetry, 2003. **74**: p. 749-759.
9. Popovic, B., et al., *Structural Changes in the Fabrication and Ageing of PA66 Textured Yarn.* Macromolecular Materials and Engineering, 2005. **290**: p. 143-148.
10. Qui, W., A. Habenschuss, and B. Wunderlich, *The Phase Structure of Nylon 6,6 as Studied by Temerature-Modulated Calorimetry and Their Link to X-ray Structure and Molecular Motion.* Polymer, 2007. **48**(6): p. 1641-1650.
11. Simal, A.L. and A.R. Martin, *Structure of Heat-Treated Nylon 6 and 6.6 Fibres I: The Shrinkage Mechanism.* Journal of Applied Polymer Science, 1998. **68**: p. 441-452.
12. Thanki, P.N., C. Ramesh, and R.P. Singh, *Photo-irradiation Induced Morphological Changes in Nylon 66.* Polymer, 2001. **42**: p. 535-538.
13. Gordon, G.A., *Glass Transitions in Nylons.* Journal of Polymer Science Part A-2, 1971. **9**: p. 1693-1702.
14. Toivonen, A.L., *Investigating the Effect of Cold Winter Conditions on Fishing Gear Materials.* Journal of the Textile Institute, 1992. **83 Part 1**: p. 163-177.
15. Affolter, S., A. Ritter, and M. Schmid, *Interlaboratory Tests on Polymers by Differential Scanning Calorimetry (DSC): Determination of Glass Transition Temperature (Tg).* Macromolecular Materials and Engineering, 2001. **286**: p. 605-610.
16. Gabbott, P., *A Practical Introduction to Differential Scanning Calorimetry*, in *Principles and Applications of Thermal Analysis*, P. Gabbott, Editor. 2008, Blackwell Publishers: Oxford.
17. Turi, E.A., *Thermal Characterization of Polymeric Materials*. 2nd ed. Vol. 2. 1997, London: Academic Press.
18. Bershtein, A. and V.M. Egavor, *DSC of Polymers: Physics, Chemistry, Analysis, Technology*. 1994, New York: Ellis Hardwood.
19. Hohne, G., W. Hemminger, and H.-J. Flammersheim, *Differential Scanning Calorimetry: An Introduction for Practitioners*. 1996, Heidelberg: Springer-Verlag.

20. Griffin, V.J. and P.G. Laye, *Thermal Analysis - Techniques and Applications*, ed. E.L. Charsely and S.B. Warrington. 1992, Cambridge: The Royal Society of Chemistry.
21. Vasanthan, N., S.B. Ruetsch, and D.R. Salem, *Structure Development of Polyamide-66 Fibres During Drawing and Their Microstructure Characterization.* Journal of Polymer Science Part B: Polymer Physics, 2002. **40**: p. 1940-1948.
22. Murthy, N.S., et al., *Drawing and Annealing of Nylon 6 Fibres: Studies of Crystal Growth, Orientation of Amorphous and Crystalline Domains and Their Influence on Properties.* Polymer, 1995. **36**(20): p. 3863-3873.

Chapter 11: Unloaded and Loaded Test Samples

Standard pest control measures in museums involve subjecting artefacts to low (-30°C) or raised (58°C) temperatures. This Chapter discusses the results from experiments which were designed to investigate whether such treatments might adversely affect polyamide 6,6 in collections. To this end, the previously characterised unaged and artificially aged polyamide textiles were subjected to temperatures of 58°C and -30°C. Thermal treatments were carried out on both loaded and unloaded samples, to determine whether textiles would suffer further deterioration if treated while hanging, for example on a manikin. The results follow on from the preliminary studies presented in the previous chapter into the behaviour of the samples at room temperature.

The analytical techniques, protocols and data interpretation presented here follow the same methods as described in Chapters 9 and 10. Table 11.1 serves as a reminder of their applications.

Technique	Sampling Volume	Information
Tensile Tests	Bulk	Breaking Load
		Percentage Strain
		Energy at Break
		Young's Modulus
Pol ATR	Surface (2-4µm)	Polymer Orientation
DSC	Bulk	Percentage Crystallinity
		Crystal Homogeneity
		Glass Transition Temperature
DMTA	Bulk	Creep/Recovery
		Percentage Strain

Table 11.1 List of analytical techniques and their application

11.1 Unloaded Test Samples

The undyed samples Con A and Con C were subjected to the treatments above and below room temperature (Table 11.2).

Sample	Ageing and Treatment Regimes
Con A 23	Unaged, 23°C
Con A 58	Unaged, 58°C, 2hrs (> 50°C 5hrs)
Con A -30	Unaged, -30°C, 72hrs
Con C 23	UV + Heat Aged, 23°C
Con C 58	UV + Heat Aged, 58°C, 2hrs (> 50°C 5hrs)
Con C -30	UV + Heat Aged, -30°C, 72hrs

Table 11.2 Ageing and treatment regimes for the unloaded test samples

11.1.1 Unloaded Test Sample Results

Table 11.3 shows the tensile properties relating to the unloaded samples after being subjected to the raised and lowered temperature regimes. It is clear that there is no significant effect on the majority of the tensile properties of the material. However, the modulus for the aged samples subjected to raised and lowered temperatures have increased from 7.6 ±0.1 (Con C 23) to 9.5 ±0.2 and 9.1 ±0.2 (Con C 58 and Con -30 respectively). This affect can be seen in Figure 11.2.

It should be noted that the artificially aged samples exhibit reduced tensile properties. These differences have been described fully in Section 10.1, Chapter 10. It is the 'within group' variations that are of particular interest here.

Sample	Breaking Load/N	Strain/%	Energy at Maximum Load/J	Young's Modulus
Con A 23	286.7 ±7.8	34.0 ±0.7	3.7 ±0.2	8.3 ±0.2
Con A 58	290.8 ±8.9	34.0 ±0.9	3.8 ±0.2	8.7 ±0.4
Con A -30	294.5 ±8.6	33.6 ±0.4	3.8 ±0.1	9.2 ±0.2
Con C 23	144.1 ±3.8	18.9 ±0.5	1.0	7.6 ±0.1
Con C 58	156.5 ±11.7	19.3 ±0.9	1.1 ±0.1	9.5 ±0.2
Con C -30	148.3 ±5.4	19.0 ±0.4	1.0 ±0.1	9.1 ±0.2

Table 11.3 Tensile properties of the unloaded test samples

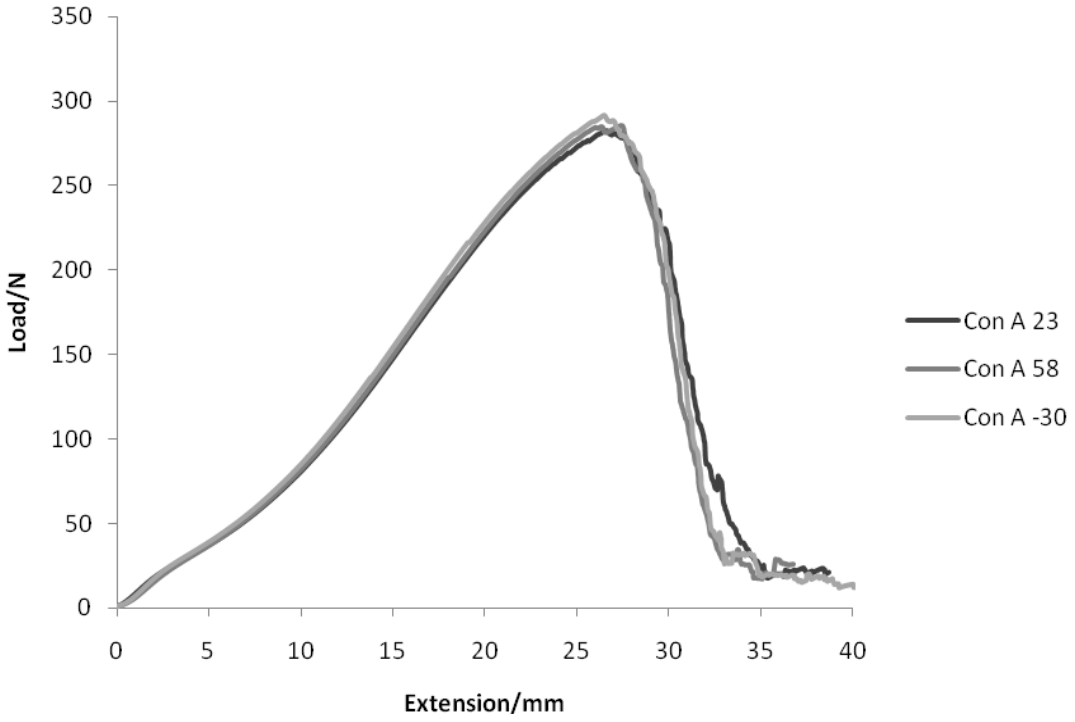

Figure 11.1 Averaged force vs elongation curve for Con A unloaded test samples, resulting from the average of seven repeat measurements for Con A23, A58 and A-30 (gauge length of 80mm)

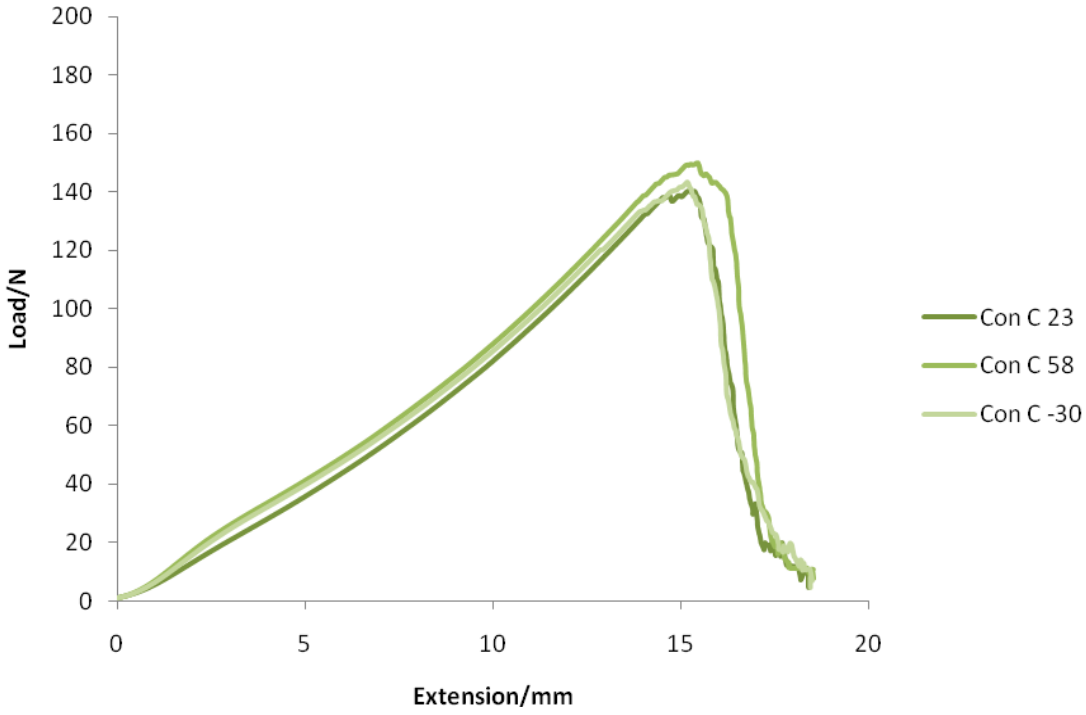

Figure 11.2 Averaged force vs elongation curve for Con C unloaded test samples, resulting from the average of seven repeat measurements for Con C23, C58 and C-30 (gauge length of 80mm)

The results for the Pol ATR data (Table 11.4) show that within the experimental error, there are no significant changes in the anisotropy of the unaged samples when subject to raised and lowered temperatures, Con A 58 and Con A -30 respectively. However, there does appear to be a decrease in the structural order when the aged material is treated with the different temperature regimes (Con C 58 and Con C -30). The D_{1196} ratio is seen to decrease after treatment, whilst D_{1416} and D_{1631} are shown to increase.

Sample	**Ratio 0/90 D_{1196}**	**Ratio 0/90 D_{1416}**	**Ratio 0/90 D_{1631}/D_{1530}**
Con A 23	1.89 ±0.06	0.34 ±0.01	0.38 ±0.03
Con A 58	2.04 ±0.23	0.30 ±0.01	0.41
Con A -30	1.76 ±0.17	0.35 ±0.04	0.47 ±0.04
Con C 23	1.94 ±0.03	0.30 ±0.02	0.33 ±0.02
Con C 58	1.57 ±0.12	0.38 ±0.04	0.46 ±0.02
Con C -30	1.49 ±0.07	0.41 ±0.02	0.50 ±0.02

Figure 11.4 Dichroic ratios for the unloaded test samples

Calculations of the percentage crystallinity using the DSC data also show a small decrease after treatment (Table 11.5). For the unaged samples this decrease is greatest in the sample subject to -30°C. Whereas in the aged material greatest decrease is seen in the sample treated at 58°C in the Thermo Lignum® process.

For samples treated at elevated temperature there is a small increase in the glass transition temperature. For the unaged material, there appears to be a decrease in the Tg when treated at -30°C. This may be caused by the plasticisation effect of moisture, present as condensation as the sample was brought back to room temperatures (Section 4.1.3, Chapter 4).

Sample	Crystallinity/%	Variance/%	Tm/°C	Variance/°C	Tg/ °C	Variance/°C
Con A 23	54.7		266.8		35.3	
Con A 58	52.7		267.7		37.3	
Con A -30	50.0		265.9		31.9	
Con C 23	51.9	0.8	263.2	0.2	33.2	0.6
Con C 58	48.4		264.0		35.9	
Con C -30	52.9		264.9		35.4	

Table 11.5 Percentage crystallinity and thermal transitions for the unloaded test samples as determined by DSC

The unprocessed DSC heating curves for the unaged samples Con A 23, Con A 58 and Con A -30 are shown in Figure 11.3. Qualitatively, all three samples apear to show similar behaviour. On close inspection of the shape of the melting endotherm the shoulder seen at 259°C in Con A 23 is reduced in Con A 58 after treatment above room temperature (Figure 11.4).

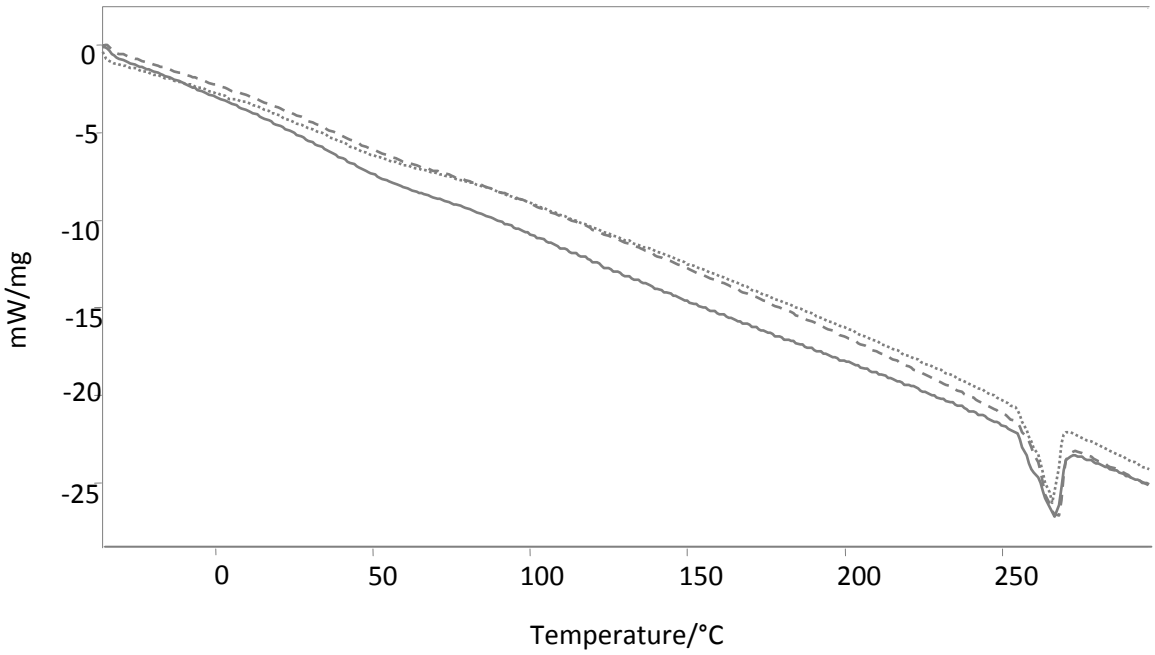

Figure 11.3 DSC Heating Curves for Con A unloaded test samples, Con A 23 (solid), Con A 58 (dashed) and Con A -30 (dotted)

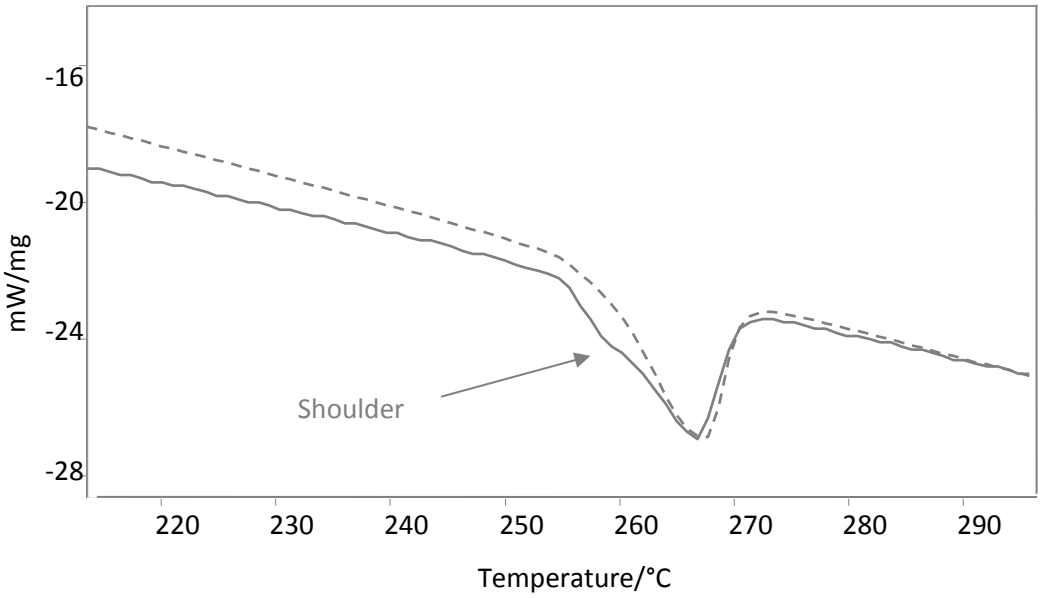

Figure 11.4 Expanded region of the DSC heating curves for Con A unloaded test samples, Con A 23 (solid) and Con A 58 (dashed)

The unprocessed DSC heating curves for the aged samples Con C 23, Con C 58 and Con C -30 are shown in Figure 11.5. Although it is apparent that there is a slight shift of the melting endotherm to higher temperatures following pest control treatment, 263°C to 264°C and 264.9°C , the shape of the peak apears to be consistent for all three aged samples.

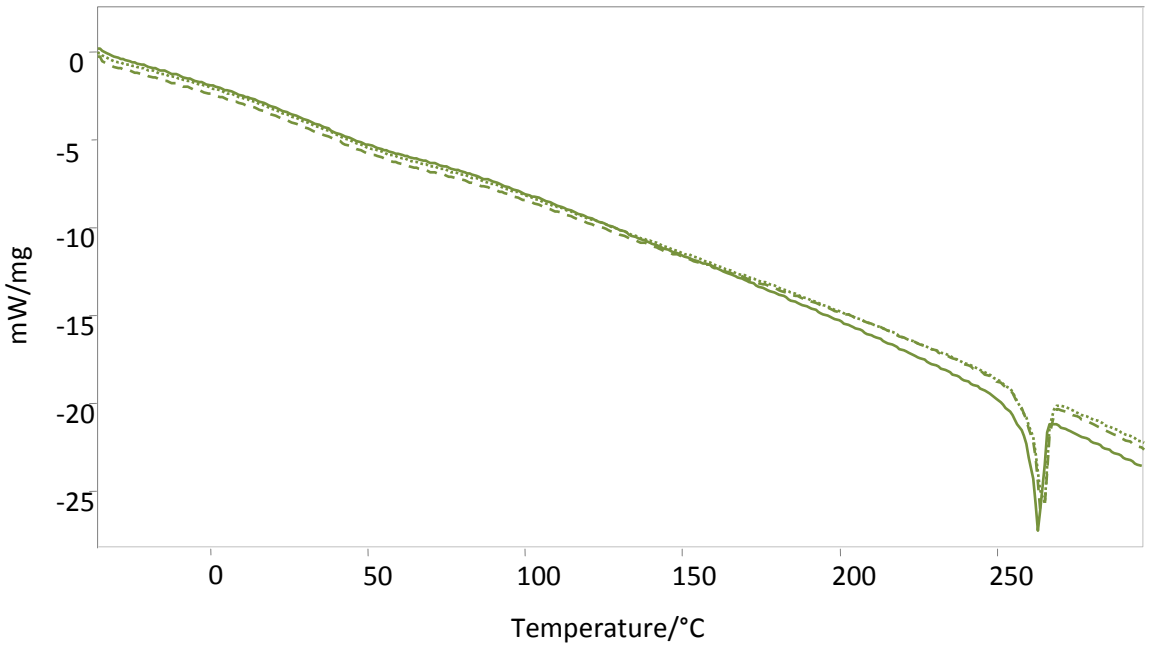

Figure 11.5 DSC Heating curves for Con C unloaded test samples, Con C 23 (solid), Con C 58 (dashed) and Con C -30 (dotted)

11.1.2 Unloaded Test Sample Discussion

A summary of the results for the unloaded test samples are presented below.

Sample	Breaking Load/N	Strain/%	Young's Modulus	Ratio 0/90 D_{1196}	Ratio 0/90 D_{1416}	Ratio 0/90 D_{1631}	% Crystallinity DSC
Con A 23	286.7 ±7.8	34.0 ±0.7	8.3 ±0.2	1.89 ±0.06	0.34 ±0.01	0.38 ±0.03	54.7
Con A 58	290.8 ±8.9	34.0 ±0.9	8.7 ±0.4	2.04 ±0.23	0.30 ±0.01	0.41	52.7
Con A -30	294.5 ±8.6	33.6 ±0.4	9.2 ±0.2	1.76 ±0.17	0.35 ±0.04	0.47 ±0.04	50.0
Con C 23	144.1 ±3.8	18.9 ±0.5	7.6 ±0.1	1.94 ±0.03	0.30 ±0.02	0.33 ±0.02	51.9 ±0.8
Con C 58	156.5 ±11.7	19.3 ±0.9	9.5 ±0.2	1.57 ±0.12	0.38 ±0.04	0.46 ±0.02	48.4
Con C -30	148.3 ±5.4	19.0 ±0.4	9.1 ±0.2	1.49 ±0.07	0.41 ±0.02	0.50 ±0.02	52.9

Table 11.6 Results summary for unloaded test samples

The reader is reminded that it is the 'within group' variations that are of most interest.

As discussed in Chapter 8, the Thermo Lignum® treatment takes place at 20 °C or more above the apparent glass transition temperatures of the samples, so that the amorphous regions should become somewhat mobile. The freezing treatment might be expected to influence the internal structure of sorbed moisture within the polyamide fibres. Nonetheless, the unaged material does not appear to exhibit any alterations in the underlying internal order when subject to either pest control method, according to the Pol ATR data.

It is also shown that there are no significant changes in the tensile properties or surface isotropy of the unaged material after treatment at raised temperatures (Con A 58). On inspection of the DSC melting endotherm (Figure 11.4), the crystalline regions appear to be more homogenous. This behaviour is accompanied by a small increase in the glass transition, which suggests that at elevated temperatures there has been a degree of re-organisation of the crystallites.
There does appear to be a small increase in the modulus after treatment at -30°C (Con A -30). This shows that there has been a stiffening of the sample. The reasons for this effect at lowered temperatures are not apparent. At the point of testing, the samples had equilibrated at ambient temperatures for over one week. Therefore, the brittle properties found at sub-ambient temperatures would have been reversed. The increase in modulus is accompanied by a drop in the percentage crystallinity and a reduction in the glass transition temperature. These latter properties may indicate the penetration of moisture into the structure, but are anomalous with the change in ductility at low stresses.

The aged samples show a significant drop in anisotropy after treatment with both raised and lowered temperatures (Con C 58 and Con C -30). This is accompanied by an increase in the modulus for both. Con C 58 also exhibits a decrease in percentage crystallinity and a small increase in Tg. The relative humidity remained constant during the Thermo Lignum® treatment (Section 8.3.1, Chapter 8). Therefore the alterations to the structure of the material may be attributed to the elevated temperatures. The results suggest that there may be two concurrent mechanisms. One of cross-linking at scission points causing an increase in the modulus. The second being chain scission, propagated by elevated temperatures, disrupting the zones peripheral to the crystalline regions and reducing order. In contrast, the significant reduction in anisotropy in Con C -30 after treatment at sub-ambient temperatures may be caused by changes in intermolecular bonding consequent

upon rearrangement of water molecules within the amorphous regions of polyamide. Echalier *et al* [1] showed that at temperatures below 0°C microvoids along the fibre result in stress concentrations. Such voids may be responsible for increasing the breakdown of the polymer chains at the surface of the fibres.

11.1.3 Conclusions for Unloaded Test Samples

The pest control methods have not caused any major changes in the tensile properties of either the unaged or aged samples. However, there does appear to be some reduced ductility in Con A -30, Con C 58 and Con C -30.

For the unaged samples there are some underlying structural changes. At elevated temperatures there is the suggestion of an increase in crystal perfection, although these differences are small. For sub-ambient conditions, the alterations are more significant. However the mechanisms of change are less easily resolved. Comparing the results for unaged, unloaded material suggests that the low temperature treatment poses the marginally higher risk.

Regarding the aged material, the treatments have caused a decrease in order, accompanied by a reduction in crystallinity at raised temperatures. These alterations are attributed to different mechanisms. The magnitude of change is perhaps somewhat greater at elevated temperatures, indicating that the sub-ambient treatments may be the preferred method where unloaded, aged polyamides are concerned.

11.2 Creep/Recovery and *in situ* Loaded Test Samples

The following section will discuss the results from the creep/recovery experiments at raised and lowered temperatures, along with the corresponding samples that were loaded *in situ* during the pest eradication treatments.

As described in Chapter 9, the creep/recovery experiments were carried out using a DMTA. After an initial five minute soak time, where the sampling chamber equilibrates at temperature, a stress of 0.31MPa was applied and the sample crept for 150 minutes. After which time the stress was removed and the sample was allowed to recover for 300 minutes. The nature of the experimental programme meant that the instrument could not be programmed to apply the stress to the textile before reaching the desired temperature. Therefore, these experiments are not a direct representation of a textile being treated hanging under its own weight. This must be borne in mind when interpreting the results and drawing inferences regarding textile garments. However, low stress creep testing should give a useful insight into the sensitivity of the materials to the differing processing conditions.

In the true case the textile yarns would already be under load prior to changing the temperature, and this would remain in place as the temperature profile was brought back to ambient conditions. This is why a test set of specimens were treated *in situ*, which were suspended from wooden frames and 50g loads applied directly to the bottom of the textile. In this case the loads were applied prior to reaching the temperature of interest and removed subsequent to reaching room temperature again.

11.2.1 Unaged Creep/Recovery and *in situ* Loaded Test Sample Results

The table below lists the conditions applied to each of the unaged samples.

Sample	Ageing and Treatment Regimes
Con A DMTA 23	Unaged + creep @ 23°C
Con A DMTA 58	Unaged + creep @ 58°C
Con A DMTA -30	Unaged + creep @ -30°C
Con AL 23	Unaged, 23°C + loaded *in situ*, 72 hrs
Con AL 58	Unaged, 58°C + loaded *in situ*, 58°C, 2hrs (> 50°C 5hrs)
Con AL -30	Unaged, -30°C + loaded *in situ,* 72hrs

Table 11.7 Treatment regimes for Con A creep/recovery and *in situ* loaded test samples

Due to access constraints on the equipment, it was not possible to run repeat analyses for each experimental condition to determine the error. Therefore statements regarding the numerical outputs should be treated as tentative. However, for one sample, a double run on two separate days was performed to give an indication of the reproducibility of the method and consistency in the sample behaviour. The overlaid graphs are shown in Figure 11.6. It can be seen, that not only do the two sets of data follow the same trend qualitatively, but from a quantitative view point they also lie in close proximity to each other. Curve 1 is, on average, 0.3% higher than Curve 2 in the creep part of the graph. From this data, and that of the tensile work discussed in previous sections, it would suggest that the material is behaving in a consistent manner and any variations in the creep behaviour at different temperatures are likely to be true effects.

The details of these curves will be covered in Section 11.2.1.1.

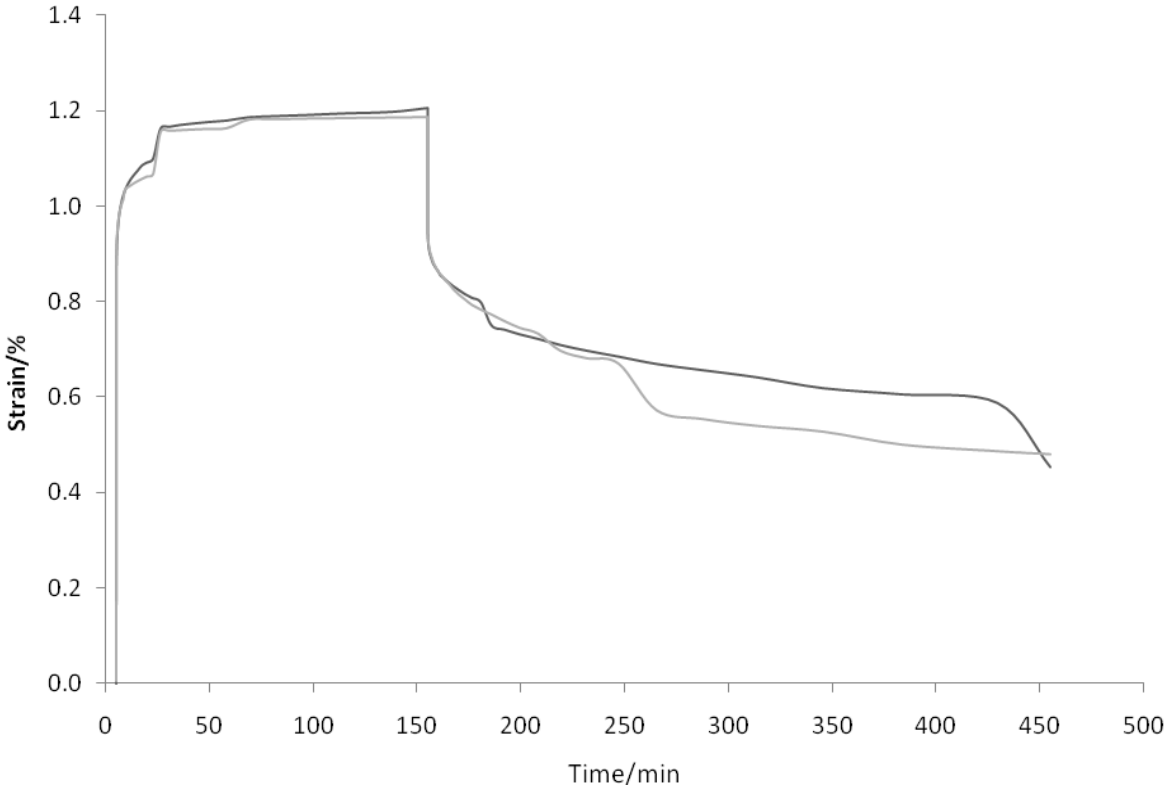

Figure 11.6 Repeat creep/recovery curves for Con A DMTA 58 illustrating the reproducibility, Curve 1 (dark grey) and Curve 2 (pale grey)

11.2.1.1 Creep/Recovery Experiments for Unaged Test Samples at Elevated Temperatures

Figure 11.7 shows the creep/recovery curves for the unaged material at 23°C and 58°C, Con A DMTA 23 and Con A DMTA 58 respectively.

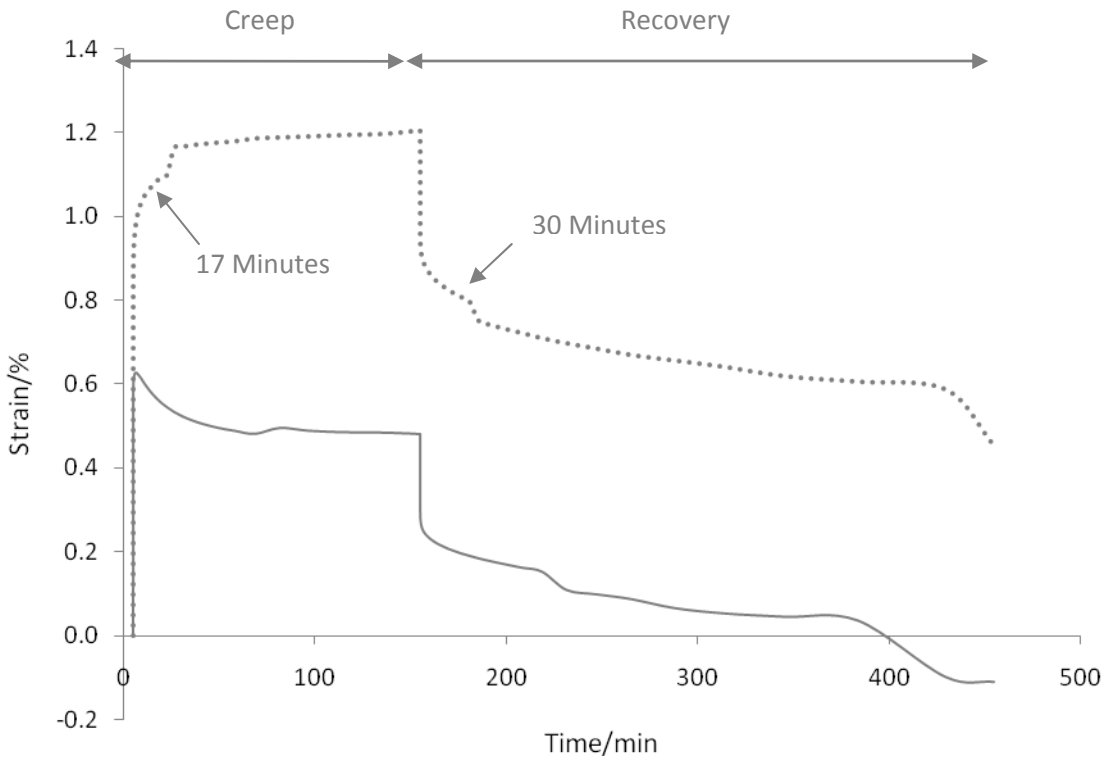

Figure 11.7 Creep/recovery curves for Con A DMTA 23 (solid) and Con A DMTA 58 (dotted)

The reader is referred back to Section 10.2.1, Chapter 10 for a full discussion of Con A DMTA 23, but reminded that the contraction behaviour seen in the creep section of the curve was attributed to strain induced crystallisation. In contrast, Con A DMTA 58 shows a completely different type of behaviour. As previously described for Con A DMTA 23, loading the sample causes an initial positive strain, attributed to the physical displacement of yarns. This displacement was followed by a negative strain, or contraction. For Con A DMTA 58, after the initial, rapid displacement of the yarns, the strain continues to increase, but at a slower rate. This is attributed to the extension and rearrangement of the amorphous polymer chains under load above Tg. Seventeen minutes into the creep

experiment there is a discontinuous increase in the displacement of the sample followed by a constant low creep rate (Figure 11.7).

The initial contraction seen at 23°C in Con A DMTA 23 is not present at 58°C. Although the sudden positive strain is visible at 23°C and 58°C, it is clear that there is a second, overriding mechanism, masking the initial load induced contraction experienced at room temperature (Section 10.1.1, Chapter 10).
In order to further examine the onset of these two differing behaviours, two supplementary experiments were carried out at intermediate temperatures, 35°C and 45°C.

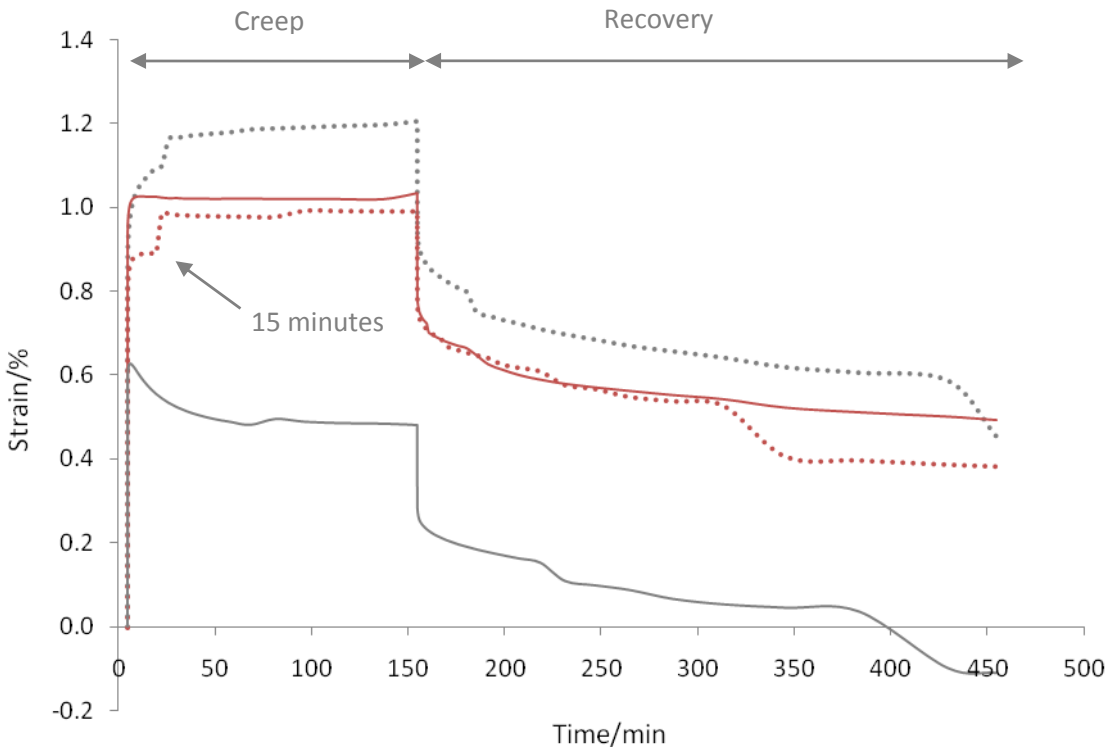

Figure 11.8 Creep/recovery curves for Con A samples at elevated temperatures. Con A DMTA 23 (solid grey), Con A DMTA 35 (solid red), Con A DMTA 45 (dotted red) and Con A DMTA 58 (dotted grey)

For Con A DMTA 35, it is still possible to see a small degree of strain induced contraction when the sample is subject to loading at 35°C (solid red line in Figure 11.8). However, at 45 °C this has completely disappeared and the sample is showing similar behaviour to Con A

DMTA 58 at 58°C. The point of discontinuity in Con A DMTA 45 occurs at approximately 15 minutes into the creep experiment.

This particular test occurs at the mid-point of the glass transition temperature for the unaged material, shown to be 35°C for the unaged, unloaded control sample Con A (Section 10.2.1, Chapter 10). As previously discussed, the Tg is not a single temperature value, but refers to a range of temperatures over which the material experiences a change in its viscoelastic properties.

11.2.1.2 Creep/Recovery Experiments for Unaged Test Samples at Lowered Temperatures

Figure 11.9 compares the creep/recovery curves for the unaged material at 23°C and -30°C, Con A DMTA 23 and Con A DMTA -30 respectively.

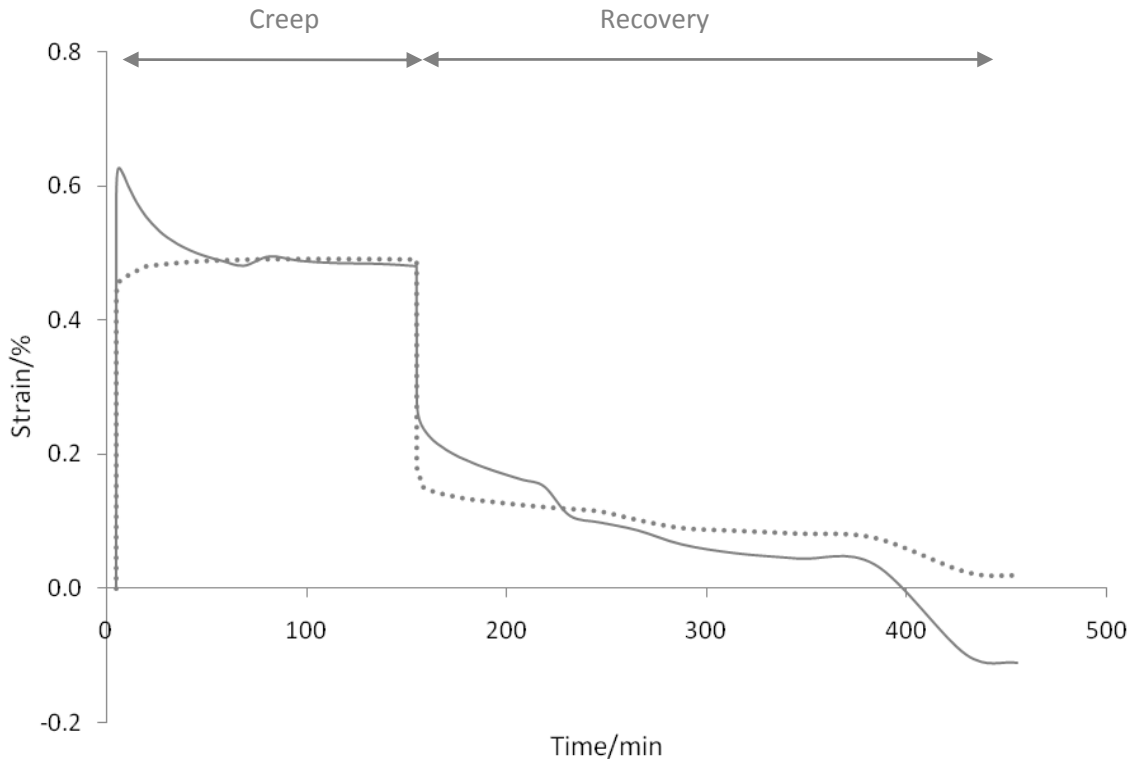

Figure 11.9 Creep/recovery curves for Con A DMTA 23 (solid) and Con A DMTA -30 (dotted)

For the sub-ambient sample Con A DMTA -30, the initial displacement is reduced, due to a more rigid structure. The low temperatures reduce chain mobility, possibly with the

additional constraint of the freezing of sorbed moisture. It is clear that the strain induced contraction does not occur. There is insufficient energy to allow for rearrangement and subsequent crystallisation. On removal of the load the sample returns to its original length in a typical viscoelastic manner.

As with the raised temperatures, supplementary experiments were carried out between room temperature and -30°C to help bridge the temperature gap. These were carried out at 0°C and -15°C, and are presented in Figure 11.10.

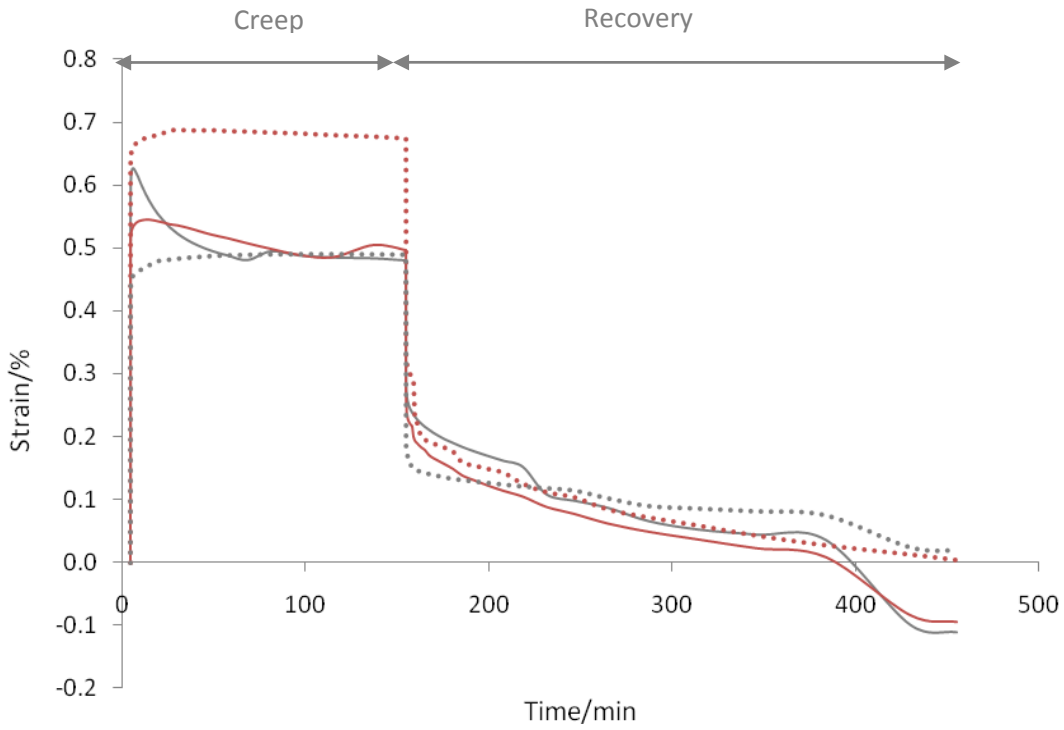

Figure 11.10 Creep/recovery curves for Con A samples at sub-ambient temperatures. Con A DMTA 23 (solid grey), Con A DMTA 0 (solid red), Con A DMTA -15 (dotted red) and Con A DMTA -30 (dotted grey)

It is apparent that at 0°C there is still a small degree of contraction present after the initial displacement (solid red line in Figure 11.10). This suggests the temperature is still sufficiently high to allow some degree of rearrangement and crystallisation. This effect is not seen in the sample loaded at -15°C (dotted red line). This resembles the same behaviour as Con A DMTA -30. Con A DMTA -15 shows a significantly greater deformation

than the other sub-ambient samples. The reasons for this difference are not immediately apparent.

The final creep strain is plotted against temperature for all of the unaged samples. It is quite clear that raising the temperature above ambient causes increased displacement. At 58°C the final strain is 0.7% higher than at 23°C. The general trend below room temperature is one of restricted deformation.

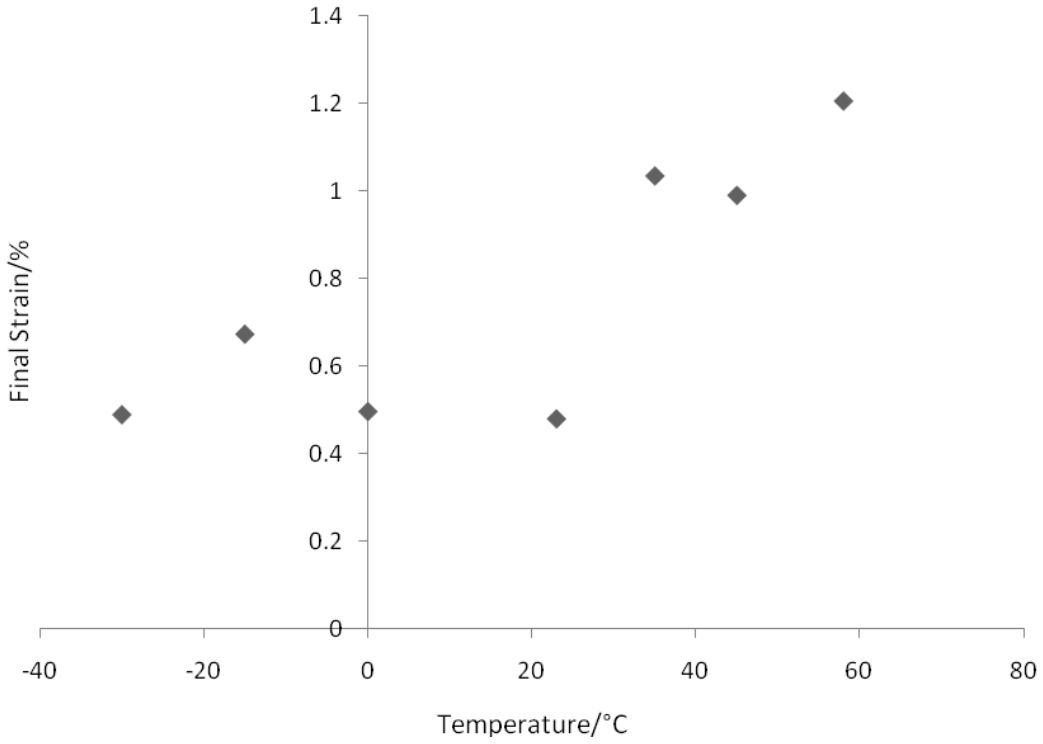

Figure 11.11 Final creep strain vs temperature for Con A DMTA samples

11.2.1.3 Post Analyses for Creep/Recovery and *in situ* Loaded Unaged Test Samples

The following results relate to the analyses carried out on the samples subjected to creep/recovery tests and *in situ* loading.

The dichroic ratios for the Pol ATR experiments are presented in Table 11.8. The results show an increase in the anisotropy of all unaged material after treatment at 58°C and -30°C. This is seen as a decrease in the D_{1196} ratio and an increase in the D_{1416} and D_{1631} ratios.

Sample	Ratio 0/90 D_{1196}	Ratio 0/90 D_{1416}	Ratio 0/90 D_{1631}/D_{1530}
Con A DMTA 23	1.87 ±0.32	0.33 ±0.06	0.39 ±0.07
Con A DMTA 58	1.58 ±0.17	0.45 ±0.07	0.54 ±0.05
Con A DMTA -30	1.49 ±0.03	0.45 ±0.02	0.55 ±0.02
Con AL 23	1.78 ±0.02	0.40 ±0.03	0.46 ±0.05
Con AL 58	1.57 ±0.02	0.44 ±0.02	0.54 ±0.03
Con AL -30	1.61 ±0.05	0.43 ±0.01	0.53 ±0.02

Table 11.8 Dichroic ratios for Con A creep/recovery and *in situ* loaded test samples

Figure 11.12 and 11.13 show the DSC heating curves for the creep/recovery and in situ loaded samples, respectively. The characteristics of the melting endotherms do not indicate any large scale alterations in the underlying structure. It is worth noting the differences in scale on the Y axis for the two figures. As discussed in Section 10.2.1 the application of a load has induced a significant change in the slope of the samples. The reasons for this are not fully understood at this time.

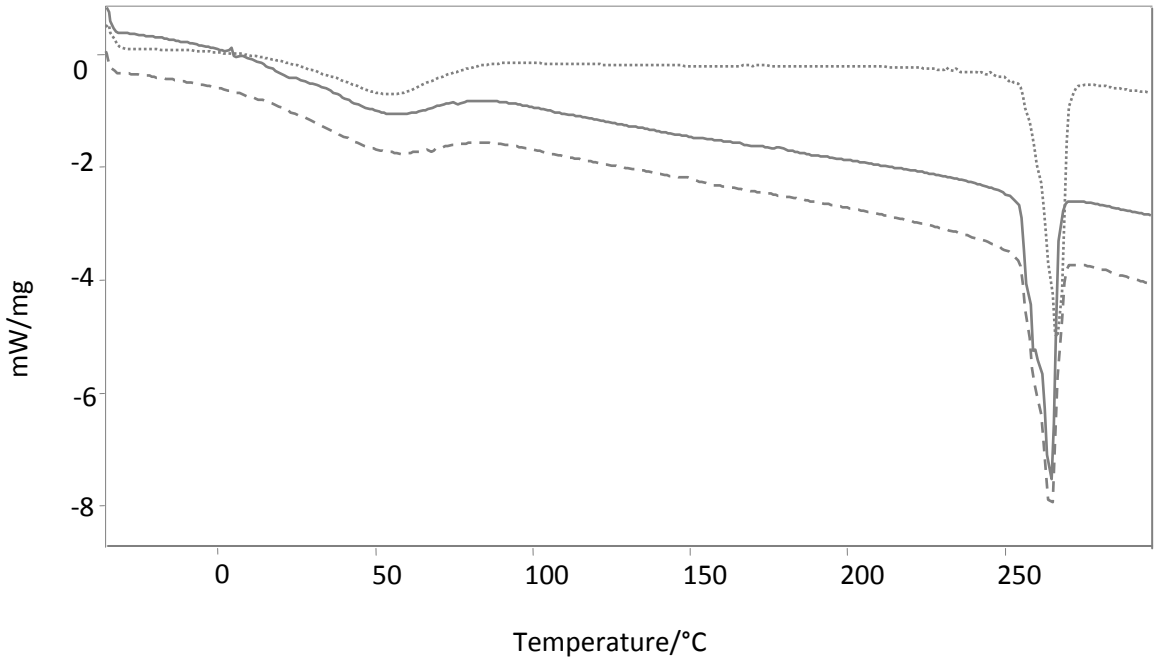

Figure 11.12 DSC heating curves for Con A creep/recovery samples. Con A DMTA 23 (solid) Con A DMTA 58 (dashed) and Con A DMTA -30 (dotted)

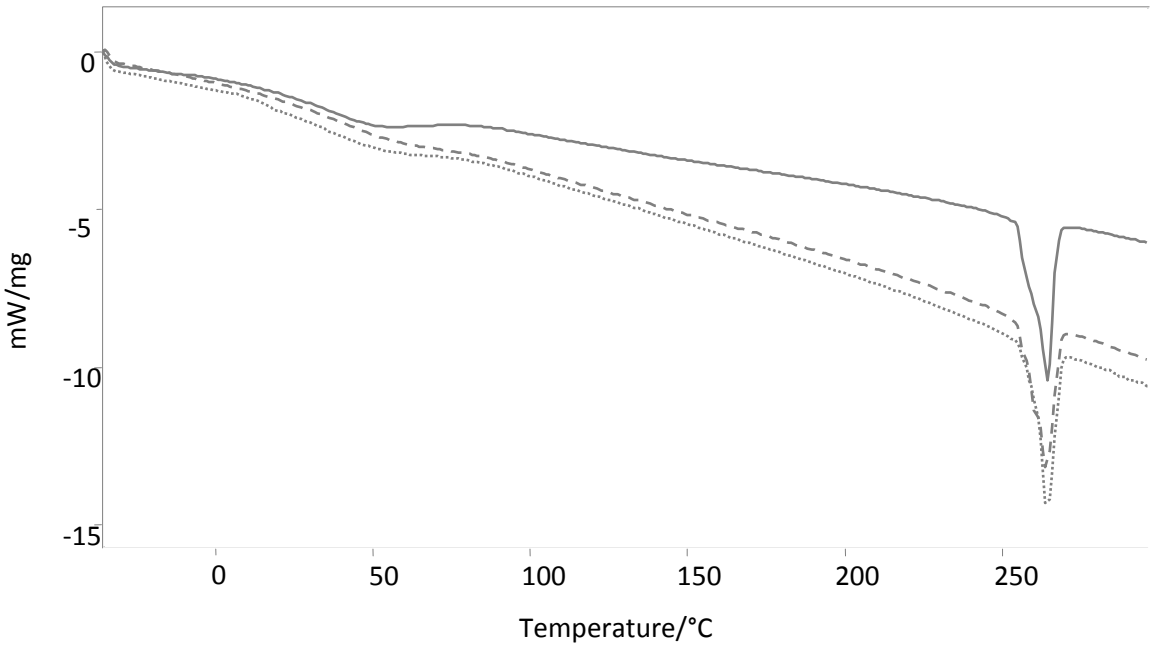

Figure 11.13 DSC heating curves for Con A loaded test samples, Con AL 23 (solid), Con AL 58 (dashed) and Con AL -30 (dotted)

The polarized ATR data and DSC data show that there is a decrease in the anisotropy of the material and crystallinity, above and below room temperature. This follows the same behaviour for both the creep/recovery samples and those loaded *in situ*, though the decrease in crystallinity is less pronounced for Con AL 58.

Sample	Crystallinity/%	Tm/°C	Tg/ °C
Con A DMTA 23	57.2	264.2	35.7
Con A DMTA 58	53.2	265.0	32.3
Con A DMTA -30	52.4	266.9	36.1
Con AL 23	58.1	264.1	33.9
Con AL 58	57.1	264.1	38.6
Con AL -30	52.2	264.1	36.1

Table 11.9 Percentage crystallinity and thermal transitions for Con A creep/recovery and *in situ* loaded test samples as determined by DSC

11.2.2 Unaged Creep/Recovery and *in situ* Loaded Test Sample Discussion

The results for the unaged loaded samples are summarised below.

Sample	Initial Strain /%	Final Strain Under Load/%	Final Strain After Recovery/%	Ratio 0/90 D_{1196}	Ratio 0/90 D_{1416}	Ratio 0/90 D_{1631}	Crystallinity/ %
Con A DMTA 23	0.56	0.48	-0.11	1.87 ±0.32	0.33 ±0.06	0.39 ±0.07	57.2
Con A DMTA 58	0.82	1.2	0.45	1.58 ±0.17	0.45 ±0.07	0.54 ±0.05	53.2
Con A DMTA -30	0.41	0.49	0.02	1.49 ±0.03	0.45 ±0.02	0.55 ±0.02	52.4
Con AL 23				1.78 ±0.02	0.40 ±0.03	0.46 ±0.05	58.1
Con AL 58				1.57 ±0.02	0.44 ±0.02	0.54 ±0.03	57.1
Con AL -30				1.61 ±0.01	0.43 ±0.01	0.53 ±0.02	52.2

Table 11.10 Results summery for unaged loaded test samples

The creep/recovery curve at 58°C exhibits a very different behaviour to the room temperature test (Figure 11.7). It is proposed that the discontinuity 17 minutes into the experiment is caused by a slippage movement in the crystal structure of the polymer. As the extended polymer chains are uniaxially drawn, the closely packed crystal regions slip past each other to reach a different conformation. The stress within the polymer system causes the crystal units to tilt and re-orientate, and glide over each other. This is a similar behaviour to drawing of crystalline fibres, such as polyethylene. The crystals are found to deform via stack rotation, sliding of lamellae and chain slip [2].

Zaukelies [3] proposed a model for the slippage of polyamide 6,6 crystallites in bristles, similar to those found in inorganic crystalline materials; with the crystal regions consisting of vacancies, dislocations and grain boundaries. The study focused on the compression/slippage behaviour of the filaments, but it would be justified to propose the opposite behaviour is occurring during creep.

Once this reorientation has occurred the strain remains almost constant. The crystal bonds are not broken, they are only stretched. This is apparent from the recovery section of the curve. Once the load is removed the effect is reversed.

Although it is the creep section of the curve that is of primary interest, the recovery of the polymer mirrors the creep behaviour. The initial negative strain is caused by contraction of the yarns on removal of the load. This is seen to taper off more slowly as the elastic amorphous regions recoil. Because the sample is still at elevated temperatures the crystal regions are pulled back to their original conformation by the tie molecules, seen as a rapid negative strain at approximately 30 minutes into the recovery. At 450 minutes the sample has not recovered fully. This may suggest that applying a load to the sample at elevated temperatures had caused a degree of rupture to the polymer chains, preventing complete elastic recovery. Alternatively, simple slippage without rupture may not be fully recoverable.

The creep tests at 35°C and 45°C provide useful insight into the intermediate behaviour of the unaged samples. The results illustrate that as the sample is nearing its Tg the creep behaviour will start to exhibit greater deformation when under load, but may still retain some lower temperature characteristics. As the temperature is increased further (Con A DMTA 45) these initial mechanisms become dominated by another process as proposed above, made possible by the higher temperatures.
On application of a load at room temperature to the control samples, there was an apparent increase in crystallinity e.g. Con A 23 → Con AL 23 (Section 10.2.1, Chapter 10). This result was in keeping with the expected behaviour of a polyamide on uniaxial drawing. On exertion of the same load above the glass transition temperature it might be expected that the degree of order and crystallinity would increase, as mobility restrictions are reduced and the polymer chains might more readily align along the fibre axis. In fact, the opposite behaviour is seen. Con A DMTA 58 experiences a decrease in the anisotropy and percentage crystallinity, compared to Con A DMTA 23. Similar behaviour is seen when the samples were loaded *in situ* (Con AL 58), but to a lesser extent. It would appear that the enhanced chain mobility has inhibited strain induced crystallisation. This behaviour may confirm that there has been a degree of rupture, which is manifest as an incomplete recovery in the creep/recovery curve.

For the three creep/recovery samples at elevated temperatures, the final strain under load is double that seen at room temperature (Figure 11.12). Con A DMTA 58 is 0.7% longer at the end of the creep test than Con A DMTA 23. If the final strain in the creep section of Con A DMTA 23 is regarded as the baseline for comparison, the results suggest that applying

raised temperature treatments to a hanging garment may have a noticeable effect on the fabrics dimensions.

The low temperature creep experiments exhibit a clear reduction in mobility. The strain induced crystallinity that occurs at ambient temperatures does not occur. This is caused by a decrease in energy, resulting in reduced molecular mobility. The mobility in the polymer chains are restricted, preventing rearrangement to new conformations. The initial displacement of the fibres is also reduced from 0.56% to 0.41%, in Con A DMTA 23 and Con A DMTA -30 respectively. However, at the end of the creep section of the curve, the final strain at -30°C is equal to that at 23°C.

The two additional experiments at intermediate temperatures provided useful information on the temperature dependence of the different behaviours. At zero degrees centigrade there still appears to be a small degree of contraction in the sample subsequent to the initial displacement. This suggests that there is still sufficient energy in the system for rearrangement. On lowering the temperature further to -15°C, the contraction disappears and the sample qualitatively behaves like that sample at -30°C. However, the initial extension is considerably increased. A result that is anomalous with the expected behaviour.

On removal of the load, Con A DMTA -30 recovers fully at 450 minutes. This suggests that the underlying structure is unaltered by the application of a load. However, on inspection of the post creep/recovery and *in situ* loading analysis, it is clear that there has been a reduction in the percentage crystallinity and anisotropy during low temperature treatment (Table 11.10). These results are consistent with those found at sub-ambient temperatures without loading (Table 11.6). In the case of Con A -30 the changes were attributed to disruption of intermolecular bonds caused by changes in moisture distribution. This is accompanied by surface fracture, induced by loading at sub-ambient temperatures.

11.2.3 Conclusions for Unaged Creep/Recovery and *in situ* Loaded Test Samples

Loading of the samples above and below room temperature has caused a decrease in the anisotropy and the percentage crystallinity. At raised temperatures this is attributed to a small degree of irrecoverable deformation and chain rupture. At low temperatures the reasons are attributed to moisture effects and surface cracking.

Although both raised and lowered temperatures appear to have induced alterations to the internal structure, on inspection of the creep/recovery curves it is apparent that at freezing temperatures there is less irrecoverable strain than at high temperatures. This indicated that for unaged hanging material the low temperature treatments pose a reduced risk.

11.2.4 Aged Creep/Recovery and in situ Loaded Test Sample Results

Table 11.11 lists the loading treatments applied to the aged material.

Sample	Ageing and Treatment Regimes
Con C DMTA 23	UV + heat aged + creep @ 23°C
Con C DMTA 58	UV + heat aged + creep @ 58°C
Con C DMTA -30	UV + heat aged + creep @ -30°C
Con CL 23	UV + heat aged, 23°C + loaded *in situ,* 72 hrs
Con CL 58	UV + heat aged, 58°C + load *in situ,* 58°C, 2hrs (> 50°C 5hrs)
Con CL -30	UV + heat aged, -30°C + loaded *in situ,* 72hrs

Table 11.11 Treatment regimes for Con C creep/recovery and *in situ* loaded test samples

11.2.4.1 Creep/Recovery Experiments for Aged Test Samples at an Elevated Temperature

The creep/recovery curves for the aged material at 23°C and 58°C are presented in Figure 11.14.

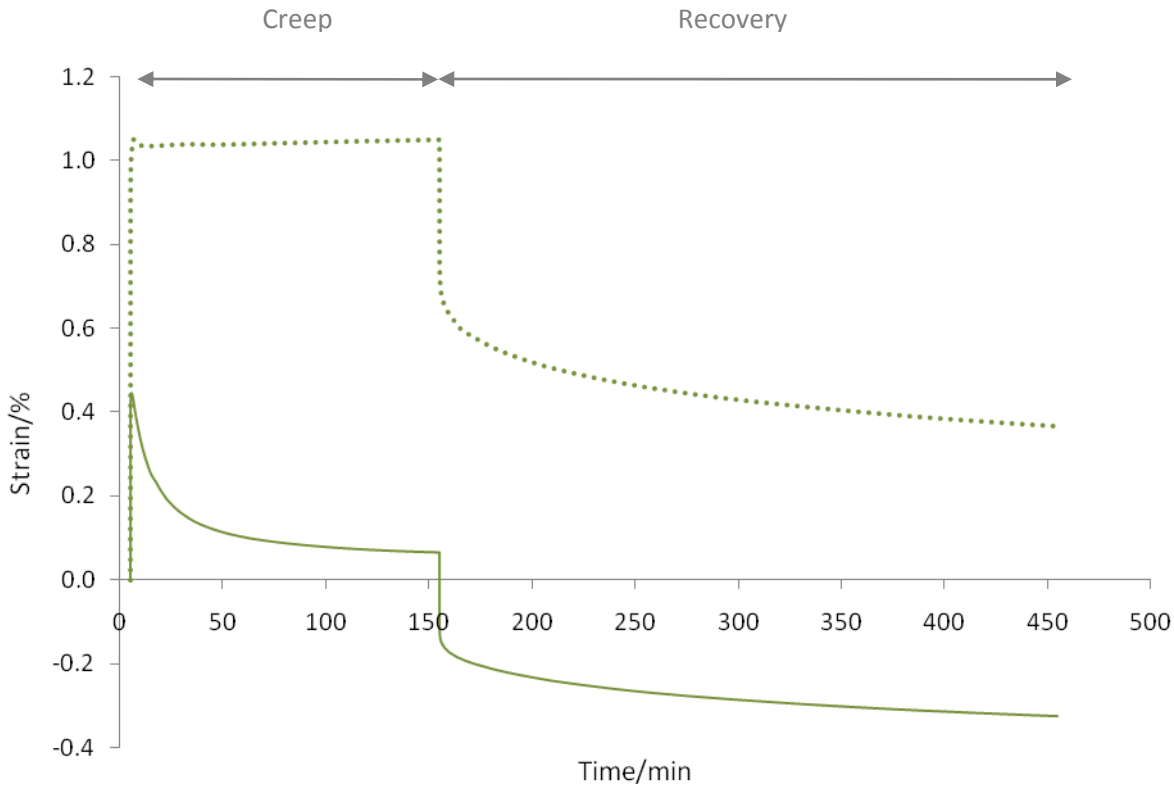

Figure 11.14 Creep/recovery curves for Con C DMTA 23 (solid) and Con C DMTA 58 (dotted)

As discussed in Section 10.2.1, Chapter 10, Con C DMTA 23 shows the same trend as Con A DMTA 23, but at 0.17% lower strain. On applying a load at elevated temperatures, the same pattern emerges. Con C DMTA 58 shows a reduced strain compared to Con A DMTA 58.

It is apparent that the slippage in the crystalline regions previously shown to occur in the unaged sample Con A DMTA 58 does not occur in the aged material. Con C DMTA 58 shows an increased initial displacement to the sample at room temperature, but does not experience the increasing extension of the amorphous regions and the crystal slip.

After the initial displacement it appears that there is a small amount of contraction in the sample, possibly indicating a degree of strain induced contraction. The over-riding slip behaviour shown to occur at and above the glass transition in the unaged samples no longer occurs.

11.2.4.2 Creep/Recovery Experiments for Aged Test Samples at a Lowered Temperature

The creep/recovery curves for the aged material at room temperature and minus 30°C are presented in Figure 11.15.

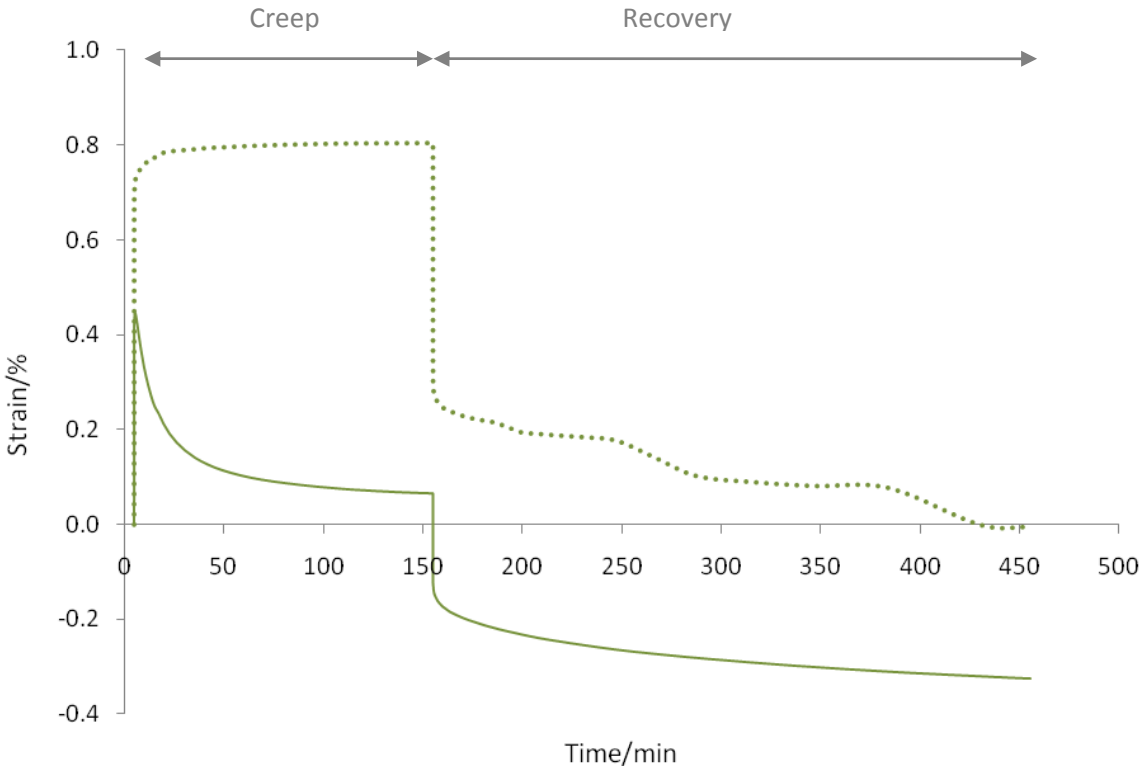

Figure 11.15 Creep/recovery curves for Con C DMTA 23 (solid) and Con C DMTA -30 (dotted)

As was shown to be the case with Con A DMTA -15, the initial displacement in Con C DMTA -30 is considerably higher than the sample treated at ambient temperatures. The reason behind this is not clear. The initial displacement is followed by a rapidly falling strain rate. The strain induced contraction seen at room temperature does not occur. Here, and as seen in the unaged samples below freezing (Con A DMTA -30), there is insufficient energy for rearrangement of the polymer chains preventing crystallisation. In the recovery section of the curve, it can be seen that after removal of the stress the sample returns to its original length.

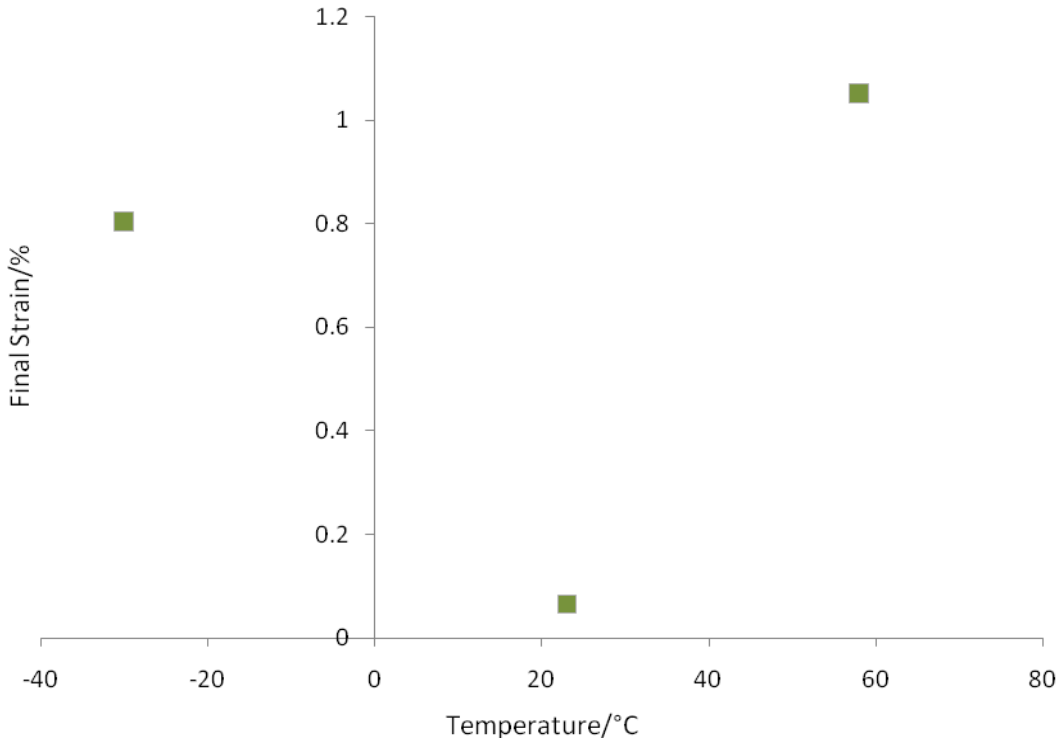

Figure 11.16 Final creep strain vs temperature for Con C DMTA samples

11.2.4.3 Post Analyses for Creep/Recovery and *in situ* Loaded Aged Test Samples

The dichroic ratios for the aged samples after loading are presented in Table 11.12.

For the aged material, the samples treated above 58°C show differing behaviour. For the creep/recovery sample Con C DMTA 58 there is an increase in order, even after accounting for the high deviations. Whereas the sample loaded in situ and treated at 58°C shows a decrease in anisotropy.

In situ loading at -30°C (Con CL -30) does not show a significant alteration in the directionality of the polymer chains. However, after creep/recovery the samples show a significant increase in orientation.

Sample	**Ratio 0/90** D_{1196}	**Ratio 0/90** D_{1416}	**Ratio 0/90** D_{1631}/D_{1530}
Con C DMTA 23	1.49 ±0.08	0.46 ±0.08	0.43 ±0.09

Con C DMTA 58	1.76 ±0.14	0.32 ±0.05	0.41 ±0.04
Con C DMTA -30	1.85 ±0.02	0.35 ±0.01	0.45 ±0.01
Con CL 23	1.74 ±0.17	0.35 ±0.06	0.39 ±0.05
Con CL 58	1.43 ±0.07	0.46 ±0.02	0.56 ±0.03
Con CL -30	1.71 ±0.16	0.36 ±0.04	0.46 ±0.04

Table 11.12 Dichroic ratios for Con C creep/recovery and *in situ* loaded test samples

After subjecting the aged sample to lowered temperatures (Con C DMTA -30) the DSC results indicates only a decrease in percentage crystallinity, whilst at raised temperatures the sample remains unchanged.

The opposite is true for Con CL -30 and CL 58, where the former is unchanged and the latter shows a small increase in crystallinity. It should be noted that it was not possible to establish a glass transition in the heating curve of Con CL -30 (Figure 11.18).

Sample	**Crystallinity/%**	**Tm/°C**	**Tg/ °C**
Con C DMTA 23	56.3	265.0	31.6
Con C DMTA 58	55.3	264.1	33.0
Con C DMTA -30	53.2	263.2	31.3
Con CL 23	54.3	265	32.7
Con CL 58	56.4	262.2	33.5
Con CL -30	54.7	263.1	

Table 11.13 Percentage crystallinity and thermal transitions for Con C creep/recovery and *in situ* loaded test samples as determined by DSC

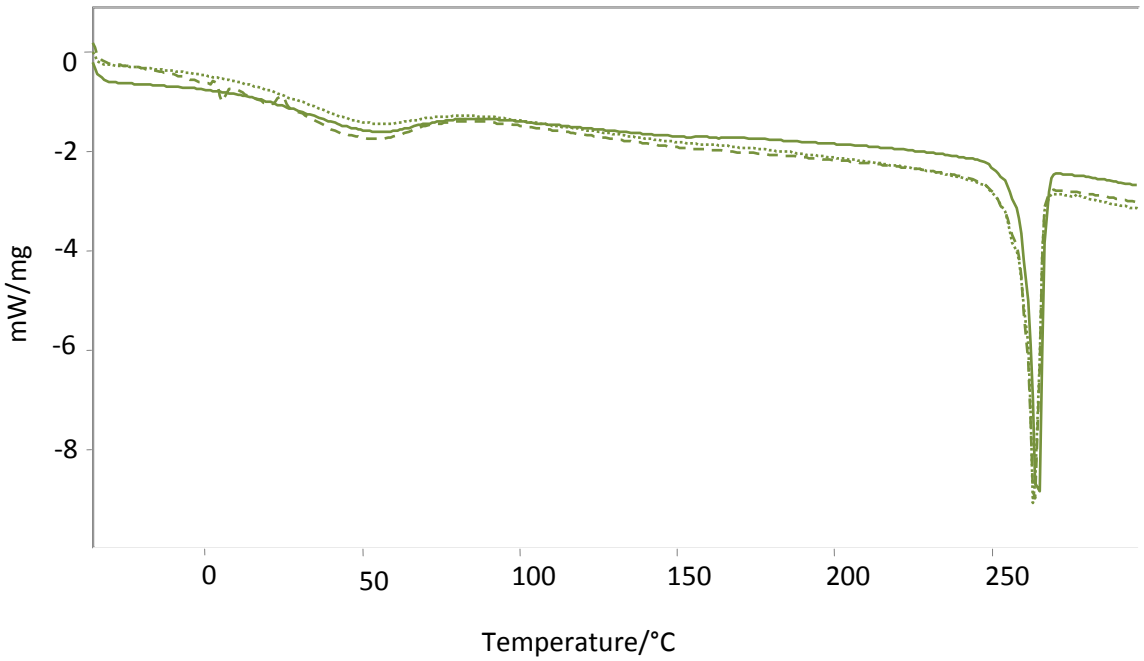

Figure 11.17 DSC heating curves for Con C creep/recovery samples. Con C DMTA 23 (solid), Con C DMTA 58 (dashed), Con C DMTA -30 (dotted)

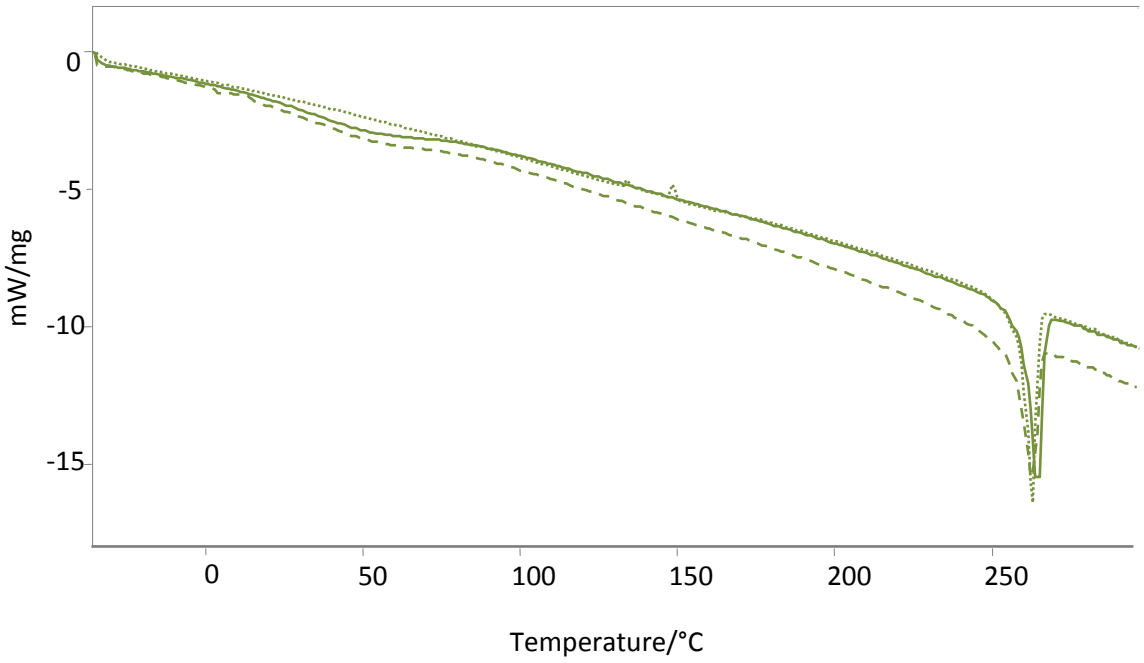

Figure 11.18 DSC heating curves for Con C loaded test samples, Con CL 23 (solid), Con CL 58 (dashed) and Con CL -30 (dotted)

11.2.5 Aged Creep/Recovery and *in situ* Loaded Test Sample Discussion

The results for the unaged loaded samples are summarised below.

Sample	Initial Strain /%	Final Strain Under Load/%	Final Strain After Recovery/%	Ratio 0/90 D_{1196}	Ratio 0/90 D_{1416}	Ratio 0/90 D_{1631}	Crystallinity/ %
Con C DMTA 23	0.39	0.07	-0.32	1.49 ±0.08	0.46 ±0.08	0.43 ±0.09	56.3
Con C DMTA 58	0.89	1.05	0.37	1.76 ±0.14	0.32 ±0.05	0.41 ±0.04	55.3
Con C DMTA -30	0.64	0.80	0.00	1.85 ±0.02	0.35 ±0.01	0.45 ±0.01	53.2
Con CL 23				1.74 ±0.17	0.35 ±0.06	0.39 ±0.05	54.3
Con CL 58				1.43 ±0.07	0.46 ±0.02	0.56 ±0.03	56.4
Con CL -30				1.71 ±0.16	0.36 ±0.04	0.46 ±0.04	54.7

Table 11.14 Results summery for aged loaded test samples

The creep/recovery curve for the aged sample at an elevated temperature shows a reduced displacement when compared to the unaged material subjected to the same conditions (Section 11.2.1.1). It is also apparent that the delayed displacement attributed to slipping of the crystallites in the unaged sample does not occur. With the experimental conditions remaining constant, these differences in behaviour can be attributed to the structure of the starting materials. It is possible that the increased anisotropy and crystal perfection (Section 10.1 and 10.2, Chapter 10) has imparted mobility restrictions on the polymer chain. This restricted conformation prevents the reversible slip mechanism seen in the unaged sample.

The corresponding analyses show that there has been an increase in surface directionality for the creep/recovery sample and a decrease for the loaded in situ sample; Con C DMTA 58 and Con CL 58 respectively. The explanation of these differences is unclear.

For the aged sample treated at -30°C, there is an increased extension to that seen at room temperature. This is anomalous with what might be expected when considering the lower temperature and therefore reduced energy. However, this behaviour is similar to that of the unaged material treated at -15°C (Figure 11.10).

On removal of the load, the sample completely recovers back to its original length. The corresponding analyses show that for the creep recovery sample there is an increase in surface orientation and a decrease in bulk crystallinity. However, for the sample loaded in situ, lowering the temperature to -30°C has not caused any significant alterations in the underlying structure of the aged polyamide.

11.2.6 Temp vs Final Strain

The shape of the temperature vs final strain plotted in Figure 11.19 follow the same pattern for both aged and unaged material. This suggests that there is similar behaviour for the unaged and aged samples at the different temperatures. It is shown that there is a drop in the final strain between -15 and -30°C in the unaged sample. This is not shown to be the case in the aged material. However, this drop must eventually occur, as the lower temperatures will eventually impose mobility restrictions on the material. The aged material has not yet reached this point. It is clear, that in all cases the low temperatures cause less irrecoverable strain than high temperature treatments[I].

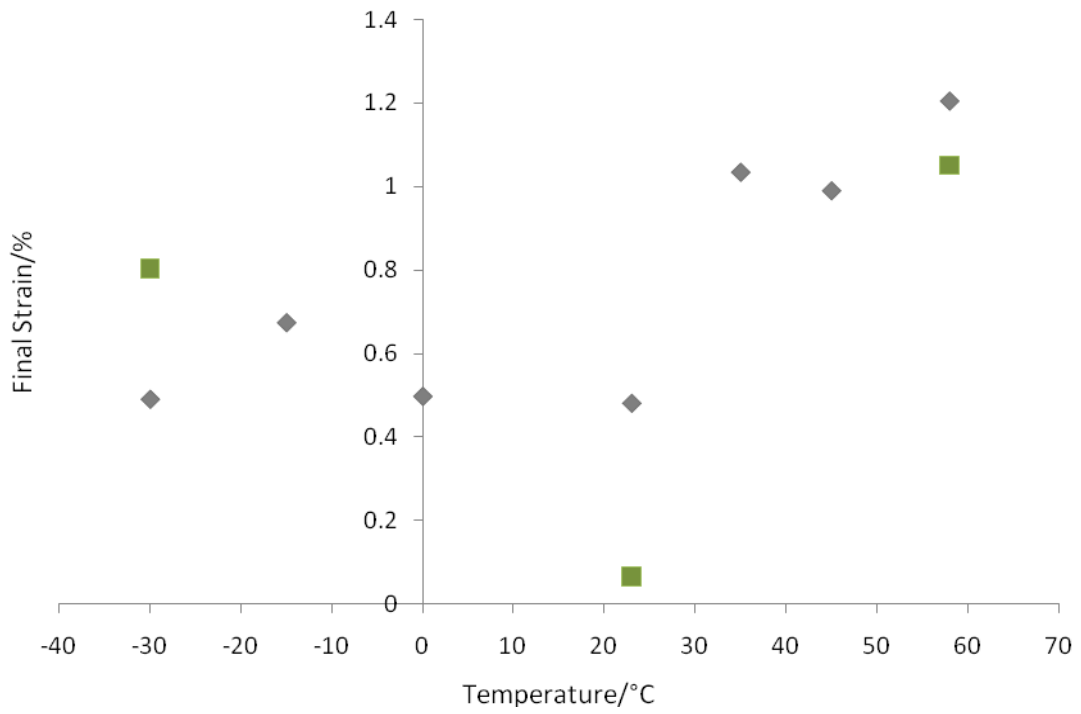

Figure 11.19 Final creep strain vs temperature for unaged (grey) and aged (green) samples

[I] Private communication with John Barnes, NIS Regional Director, INVISTA Performance Surfaces and Materials, 24 February 2009.

11.2.7 Conclusions for Creep/Recovery and in situ Loaded Test Samples

For the unaged material, the final displacement under load was significantly higher at 58°C than at room temperature. Although it is the creep section that is of primary interest, the fact that the sample did not fully recover after 450 minutes indicates permanent deformation, associated with underlying structural changes. At -30°C, the sample displacement at the end of the creep section was found to be equal to that at 23°C. This, coupled with the fact that the sample recovered fully, indicates that the low temperature treatment of unaged polyamide would be the preferred method for pest eradication.

For the aged material at 58°C, the underlying structure induced differing behaviour. After the initial displacement, the creep curve remained constant until the stress was removed. The final strain under load was greater than that at room temperature. The recovery section of the curve suggested non-elastic deformation. Contradictory results were seen in the post analyses. However, both indicated underlying structural changes had occurred. At -30°C the aged sample was shown to displace to a greater extent than at room temperature. This seems to be an anomalous result bearing in mind the reduced energy and mobility at sub-ambient temperatures, but the sample recovered to its original length after 450 minutes. For the creep/recovery sample the corresponding analyse suggested a decrease in percentage crystallinity. Whereas the sample treated *in situ* did not exhibit any underlying structural alterations after low temperature treatment.

Although there remain some unexplained results, the general pattern indicated that both the loaded unaged and loaded aged samples are more stable at sub-ambient temperatures. The final displacement under load and final strain after recovery indicate that sample deformation is reduced at lowered temperature than at elevated temperatures. However, there are clearly effects that override those seen at room temperature for a loaded sample and the outcomes may suggest that treatment of textile artefacts, both new and aged, should not be carried out whilst they are hanging under their own weight. When textiles are to be subject to these pest control treatments, where possible they should be removed from their manikins or frames and laid horizontal to minimise stress.

11.3 Conclusions

In the previous chapter, the unaged staring material had been shown to be highly oriented with reproducible tensile properties. Artificial ageing induced reduced tensile properties attributed to scission along the polymer chain, and increased surface orientation indicating some cross-linking. These two control materials were subsequently subjected to pest control treatments. Three sets of tests were carried out, where the samples were treated in their unloaded state, the samples were loaded *in situ* during treatment, and where the samples were subjected to creep/recovery loading using a DMTA.

For the unaged, unloaded material, there were no significant changes in tensile or surface properties after treatment at raised temperatures. However, there was a slight increase in the crystalline perfection. This was seen as a more highly resolved melting endotherm, attributed to an annealing effect. At lowered temperatures, the unaged material indicated the possibility of a small degree of moisture penetration into the sample.
For the aged material, the Thermo Lignum® treatment induced an apparent decrease in order and crystallinity, attributed to chain scission propagated at raised temperatures.
At the sub-ambient temperatrure, disruption of inter-molecular bonds by alterations in moisture distribution and an increase in surface voids probably induced a reduction in anisotropy.

To ascertain the stability of load baring polyamides subjected to such treatments, a number of experiments were set up, applying a load directly to the suspended samples in situ, and by applying a static creep stress using a DMTA.

For the unaged material, the creep/recovery tests exhibited interesting patterns of behaviour. At elevated temperatures, the strain induced crystallisation that had been apparent at room temperature was prevented, due to increased chain mobility. It was found that after the initial displacement there was a slow increase in strain associated with the extension of the amorphous regions. This was followed by a sudden displacement, before reaching a constant creep rate. This discontinuity was assigned to a tilting and slippage in the crystalline regions. To investigate this behaviour further, two experiments at intermediate temperatures were carried out. The results of these appeared to indicate that

the transition between the occurrence of strain induced crystallisation and that of crystalline slip corresponds with the glass transition of the polyamide.
The creep behaviour was shown to be partially reversible, as the same effect was seen in the recovery section of the curve. However, the final strain after recovery indicated that there had been some non-elastic deformation. The accompanying analyses for the creep/recovery samples and those samples loaded in situ indicated that there had been disordering of the structure, attributed to chain rupture. This correlated with the incomplete recovery in the creep experiment.

At sub-ambient temperatures, the unaged material was hindered by mobility restrictions. This resulted in reduced initial displacement and prevented strain induced crystallisation. Again, two supplementary creep experiments were carried out at intermediate temperatures. The results of these suggested that at 0°C, there was still sufficient energy to allow for a small amount of molecular reorientation and strain induced crystallisation. At -15°C this behaviour had disappeared and the shape of the curve was found to be the same as that at -30°C. It should be noted that the initial displacement at -15°C was greater than those at 23°C, 0°C and -30°C. The reasons for this are unclear.
The final recovery strain indicated that treated and unaged, loaded polyamide at -30°C would not suffer any permanent deformation. However, the subsequent analyses of the creep/recovery sample and the in situ samples indicated that sub-ambient loading had caused some underlying disruption and surface fracture.

The aged material presented different behaviour to that exhibited by the unaged samples. With all other parameters being equal, these differences were attributed to the structure of the starting material.
At an elevated temperature the sample did not show the strain induced contraction shown to occur at room temperature. On loading, the initial displacement was lower than that found for the unaged material at the same temperature. This suggested a degree of restriction, possibly caused by cross-links. After the initial displacement the sample maintained a constant strain until the load was removed at 150 minutes. After 450 minutes the sample had not fully recovered.
The pol ATR results for the creep/recovery experiments showed anomalous results when compared to the samples loaded *in situ*. The former indicating an increase in order, whilst the latter showing a decrease in anisotropy. The reasons for this difference are not clear.

The low temperature treatment of the aged sample follows the same creep behaviour as for the unaged sample; initial displacement followed by a constant strain. The reduced energy preventing strain induced crystallisation. In the case of the aged material, the initial displacement is larger than that seen at room temperature. This is similar to the unaged sample subjected to -15°C. These results are contrary to what might be expected at temperatures where molecular motion is restricted and have not been interpreted further. On removal of the load, the sample is seen to fully recover to its original length. The corresponding analysis indicate a decrease in crystallinity after creep/recovery loading. However, for the *in situ* loaded samples there are no alteration in the crystallinity or anisotropy. This indicates that there has been no detrimental effect to the sample when treated *in situ*. This is an important point to note. The creep/recovery experiments were carried out as a means of supplementing the results from the real treatments. However, as noted in Section 11.2 the experimental parameters did not exactly mirror those of the pest control methods. Therefore, they can only serve as an indication of how the unaged and aged material may behave under such treatments. It is the *in situ* loading that represents the true experimental practice, rather than the creep/recovery experiments.

Although there are clear limitations with regards to the size of the data set, the generally consistent pattern that was shown to occur in the control material suggests that the latter behaviour will also be reproducible. Where there was the opportunity to carry out repeat measurements, this was shown to be the case.

With this in mind, the following conclusions can be drawn with regards to the pest control treatment of polyamide 6,6:

1 For unaged, unloaded polyamides the results suggest that both raised and lowered temperatures should be safe. However, the unloaded aged samples did exhibit larger structural changes that indicated that low temperature treatments would be preferable to elevated temperatures.
2 In relation to the loaded textiles, the analyses clearly showed a greater degree of strain and irreversible creep behaviour when at raised temperature, for both unaged and aged samples. In contrast, the samples proved quite stable at sub-ambient temperatures.

3 The results indicate that treatment of loaded samples may induce irreversible effects to polyamide 6,6. This suggests that textile artefacts should be removed from manikins or frames prior to treatment.

11.4 References

1. Echalier, B., P. Bluet, and F. Lefebvre. The Ductile/brittle Transition in Polyamide 11 at Low Temperature. in Polymers at Low Temperatures. 1987. London: Polymer Properties Group, Institute of Marine Engineers.
2. Peterlin, A., Molecular Model of Drawing Polyethylene and Polypropylene. Journal of Material Science, 1971. **6**: p. 490-507.
3. Zaukelies, D.A., Obeservation of Slip in Nylon 66 and 610 and Its Interpretation in Terms of a New Model. Journal of Applied Physics, 1962. **33**(9): p. 2797-2803.

Chapter 12: Further Work

1. Near-infrared spectroscopy has proven itself to be a viable method of non-invasive characterisation when coupled with the relevant calibration set. The major classes and polyamide sub-classes were readily identified when coupled with commercial library software and multivariate techniques. However, the limitations were evidenced in Section 7.1.4, Chapter 7, *Case Study II: Schiaparelli Thai Silk Under Dress*, where it was shown that blended textiles could not be readily resolved into their separate components. Although it is often possible to see multiple components in the raw NIR spectrum, objective classification would necessitate a quantitative multivariate approach. To enable this, a large sample set of polymer blends would be required, with known percentage quantities of each component. The calibration could then be approached in one of two ways. Either via a simple principal component method, such as *Soft Independent Modelling of Class Analogies,* where each set of polymer blends were modelled separately. However, problems could arise from this if boundaries in PC space were in close proximity. The alternative route, and probably the most appropriate, would be via a quantitative *partial least squares regression* method. This would allow the known concentrations to be included in the decomposition of the X matrix and provide a robust prediction of polymer content.

2. An additional factor that may need to be addressed in future extension to the classification work is the age of the material. In the research presented here the reference samples used to build the searching library and multivariate models were new, unaged material. Ageing is unlikely to significantly influence the NIR spectra to an extent where the distinctly different polymers can no longer be identified. However, for sub-class determination alterations in the underlying structure of material may prevent successful differentiation where the spectral differences are already small.

3. Focus of the research presented in the later part of this thesis was given to investigating the behaviour of polyamide 6,6 fabric under pest eradication conditions. This provided an understanding of how the different properties of unaged and aged textiles influenced stability at the temperatures of interest. The

4. The creep experiments undertaken across a broad temperature range produced a number of distinctly different behaviours. Although the mechanisms for these changes have been postulated, the extent of the variations, coupled with a lack of supplementary literature, suggest that further research may be warranted.

5. The results showed that the polyamide behaved in a consistent manner throughout the analyses. However, limitations of the investigation lie in the lack of repeat tests for the thermal analyses, owing to restricted access to equipment. The opportunity to carry out replicate tests would enable the real significance of change to be evaluated.

6. The lack of previous research prompted heritage professionals to voice concerns regarding the stability of synthetic material when subjected to raised and lowered temperatures. The results presented in this thesis have indicated that for unaged material these treatments can be applied safely, so long as precautions are taken to ensure an object is not weight bearing. However, the treatment of aged material indicated stability issues in both unloaded and loaded material. These findings suggest that further investigations into synthetic material may be necessary, particularly focusing on those polymers that exhibit a glass transition within the temperature regions of interest.

Chapter 13: Conclusions

1. With the aid of the relevant spectral reference set and commercial library software, near-infrared spectroscopy can be successfully applied to the rapid, *in situ* characterisation of polymeric material. Coupled with the depth sampling capabilities of shorter wavelengths employed in conventional mid-infrared spectroscopy, NIR spectroscopy becomes a powerful non-invasive method of analysis.

2. The physical nature of the examined artefacts can often cause spectral interferences, when there is a high component of specular reflectance reducing signal and increasing noise. This therefore limits the NIR technique to diffusely scattering samples, such as woven fabrics.

3. Although commercial library software proved appropriate for the classification of the major polymers found in contemporary collections, sub-class identification requires a more sophisticated multivariate approach for discrimination. Both *Soft Independent Modelling of Class Analogies* and *Partial Least Squares Discriminant Analysis* proved applicable to the discrimination of the polyamide sub-classes, with the latter giving slightly better results during validation.

4. The application of multivariate techniques enables the degree of interference from extraneous factors to be determined and isolated. Such factors include colouring agents that absorb highly in the NIR spectrum and contain information on the underlying chemistry. These are regarded as “noise” when dealing with structural classification.

5. The artificial ageing regime under daylight conditions of the polyamide 6,6 fabric indicated that degradation progressed via a chain scission mechanism. On subsequent heat ageing a degree of cross linking is induced into the polymeric structure. Evidence for this is revealed in a loss of tensile properties and an increase in anisotropy, determined by Pol ATR.

6. The temperature dependant properties of polymeric material can be directly linked to the presence of the glass transition, the temperature of which was found to be approximately 35°C for the samples studied here.

7. The unaged, unloaded polyamide samples remained unchanged after treatment at both raised and lowered temperatures. However, for aged material, the temperature treatments induced a small acceleration in degradation, shown by disruption of the inter-crystalline regions and a decrease in anisotropy. The degree of change is greater at elevated temperature than at sub-ambient temperatures.

8. The application of a low loads to both unaged and aged polyamide 6,6 resulted in strain induced crystallisation. This was seen as a contraction in the creep section of the creep/recovery curves and is accompanied by an increase in the percentage crystallinity, as determined by DSC.

9. For the loaded samples, the raised temperature treatments caused irreversible changes to both the unaged and aged polyamide 6,6. These changes are attributed to different mechanisms due to variations in the structure of the starting materials.

10. At elevated temperatures strain induced crystallisation did not occur. For the unaged material the increased chain mobility enabled partial slippage of the crystalline regions. Supplementary creep experiments at intermediate temperatures showed that this mechanism was related to the onset of the glass transition. This deformation was not fully reversible, with the post-creep analyses confirming chain rupture.

11. At sub-ambient temperatures strain induced crystallisation was inhibited by mobility restrictions. The initial displacement in creep curves was found to recover fully in both the unaged and aged samples. For the unaged material the subsequent analyses of the creep/recovery samples and the *in situ* loaded samples indicated a degree of chain disruption and fracture. For the aged material, the post-analyses indicated a decrease in crystallinity after creep/recovery loading. Conversely, the *in situ* loaded samples did not exhibit any changes in the underlying structure.

12. Although the creep/recovery experiments enabled the physical behaviour of the samples to be monitored at the relevant temperatures, it was the samples loaded *in situ* that truly represented the behaviour of polyamide material subjected to pest control methods.

13. For the unaged, unloaded polyamide 6,6 either method of pest eradication was found to be safe. However, for aged material in the unloaded states, freezing temperature is the preferred method.

14. The treatment of loaded samples was shown to cause irreversible alterations at elevated temperatures.

15. All loaded samples were shown to be stable under sub-ambient conditions.

16. Where possible, objects should be treated in their unloaded state. Where this is not possible, then low temperature treatments should be used.

Appendix 1: Synthetic Polymers Found in Textile Collections

Organic polymeric materials are long chain macromolecules made up of many repeat units of smaller organic monomers. Depending on the stereochemistry and functionality of the initial reactants the resulting polymer will have a linear, branched or three dimensional network. Polymerisation can occur between monomer units of the same species, or from two or more different reactants. The former polymerisation route derives homopolymers with the latter group producing copolymers of differing repeat units [1]. In production of copolymers the beneficial characteristics of the individual molecules can be employed within one material.

The microstructure of fibres shows a two phase morphology; well ordered, closely packed crystalline regions and low order, randomly orientated amorphous regions. The crystalline regions are formed by folded polymer lengths, called lamellae, with a high degree of intermolecular bonding between adjacent polar groups along the polymer. The amorphous regions contain disoriented polymer chains, many having large side groups, branches or random stereochemistry that reduce packing, orientation and forces of attraction. The polymerisation of monosubstituted alkenes often produces highly amorphous polymers, where the chains possess varying stereochemistry dependent on the asymmetry of the carbon group. When the substituted group is positioned in a random manner along the polymer backbone the polymer is said to be atactic. Polymers possessing group conformations on the same side of the polymer backbone are isotactic and on alternating sides syndiotactic. The atactic conformation prevents the chains from closely aligning with adjacent lengths producing polymers of low crystallinity [2].

Crystallinity, orientation and forces of attraction all have an effect on the physical characteristics of polymers, such as strength, melting point (Tm) and the glass transition temperature (Tg). A high proportion of crystalline regions within a fibre will lead to increased polymer strength. However, this also produces a rigid polymer backbone, reducing flexibility and increasing brittleness. For these polymers, plasticisers are often added to intersperse within the matrix, thus enabling increased freedom of the molecular chains [3].

A1. Manmade and Synthetic Fibres in Textile Collections

The following two sections give an overview to the chemistry of the most commonly employed manmade and synthetic polymers used in fibre production. This is accompanied by a brief description of the physical properties of each class of polymer and a near infrared absorption spectrum of a standard reference material. Although the spectra appear less well resolved than those produced by mid-infrared spectroscopy, it is clear that the raw data are still sufficiently characteristic to enable reliable identification. Thus enabling the major classes of synthetic textiles to be readily analysed using a non-invasive sampling technique.

Manmade and synthetic polymers are grouped into two distinct categories of materials, owing to their origin. Manmade or semi-synthetic materials are those that have been derived from naturally occurring polymers. In contrast, synthetic polymers are formed through induced polymerisation reactions of small molecular weight hydrocarbons.

A1.1Manmade Fibres

Manmade polymers can be derived from modified and regenerated cellulose or proteins; the most common being employed for fibre production are cellulose acetate and cellulose xanthate. Cellulose xanthate reacts to reform cellulose; the product is commercially known as Viscose, owing to the viscous solution produced during the regeneration process.

Cellulose derived polymers are produced by dissolution, modification and regeneration of cellulose fibres [4]. These fibres originate from the fibrous cells of seed cases, leaves and stems of plant matter. The primary reason for cellulose modification is to form a soluble, viscous polymer that can be manipulated into fibres of various physical forms.

Plant cell walls are primarily comprised of the linear polysaccharide, cellulose. Cellulose is formed by the polymerisation of glucose units. Glucose forms a glycosidic link between the first and fourth carbon atom of a second molecule, giving a conformation of 1,4-β-D-glucopyranose [5]. Each glucose residue is orientated by 180° to the next within the chain, forming a celloboise dimer.

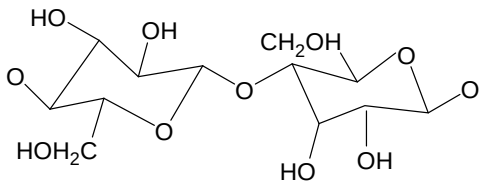

Figure A1.1 The cellobiose repeating unit in cellulose

The degree of polymerisation (DP) of non-degraded cellulose cotton is in the region of 6,000-10,000; for Viscose the DP is just 300-400 [6]. The differences in chain lengths are due to the dissolution of the cellulose fibres and polymer cleavage during processing. Through intra and intermolecular hydrogen bonding the long polymer chains of cellulose form crystalline structures. These approximate at 70-75% crystallinity for cotton and 25-30% for Viscose [6]. The degree of polymerisation and crystallinity provide the cellulose chains with relatively high resistance to chemical and physical degradation.

A1.1.1 Viscose Rayon

Viscose Rayon is formed through the alkali conversion of cellulose into cellulose xanthate followed by subsequent regeneration via an acid treatment.

Cellulose is steeped with sodium hydroxide to form alkali cellulose and then further reacted with carbon disulfide to form sodium cellulose xanthate. This soluble material is then dissolved in further sodium hydroxide, producing a viscous solution suitable for extrusion [7]. Extrusion occurs through an acidic coagulation bath, containing sodium bisulfate, zinc sulfate and sulfuric acid, where the xanthate is regenerated into a cellulose fibre of given length and form [8].

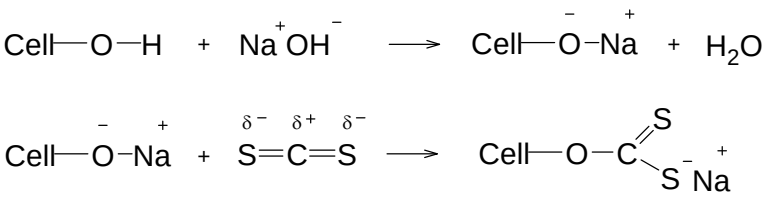

Figure A1.2 Formation of cellulose xanthate

Following extrusion, the fibres are drawn to impart orientation and increase crystallisation. This increases tensile strength to approximately 0.13-0.22 N/Tex [9]. Where one Tex is defined as the weight in grams of 1,000 meters of linear material.

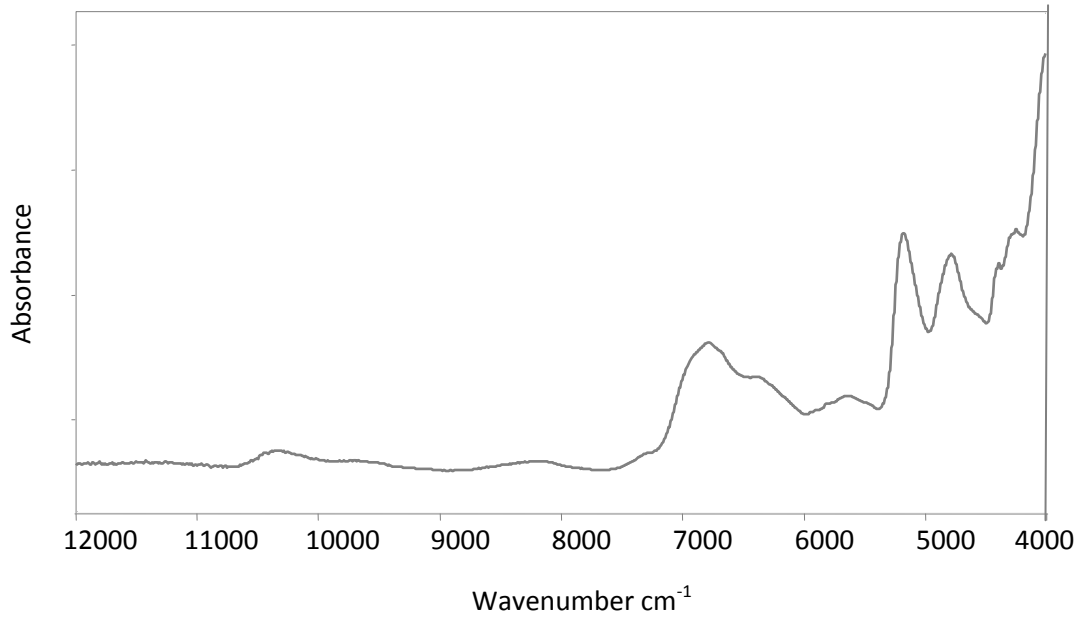

Figure A1.3 NIR absorbance spectrum of viscose

A1.1.2 Cellulose Triacetate and Cellulose Acetate

Cellulose acetate is formed through the acetylation of cellulose with acetic anhydride. Cellulose is steeped in acetic acid at 50°C to open up the fibre for reagent penetration. This is then added to a mixture of acetic anhydride, sulfuric acid and methylene chloride. The acetic acid and methylene chloride act as solvents, whilst the sulfuric acid provides the acidic conditions required for acetylation with acetic anhydride [8] (Figure A1.4).

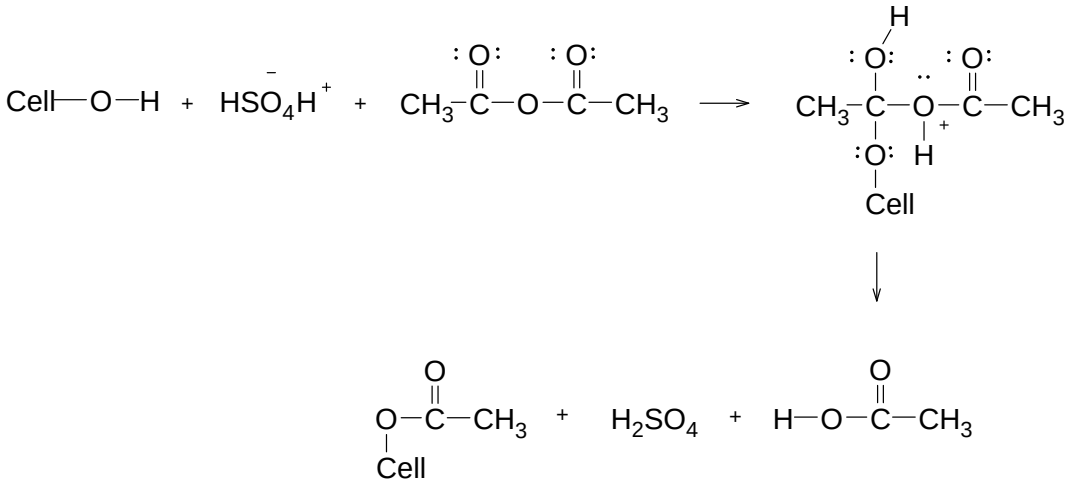

Figure A1.4 Formation of cellulose triacetate

The cellulose is completely reacted after eight hours, when the degree of substitution is three. This refers to the number of hydroxyl groups that have been converted per glucose unit, hence the name cellulose triacetate.

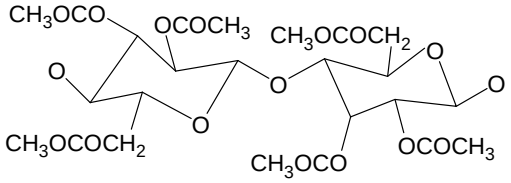

Figure A1.5 Structure of cellulose triacetate

Cellulose acetate relates to a material where the average degree of esterification within fibres is 2.3-2.4 [9]. This lower degree of substituted hydroxyls can only be formed through the hydrolysis of triacetate. The reaction is initiated by the addition of aqueous acetic acid, where the acetic acid acts as a solvent for the triacetate to prevent precipitation and the water causes hydrolysis [9].

Both forms of acetate fibre are dry spun through a spinneret and concurrently heated to evaporate the acetone solvent. The resulting tensile strength of cellulose triacetate and cellulose acetate fibres are 0.11-0.19 N/Tex and 0.09-0.13N/Tex respectively.

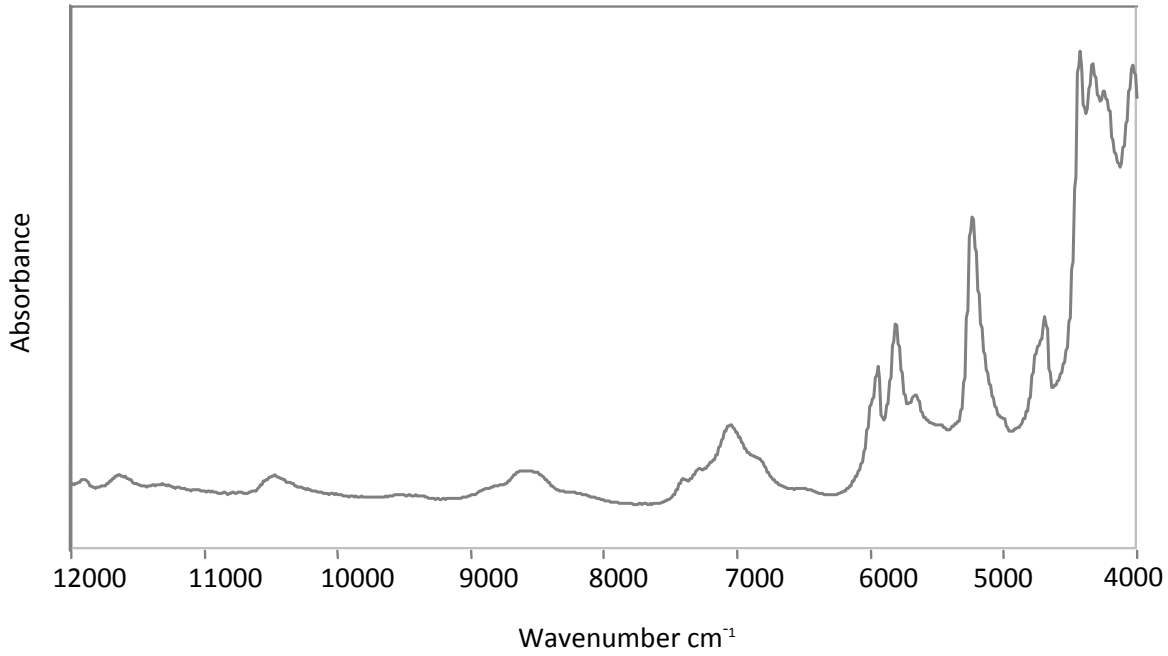

Figure A1.6 NIR absorbance spectrum of cellulose acetate

The assignment of peaks in the NIR region are tentative, but distinct regions can be assigned. The peaks in the region of 4000-4250cm^{-1} are related to the carbon-hydrogen combination vibrations, with the first and second overtones in at approximately 5700-6000cm^{-1} and 7100cm^{-1} respectively. Those relating to the 1st and second overtones of the carbonyl vibrations are seen between 5100 and 5400cm^{-1}.

A1.2 Synthetic Fibres

The formation of synthetic polymers requires that the initial monomer molecules have a functionality of two or more. This allows for linkages to be formed at these activation sites. Many types of reaction are possible, but most can be classified as either step polymerisation reactions or chain polymerisation reactions. The process of synthesis for the major classes of polymeric fibres will be outlined below.

Step polymerisation occurs when two difunctional molecules (monomers) react with each other to form a product that also contains two functional end groups. The molecular mass of the polymer increases as a function of reaction time [10]. This relationship is, however, governed by factors such as the reactivity of the functional groups and the degree of intramolecular reactions competing with intermolecular reactions [3]. This process can be

divided into two categories: Polycondensation and Polyaddition. The former are those reactions where small molecules are eliminated, with the resultant polymer units containing fewer atoms than the original monomer units [1]. Polyaddition reactions do not eliminate molecules during polymer formation. Any side products are retained in the material.

Chain polymerisation can follow a number of reaction routes. These include ionic polymerisation, Ziegler-Natta coordination polymerisation, ring opening polymerisation and free radical polymerisation [1]. Chain polymerisation follows three steps during reaction; initiation, propagation and termination.

The degree of polymerisation (DP) is a measure of the average number of monomer units per polymer chain. It is determined statistically and is based on the stoichiometric balance of the reaction. The reader is referred to the literature for an in depth discussion on the subject [1, 10, 11], but it is suffice to say that the type of monomer units and the degree of polymerisation will govern the molecular weight of the material. If reactant quantities are not stoichiometric then the degree of polymerisation is reduced, because the reaction is terminated by the monomer in excess. This can often be used to the advantage of manufacturing, enabling the control the length of the polymer chains, and therefore manipulating the physical properties of the material. Other methods employed to control molecular weights rely on the inclusion of monofuntional groups, such as acetic acid, which will react to terminate the chain.

A1.2.1 Step Polymerisation

A1.2.1.1 Polycondensation

A1.2.1.1.1 Polyamide (Nylon)

Polyamides are generally formed through the reaction between a carboxylic acid and an amine. The product is an amide and the general equation for the reaction is:

$$n\text{HOOC-R-COOH} + n\text{H}_2\text{N-R}_2\text{-NH}_2 \rightarrow [\text{-OC-R-CONH-R}_2\text{-NH-}]_n + n\text{H}_2\text{O}$$

Figure A1.7 The reaction between a carboxylic acid and an amine in the formation of polyamide

Where R is any aliphatic or aromatic species that does not exceed more than 15% aromatic on either side of one amide group [6]. The degree of polymerisation for polyamines is in the region of 50-80 repeat units.

The commercial name for the aliphatic polyamide family is Nylon. There are a number of polyamides available, but those most frequently employed in the textile industry are polyamide 6,6 and polyamide 6. The numbering system denotes the number of carbons present on the amine and acid monomers, respectively.

The chemical name for polyamide 6,6 is polyhexamethylene adipamide and it is formed through a polycondensation reaction between the monomer units adipic acid and hexamethylene diamine (Figure A1.8 and A1.9).

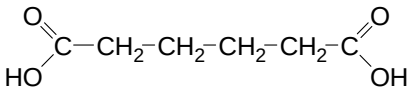

Figure A1.8 Chemical structure of adipic acid

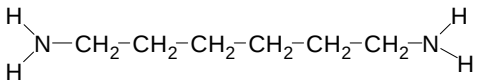

Figure A1.9 Chemical structure of hexamethylene diamine

The mechanism for production is catalysed by an acid, which is either introduced into the system or self-catalysing due to the presence of adipic acid. The adipic acid protonates the carbonyl of a second acid molecule, this is followed by nucleophilic nitrogen attack by the diamine monomer.

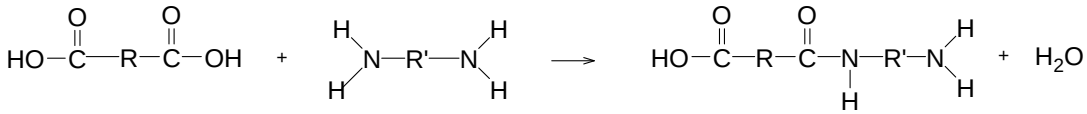

Figure A1.10 Formation of polyamide 6,6

Where HOOCRCOOH is adipic acid (Figure A1.8) and $H_2NR'NH_2$ is hexamethylene diamine (Figure A1.9). The linear product goes on to polymerise with further molecules of diamine, diacid or with other linear products.

The chemical name for polyamide 6 is polycaproamide. Polyamide 6 is formed by self-polymerisation of caprolactam (Figure A1.11).

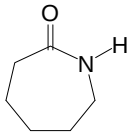

Figure A1.11 Chemical structure of caprolactam

When caprolactam is heated to approximately 250°C in the presence of water, hydrolysis results in ring opening (Figure A1.12) . The resulting amino acid then reacts directly with a caprolactam molecule, and the polymer chain grows as the reaction continues between further caprolactam molecules and the hydroxyl end group of the newly formed linear amino acid.

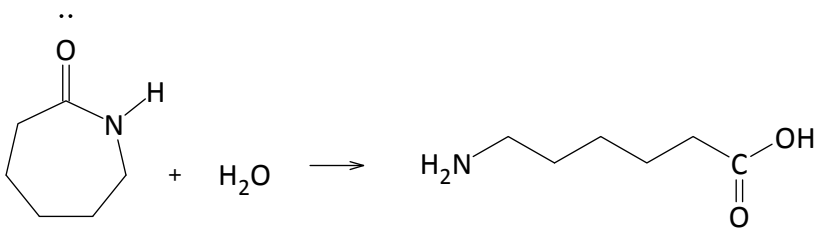

Figure A1.12 Ring opening of caprolactam in the formation of polyamide 6

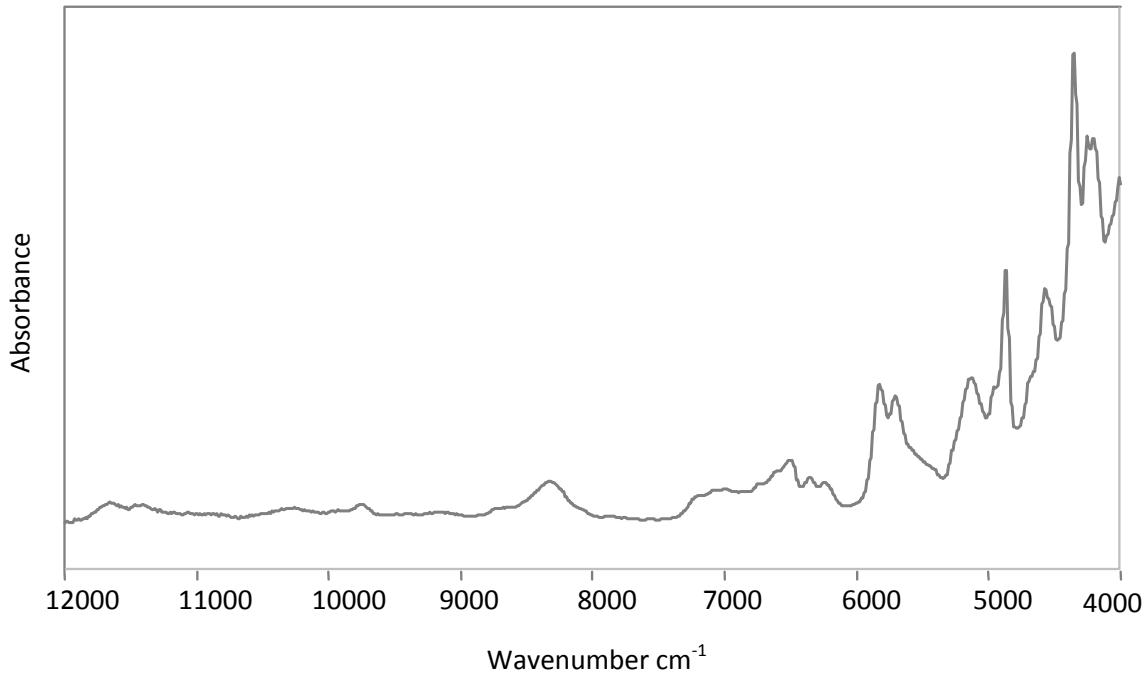

Figure A1.13 NIR absorbance spectrum of polyamide 6,6

The bands associated with the combination and increasing overtone vibrations of the amide groups are seen in the region of 4610-5000cm^{-1}, 6000-6800cm^{-1} and 8900-9600cm^{-1} respectively. Carbon hydrogen overtone vibrations are seen at approximately 7800 and 8500cm^{-1}.

Polyamide fibres are formed through the extrusion of the molten polymer after reaction. The fibre is cooled by air and then drawn, which increases alignment of the polymer chains along the fibre axis and in turn increases the degree of crystallisation [12]. Linear aliphatic polyamides, such as polyamide 6,6 and polyamide 6, form aligned semi-crystalline material through intermolecular hydrogen bonds. The polymer units orientate themselves in parallel or anti-parallel conformations, respectively, and form hydrogen bonds between adjacent carbonyl and amino parts of the amide moieties [13]. Crystallinity in fibres is in the region of 55-85%.

The tensile strength of both the polyamides described above is in the region of 0.4-0.6 N/Tex.

A1.2.1.1.2 Polyester

Polyesters are formed through the reaction between a difunctional alcohol and a carboxylic acid. There are a number of polyesters available commercially, such as poly(1,4-butylene terephthalate) and poly(1,4-cyclohexylenedimethylene terephthalate), but the dominant polymer used for fibre formation is Poly(ethylene terephthalate), also known as PET [6]. PET is formed through the ester interchange of dimethyl terephthalate (Figure A1.14) and ethylene glycol (Figure A1.16) or the esterifiction of terephthalic acid (Figure A1.15) with ethylene glycol [14].

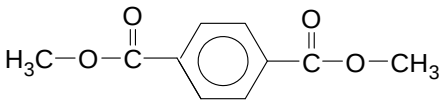

Figure A1.14 Chemical structure of dimethyl terephthalate

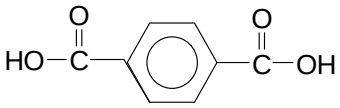

Figure A1.15 Chemical structure of terephthalic acid

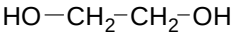

Figure A1.16 Chemical structure of ethylene glycol

The product formed be either route is *bis*(2-hydroxyethyl)terephthalate and this is the starting material for the polycondensation reaction of PET formation. The former route eliminates methanol, whist the later causes the elimination of water. Both are reversible reactions and therefore require distillation of the by-products to drive the system forward [13].

Once *bis*(2-hydroxyethyl)terephthalate has been produced, the polymerisation reaction is catalysed at temperatures ranging from 150-250°C. The degree of polymerisation is typically on the order of 115-140.

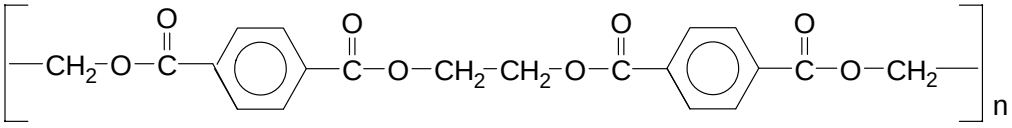

Figure A1.17 Chemical structure of polyethylene terephthalate

The fibre lengths are formed via extrusion and spinning. Varying degrees of extrusion speed can be applied, which alter the internal alignment of the polymer chains. The higher the extrusion speed the higher the degree of orientation. For those fibres spun at slow speeds, it is possible to increase orientation through drawing the fibre just above the glass transition temperature at approximately 90-100°C [13]. Polyester fibres are semi-crystalline in structure, with the degree of crystallinity approximating 35% with a tensile strength of approximately 0.7 N/Tex.

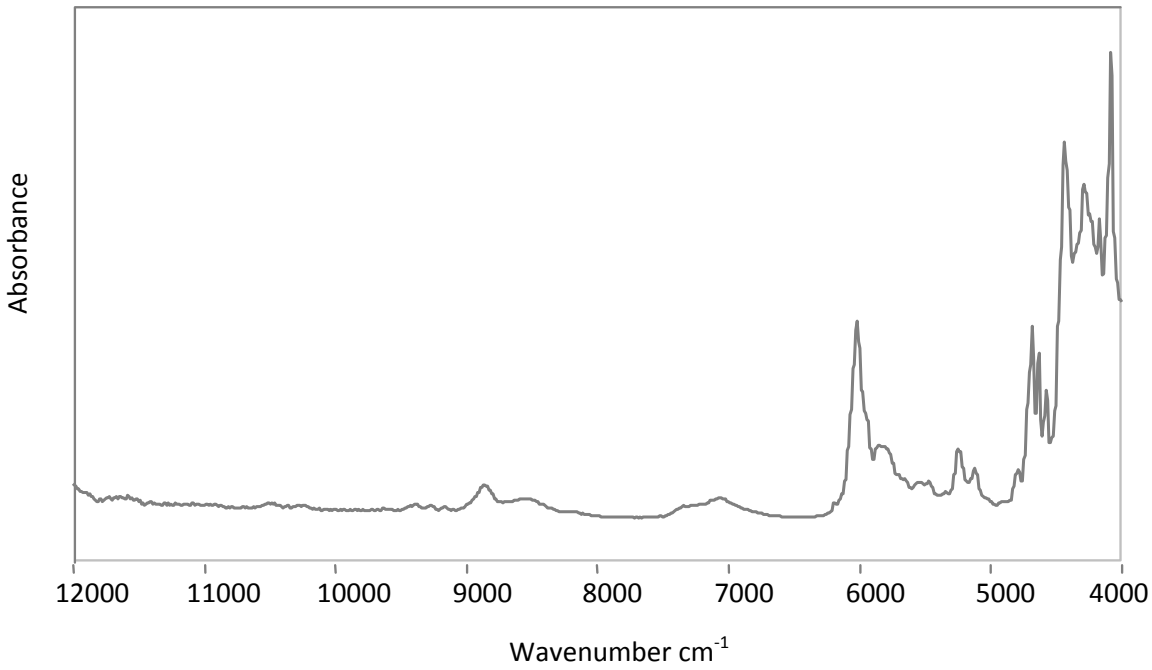

Figure A1.18 NIR absorbance spectrum of polyethylene terephthalate

The sharp peak centred at 5950cm^{-1} is due to the first overtone of the aromatic benzene ring, with the second overtone experienced in the region of 8800cm^{-1}. The small peaks between 5130cm^{-1} and 5210cm^{-1} are assigned to the 2nd overtone of the ester linkages.

A1.2.1.2 Polyaddition

A1.2.1.2.1 Polyurethane

Polyurethane's are generally formed through the reaction of a diisocyanate and a polyol (usually a diol), an aminoalcohol or a diamine. The more common are those derived from polyether and polyester diols. The structure of a typical polyurethane polyether is shown in Figure A1.21. The precursors in this case are 4,4'-diphenylmethane diisocyanate (Figure A1.19) and ethylene glycol (Figure A1.20).

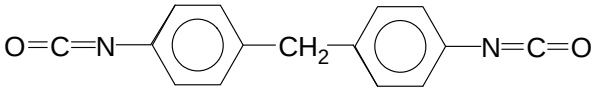

Figure A1.19 Chemical structure of 4,4'-diphenylmethane diisocyanate

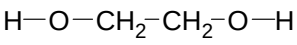

Figure A1.20 Chemical structure of ethylene glycol

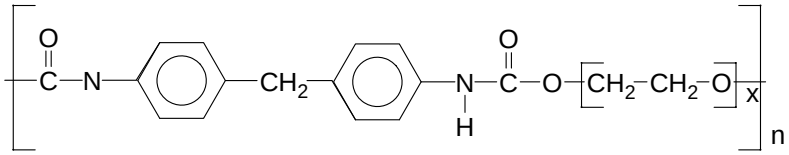

Figure A1.21 Chemical structure of a polyurethane polyether

The diol monomers used during urethane formation have usually been polymerised before reaction to a degree of 20-45. These long polymer lengths form what is called the soft segment of the polymer, whilst the isocyanate sections form the hard segment. The soft segments do not form strong intermolecular bonds, and are therefore free to move and re-orientate themselves. The hard segments are crystalline and structured with intermolecular hydrogen bonds and van der Waals forces form between adjacent urethane groups and benzene rings, respectively. This prevents elongation and movement. This polymeric structure allows the polymer to be extended and compressed, without permanent deformation to the chains. Such polymers are called elastomers and form the basis of Lycra and Spandex [6].

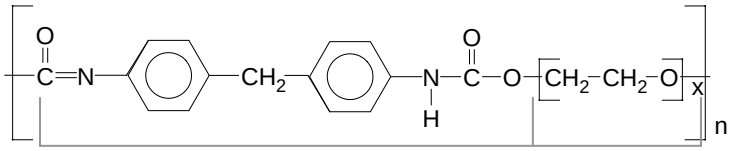

Hard Segment **Soft Segment**

Figure A1.22 Hard and soft segments of a polyurethane elastomer

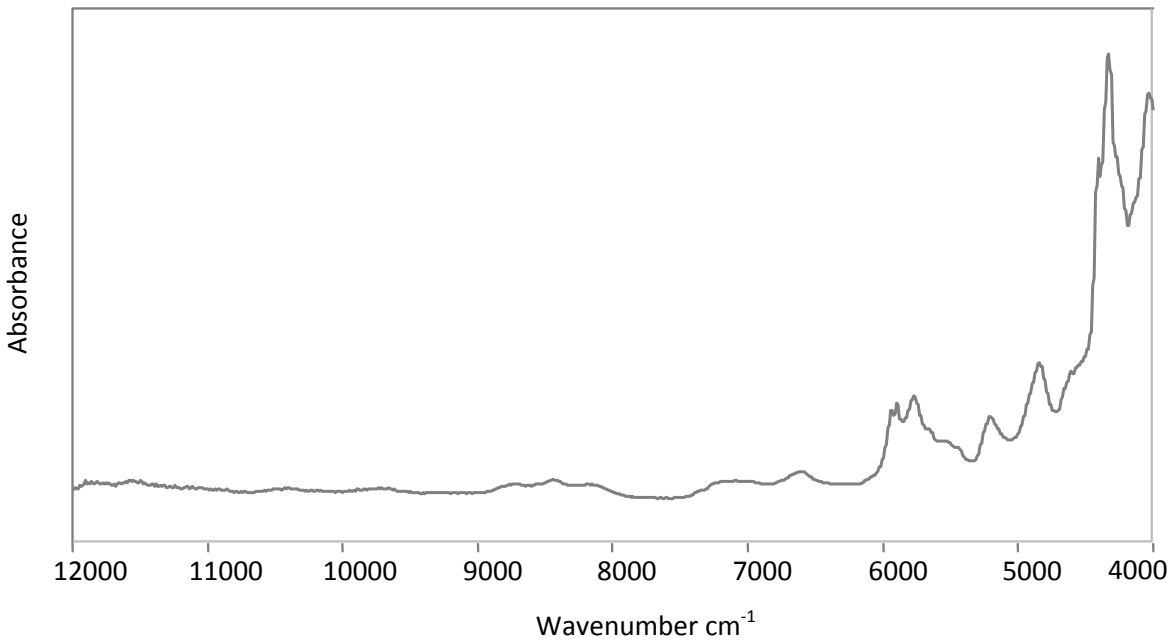

Figure A1.23 NIR absorbance spectrum of a diphenylmethane polyurethane polyether

The first overtone of the benzene vibration is centred at 5950cm^{-1}. The peak in the region of 5200cm^{-1} is the second overtone of the ester group. Combination and increasing overtone vibrations of the amide groups are seen in the region of 4610-5000cm^{-1}, 6800cm^{-1} and 8900cm^{-1} respectively.

Polyurethane fibres are formed via solution spinning or reaction spinning. Solution spinning requires the polymer to be dissolved in a polar solvent, such as dimethylformamide, and then extruded through a spinneret. Reaction spinning involves the extrusion of the isocyanate monomer through an aqueous solution of the diol. The reaction occurs at the surface of the fibre [9].

The elastomeric nature of polyurethane polymer is often employed for the production of foams. Foam formation occurs through a simultaneous reaction of the isocyanate and diol, and isocyanate and water, at high temperatures and under catalytic conditions. The two reactions produce polyurethane and carbon dioxide respectively, with the latter product imparting an open three dimensional structure. Polyurethane foams may be found as interlinings or padding in some garments [15].

A1.2.2 Chain Polymerisation

Chain polymerisation can follow a number of reaction routes. These include ionic polymerisation, Ziegler-Natta coordination polymerisation, ring opening polymerisation and free radical polymerisation [1]. The last is the most common reaction used for polyalkene production, and will be outlined below as a guide to the formation of vinyl fibres.

Chain polymerisation follows three steps during reaction: initiation, propagation and termination. During the *initiation* step (Figure A1.24), free radicals called initiators are formed under catalytic conditions (1). Due to their highly reactive nature, these often break down further into smaller radicals with the elimination of a molecule (2). The free radical is then available to react with the double bond of an alkene, of general formula CH_2CHX (3). The new carbon radical can then go on to react with a monomer unit. This *propagation* step is repeated many times to form the polymer chains (4) [2].

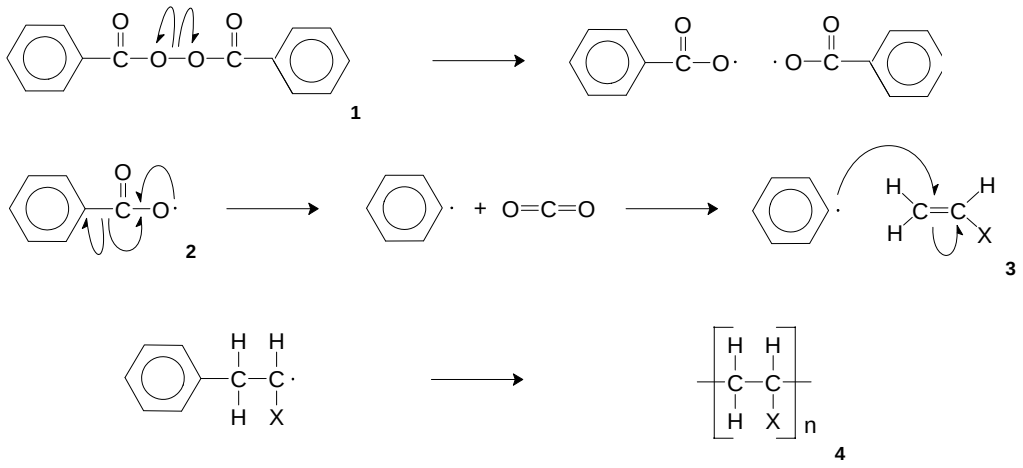

Figure A1.24 Free radical initiation from benzoyl peroxide and propagation reaction to form a polyalkene

The polymerisation reaches *termination* when the radicals are all consumed (Figure A1.25). The most common of these reactions are combination and disproportionation [1]. During the combination mechanism, two carbon radicals come together to form a bond and a single polymer chain (5a). Disproportionation occurs when a hydrogen atom is removed from one carbon radical to another. The result is the retardation of one radical, with the other gaining a second unpaired electron (5b). The molecule is then stabilised by the formation of a double bond (6).

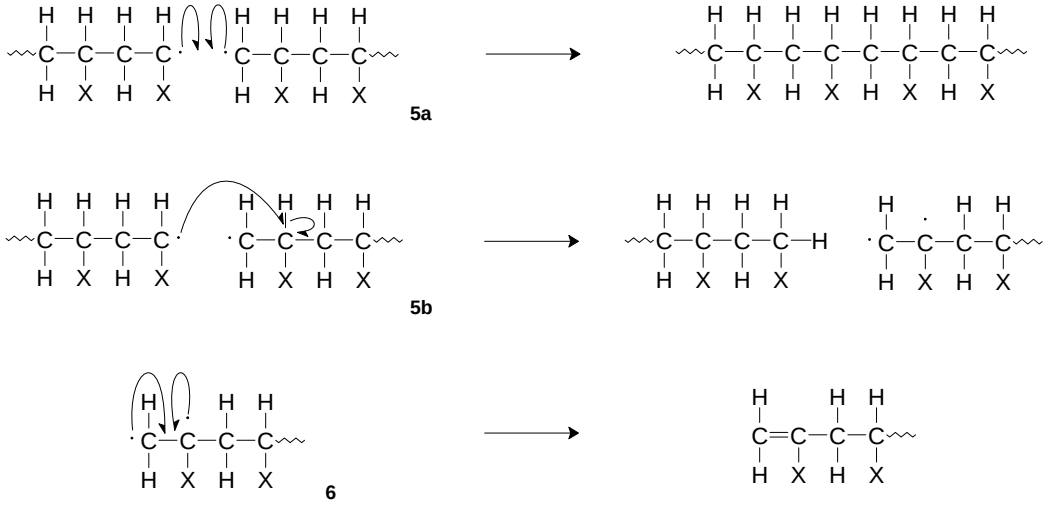

Figure A1.25 Free radical termination

If the disproportionation radical attack occurs along the polymer backbone, the energy cannot be dissipated through step 6. Therefore the newly formed radical will go on to react with further alkene molecules forming a branched or network polymer structure [16].

Free radical polymerisation of substituted alkenes often produces polymer chains that possess random, atactic stereochemistry [2]. Polymers that possess isotactic and syndiotactic conformations are formed through a process known as Ziegler-Natta polymerisation. The exact mechanistic route is not fully understood, but polymerisation occurs through coordination of the alkene's bonding and antibonding orbitals with an organometallic transition metal complex [2], with consequent stereo selectivity.

A1.2.2.1 Polyethylene and Polypropylene

Polyethylene is a vinyl polymer formed through the polymerisation of ethylene molecules.

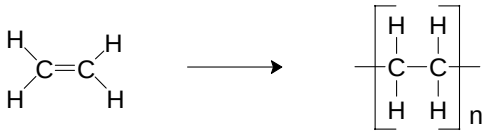

Figure A1.26 Chemical structure of polyethylene

The polymer chains can be formed through the two reaction routes described in Section A1.2.2. Free radical polymerisation produces a low density, low tenacity semi-crystalline material. Its use in textiles requires a course fibre, limiting its general use to upholstery and outdoor material. High density polyethylene is formed via the Ziegler-Natta process, producing a linear polymer with high tenacity and crystallinity. The degree of polymerisation is in the region of 200-500. This material is employed for specialist applications such as ballistic vests [6].

Polypropylene is made by polymerisation of propylene with transition metal catalysts (Section A1.2.2). The fibre lengths are formed through extrusion of the polymer melt. Polypropylene is prone to oxidation during and after fibre production. Stabilisation is achieved through the addition of antioxidants that sacrificially react with radicals [17]. Textile fibres are formed from helical isotactic polypropylene, imparting orientation and crystallinity to the polymer lengths. The tensile strength is in the region of 0.6 N/Tex.

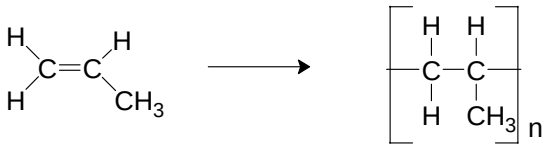

Figure A1.27 Chemical structure of polypropylene

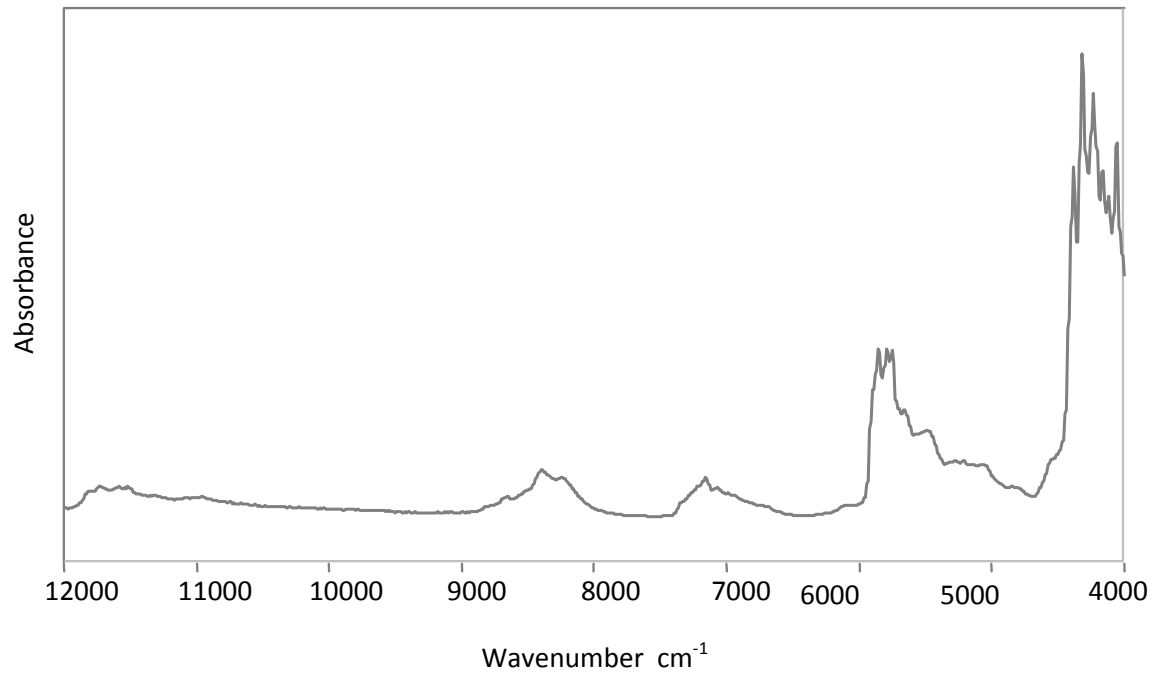

Figure A1.28 NIR absorbance spectrum of polypropylene

All bands can be assigned to the combination and overtone vibrations of the methylene and methyl groups along the polymer backbone.

A1.2.2.2 Polyvinyl Chloride (PVC)

Polyvinyl chloride is formed though the polymerisation of vinyl chloride monomers.

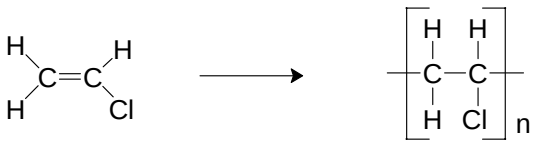

Figure A1.29 Chemical structure of polyvinyl chloride

Due to high thermal instability, once the polymer chains have been formed it is not possible to extrude the fibre through melt spinning. The polymer is therefore dissolved in solvent mixtures of acetone and benzene and dry spun. The degree of polymerisation ranges from 800-2000 repeat units [18]. The free radical polymerisation produces an atactic backbone and a highly amorphous material, in the region of 85-90% [19].

PVC is often applied as a coating to textile substrates. The additional processing involved requires a number of additives, such as plasticizers and heat stabilisers. Plasticizers work to reduce the intermolecular forces between polymer chains. The stabilisers prevent dehydrochorination and subsequent conjugation of the polymer chains [19].

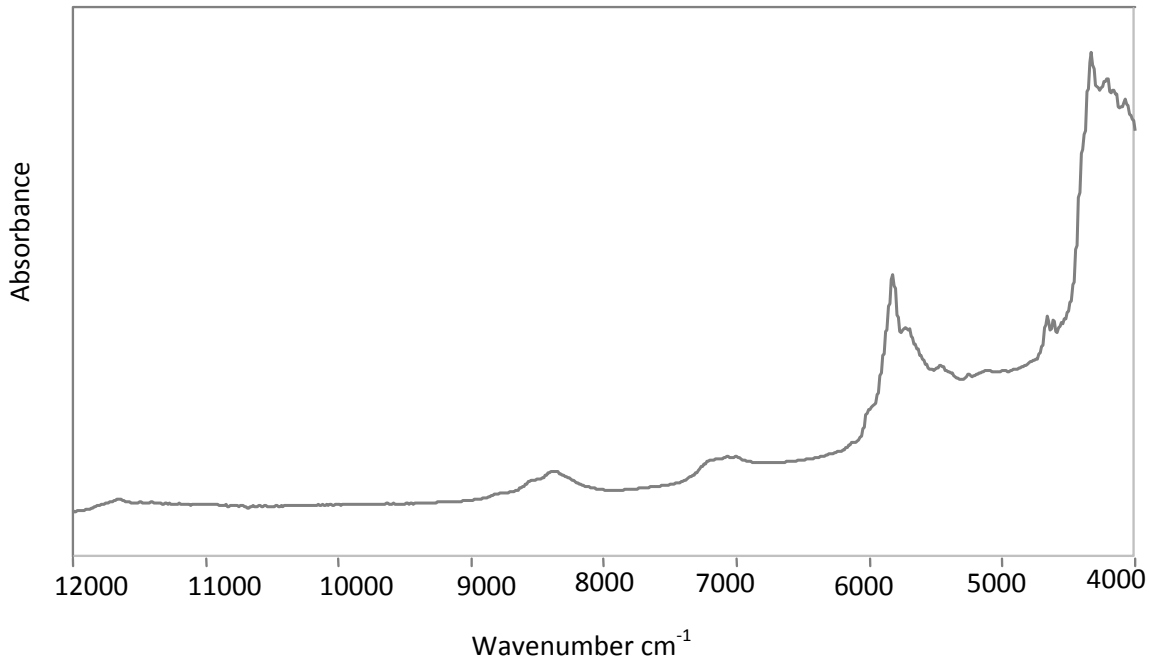

Figure A1.30 NIR absorbance spectrum of polyvinyl chloride

Two primary vibration functions have been identified as CH_2 and CHCl. De Araujo et al [20] have assigned the peaks in the region of 5700 and 8400cm^{-1} as CH_2 stretching modes and those at 5850, 7000 and 8500cm^{-1} to CHCl stretching vibrations.

A1.2.2.3 Polyacrylates

Acrylate monomers are vinyl esters, with the basic polymeric group being polymethacrylate:

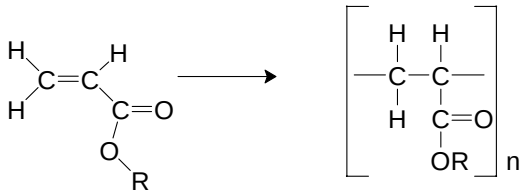

Figure A1.31 Chemical structure of polymethacrylate (R = CH_3)

By substitution of the R group and the hydrogen on the α-carbon, a wide variety of polymers are formed with differing chemical and physical properties. The polymer used for fibre production is a derivative of the acrylate family, polyacrylonitrile.

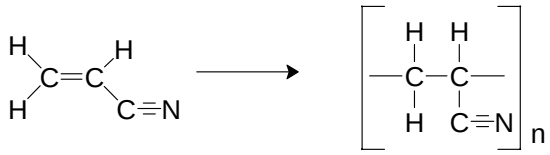

Figure A2.32 Chemical Structure of polyacrylonitrile

The homopolymer is very strong and chemically resistant, but does not allow for fibre dying due to a closely packed structure. Therefore, acrylonitrile is usually reacted with acrylate monomers to form a copolymer in a ratio of approximately 6:1 respectively [21]. This provides the fibre with increased access for surfactants, but reduces strength.

Fibres are formed through cold water extrusion from a solvent solution, followed by drawing at raised temperatures. The structure and degree of crystallinity are not fully determined. A two phase structure has been proposed consisting of lateral crystal chains bridged by tie molecules in amorphous regions [13, 21]. The nitrile groups allow for repulsive and attractive forces, dependent on their orientation.

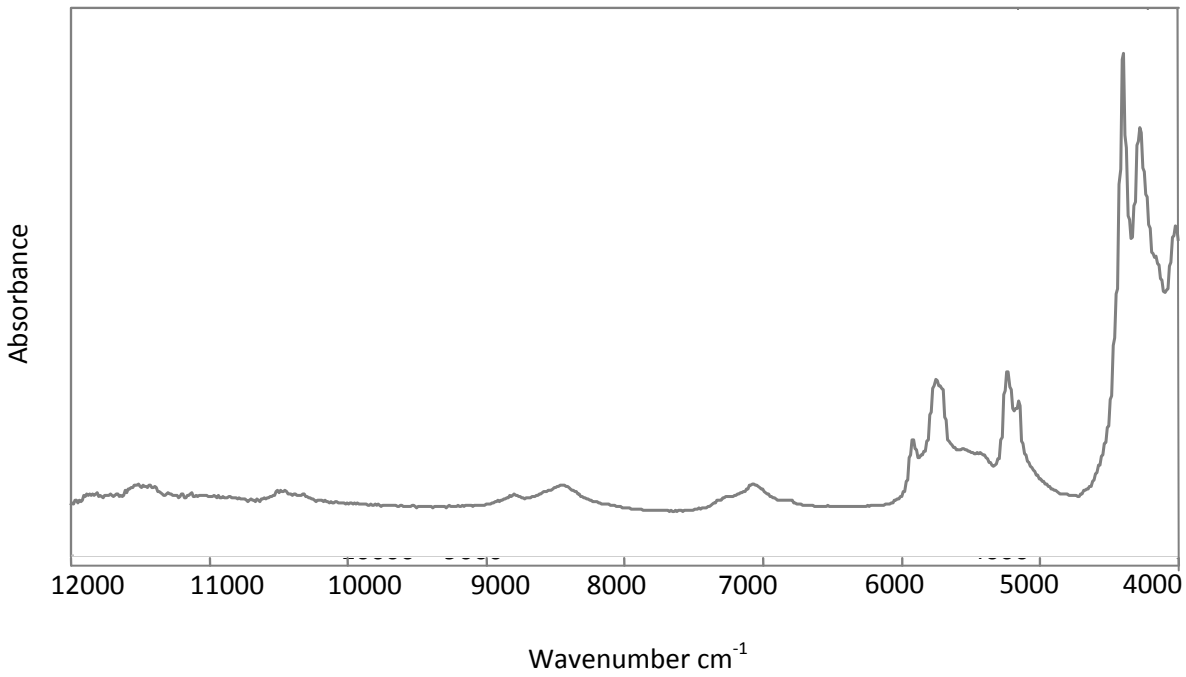

Figure A1.33 NIR absorbance spectrum of polyacrylonitrile

Methylene groups show absorption at 4300, 5500-5700 and 8300-8500cm^{-1}, with carbon hydrogen bonds vibrating at a frequency of 5700 and 8400cm^{-1} [22]. Band assignment for the CHCN vibrations have not been made.

A1.3 Polymer Degradation

One of the primary reasons for the identification of the different classes of synthetic material within contemporary collections is the desire to mitigate deterioration. Synthetic polymers pose significant challenges for conservation professionals due to the varied routes of manufacture and processing presenting a wide range of degradation issues. This section serves as a brief overview of the types of deterioration that could be expected to cause damage to synthetic polymers. The primary focus of this work is the stability of polyamide material and therefore a more in depth discussion is given in Chapters 5, 10 and 11.

A1.3.1 Thermal Decomposition

On application of heat organic polymers will undergo thermal degradation via two main routes. These are the random scission of condensation polymers and depolymerisation of addition and vinyl polymers [23].

Random degradation occurs for those polymers formed via a polycondensation mechanism. Free radicals are formed at random rupture points along the polymer backbone [24]. This causes macromolecules to split at varying lengths producing two molecules. Termination of the scission reaction can occur with the formation of an unsaturated end group, or via the reaction of two different radicals producing a new macromolecule of higher molecular weight [24]. This type of reaction produces alkanes, alkenes and dienes.

The depolymerisation reaction, or depropagation, is induced in vinyl and addition polymers by heat. This can be a free radical mechanism, where the polymer reverts back to the monomer unit, or an elimination reaction involving the removal of small molecules from the polymer backbone. The former pathway is seen in polyacrylates which revert to monomeric acrylates, and the latter in the depolymerisation of polyvinyl chloride to a polyene with the elimination of hydrogen chloride [24].

A1.3.2 Photo-oxidative Decomposition

Ultraviolet radiation in the region of 290-400 nm, is sufficiently energetic to cause the dissociation of many single covalent bonds [25]. Photon energy is absorbed by the material through chromophores, usually present in small quantities as impurities. Without such activation sites, many polymers would not absorb wavelengths energetic enough to cause photo-degradation [23]. These chromophores are in the form of carbonyls and peroxides which are residual by-products from the manufacturing and processing.

In the presence of oxygen and metal ion impurities, a photo-oxidiative reaction is induced causing chain scission. The initiation step produces a macroradical through absorption of radiation. These radicals readily react with oxygen to form a highly reactive peroxy radical which in turn abstracts a hydrogen atom from the polymer chain. Further radicals are formed until termination occurs in a similar manner to that described in Section 3.2.2 [1]. In order to perturb these reactions it is often necessary to add stabilisers to the polymer during production. These can be in the form of UV absorbers which dissipate the energy through the polymer as heat. Alternatively, antioxidants can be used which react preferentially with free radicals formed during the initiation reactions [23].

A1.3.3 Chemical Decomposition

The chemical degradation of a polymer is not only dependent on its chemical structure and reactive sites, but also its physical nature. Organic polymeric materials will react via the same mechanisms as smaller organic molecules, but the extent of these reactions is very much governed by the ability of reagents to penetrate the microstructure. For highly crystalline materials reactions may only occur on the fibre surface. For example, polypropylene is hydrophobic and highly crystalline and so resistant to swelling because the structure prevents moisture penetration. In contrast, viscose fibres are hydrophilic with a lower degree of crystallinity and so readily take up moisture, and are consequently the more likely to be affected by atmospheric pollutants.

Numerous types of reactions are possible for each fibre. Their resistance, or otherwise, to degradation are presented in Table A1.1.

Polymer	Thermal	Photo-oxidation	Moisture	Acids	Alkalis
Cellulose Acetate	Degrade above 260ºC	Resistant	Resistance increase with increase in substitution	Degrades at high conc.	Saponifies - Reverts to cellulose
Viscose	Degrade above 130ºC	Yellow	Swells	Degrades	Swells
Polyamides	Degrade above 280 ºC	Yellow	Hydrolysis	Aqueous H^+ Degrade	Aqueous OH^- Degrade
Polyesters	Degrade above 300ºC	Resistant	Resistant	Degrades at high conc.	Degrades
Polyurethanes	Degrade above 230ºC	Yellow	Hydrolysis of Polyester Form	Oxidation of Polyether form	Hydrolysis of Polyester form
Polypropylene	Degrade above 165ºC	Yellows	Resistant	Degrades at high conc.	Resistant
Polyvinyl Chloride	Degrades	Degrades and yellows	Resistant	Resistant	Resistant
Acrylic	Yellows	Resistant	Resistant	Degrades at high conc.	Degrades

Table A1.1 Overview of the degradation processes of manmade and synthetic fibres

A1.4 References

1. Young, R.J. and P.A. Lovell, *Introduction to Polymers*. 2nd ed. 1991, London: Chapman & Hall.
2. McMurry, J., *Organic Chemistry*. 2nd ed. 1988, California: Brooks/Cole Publishing Company.
3. Nicholson, J.W., *The Chemistry of Polymers*. 2nd ed. 1997, Cambridge: The Royal Society of Chemistry.
4. Timar-Balazsy, A. and D. Eastop, *Chemical Principles of Textile Conservation*. Conservation and Museology, ed. A. Oddy. 1998, Oxford: Butterworth-Heinemann. 444.
5. Garside, P., *Investigations of Analytical Techniques for the Characterisation of Natural Textiles Fibres Towards Informed Conservation*. 2002, Department of Chemistry, University of Southampton.
6. Hatch, K.L., *Textile Science*. 1993, Saint Paul: West Publishing Company. 471.
7. Pelatt, D.L., *Viscose Rayon Production* Textile Manufacturers Manuals. 1931, Manchester: Emmott & Co Ltd.
8. Carrerah, C.E., *Polymer Chemistry*. 5th ed. Undergraduate Chemistry, ed. J.J. Lagowski. 2000, New Yrok: Marcel Dekker Inc.
9. Saunders, K.S., *Organic Polymer Chemistry*. 1988, New York: Chapman & Hall.

10. Brydson, J., *Plastics Materials*. 7th ed. 1999, Oxford: Butterworth-Heinemann.
11. Walton, D. and P. Lorimer, *Polymers*. Oxford Chemistry Primers, ed. R.G. Compton. 2001, Oxford: Oxford University Press.
12. Brooks, M. and P. Gardside. *Probing The Microstructure of Protein and Polyamide Fibres*. in *AHRC Research Centre for Textile Conservation and Textile Studies Second Annual Conference: The Furture of the 20th Century - Collecting, Interpreting and Conserving Modern Materials*. 2005. Winchester: Archetype Publications.
13. Lewin, M. and E.M. Pearce, *Handbook of Fibre Chemistry*. 2nd ed. International Fibre Science and Technology Series, ed. M. Lewin. 1998, New York: Marcel Dekker Inc.
14. Bendak, A. and S.M. El-Marsafi, *Effects of Chemical Modifications on Polyester Fibres.* Journal of Islamic Academy of Science, 1991. **4**(4): p. 275-284.
15. Wickens, J., *Eero Aarnio's Globe: A Platform for an Investigation of Challenges and Possibilities Related to the Conservation of Twentieth Century Foam Upholstered Furniture*, in *School of Arts*. 2007, University of Southampton: Southampton.
16. Mathias, L. 2005, Department of Polymer Science, The University of Mississippi.
17. Billmayer, F.W., *Textbook of Polymer Science*. 2nd ed. 1971, Chichester: Wiley-Interscience.
18. Carr, C.M.e., *Chemistry of the Textile Industry*. 1995, Cambridge: Chapman & Hall.
19. Sen, A.K., *Coated Textiles: Principles and Applications*. 2001: CRC Press.
20. De Araujo, S., C and Y. Kawano, *Near-infrared Spectra of Polyamide 6, Poly(vinyl cloride), and Polychlorotrifluoroethylene.* Journal of Applied Polymer Science, 2002. **85**: p. 199-208.
21. Blanco, M., et al., *Use of Near-infrared Spectroscopy in Control Analyses of Acrylic Fibre Manufacturing Processes.* Analytica Chimica Acta, 1999. **383**: p. 291-298.
22. Siesler, H.W., *Near-Infrared Spectroscopy: Principles, Instrumentation, Applications*, ed. H.W. Siesler, et al. 2002, Weinheim: Wiley-VCH.
23. Van Krevelen, D.W., *Properties of Polymers*. 1st ed. 1997, Amsterdam: Elsevier Science B.V. 875.
24. Hamid, S.H., M.B. Amin, and A.G. Maadhah, *Handbook of Polymer Degradation*. 1992, New York: Marcel Dekker Inc.
25. Feller, R.L., *Accelerated Ageing: Photochemical and Thermal Aspects*. Research in Conservation, ed. D. Berland. 1994, Los Angeles: Getty Conservation Institute.

Appendix 2: FTIR-ATR Spectra of the Schiaparelli Thai Silk Under Dress

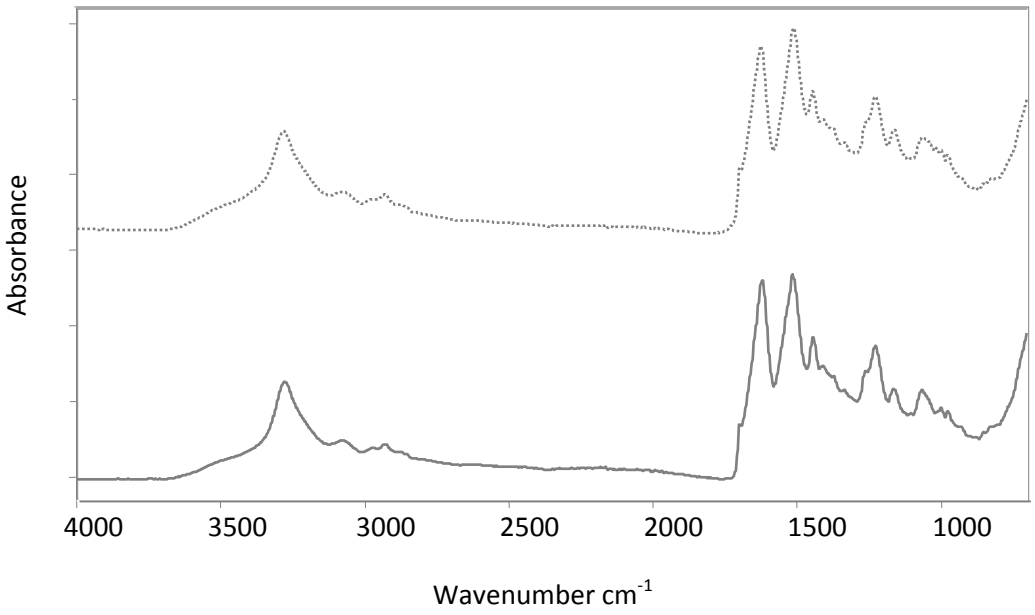

Figure A2.1 FTIR-ATR absorbance spectra of the warp fibres of the Sciaparelli under dress (dotted) and a silk reference (solid)

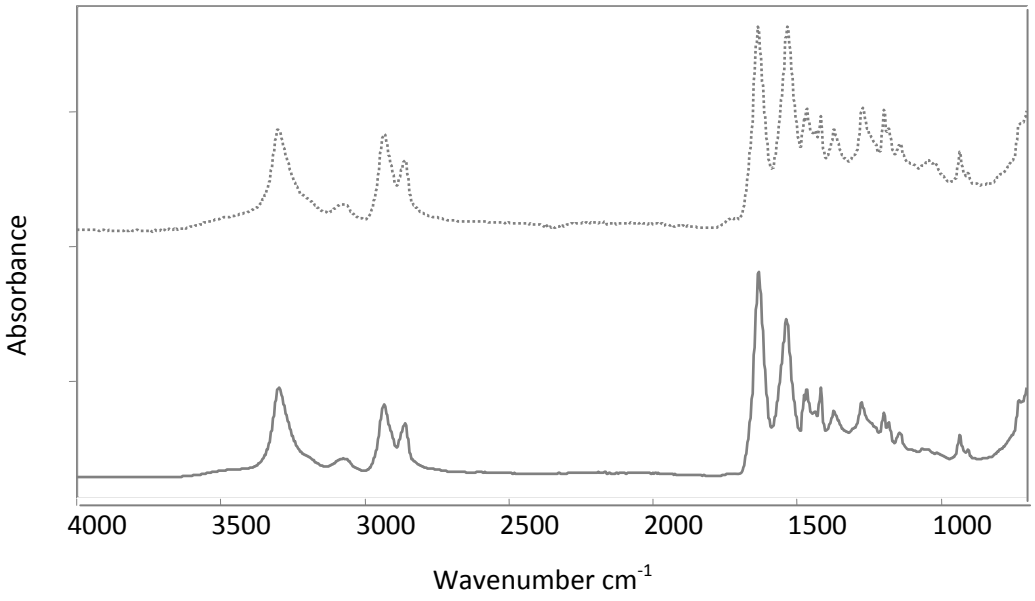

Figure A2.2 FTIR-ATR absorbance spectra of the weft fibres of the Sciaparelli under dress (dotted) and a polyamide reference (solid)

Appendix 3: Error in the FTIR Fractional Crystallinity Calibration Line

In order to determine the error in the fractional crystallinity calibration line (P1), that is the error in the slope (a) and intercept (b), the average X and Y values are used to calculate the most probable slope and intercept and the residuals given as [1]:

$$d_s = ax_s + b - y_s$$

Eq A3.i

Where:

d_s = residuals

a = slope

b = intercept

x_s = sample X value

y_s = sample Y value

The mean square error (α^2) in P1 is given as:

$$\alpha^2 = \frac{\sum dd}{n-2}$$

Eq A3.ii

The standard errors for a and b are:

$$\frac{\alpha_a^2}{n} = \frac{\alpha_b^2}{\sum xx} = \frac{\alpha^2}{\Delta}$$

Eq A3.iii

Where Δ is:

$$\Delta = n\sum xx - (\sum x)^2$$

Eq A3.iv

Where:

n = number of samples

∑xx = sum of the X^2 values

$(\sum x)^2$ = sum of the X values squared

Therefore, the mean square error in the slope and the intercept are derived by:

$$a = \alpha_a^2 = n\frac{\alpha^2}{\Delta}$$

Eq A3.v

$$b - \alpha_b^2 - \Sigma dd\,\frac{\alpha^2}{\Delta}$$

Eq A3.vi

A3.1 References

1. Topping, J., *Errors of Observation and Their Treatment*. 3rd ed. 1962, London: Chapman and Hall Ltd.

Appendix 4: Publications and Conference Papers

Publications:

Richardson. E, Martin.G, Wyeth. P and X. Zhang, *State of the Art: Non-invasive Interrogation of Textiles in Museum Collections*, 2008, Microchimica Acta, Vol. 162, No. 3-4, pp. 303-312.

Richardson. E, Martin.G, and P. Wyeth, *Collecting a Near-Infrared Spectral Database of Modern Textiles for use of On-site Characterisation,* 2007, published in the postprints of the conference, Textiles and Text**,** AHRC Research Centre for Textile Conservation and Textile Studies Second Annual Conference (Archetype Publications) held at The Textile Conservation Centre, Winchester, June 2006, pp.257-263.

Thickett, D and E. Richardson, *Preventive Conservation Research for Plastics on Open Display,* in the postprints of the Plastics: Looking at the Future and Learning from the Past (Archetype Publications), held at the Victoria and Albert Museum, London, May 2007, pp. 89-96.

Richardson. E, Martin.G, and P. Wyeth, *On-site Collections Management: NIR Characterisation and Condition Monitoring of Modern Textiles,* in the postprints of Conservation Science 2007 (Archetype Publications), held at the Politecnico di Milano, Milan, May 2007, pp.262-269.

Richardson, E and P. Garside, *The Use of Near-Infrared Spectroscopy as a Diagnostic Tool for Historic Silk Artefacts,* awaiting publication in the postprints of the IRUG Biannual conference (Journal of ePreservationScience), held at the Academy of Fine Arts, Vienna, March 2008.

Conference Papers:

Richardson. E, Martin.G, and P. Wyeth, *Collecting a Near-Infrared Spectral Database of Modern Textiles for use of On-site Characterisation,* 2007, Textiles and Text**,** AHRC Research Centre for Textile Conservation and Textile Studies Second Annual Conference held at The Textile Conservation Centre, Winchester, June 2006.

Thickett, D and E. Richardson, *Preventive Conservation Research for Plastics on Open Display,* Plastics: Looking at the Future and Learning from the Past, held at the Victoria and Albert Museum, London, May 2007.

Richardson. E, Martin.G, and P. Wyeth, *On-site Collections Management: NIR Characterisation and Condition Monitoring of Modern Textiles,* Conservation Science 2007, held at the Politecnico di Milano, Milan, May 2007.

Richardson, E and P. Garside, *The Use of Near-Infrared Spectroscopy as a Diagnostic Tool for Historic Silk Artefacts,* IRUG Biannual conference, held at the Academy of Fine Arts, Vienna, March 2008.

Richardson. E, Martin.G, and P. Wyeth, *On-site Characterisation of Polyamide Material by Near-Infrared Spectroscopy and Principal Component Analysis,* COST D42 workshop on NIR and Chemometrics in Cultural Heritage, Ljubljana, November 2008.

Richardson. E, Garside.P, Martin.G, and P. Wyeth, *Enhancing Collections Management: On-site NIR Characterisation and Condition Monitoring of Textile Artefacts,* 47th Eastern Analytical Symposium, held at the Garden State Exhibition Centre, Somerset, New Jersey, November 2008.